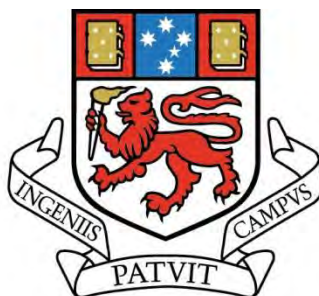


Porous polymer monolith supported Suzuki-Miyaura catalysis in microreactors



UNIVERSITY
OF TASMANIA

Jeremy Alan Deverell

B.Sc Hons (University of Tasmania)

Submitted in fulfilment of the requirements
for the degree of

Doctor of Philosophy

School of Chemistry
University of Tasmania
Hobart, Tasmania
Australia
September 2011

Declaration of originality

This thesis contains no material which has been accepted for a degree or diploma by the University or any other institution, except by way of background information and duly acknowledged in the thesis, and to the best of my knowledge and belief no material previously published or written by another person except where due acknowledgement is made in the text of the thesis, nor does the thesis contain any material that infringes copyright.

Authority of access

This thesis is not to be made available for loan or copying for two years following the date this statement was signed. Following that time the thesis may be made available for loan and limited copying in accordance with the Copyright Act 1968.

A handwritten signature in black ink that reads "Jeremy Deverell". The signature is written in a cursive style with a large, looped 'J' and a clear, legible 'Deverell'.

Jeremy Alan Deverell

September, 2011

Statement of co-authorship

Several people within the microreactor group contributed towards research reported in publications, and the contribution of each author is estimated to be approximately as documented below.

Paper 1: "Microfluidic devices for flow-through supported palladium catalysis on porous organic monolith".

Jeremy A. Deverell (75%, experimental and planning), Allan J. Canty (5%, planning and writing), Anissa Gömann (5%, experimental and planning), Rosanne M. Guijt (5%, planning and writing), Thomas Rodemann (5%, planning and writing), and Jason A. Smith (5%, planning and writing).

Paper 2: "Palladium-mediated organic synthesis using porous polymer monolith formed in situ as a continuous catalyst support structure for application in microfluidic devices".

Jeremy A. Deverell (65%, experimental and planning), Allan J. Canty (5%, planning and writing), Anissa Gömann (5%, experimental and planning), Rosanne M. Guijt (5%, planning and writing), Thomas Rodemann (5%, planning and writing), Jason A. Smith (5%, planning and writing), Katrina F. Munting (5%, experimental and planning), and Roderick C. Jones (5%, experimental and planning).

Paper 3: "Supported palladium catalysis using a heteroleptic 2-methylthiomethylpyridine-N,S-donor motif for Mizoroki-Heck and Suzuki-Miyaura coupling, including continuous organic monolith in capillary microscale flow-through mode".

Jeremy A. Deverell (35%, experimental and planning), Roderick C. Jones (35%, experimental, planning and writing), Allan J. Canty (5%, planning and writing), Michael G. Gardiner (5%, planning and writing), Rosanne M. Guijt (5%, planning

and writing), Thomas Rodemann (5%, planning and writing), Jason A. Smith (5%, planning and writing), and Vicki A. Tolhurst (5%, planning and writing).

Paper 4: "UV initiated formation of polymer monoliths in glass and polymer microreactors".

Jeremy A. Deverell (80%), Thomas Rodemann (5%, planning and writing), Jason A. Smith (5%, planning and writing), Allan J. Canty (5%, planning and writing), and Rosanne M. Guijt (5%, planning and writing).

Paper 5: "Macroporous monolith supports for continuous flow capillary microreactors".

Jeremy A. Deverell (40%, experimental and planning), Katrina F. Bolton (30%, experimental and planning), Allan J. Canty (5%, planning and writing), Rosanne M. Guijt (5%, planning and writing), Emily F. Hilder (5%, planning and writing), Thomas Rodemann (5%, planning and writing), and Jason A. Smith (5%, planning and writing).

Signed: _____

Prof. Allan Canty

Dr Greg Dicinoski

Supervisor

Head of School

School of Chemistry

School of Chemistry

University of Tasmania

University of Tasmania

September 2011

Acknowledgements

First and foremost I would like to express my deepest gratitude to my supervisors Dr Thomas Rodemann, Dr Rosanne Guijt, and Prof. Allan Canty. This document would not exist if not for their guidance, encouragement, and incredible fortitude in persevering with me for all these years.

Thomas has been more than a supervisor, he has also been a mentor in both academia and in life. He is a dear friend, without whom I know I probably would not be here now. It was he that originally encouraged me to pursue a doctorate, for which I will always be grateful.

Rosanne is truly an amazing woman, for whom I have nothing but the deepest respect for as an academic and as a person. Her strength and objectivity were invaluable and allowed the project to continually move forward.

Allan's international fame as a master of palladium chemistry is very well deserved. I often found his wealth of knowledge and experience astonishing and almost always learned something new from him during each conversation.

Other than my supervisors, I would like to thank Dr Jason Smith for his invaluable insight and mastery of organic chemistry, Dr Emily Hilder for all her support both as a polymer monolith expert and as graduate research coordinator, and Dr Michael Breadmore for sharing his years of experience in all things microfluidic.

I especially need to thank the staff of the School of Chemistry, the Document Delivery service and the Graduate Research Office.

Special thanks to my grandfather, who sadly passed away during my studies, and my good friend Pam Mansfield for their love and support.

I must thank Dr Doug McLean for rocking, for his encouragement, and for his friendship.

Thank you to the talented staff of the Central Science Laboratory whom made this work possible, specifically Peter Dove, Mike Brandon, Dr Karsten Gömann, Dr Ashley Townsend, Dr James Horne, and John Davis.

And finally I would like to thank everyone who contributed to work: Katrina Munting, Dale Brandon, Paul Harvey, Peter Molesworth, Oscar Potter, Dr Andrew Grosse, Graham Meredith, Simon Stephens, Dr Anissa Gömann, Dr Joselito Quirino, Dr Mohamed Dawod, Dr Anna Nordborg, Dr Joe Hutchinson, and Adam James.

Table of contents

	Page no.
Declaration of originality	II
Authority of access	II
Statement of co-authorship.....	III
Acknowledgements	V
Table of contents	VII
Abstract	1
Publications and presentations	3
Glossary.....	5
Chapter 1 Literature Review	7
1.1 Introduction.....	7
1.2 Microreactor design, fabrication, and operation.....	9
1.3 Palladium mediated catalysis in microreactors.....	16
1.4 Supports for palladium catalysis.....	27
1.5 Aims.....	31
1.6 References.....	32
Chapter 2 Porous polymer monoliths	42
2.1 Introduction.....	42
2.2 Thermally initiated polymer monoliths	48
2.3 Photoinitiated polymer monoliths.....	55
2.4 Photopolymerised PPM in plastic devices.....	89
2.5 Photopolymerised PPM in large ID glass columns	121

2.6	Preparation and characterisation of photopolymerised bulk monolith	128
2.7	Conclusions.....	135
2.8	Experimental.....	140
2.9	References.....	150
Chapter 3	Catalyst immobilisation on porous polymer monolith.....	156
3.1	Introduction.....	156
3.2	Immobilisation of 5-NH ₂ phen	158
3.3	Immobilisation of Me-im.....	175
3.4	Palladium attachment to PPM with immobilised ligand	182
3.5	Conclusions.....	191
3.6	Experimental.....	194
3.7	References.....	202
Chapter 4	Suzuki-Miyaura reactions	205
4.1	Introduction.....	205
4.2	Considerations	206
4.3	Continuous flow reaction results	213
4.4	Reactor catalysis validation, palladium leaching, and homogeneous catalysis.....	227
4.5	Alternative reactor system	228
4.6	Conclusions.....	232
4.7	Experimental.....	233
4.8	References.....	238
Chapter 5	Engineering	240

5.1	Flow-through devices and interfaces	240
5.2	Development of a UV initiated bulk monolith polymerisation container	249
5.3	Conclusions.....	254
5.4	References.....	254
Chapter 6	Conclusion and outlook.....	255
	Appendices	258

Abstract

Miniaturisation of reactions to the sub-millilitre scale, through the use of microreactor technology, has the potential to reduce costs by drastically reducing reaction times, improving yields and selectivities, as well as decreasing the environmental impact by reducing reagent and solvent use. Further improvements can be achieved by utilising heterogeneous and supported catalysts within microreactors in order to increase reaction efficiency, reduce energy requirements, and simplify product purification. This should also enable the integration of microreactors with other existing microfluidic technologies allowing synthesis, purification, analysis, and bio-testing to be performed on a single device in an automated fashion.

In this work, novel microreactors were fabricated utilising porous polymer monoliths (PPM's) prepared *in situ* within microfluidic devices as a support for the immobilisation of palladium complexes. Poly(glycidyl methacrylate-*co*-ethylene glycol dimethylacrylate) and poly(chloromethylstyrene-*co*-divinylbenzene) monoliths were prepared by either thermal or UV initiated radical polymerisation in several formats, including capillary, microchip, and column using both glass and polymer substrates. This required the development of new methods for anchoring PPM within polymer substrates with poor transmission in the deep UV region, which is necessary for photografting, thus enabling the use of polymer substrates with greater thermal resistance. The development of polymeric microreactors was pursued as mass production of microfluidic devices with multiple components is considerably easier and more economical compared to other substrates. Additionally, conditions were developed to allow the formation of PPM in columns with an internal diameter (ID) greater than 1 mm without the need for external compression to avoid shrinkage. The preparation of PPM using light emitting diode light sources was

investigated with the aim of reducing the cost associated with development of photoinitiated PPM's, enabling greater access to this technique. The PPM's were utilised to immobilise ligands that will bind palladium, 5-hydroxy-1,10-phenanthroline, 5-amino-1,10-phenanthroline, and an *N*-methylimidazolium salt. In order to demonstrate the feasibility of this technology, the Suzuki-Miyaura coupling of iodobenzene and *p*-tolylboronic acid was performed under continuous flow in the reactors, which produced quantitative yields with less than 0.01% of the immobilised palladium leached over a 24 h reaction period. This is the first reported use on a polymer microchip for supported Suzuki-Miyaura catalysis and also the first demonstration of non-room temperature supported palladium catalysis within a polymer microreactor. Novel technology was developed to allow easy interfacing with a broad range of microchips and for producing PPM in batch via UV initiation using low intensity light sources.

Publications and presentations

Publications (copies provided in the appendix)

"Microfluidic devices for flow-through supported palladium catalysis on porous organic monolith".

Allan J. Canty, Jeremy A. Deverell, Anissa Gömann, Rosanne M. Guijt, Thomas Rodemann and Jason A. Smith: *Australian Journal of Chemistry*, **2008**, 61(8), 630-366.

"Palladium-mediated organic synthesis using porous polymer monolith formed in situ as a continuous catalyst support structure for application in microfluidic devices".

Anissa Gömann, Jeremy A. Deverell, Katrina F. Munting, Roderick C. Jones, Thomas Rodemann, Allan J. Canty, Jason A. Smith, and Rosanne M. Guijt: *Tetrahedron*, **2009**, 65(7), 1450-1454.

"Supported palladium catalysis using a heteroleptic 2-methylthiomethylpyridine-N,S-donor motif for Mizoroki-Heck and Suzuki-Miyaura coupling, including continuous organic monolith in capillary microscale flow-through mode".

Roderick C. Jones, Allan J. Canty, Jeremy A. Deverell, Michael G. Gardiner, Rosanne M. Guijt, Thomas Rodemann, Jason A. Smith, and Vicki A. Tolhurst: *Tetrahedron*, **2009**, 65(36), 7474-7481.

"UV initiated formation of polymer monoliths in glass and polymer microreactors".

Jeremy A. Deverell, Thomas Rodemann, Jason A. Smith, Allan J. Canty, and Rosanne M. Guijt: *Sensors and Actuators B: Chemical*, **2010**, in press.

"Macroporous monolith supports for continuous flow capillary microreactors".

Katrina F. Bolton, Allan J. Canty, Jeremy A. Deverell, Rosanne M. Guijt, Emily F. Hilder, Thomas Rodemann, and Jason A. Smith: *Tetrahedron*, **2006**, 47(52), 9321-9324.

Presentations

ACROSS Symposium on Advances in Separation Science

Hobart, Tasmania, December 2008.

Poster entitled "Photo-initiated radical polymerisation of porous polymer monoliths in microchips with low-intensity near UV light sources".

Glossary

The following abbreviations have been used throughout this thesis:

1,10-phen	1,10-phenanthroline
5-NH ₂ phen	5-amino-1,10-phenanthroline
5-OHphen	5-hydroxy-1,10-phenanthroline
AIBN	azoisobutyronitrile
BAPO	bis(2,4,6-trimethylbenzoyl)phenylphosphine oxide
bipy	2,2'-bipyridine
BP	benzophenone
CEC	capillary electrochromatography
CMS	Chloromethylstyrene
COC	cyclic olefin co-polymer
COP	cyclic olefin polymer
DMABP	4,4'-bis(dimethylamino)benzophenone
DMF	dimethylformamide
DMPAP	2,2-dimethoxy-2-phenylacetophenone
DMSO	dimethyl sulphoxide
DVB	divinylbenzene
EA	elemental analysis
EDA	ethylene glycol diacrylate
EDMA	ethylene glycol dimethacrylate
EOF	electromotive force
eq.	equivalent/s
GC	gas chromatography
GC-MS	gas chromatography–mass spectrometry
GMA	glycidyl methacrylate
HPLC	high pressure liquid chromatography
ICP-MS	inductively coupled plasma-mass spectrometry

ID	internal diameter
LED	light emitting diode
Me-im	1-methylimidazole
MIP	mercury intrusion porosimetry
MMA	methyl methacrylate
OD	outer diameter
PDMS	poly(dimethylsiloxane)
PEEK	polyetheretherketone
PMMA	Poly(methyl methacrylate)
PPM	porous polymer monolith
PTFE	polytetrafluoroethylene
SEM	scanning electron microscopy
TBAH	tetrabutylammonium hydroxide
TBAM	tetrabutylammonium methoxide
THF	tetrahydrofuran
TMPTA	trimethylolpropane triacrylate
TOF	turnover frequency
TON	turnover number
UV	ultraviolet
UV-VIS	ultraviolet-visible

Chapter 1 Literature Review

1.1 Introduction

Synthetic chemists have developed a multitude of successful strategies for assembling molecules utilising established and developing technologies [1]. A majority of the techniques traditionally employed are inherently wasteful, requiring relatively large quantities of reagents and solvents to produce analytically pure compounds. It is estimated, that in the production of fine chemicals, for every kilogram of product between 5-20 kg of waste is produced. This can be as high as 100 kg of waste in the production of pharmaceuticals [2]. Due to changes in the economic and political climate in recent years, it has become apparent that these methods for performing synthetic chemistry are not sustainable and must be changed. There is a great need to reduce consumption of expensive reagents, decrease waste, and use more environmentally friendly synthetic pathways. A number of different strategies have been pursued to advance the sustainability of synthetic chemistry including catalysis and cascade sequences (multi-step one-pot reactions) [3, 4]. An important and versatile approach is optimisation of reaction engineering, known as process intensification through the use of microreactor technology [5].

A microreactor is a device for performing chemical transformations in which fluids are manipulated within a network of channels with dimensions in the sub-millimetre region. Microreactor technology is a subset of the large field of microfluidics, which has become well established in separation science and to-date a large variety of separation techniques have been demonstrated in microfluidic devices, including CE, HPLC, and IC [6-10]. Separations performed at the microfluidic scale have been shown to be more efficient and afford lower detection limits. At present microfluidic devices are routinely used for analysis and there are

several commercial instruments available from companies such as Agilent Technologies Inc., Caliper Life Sciences Inc., Fluidigm Corporation, and Gyros. Analytical microfluidic devices have become common place in bio-applications, especially in proteomics and genomics [11], as well as drug discovery [12, 13].

One of the most attractive aspects of microfluidics is integration, which completely revolutionised the electronics industry in a similar fashion more than 50 years ago. This has several potential benefits, such as automation, safety, and preventing contamination. The ultimate goal is the ability to perform synthesis, separation, analysis, and bio-testing in an automated fashion, which has become known as the 'lab-on-a-chip' concept.

The idea of utilising microfluidic devices for performing chemical and biochemical transformations was first discussed at a workshop in Mainz in 1995 [14]. While initially there was relatively little interest in this area, the last ten years has seen amazing growth in microreactor research, illustrated by reviews during this period [5, 14-36]. It has been discovered that performing synthesis using microreactors has several important benefits other than just the reduction in use of solvents and reagents. These include controlled mixing, greater temperature control, improved selectivity and yield, rapid reaction optimisation and compound library generation, increased production by parallelisation, continuous automated processing, increased safety, and on-demand synthesis.

Microreactor technology has the potential to revolutionise drug discovery. Presently, only 10% of drugs developed make it to market, and about half fail at Phase II clinical trials where 80% of the cost has already been incurred [33]. Microreactors have the potential to greatly reduce this cost by improving the drug development cycle through coupling of the microreactors with on-line purification,

analysis, and bio-testing. Utilising a large number of such devices in parallel could drastically accelerate compound library generation. Loss after synthesis is minimised as synthesis and purification are performed within a single device, enabling complete testing with only picograms of material [33]. Currently there are several commercial microreactor producers, including Chemtrix BV, CPC-Cellular Process Chemistry Systems GmbH, Ehrfeld Mikrotechnik, Micronit/Future Chemistry, Microinnova Engineering GmbH, Mikrogas Chemtech GmbH, and Syrris.

The main focus of this review is supported catalysis within microreactors, with particular emphasis on palladium mediated catalysis. As such, only a basic overview of continuous flow microreactors in general will be presented as there are several excellent comprehensive reviews of microreactor science [16, 30, 32]. Finally catalyst support structures will be discussed, with particular focus on polymer resins and porous polymer monoliths.

1.2 Microreactor design, fabrication, and operation

A microreactor in its simplest form is a length of sub-millimetre ID column, which can either have a single inlet and outlet through which a fluid is pumped, or can utilise manifolds, such as three-way fittings, in order to combine reagent streams. Microchip-based reactors can readily accommodate multiple inlets and outlets without the need for complex manifolds and offer precise control over how the reagent streams are combined with significantly more complex flow pathways than can be achieved in column reactors. Due to the greater potential of microchip reactors, their design requires careful selection of several factors including the channel layout and dimensions, thermal properties, chemical and solvent compatibility, fluid flow properties, and fabrication volume. Several of these considerations relate directly to the choice of substrate material from which the

device is fabricated. There is no universal microreactor design and substrate, and a variety of different substrates have been used for the fabrication of microreactors, including: quartz [37, 38], glass, silicon [39], metals [40], plastics [41-43], and ceramics [44]. The choice of substrate determines the thermal and chemical properties of the reactor, as well as those methods that can be utilised for their fabrication.

1.2.1 Fabrication and substrate choice

Early microreactors were fabricated using techniques borrowed from the microelectronics industry using silicon and glass substrates. As the field has grown, techniques have been developed for fabrication in a variety of materials. These fabrication methods can be broadly categorised into direct fabrication and replication techniques. Direct fabrication methods produce features directly in the substrate and are generally employed for fabricating microreactors in quartz, glass, polymers, and metals utilising techniques such as wet [45]/dry [46] etching, laser ablation [47], lamination [48], and micro-milling [49]. The disadvantage of this approach is that each fabrication only yields a single device, hence this inevitably leads to variation in feature dimensions due to changes in the fabrication conditions rendering this approach unsuitable for mass production of devices with exact features. Also, etching techniques often require the use of highly toxic and hazardous chemicals, such as hydrofluoric acid, increasing the environmental burden with their use [12]. Replication methods make use of a master, generally fabricated using direct fabrication techniques, to transfer features into the substrate, and includes techniques such as hot embossing [50], injection molding [51], and soft embossing [52]. These techniques are almost exclusively used for fabrication of polymer devices, with the exception that hot embossing of glass has been recently demonstrated [53]. The

advantage of replication methods, in that a single master can be used to produce many exact replicates, make this approach perfectly suited to mass production.

Glass has traditionally been the material of choice for synthetic applications due to its chemical inertness to most reagents and transparency for visual inspection of reaction conditions. The poor thermal conductivity of glass limits its application to reactions which do not require high temperatures or pressures; these conditions generally require materials such as silicon, metal, or ceramics.

Silicon is a useful substrate for microreactors, and microfluidic devices in general, as fabrication techniques are well established, allowing fabrication of complex structures with high aspect ratios. The high heat transfer coefficient of silicon also makes it useful for exothermic reactions, but silicon is incompatible with bases and is not transparent making visual inspection and online optical detection impossible.

Metals, such as stainless steel, are the preferred material for fabrication of column-based microreactors for production applications as they can be operated under extreme conditions. Metals are generally not used for fabrication of microchip reactors due to difficulties producing high aspect-ratio features in these materials and the inability to visually inspect the reaction.

Ceramic microdevices have excellent resistance to extreme temperatures and pressures, and are highly inert. Unfortunately, fabrication of microstructures in ceramics is exceedingly difficult.

Polymers have gained popularity recently for the fabrication of biocatalyst reactors as they are relatively inexpensive and allow the use of rapid prototyping techniques such as soft embossing used with widely used poly(dimethylsiloxane) (PDMS). Polymers are comparatively limited in terms of solvent and thermal

compatibility, restricting their application mostly to aqueous chemistry at low pressures and temperatures. They can however be mass produced at a low unit cost, allowing them to be disposable [54]. Due to the wide variety of different commercially available polymers, the chemical and physical properties are highly configurable, enabling tailoring of the material to the application.

1.2.2 Interfacing and fluid transport

Fabrication of microscale structures, which create the microchannel network within the device, is important, the ability to interface the device and control the fluid flow within is equally important. Interfacing a microreactor depends heavily on the design and reactor type. Column reactors can be interfaced using simple adapters, however microchip reactors generally require a custom fabricated interface using specialised microfluidic fittings to allow the channels to be connected to external tubing.

A variety of different microfluidic fluid transport techniques have been demonstrated [30, 35], however the two most commonly utilised in microreactors are pressure-driven and electrokinetic. Pressure-driven, or hydrodynamic, flow, relies on the creation of a pressure differential between the inlet and outlet of the microchannel, and is usually created by an external pump [55, 56]. The advantage of this approach is that it is relatively simple and can be utilised with any fluid and any device substrate, provided the seal is strong enough to withstand the backpressure. Typically large external syringe pumps or HPLC pumps are used, but internal pumps with complex small moving parts have also been fabricated [57]. Pressure-driven flow is best suited to simple flow systems as it does not allow for accurate flow control within devices with complex channel pathways. Pressure-driven flow is known to generate a parabolic velocity profile [12] as a result of flow resistance, which does not affect continuous flow systems but can adversely affect pulsed flow

systems or 'bubble' reactors. Electrokinetic flow is the movement of the liquid inside a channel by application of a potential bias between the inlet and outlet [58, 59]. Flow results from the movement of ions in solution towards the oppositely charged electrode, and also from electro-osmotic flow which arises from the electrical double layer that polar solvents form on charged surfaces. This restricts the use of this technique to polar solvents such as water, methanol, acetonitrile, and to materials that form charged surfaces, such as glass and silicon. The main benefit of electrokinetic flow is that it enables precise control over fluid flows within a complex microchannel network, as fluid velocity is directly proportional to voltage which can be computer controlled. Another advantage is that this type of flow generates a flat velocity profile as it is generated at the wall [30].

1.2.3 Benefits of microreactors

Most of the benefits associated with microreactors arise from their sub-millimetre dimensions, which give rise to rapid mixing and heat transfer. Microreactor dimensions fluid flow is typically laminar, where internal forces dominate and turbulence is absent [60]. Here mixing occurs solely by molecular diffusion, which is relatively slow and channel cross-sections in the tens of microns range are required to achieve complete mixing within seconds [5]. These narrow channels usually result in excessively large pressure differentials over the length of channel, drastically increasing the force required to achieve flow. In order to address this problem, microfluidic devices, known as micro-mixers, have been developed to improve mixing while having acceptable pressure differentials. Micro-mixers can either be passive [60-62] where mixing is induced by using creative microchannel design to increase the interfacial surface area between reagent streams or create chaotic advection, or active [63, 64] where the external input of energy induces mixing, such as an ultrasonic transducer [65].

The small dimensions of microreactors also give them a relatively large surface area-to-volume ratio, which can be up to 500 times larger than for conventional reactors [19]. The large surface area of the microchannel allows for rapid heat transfer between the reactor and reaction mixture. Coupled with rapid mixing, this helps prevent the formation of „hot spots’ during reactions resulting in a narrow temperature distribution which greatly improves selectivity and yield of the target product [30]. Under batch reaction conditions, concentration gradients and the formation of „hot spots’ can alter the reaction selectivity, resulting in reduced yield. The rapid heat transfer coupled with the small reaction volume allows highly exothermic reactions and the synthesis of unstable, potentially explosive, or toxic compounds to be performed safely. For example fluorinations [66, 67] and diazo transfer reactions [68] have been shown to be significantly safer when performed in microreactors.

Multi-step reactions are another area where microreactor technology has considerable potential. In traditional batch synthesis, multi-step synthetic pathways can often be quite complex, requiring purification and isolation of the product between reactions steps. Microreactor technology, by careful design of the microchannel network and precise control over the reagent stream flows, allows multiple reactions to be performed in a specific sequence, all within a sealed reaction vessel with minimal loss between reaction steps. Several examples of multi-step synthesis in microreactors have already been presented [69-71]. Integration of multi-step reactors with existing microfluidic technology for on-line separation, purification, and analysis with computer control is very attractive for reaction optimisation, compound library generation, or on-demand synthesis of unstable compounds [72, 73]. Addition of on-line bio-assay to such a system could potentially revolutionise drug discovery, allowing for rapid identification of drug leads, saving

many of hours, drastically reducing waste and accelerating the drug development process [33]. This is arguably the most important potential application of this technology.

A major challenge in pharmaceutical and fine chemical production is the scaling-up of a laboratory optimised synthesis to production scale, in which a variety of issues are generally incurred such as reduced yield and selectivity due to the formation of thermal and concentration gradients in large reaction vessels [19, 74]. Microreactors offer alternative approaches to increasing product other than increasing the reactor dimensions. The first is to use the reactor for long periods of time in order to accumulate the desired amount of product, and the second is to operate multiple identical microreactors in parallel. The latter approach is referred to as „numbering-up’ or „scale-out’. There have been several pilot plants based on microreactor technology which have utilised the scale-out approach [75-77].

1.2.4 Catalysis in microreactors

Further improvements in reaction efficiency can be obtained by utilising catalytic reactions within microreactors. Catalysts work by reducing the activation energy required for chemical transformations. This allows reactions to be performed using milder conditions, which enables the use of a wider variety of microreactor substrates for fabrication. Catalysis is generally categorised as either homogeneous, where a dissolved species in the same phase as the reaction acts as the catalyst, or heterogeneous, where reactions are believed to occur at a solid surface of which the active site is part of. Heterogeneous catalysts are not to be confused with supported catalysts, where a homogeneous catalytic centre is immobilised on a support, usually a solid [78]. Homogeneous catalysts are more commonly utilised as they are simply added to a reaction and mixed with the reagents in solution [58, 72, 79-85]. An obvious draw-back to the use of homogeneous catalysts is that that they must be

isolated from the product. Often the purification process deactivates the catalyst preventing reuse and hence increasing the environmental burden. A solid heterogeneous catalyst, or a solid support for a supported catalyst, can be removed from the reaction medium by simple filtration and potentially reused repeatedly. Hence, heterogeneous and supported catalysts are attractive from an environmental and economic stand-point. They can be immobilised in continuous flow-through reactors, which greatly simplifies product isolation and enables the possibility of connecting several reactors in series for multi-step catalytic reactions.

A variety of different catalytic reactions have been demonstrated, and have been extensively discussed in recent reviews [21, 30, 35, 36], including transition metal catalysts, organometallic complexes, organic catalyst, enzymatic and bio-reactors. Supported catalysts generally have the same or better performance than their homogeneous analogues [86]. Transition metal catalysts are very important in the pharmaceutical and fine chemical industries as several key molecule building reactions utilise these catalysts. In particular, palladium catalysts are important in the production of biaryls which are the starting materials for many important pharmaceutical and fine chemical products [86-88].

1.3 Palladium mediated catalysis in microreactors

Palladium is commonly utilised to catalyse coupling reactions, such as the Mizoroki-Heck, Suzuki-Miyaura, Sonogashira, and Stille reactions, as well as hydrogenation reactions, which are selective with high turnover numbers and relatively mild conditions [89]. Homogeneous palladium catalysis has been demonstrated in both microreactors [58, 72, 79-84] and minireactors (>1 mm ID) [84, 90, 91], which generally showed equal or better performance than the equivalent batch reactions. As stated previously, heterogeneous and supported catalysts are of

particular interest due to their potential application in lab-on-a-chip devices and hence a detailed discussion of homogenous palladium catalysis in microreactors will not be presented.

Heterogeneous palladium catalysis within a microreactor was first reported by Greenway *et al.* in 2000 [59]. Their microchip reactor was fabricated from glass and featured a T-shape microchannel (300 μm wide and 115 μm deep), shown in **Figure 1.1**, prepared by wet etching. The heterogeneous catalyst, 1.8 wt% palladium on silica, was loaded into the etched trough prior to bonding of the top sealing plate which forms the microchannel.

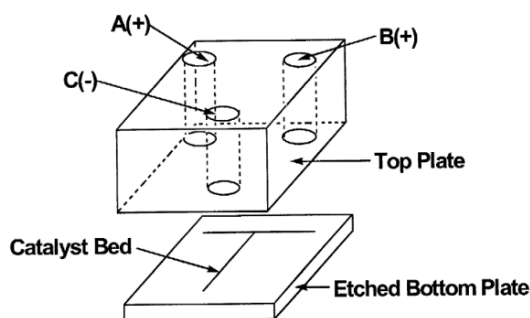
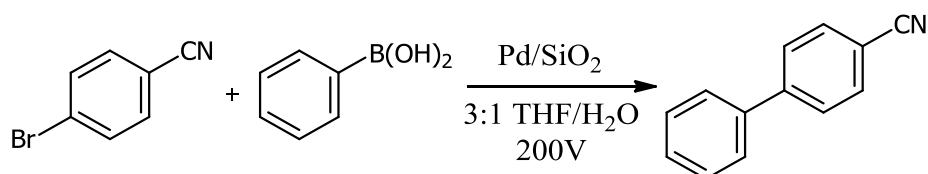


Figure 1.1 T-shape glass microreactor. Figure adapted from Greenway *et al.* [59].

Electromotive force (EOF) was used to induce fluid transport within the reactor by the application of a positive potential at the inlet reservoirs, A and B, and a negative potential at the outlet, reservoir C. Under these conditions the microporous silica also acted as a micro-pump, assisting the fluid flow. The Suzuki-Miyaura coupling of 4-bromobenzonitrile and phenylboronic acid, shown in **Scheme 1.1**, was used as a model reaction for testing the microreactor.



Scheme 1.1 Suzuki-Miyaura coupling of 4-bromobenzonitrile and phenylboronic acid.

Reactions were performed in 3:1 tetrahydrofuran (THF)/water, with a solution of phenylboronic acid (0.1M) added to reservoir B of the reactor while a solution of 4-bromobenzonitrile (0.1M) was added to reservoir A. The voltages were manipulated such that the continuous flow of the phenylboronic acid solution moved from reservoir B to C, while aliquots of the 4-bromobenzonitrile solution were selectively injected into the continuous stream of phenylboronic acid. Samples were taken from reservoir C for GC-MS analysis in order to determine reaction yield. The authors found that the addition of a base was not required for the reaction, which they attributed to the generation of hydroxide by the silica in the microreactor channel. Under optimised conditions, a yield of $67\pm 7\%$ was obtained at a flow rate of $0.8\ \mu\text{L min}^{-1}$. For comparison a batch reaction was performed under reflux for 8 h using sodium carbonate as a base, affording a yield of 10%. In this particular example the microreactor clearly outperforms the equivalent batch reaction.

He *et al.* also utilised particle packed column and microchip reactors to perform heterogeneous Suzuki-Miyaura catalysis [56, 86]. The column reactor consisted of a U-shaped 800 μm ID glass tube, 138 mm in length, packed with either 2 wt% palladium on silica or 5 wt% palladium on alumina [86]. The catalyst particles, 355-420 μm in diameter, were retained within the column by insertion of 300 μm OD glass rods into both ends of the tube, with one side connected to a syringe pump via PTFE tubing. The packed catalyst bed was heated by microwave-induced heating. Due to the relatively small reactor cross-section, 15 mm of the U-bend was sputter coated with gold, as shown in **Figure 1.2**, to improve absorption of the microwave energy.

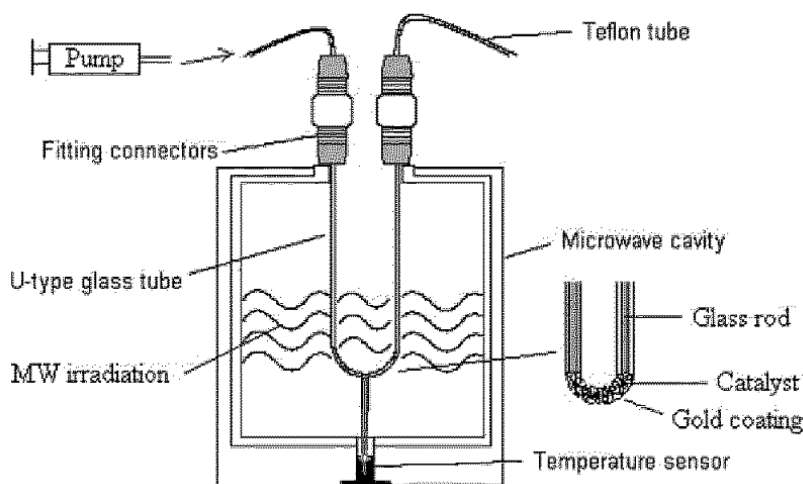
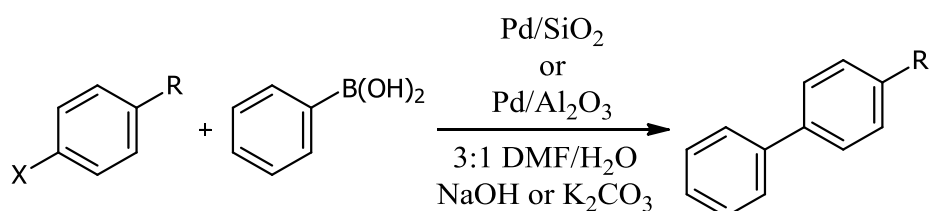


Figure 1.2 Diagram of microwave-assisted column microreactor. Figure adapted from He *et al.* [86].

The Suzuki-Miyaura coupling of 4-bromobenzonitrile and phenylboronic acid in 3:1 dimethylformamide (DMF)/water, shown in **Scheme 1.2**, was used for the optimisation of several different reaction conditions, which included investigation of the base, heating source, flow rate, and catalyst support.



Scheme 1.2 Suzuki-Miyaura couplings utilised by He *et al.* in column microreactor.

X = I, Br and R = CH₃, CHO, OCH₃, CN, NO₂.

The optimal conditions involved the use of potassium carbonate as the base, heating via microwave with a gold coating on the column, and a flow rate of 0.04 μL min⁻¹. Palladium immobilised on alumina was found to give superior results to silica, which the authors attributed to its more efficient absorption of microwave energy. Under the optimised conditions, a yield of over 69% was obtained with a reaction time of 15 s. Coupling of phenylboronic acid and an additional two aryl bromides and two aryl iodides were demonstrated using the optimised conditions, with the microwave

power adjusted to give a reaction temperature of 50 °C. The yields obtained for these reactions were between 30-74%.

Based in their findings using the column microreactor, *He et al.* developed a glass microchip reactor also utilising a packed particle catalyst bed, microwave heating, and pressure-driven flow via syringe pump [56]. Two different microchip designs were investigated, shown in **Figure 1.3**.

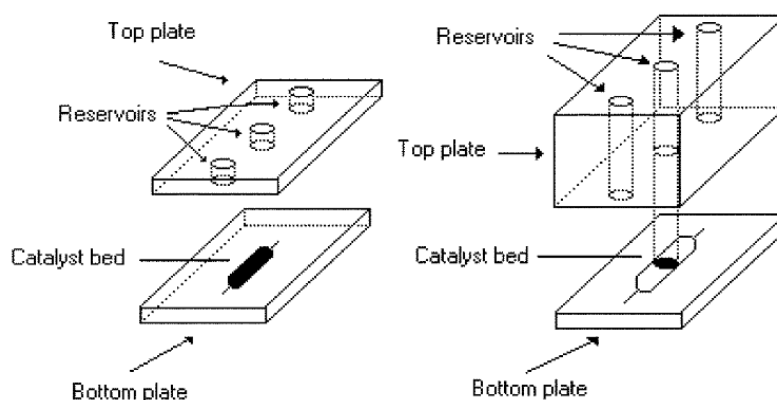
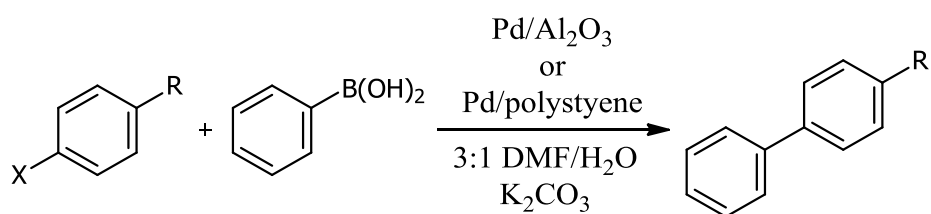


Figure 1.3 Microwave-assisted microchip reactors, (left) design A and (right) design B. Figure adapted from He *et al.* [56].

Design A featured a 1.5 mm wide, 80 μm deep, and 15 mm long catalyst channel connected to the inlet and outlet reservoirs by channels (130 μm wide and 50 μm deep). The only significant difference in design B was that the catalyst channel was 50 μm , 30 μm shallower than in design A. Both designs featured an reservoir in the centre of the channel for packing the catalyst which was sealed with a tight fitting polyether ether ketone (PEEK) rod. Catalyst was introduced as a dry powder through the central reservoir and then located in the microchannel using air pressure generated from a hand-held syringe.

The catalyst, 5 wt% palladium on alumina, consisted of particles with a size 45-63 μm . These particles completely filled the catalyst bed in design A, forming a monolayer, and were retained by the keystone effect. However, particles were too

big to fit within the catalyst bed of design B and were located only within the central reservoir in a plug 0.5-1 mm deep, as shown on the right of **Figure 1.3**. As the depth of the channel at the catalyst bed is the same as the plug height, it is questionable whether or not design B is a true microreactor. Due to this relatively large catalyst bed, the catalyst present in the design B microreactor (6 mg) was four times greater than present in design A (1.5 mg). The authors compared several heating configurations using the Suzuki-Miyaura coupling of 4-bromobenzonitrile and phenylboronic acid in 3:1 dimethylformamide (DMF)/water using potassium carbonate as the base, as shown in **Scheme 1.3**.



Scheme 1.3 Suzuki-Miyaura couplings utilised by He *et al.* in a microchip reactor.

X = I, Br and R = CH₃, CHO, OCH₃, CN, NO₂.

Using design B they were able to obtain quantitative yields when using microwave heating with a 15 nm sputtered gold coating below the catalyst bed. Using these conditions, coupling reactions of several different aryl iodides and bromides with phenylboronic acid were demonstrated in microreactor design B, affording yields between 58-99%. The two microreactor designs were compared by performing reactions using several different aryl bromides with phenylboronic acid at the same flow rate. Despite having a shorter contact time due to its shallower channel depth, the design B reactor was found to consistently outperform the design A reactor. In order to evaluate the stability of the proposed packing methodology to deal with polymeric-based catalysts, a 4 wt% palladium on polystyrene support was used in the design B microreactor. The authors found that packing the channel of the

microreactor design A with the polystyrene support was practically very difficult, however filling design B was straightforward. Despite having 20% lower palladium loading than the alumina support, the Pd-polystyrene catalyst gave comparable product yield.

In 2005 Kobayashi *et al.* presented the first example of a microreactor system using supercritical carbon dioxide as the reaction medium for hydrogenation of terminal and trans olefins and phenylacetylenes [92]. The microreactor system, shown in **Figure 1.4**, features a microchip with a 40 cm long reaction channel 200 μm wide and 100 μm deep.

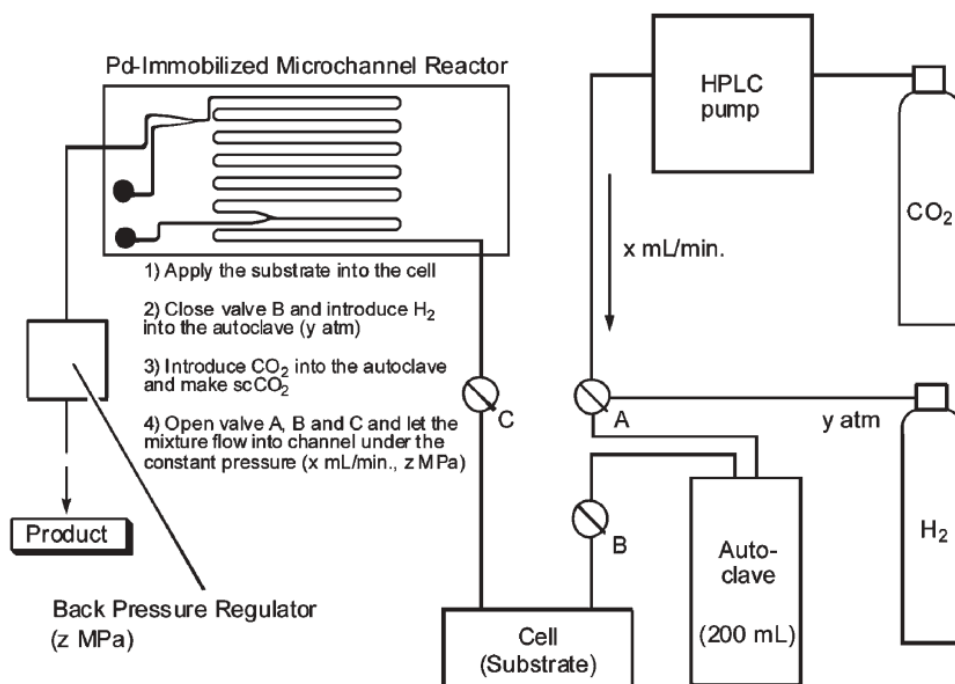


Figure 1.4 Hydrogenation in supercritical carbon dioxide microreactor system.

Figure adapted from Kobayashi *et al.* [92].

Kobayashi *et al.* immobilised polymer encapsulated palladium onto the walls of the reactor *in situ*, removing the difficulty associated with introduction and retention of a particulate catalyst within the microchannel. This was done by treating the surface of the microchannel with an amino alkoxysilane reagent, after which polystyrene encapsulated palladium was introduced and cross-linked to the amino groups by

heating, affording a thin surface layer. The authors estimated the palladium content of the reactor to be 10 μg from ICP-MS analysis. Reactions were performed using supercritical carbon dioxide at 9 MPa at a flow rate of 1 mL min^{-1} with 9 atm of hydrogen gas, which allowed near quantitative yields with average contact times of less than one second.

Ueno *et al.* used a similar approach to Kobayashi *et al.* for catalyst immobilisation in a capillary reactor, utilising polysilane encapsulated palladium with metal oxide additives for performing hydrogenation reactions [93]. Capillary reactors were fabricated from 50 cm long 530 μm ID fused silica by coating the inner capillary surface with a mixture of palladium acetate and a metal oxide in polysilane, followed by crosslinking of the polysilane at 120 $^{\circ}\text{C}$ for 12 h. The authors found that the addition of a metal oxide to the catalyst layer significantly improved the reaction yield. Several metal oxides were trialled and titanium oxide was found to improve the reaction yield by 20%, giving quantitative yields for the hydrogenation of 2,4-diphenyl-4-methyl-1-pentene. The authors found the capillary reactor could be used at least 15 times without loss of activity, and no leaching of palladium occurred under the conditions investigated.

Hornung *et al.* developed a microreactor of palladium catalysed transfer hydrogenation reaction, and in doing so were the first group to demonstrate heterogeneous palladium catalysis within a polymer microreactor [94]. Similarly to the microreactors developed by Kobayashi *et al.* and Ueno *et al.*, this microreactor utilised a heterogeneous palladium catalyst immobilised on the microchannel walls. Their reactor consisted of a polymer „ribbon’, shown in **Figure 1.5**, containing 19 channels, each with an average diameter of 146 μm and a length of 10-15 m.

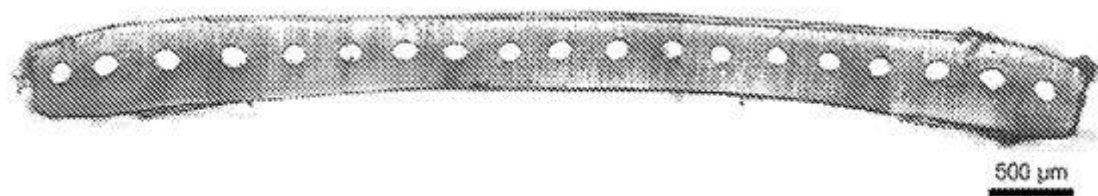
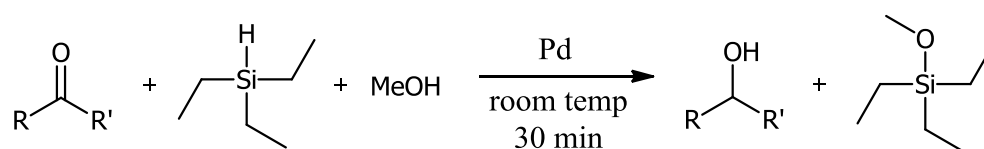


Figure 1.5 Cross-section of polymer ‘ribbon’ reactor. Figure adapted from Hornung *et al.* [94].

The reactor was fabricated by extrusion from poly(ethylene-*co*-vinyl alcohol), a copolymer containing pendant hydroxyl groups, which was treated with *N*-trimethoxysilylpropyl-*N,N,N*-trimethylammonium chloride in order to introduce quaternary ammonium groups to the microchannel surface. Palladium was immobilised in the reactor by passing through a solution of disodium tetrachloropalladate followed by reduction with sodium borohydride to form palladium(0). This afforded a reactor with a palladium content of $31 \mu\text{g m}^{-1}$, determined by ICP-MS. The reactor was successfully utilised for the reduction of a variety of functional groups, such as carbonyl, imine, nitro, alkene, and alkyne groups. Reactions were performed at room temperature using triethylsilane as a hydrogen source as shown in **Scheme 1.4**, with a contact time of 30 min.



Scheme 1.4 Palladium catalysed transfer hydrogenation for reduction of a ketone performed by Hornung *et al.*.

Initially, the authors attempted to perform reactions while heating the microreactor to 60-70 °C, however the polymer was found to soften at these temperatures causing the channels to expand when pressure was applied from the HPLC pump. Despite being limited to room temperature reactions, reasonable yields ranging between 42-97% were obtained.

In 2006 Uozumi *et al.* reported a unique method for catalyst immobilisation that utilised the laminar flow conditions present within microreactors [95]. They formed a polymer membrane via self-assembling complexation of a polymeric phosphine ligand and palladium species at the interface of two parallel laminar flows within the microchannel, as shown in **Figure 1.6**.

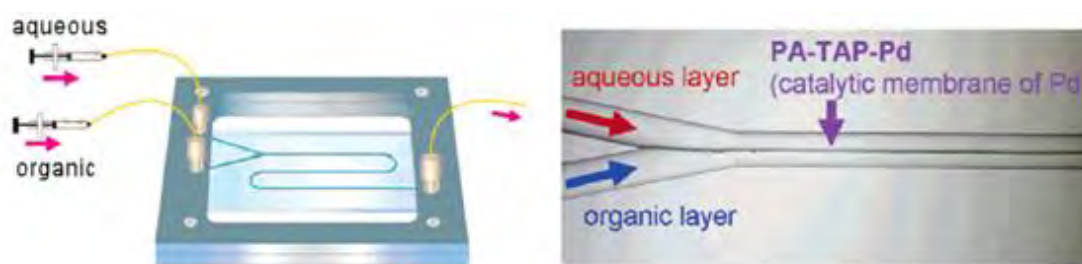
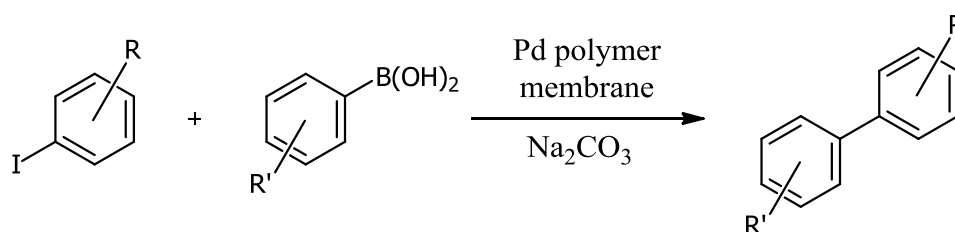


Figure 1.6 Microreactor design (left) and formation of the catalyst membrane (right). Figure adapted from Uozumi *et al.* [95].

The microchip featured a 14 cm long channel, 100 μm wide and 40 μm deep, two inlet reservoirs meeting at a Y-junction, and a single outlet reservoir. The poly(acrylamide)-triarylphosphine-palladium (PA-TAP-Pd) membrane was formed by passing a solution of poly(acrylamide)-triarylphosphine in ethyl acetate in one inlet and an aqueous solution of ammonium tetrachloropalladate in the other, precipitating a 1.3 μm wide polymer membrane at the interface. Application of the microreactor was demonstrated by performing Suzuki-Miyaura coupling reactions between four different aryl iodides and aryl boronic acids.



Scheme 1.5 Suzuki-Miyaura couplings utilised by Uozumi *et al.* in a microchip reactor. R = H, 3-EtOCO, 3-Cl, 4-CF₃, and R' = 4-MeO, 3-Me, 2-Me.

Reactions were performed at 50 °C by passing a solution of aryl iodide in ethyl acetate/isopropanol (2:5) in one inlet and aqueous aryl boronic acid with sodium carbonate in the other inlet. The resulting organic/aqueous stream was collected from the outlet of the microreactor, affording quantitative yields for almost all reactions investigated within the 4 s contact time. The authors estimated the palladium content of the reactor to be 3.2 μmol , which gives a turnover frequency (TOF) for the 99% yield coupling of iodobenzene and p-methoxyphenylboronic acid of 600 h^{-1} .

Uozumi *et al.* later extended their investigation to include a nitrogen coordinative membrane formed from poly(4-vinylpyridine) (membrane 2) and an ionic membrane formed from poly{(4,4'-bipyridyl)-*co*-[1,4-bis(bromomethyl)benzene]} (membrane 3) [96]. Together with the previously presented PA-TAP-Pd membrane (membrane 1), these devices were utilised for Suzuki-Miyaura coupling reactions of aryl, heteroaryl, and alkenyl halides with arylboronic acids and sodium tetraarylborates. Additionally allylic arylation reactions of *allylic* esters with aryl-boron reagents were investigated. Membrane 1 was found to give far superior performance to the other two membranes, which the authors attributed to the higher catalytic activity of the phosphine-palladium complex. Microreactors utilising membrane 1 were applied to the coupling reactions of a diverse range of aryl halides and arylboronic acids, heteroaryl halides and heteroarylboronic acids, which gave high or quantitative yields. These devices were also applied to the synthesis of several important intermediate compounds used in material science, bioactive compounds, and functional materials, all of which were obtained in high yield.

Costantini *et al.* demonstrated a unique approach to immobilisation of metal nanoparticles within a glass microchip reactor by utilising branched polymer 'brushes' featuring carboxylic groups, which were formed *in situ* by atom-transfer

radical polymerisation [97]. The carboxylic groups were used to complex with either silver(I) or palladium(II), which were subsequently reduced to form nanoparticles. The glass microchip featured a 110 μm wide, 50 μm deep, and 300 mm long channel. The microreactor was tested by performing reduction of *p*-nitrophenol at room temp in water with sodium borohydride. Flow rates were varied between 0.1 and 20 $\mu\text{L min}^{-1}$, with UV-VIS detection used for reaction monitoring. Reactions were found to be completed within seconds for both metals, and no leaching observed. The palladium microreactor was also utilised for the Heck coupling of ethyl acrylate and iodobenzene in DMSO at 80 °C. The flow-rate was varied between 0.06 and 0.2 $\mu\text{L min}^{-1}$, with complete conversion obtained when using a 26 min contact time. Palladium leaching was observed for this reaction, which the authors attributed this to the formation of palladium(II) during the catalytic cycle.

1.4 Supports for palladium catalysis

While there has been relatively little interest in heterogeneous or supported palladium catalysis in microreactors to date, extensive research had been performed using continuous flow minireactors featuring ID's greater than 1 mm up to tens of millimetres [90, 98-110]. The main reason for this discrepancy is the difficulties associated with placement and retention of solid catalysts within microreactors [28]. As they are considerably larger than microreactors, minireactors do not feature many of the benefits associated with microreactor technology, such as rapid mixing or fast heat transfer. They are, however, considerably easier to construct and integrate into existing synthetic methodologies. An example of this is the X-cube™ from ThalesNano Nanotechnology Inc., which is a commercial flow reactor for catalyst and reaction screening. The X-cube™ employs either a 30 mm, 55 mm, or 70 mm long and 4 mm ID catalyst cartridge which can be packed with a range of

heterogeneous or supported catalysts. There have been a few examples of the X-cube™ being applied to palladium catalysis [99, 100].

Other than the techniques previous discussed for microreactors, several methods have been presented for immobilisation of palladium in minireactors, including metallic films [108, 110], polymer encapsulation [104-106], polymer-supported complexes [109], silica-coated magnetic nanoparticles [103], and polymer-modified megaporous glass [98, 111, 112].

1.4.1 Polymer resin beads

Polymer support structures have been keenly pursued for homogeneous catalysts as they are robust, easily prepared, highly configurable through choice of monomers, and can withstand a broad range of reaction conditions [89, 113-115]. One of the most widely utilised polymer catalyst supports are resin beads, which have been applied in both batch reactions [116-123] and flow-through reactors [109, 124]. A wide variety of resin beads are available with a broad range of physical and chemical properties [113]. One of the earliest developed and still widely utilised beads is Merrifield resin, which has been extensively utilised for solid supported synthesis in combinatorial chemistry [125]. Merrifield resin has a relatively low catalyst loading capacity under normal conditions due to its small surface area. This capacity can be improved by swelling the resin using halogenated or aromatic solvents, which causes separation of the cross-linked polymer strands, forming pores [126]. In a resin packed column this swelling reduces the void volume, leading to high back-pressure and irreproducible flow [124]. These issues eventually led to the development of macroporous beads, which feature greater crosslinking to reduce solvent swelling and a permanent porous structure to improve capacity [127]. Regardless of the capacity of the particulate loading capacity, randomly packed catalytic beds suffer from uncontrolled fluid dynamics which results in stagnation

zones and hot-spot formation, broad residence time distribution, low selectivity, and low process efficiency [128]. Monolithic structures overcome most of these issues associated with packed particulate columns.

1.4.2 Porous polymer monoliths

A monolithic stationary phase is a "unibody" structure containing interconnected cells or channels through which fluid can flow [129]. These continuous porous structures feature large void volumes and high surface areas, which gives a large contact area of the catalyst with the reactants while maintaining a low flow resistance [128]. Monoliths have been extensively applied in heterogeneous and supported catalysis and can be prepared in a variety of materials, including metals, metal oxides, sol-gel, glass, and polymers [130-139]. The most suitable material for monolithic structures in mini- or micro-scale flow reactors are polymers, as they are relatively simple to prepare, can be formed *in situ*, and are easily stored [125]. Polymer monoliths, also known as porous polymer monoliths (PPM's), are in essence a single continuous macroporous bead that completely fill the container, where flow is via the inter-connected pores, eliminating the void space between the particles [126]. The major benefits of PPM's over other support structures are:

- In-situ polymerisation, eliminating issues associated with packing of particulates in microreactors.
- Covalent binding to reactor wall to ensure fluid flows through pores, which also eliminates the need for a retention mechanism.
- Accurate control over region of formation in channel by photoinitiated polymerisation [140].
- Low flow resistance and non-convective mass transfer.
- Less susceptible to swelling.
- Compatibility with a broad range of solvents and pH values.

- Highly configurable through choice of monomers and polymerisation conditions.

PPM's were originally developed as solid phases for liquid chromatography in the 1990s, but have since been demonstrated in a variety of analytical applications [126, 127, 135, 141-156], as well as for immobilisation of enzymes in bio-reactors [157] and as support structures in catalysis [158-163].

1.5 Aims

The core goal of this work was to develop methodologies for the fabrication of microreactors using PPM's for the immobilisation of palladium complexes. More specifically to enable the placement of the immobilised catalyst within a specific region of a microchip reactor for the potential integration with other microfluidic technologies on-chip.

The performance of these devices was to be determined by performing Suzuki-Miyaura coupling reactions in continuous flow with analysis of the reaction yield and catalyst leaching.

Development of PPM's suitable for the immobilisation of palladium complexes within microreactors follows on from the core goal. Characterisation of the PPM's was to be performed by analysis of their flow properties, imaging via scanning electron microscopy, and measurement of porous properties using mercury intrusion porosimetry.

A secondary goal was the development of microreactors for non-room temperature supported catalysis fabricated from polymer devices to potentially enable inexpensive mass production.

The investigation of the use of alternative, inexpensive light sources for photo-polymerisation on PPM's was also pursued, with the goal of reducing fabrication costs and enabling greater access to this PPM technology.

1.6 References

1. Jas, G. and A. Kirschning, Continuous flow techniques in organic synthesis. *Chemistry-a European Journal*, 2003. **9**(23), 5708-5723.
2. Dunn, P., A. Wells, and M.T. Williams, Green Chemistry in the Pharmaceutical Industry. 2010, Weinheim, Germany: Wiley-VCH Verlag GmbH & Co. 370.
3. Nicolaou, K.C., T. Montagnon, and S.A. Snyder, Tandem reactions, cascade sequences, and biomimetic strategies in total synthesis. *Chemical Communications*, 2003(5), 551-564.
4. Bruggink, A., R. Schoevaart, and T. Kieboom, Concepts of nature in organic synthesis: Cascade catalysis and multistep conversions in concert. *Organic Process Research & Development*, 2003. **7**(5), 622-640.
5. Yoshida, J.-i., H. Kim, and A. Nagaki, Green and Sustainable Chemical Synthesis Using Flow Microreactors. *ChemSusChem*, 2010.
6. Vilkner, T., D. Janasek, and A. Manz, Micro Total Analysis Systems. Recent Developments. *Analytical Chemistry*, 2004. **76**(12), 3373-3386.
7. Reyes, D.R., D. Iossifidis, P.A. Auroux, and A. Manz, Micro total analysis systems. 1. Introduction, theory, and technology. *Analytical Chemistry*, 2002. **74**(12), 2623-2636.
8. McCreedy, T., Micro Total Analytical Systems. 2005, 10-15.
9. Jakeway, S.C., A.J. de Mello, and E.L. Russell, Miniaturized total analysis systems for biological analysis. *Fresenius' Journal of Analytical Chemistry*, 2000. **366**(6-7), 525-539.
10. Auroux, P.A., D. Iossifidis, D.R. Reyes, and A. Manz, Micro total analysis systems. 2. Analytical standard operations and applications. *Analytical Chemistry*, 2002. **74**(12), 2637-2652.
11. Yeo, L.Y., H.C. Chang, P.P.Y. Chan, and J.R. Friend, Microfluidic Devices for Bioapplications. *Small*, 2011. **7**(1), 12-48.
12. Weigl, B.H., R.L. Bardell, and C.R. Cabrera, Lab-on-a-chip for drug development. *Advanced Drug Delivery Reviews*, 2003. **55**(3), 349-377.
13. Pihl, J., M. Karlsson, and D.T. Chiu, Microfluidic technologies in drug discovery. *Drug Discovery Today*, 2005. **10**(20), 1377-1383.
14. Brivio, M., W. Verboom, and D.N. Reinhoudt, Miniaturized continuous flow reaction vessels: influence on chemical reactions. *Lab on a Chip*, 2006. **6**(3), 329-344.
15. de Mello, A. and R. Wootton, But what is it good for? Applications of microreactor technology for the fine chemical industry. *Lab on a Chip*, 2002. **2**(1), 7N-13N.
16. Fletcher, P.D.I., S.J. Haswell, E. Pombo-Villar, B.H. Warrington, P. Watts, S.Y.F. Wong, and X.L. Zhang, Micro reactors: principles and applications in organic synthesis. *Tetrahedron*, 2002. **58**(24), 4735-4757.
17. Schwalbe, T., V. Autze, and G. Wille, Chemical synthesis in microreactors. *Chimia*, 2002. **56**(11), 636-646.
18. Haswell, S.J. and P. Watts, Green chemistry: synthesis in micro reactors. *Green Chemistry*, 2003. **5**(2), 240-249.
19. Jähnisch, K., V. Hessel, H. Löwe, and M. Baerns, Chemistry in microstructured reactors. *Angewandte Chemie, International Edition*, 2004. **43**(4), 406-446.
20. Kolb, G. and V. Hessel, Micro-structured reactors for gas phase reactions. *Chemical Engineering Journal*, 2004. **98**(1-2), 1-38.

21. Křenková, J. and F. Foret, Immobilized microfluidic enzymatic reactors. *Electrophoresis*, 2004. **25**(21-22), 3550-3563.
22. Pennemann, H., P. Watts, S.J. Haswell, V. Hessel, and H. Löwe, Benchmarking of microreactor applications. *Organic Process Research & Development*, 2004. **8**(3), 422-439.
23. Doku, G.N., W. Verboom, D.N. Reinhoudt, and A. van den Berg, On-microchip multiphase chemistry-a review of microreactor design principles and reagent contacting modes. *Tetrahedron*, 2005. **61**(11), 2733-2742.
24. Hessel, V. and H. Löwe, Organic synthesis with microstructured reactors. *Chemical Engineering & Technology*, 2005. **28**(3), 269-284.
25. Watts, P. and S.J. Haswell, The application of micro reactors for organic synthesis. *Chemical Society Reviews*, 2005. **34**(3), 235-246.
26. Geyer, K., J.D.C. Codée, and P.H. Seeberger, Microreactors as tools for synthetic chemists - the chemists' round-bottomed flask of the 21st century? *Chemistry - A European Journal*, 2006. **12**(33), 8434-8442.
27. Zhang, X.L., C. Wiles, S.L. Painter, P. Watts, and S.J. Haswell, Microreactors as tools for chemical research. *Chimica Oggi-Chemistry Today*, 2006. **24**(2), 43-45.
28. Ahmed-Omer, B., J.C. Brandt, and T. Wirth, Advanced organic synthesis using microreactor technology. *Organic & Biomolecular Chemistry*, 2007. **5**(5), 733-740.
29. Brown, D., Synthetic chemistry in microreactors. *Chemistry in Australia*, 2007. **74**(7), 14-17.
30. Mason, B.P., K.E. Price, J.L. Steinbacher, A.R. Bogdan, and D.T. McQuade, Greener Approaches to Organic Synthesis Using Microreactor Technology. *Chemical Reviews (Washington, DC, United States)*, 2007. **107**(6), 2300-2318.
31. Watts, P. and C. Wiles, Micro reactors: a new tool for the synthetic chemist. *Organic & Biomolecular Chemistry*, 2007. **5**(5), 727-732.
32. Watts, P. and C. Wiles, Recent advances in synthetic micro reaction technology. *Chemical Communications (Cambridge, United Kingdom)*, 2007(5), 443-467.
33. Wong-Hawkes, S.Y.F., J.C. Matteo, B.H. Warrington, and J.D. White, Microreactors as new tools for drug discovery and development. *Ernst Schering Foundation Symposium Proceedings*, 2007(2006-03, New Avenues to Efficient Chemical Synthesis), 39-55.
34. Hartman, R.L. and K.F. Jensen, Microchemical systems for continuous-flow synthesis. *Lab on a Chip*, 2009. **9**(17), 2495-2507.
35. Fernandes, P., Miniaturization in Biocatalysis. *International Journal of Molecular Sciences*, 2010. **11**(3), 858-879.
36. Frost, C.G. and L. Mutton, Heterogeneous catalytic synthesis using microreactor technology. *Green Chemistry*, 2010. **12**(10), 1687-1703.
37. Jackman, R.J., T.M. Floyd, R. Ghodssi, M.A. Schmidt, and K.F. Jensen, Microfluidic systems with on-line UV detection fabricated in photodefinable epoxy. *Journal of Micromechanics and Microengineering*, 2001. **11**(3), 263-269.
38. Vesper, G., Experimental and theoretical investigation of H₂ oxidation in a high-temperature catalytic microreactor. *Chemical Engineering Science*, 2001. **56**(4), 1265-1273.
39. Tiggelaar, R.M., J.G.E. Gardeniers, and A. van den Berg, Silicon-based microreactors as research tools in chemistry. *Chimica Oggi-Chemistry Today*, 2006. **24**(2), 52-54.

40. Schwalbe, T., V. Autze, M. Hohmann, and W. Stirner, Novel innovation systems for a cellular approach to continuous process chemistry from discovery to market. *Organic Process Research & Development*, 2004. **8**(3), 440-454.
41. Song, H. and R.F. Ismagilov, Millisecond kinetics on a microfluidic chip using nanoliters of reagents. *Journal of the American Chemical Society*, 2003. **125**(47), 14613-14619.
42. McCreedy, T. and N.G. Wilson, Microfabricated reactors for on-chip heterogeneous catalysis. *Analyst (Cambridge, United Kingdom)*, 2001. **126**(1), 21-23.
43. Honda, T., M. Miyazaki, H. Nakamura, and H. Maeda, Facile preparation of an enzyme-immobilized microreactor using a cross-linking enzyme membrane on a microchannel surface. *Advanced Synthesis & Catalysis*, 2006. **348**(15), 2163-2171.
44. Knitter, R. and M.A. Liauw, Ceramic microreactors for heterogeneously catalysed gas-phase reactions. *Lab on a Chip*, 2004. **4**(4), 378-383.
45. Iliescu, C., F.E.H. Tay, and J.M. Miao, Strategies in deep wet etching of Pyrex glass. *Sensors and Actuators a-Physical*, 2007. **133**(2), 395-400.
46. Rossier, J.S., C. Vollet, A. Carnal, G. Lager, V. Gobry, H.H. Girault, P. Michel, and F. Reymond, Plasma etched polymer microelectrochemical systems. *Lab on a Chip*, 2002. **2**(3), 145-150.
47. Roberts, M.A., J.S. Rossier, P. Bercier, and H. Girault, UV laser machined polymer substrates for the development of microdiagnostic systems. *Analytical Chemistry*, 1997. **69**(11), 2035-2042.
48. do Lago, C.L., H.D.T. da Silva, C.A. Neves, J.G.A. Brito-Neto, and J.A.F. da Silva, A dry process for production of microfluidic devices based on the lamination of laser-printed polyester films. *Analytical Chemistry*, 2003. **75**(15), 3853-3858.
49. Schaller, T., L. Bohn, J. Mayer, and K. Schubert, Microstructure grooves with a width of less than 50 μm cut with ground hard metal micro end mills. *Precision Engineering-Journal of the American Society for Precision Engineering*, 1999. **23**(4), 229-235.
50. Becker, H. and U. Heim, Hot embossing as a method for the fabrication of polymer high aspect ratio structures. *Sensors and Actuators a-Physical*, 2000. **83**(1-3), 130-135.
51. Mair, D.A., E. Geiger, A.P. Pisano, J.M.J. Fréchet, and F. Svec, Injection molded microfluidic chips featuring integrated interconnects. *Lab on a Chip*, 2006. **6**(10), 1346-1354.
52. Duffy, D.C., J.C. McDonald, O.J.A. Schueller, and G.M. Whitesides, Rapid Prototyping of Microfluidic Systems in Poly(dimethylsiloxane). *Analytical Chemistry*, 1998. **70**(23), 4974-4984.
53. Schubert, A., J. Edelmann, and T. Burkhardt, Micro structuring of borosilicate glass by high-temperature micro-forming. *Microsystem Technologies-Micro-and Nanosystems-Information Storage and Processing Systems*, 2006. **12**(8), 790-795.
54. Fiorini, G.S. and D.T. Chiu, Disposable microfluidic devices: fabrication, function, and application. *Biotechniques*, 2005. **38**(3), 429-446.
55. Phan, N.T.S., D.H. Brown, and P. Styring, A facile method for catalyst immobilisation on silica: nickel-catalysed Kumada reactions in mini-continuous flow and batch reactors. *Green Chemistry*, 2004. **6**(10), 526-532.

56. He, P., S.J. Haswell, and P.D.I. Fletcher, Microwave heating of heterogeneously catalysed Suzuki reactions in a micro reactor. *Lab on a Chip*, 2004. **4**(1), 38-41.
57. Ramirez-Garcia, S., M. Baeza, M. O'Toole, Y.Z. Wu, J. Lalor, G.G. Wallace, and D. Diamond, Towards the development of a fully integrated polymeric microfluidic platform for environmental analysis. *Talanta*, 2008. **77**(2), 463-467.
58. Basheer, C., F.S. Jahir Hussain, H.K. Lee, and S. Valiyaveetil, Design of a capillary-microreactor for efficient Suzuki coupling reactions. *Tetrahedron Letters*, 2004. **45**(39), 7297-7300.
59. Greenway, G.M., S.J. Haswell, D.O. Morgan, V. Skelton, and P. Styring, The use of a novel microreactor for high throughput continuous flow organic synthesis. *Sensors and Actuators B-Chemical*, 2000. **63**(3), 153-158.
60. Lu, Z.H., J. McMahon, H. Mohamed, D. Barnard, T.R. Shaikh, C.A. Mannella, T. Wagenknecht, and T.M. Lu, Passive microfluidic device for submillisecond mixing. *Sensors and Actuators B-Chemical*, 2010. **144**(1), 301-309.
61. Sullivan, S.P., B.S. Akpa, S.M. Matthews, A.C. Fisher, L.F. Gladden, and M.L. Johns, Simulation of miscible diffusive mixing in microchannels. *Sensors and Actuators B-Chemical*, 2007. **123**(2), 1142-1152.
62. Hessel, V., S. Hardt, H. Löwe, and F. Schönfeld, Laminar mixing in different interdigital micromixers: I. Experimental characterization. *Aiche Journal*, 2003. **49**(3), 566-577.
63. Lin, J.L., K.H. Lee, and G.B. Lee, Active mixing inside microchannels utilizing dynamic variation of gradient zeta potentials. *Electrophoresis*, 2005. **26**(24), 4605-4615.
64. Bau, H.H., J.H. Zhong, and M.Q. Yi, A minute magneto hydro dynamic (MHD) mixer. *Sensors and Actuators B-Chemical*, 2001. **79**(2-3), 207-215.
65. Yang, Z., S. Matsumoto, H. Goto, M. Matsumoto, and R. Maeda, Ultrasonic micromixer for microfluidic systems. *Sensors and Actuators A - Physical*, 2001. **93**(3), 266-272.
66. Gustafsson, T., R. Gilmour, and P.H. Seeberger, Fluorination reactions in microreactors. *Chemical Communications*, 2008(26), 3022-3024.
67. Baumann, M., I.R. Baxendale, and S.V. Ley, The use of diethylaminosulfur trifluoride (DAST) for fluorination in a continuous-flow microreactor. *Synlett*, 2008(14), 2111-2114.
68. Wheeler, R.C., O. Benali, M. Deal, E. Farrant, S.J.F. MacDonald, and B.H. Warrington, Mesoscale flow chemistry: A plug-flow approach to reaction optimisation. *Organic Process Research & Development*, 2007. **11**(4), 704-710.
69. Schwalbe, T., D. Kadzimirsz, and G. Jas, Synthesis of a library of Ciprofloxacin analogues by means of sequential organic synthesis in microreactors. *QSAR & Combinatorial Science*, 2005. **24**(6), 758-768.
70. Hartman, R.L., J.R. Naber, S.L. Buchwald, and K.E. Jensen, Multistep Microchemical Synthesis Enabled by Microfluidic Distillation. *Angewandte Chemie-International Edition*, 2010. **49**(5), 899-903.
71. Wiles, C., P. Watts, and S.J. Haswell, The use of solid-supported reagents for the multi-step synthesis of analytically pure a,b-unsaturated compounds in miniaturized flow reactors. *Lab on a Chip*, 2007. **7**(3), 322-330.
72. McMullen, J.P., M.T. Stone, S.L. Buchwald, and K.E. Jensen, An Integrated Microreactor System for Self-Optimization of a Heck Reaction: From Micro-

- to Mesoscale Flow Systems. *Angewandte Chemie-International Edition*, 2010. **49**(39), 7076-7080.
73. Wang, J., G. Sui, V.P. Mocharla, R.J. Lin, M.E. Phelps, H.C. Kolb, and H.-R. Tseng, Integrated microfluidics for parallel screening of an in situ click chemistry library. *Angewandte Chemie, International Edition*, 2006. **45**(32), 5276-5281.
 74. Mills, P.L., D.J. Quiram, and J.F. Ryley, Microreactor technology and process miniaturization for catalytic reactions-A perspective on recent developments and emerging technologies. *Chemical Engineering Science*, 2007. **62**(24), 6992-7010.
 75. Thayer, A.M., Harnessing microreactions. *Chemical & Engineering News*, 2005. **83**(22), 43-52.
 76. Togashi, S., T. Miyamoto, T. Sano, and M. Suzuki, Microreactor system using the concept of numbering-up. *New Trends in Fluid Mechanics Research - Proceedings of the Fifth International Conference on Fluid Mechanics*, ed. F.G. Zhuang and J.C. Li. 2007, Beijing: Tsinghua University Press. 678-681.
 77. Rouhi, A.M., Microreactors eyed for industrial use. *Chemical & Engineering News*, 2004. **82**(27), 18-19.
 78. Huang, L., T.P. Ang, Z. Wang, J.Z. Tan, J.H. Chen, and P.K. Wong, On the Roles of Solid-Bound Ligand Scavengers in the Removal of Palladium Residues and in the Distinction between Homogeneous and Heterogeneous Catalysis. *Inorganic Chemistry*, 2011. **50**(6), 2094-2111.
 79. Theberge, A.B., G. Whyte, M. Frenzel, L.M. Fidalgo, R.C.R. Wootton, and W.T.S. Huck, Suzuki-Miyaura coupling reactions in aqueous microdroplets with catalytically active fluororous interfaces. *Chemical Communications*, 2009(41), 6225-6227.
 80. Park, C.P. and D.P. Kim, Dual-Channel Microreactor for Gas-Liquid Syntheses. *Journal of the American Chemical Society*, 2010. **132**(29), 10102-10106.
 81. Nagaki, A., A. Kenmoku, Y. Moriwaki, A. Hayashi, and J. Yoshida, Cross-Coupling in a Flow Microreactor: Space Integration of Lithiation and Murahashi Coupling. *Angewandte Chemie-International Edition*, 2010. **49**(41), 7543-7547.
 82. Shi, G.Y., F. Hong, Q.S. Liang, H. Fang, S. Nelson, and S.G. Weber, Capillary-based, serial-loading, parallel microreactor for catalyst screening. *Analytical Chemistry*, 2006. **78**(6), 1972-1979.
 83. Miller, P.W., N.J. Long, A.J. De Mello, R. Vilar, J. Passchier, and A. Gee, Rapid formation of amides via carbonylative coupling reactions using a microfluidic device. *Chemical Communications (Cambridge, United Kingdom)*, 2006(5), 546-548.
 84. Comer, E. and M.G. Organ, A microcapillary system for simultaneous, parallel microwave-assisted synthesis. *Chemistry - A European Journal*, 2005. **11**(24), 7223-7227.
 85. Jönsson, C.I., S. Lundgren, S.J. Haswell, and C. Moberg, Asymmetric catalysis in a micro reactor - Ce, Yb and Lu catalysed enantioselective addition of trimethylsilyl cyanide to benzaldehyde. *Tetrahedron*, 2004. **60**(46), 10515-10520.
 86. He, P., S.J. Haswell, and P.D.I. Fletcher, Microwave-assisted Suzuki reactions in a continuous flow capillary reactor. *Applied Catalysis a-General*, 2004. **274**(1-2), 111-114.

87. McChesney, J., Heck reactions for intermediate synthesis. *Speciality Chemicals*, 1999. **19**(3), 98.
88. Phan, N.T.S., M. Van Der Sluys, and C.W. Jones, On the nature of the active species in palladium catalyzed Mizoroki-Heck and Suzuki-Miyaura couplings - homogeneous or heterogeneous catalysis, a critical review. *Advanced Synthesis & Catalysis*, 2006. **348**(6), 609-679.
89. Lamblin, M., L. Nassar-Hardy, J.C. Hierso, E. Fouquet, and F.X. Felpin, Recyclable Heterogeneous Palladium Catalysts in Pure Water: Sustainable Developments in Suzuki, Heck, Sonogashira and Tsuji-Trost Reactions. *Advanced Synthesis & Catalysis*, 2010. **352**(1), 33-79.
90. Shore, G., S. Morin, D. Mallik, and M.G. Organ, Pd PEPPSI-IPr-mediated reactions in metal-coated capillaries under MACOS: The synthesis of indoles by sequential aryl amination/Heck coupling. *Chemistry-a European Journal*, 2008. **14**(4), 1351-1356.
91. Glasnov, T.N. and C.O. Kappe, Toward a Continuous-Flow Synthesis of Boscalid (R). *Advanced Synthesis & Catalysis*, 2010. **352**(17), 3089-3097.
92. Kobayashi, J., Y. Mori, and S. Kobayashi, Hydrogenation reactions using scCO₂ as a solvent in microchannel reactors. *Chemical Communications*, 2005(20), 2567-2568.
93. Ueno, M., T. Suzuki, T. Naito, H. Oyamada, and S. Kobayashi, Development of microchannel reactors using polysilane-supported palladium catalytic systems in capillaries. *Chemical Communications*, 2008(14), 1647-1649.
94. Hornung, C.H., B. Hallmark, M.R. Mackley, I.R. Baxendale, and S.V. Ley, A Palladium Wall Coated Microcapillary Reactor for Use in Continuous Flow Transfer Hydrogenation. *Advanced Synthesis & Catalysis*, 2010. **352**(10), 1736-1745.
95. Uozumi, Y., Y.M.A. Yamada, T. Beppu, N. Fukuyama, M. Ueno, and T. Kitamori, Instantaneous carbon-carbon bond formation using a microchannel reactor with a catalytic membrane. *Journal of the American Chemical Society*, 2006. **128**(50), 15994-15995.
96. Yamada, Y.M.A., T. Watanabe, T. Beppu, N. Fukuyama, K. Torii, and Y. Uozumi, Palladium Membrane-Installed Microchannel Devices for Instantaneous Suzuki-Miyaura Cross-Coupling. *Chemistry-a European Journal*, 2010. **16**(37), 11311-11319.
97. Costantini, F., E.M. Benetti, R.M. Tiggelaar, H. Gardeniers, D.N. Reinhoudt, J. Huskens, G.J. Vancso, and W. Verboom, A Brush-Gel/Metal-Nanoparticle Hybrid Film as an Efficient Supported Catalyst in Glass Microreactors. *Chemistry-a European Journal*, 2010. **16**(41), 12406-12411.
98. Mennecke, K., R. Cecilia, T.N. Glasnov, S. Gruhl, C. Vogt, A. Feldhoff, M.A.L. Vargas, C.O. Kappe, U. Kunz, and A. Kirschning, Palladium(0) nanoparticles on glass-polymer composite materials as recyclable catalysts: A comparison study on their use in batch and continuous flow processes. *Advanced Synthesis & Catalysis*, 2008. **350**(5), 717-730.
99. Irfan, M., E. Petricci, T.N. Glasnov, M. Taddei, and C.O. Kappe, Continuous Flow Hydrogenation of Functionalized Pyridines. *European Journal of Organic Chemistry*, 2009(9), 1327-1334.
100. Glasnov, T.N., S. Findenig, and C.O. Kappe, Heterogeneous Versus Homogeneous Palladium Catalysts for Ligandless Mizoroki-Heck Reactions: A Comparison of Batch/Microwave and Continuous-Flow Processing. *Chemistry-a European Journal*, 2009. **15**(4), 1001-1010.
101. Csajági, C., B. Borcsek, K. Niesz, I. Kovács, Z. Székelyhidi, Z. Bajkó, L. Üрге, and F. Darvas, High-efficiency aminocarbonylation by introducing CO

- to a pressurized continuous flow reactor. *Organic Letters*, 2008. **10**(8), 1589-1592.
102. Clark, P., M. Poliakoff, and A. Wells, Continuous flow hydrogenation of a pharmaceutical intermediate, 4-(3,4-dichlorophenyl)-3,4-dihydro-2H-naphthalenydene -methylamine, in supercritical carbon dioxide. *Advanced Synthesis & Catalysis*, 2007. **349**(17-18), 2655-2659.
 103. Ceylan, S., C. Friese, C. Lammel, K. Mazac, and A. Kirschning, Inductive Heating for Organic Synthesis by Using Functionalized Magnetic Nanoparticles Inside Microreactors. *Angewandte Chemie-International Edition*, 2008. **47**(46), 8950-8953.
 104. Baxendale, I.R., C.M. Griffiths-Jones, S.V. Ley, and G.K. Tranmer, Microwave-assisted Suzuki coupling reactions with an encapsulated palladium catalyst for batch and continuous-flow transformations. *Chemistry-a European Journal*, 2006. **12**(16), 4407-4416.
 105. Leeke, G.A., R.C.D. Santos, B. Al-Duri, J.P.K. Seville, C.J. Smith, C.K.Y. Lee, A.B. Holmes, and I.F. McConvey, Continuous-flow Suzuki-Miyaura reaction in supercritical carbon dioxide. *Organic Process Research & Development*, 2007. **11**(1), 144-148.
 106. Lee, C.K.Y., A.B. Holmes, S.V. Ley, I.F. McConvey, B. Al-Duri, G.A. Leeke, R.C.D. Santos, and J.P.K. Seville, Efficient batch and continuous flow Suzuki cross-coupling reactions under mild conditions, catalysed by polyurea-encapsulated palladium (II) acetate and tetra-n-butylammonium salts. *Chemical Communications*, 2005(16), 2175-2177.
 107. Solodenko, W., H. Wen, S. Leue, F. Stuhlmann, G. Sourkouni-Argirusi, G. Jas, H. Schönfeld, U. Kunz, and A. Kirschning, Development of a continuous-flow system for catalysis with palladium(0) particles. *European Journal of Organic Chemistry*, 2004(17), 3601-3610.
 108. Shore, G., S. Morin, and M.G. Organ, Catalysis in capillaries by Pd thin films using microwave-assisted continuous-flow organic synthesis (MACOS). *Angewandte Chemie, International Edition*, 2006. **45**(17), 2761-2766.
 109. Phan, N.T.S., J. Khan, and P. Styring, Polymer-supported palladium catalysed Suzuki-Miyaura reactions in batch and a mini-continuous flow reactor system. *Tetrahedron*, 2005. **61**(51), 12065-12073.
 110. Rahman, M.A., F.R. Garcia-Garcia, M.D.I. Hatim, B.F.K. Kingsbury, and K. Li, Development of a catalytic hollow fibre membrane micro-reactor for high purity H-2 production. *Journal of Membrane Science*, 2011. **368**(1-2), 116-123.
 111. Mennecke, K. and A. Kirschning, Immobilization of NHC-Bearing Palladium Catalysts on Polyvinylpyridine; Applications in Suzuki-Miyaura and Hartwig-Buchwald Reactions under Batch and Continuous-Flow Conditions. *Synthesis-Stuttgart*, 2008(20), 3267-3272.
 112. Mennecke, K., W. Solodenko, and A. Kirschning, Carbon-carbon cross-coupling reactions under continuous flow conditions using poly(vinylpyridine) doped with palladium. *Synthesis-Stuttgart*, 2008(10), 1589-1599.
 113. Lu, J. and P.H. Toy, Organic Polymer Supports for Synthesis and for Reagent and Catalyst Immobilization. *Chemical Reviews*, 2009. **109**(2), 815-838.
 114. Alonso, F., I.P. Beletskaya, and M. Yus, Non-conventional methodologies for transition-metal catalysed carbon-carbon coupling: a critical overview. Part 2: The Suzuki reaction. *Tetrahedron*, 2008. **64**(14), 3047-3101.

115. Yin, L.X. and J. Liebscher, Carbon-carbon coupling reactions catalyzed by heterogeneous palladium catalysts. *Chemical Reviews*, 2007. **107**(1), 133-173.
116. Bakherad, M., A.H. Amin, A. Keivanloo, B. Bahramian, and M. Raeissi, Copper- and phosphine-free Sonogashira coupling reactions of aryl iodides catalyzed by an N,N-bis(naphthylideneimino)diethylenetriamine-functionalized polystyrene resin supported Pd(II) complex under aerobic conditions. *Tetrahedron Letters*, 2010. **51**(43), 5653-5656.
117. Jones, R.C., A.J. Canty, J.A. Deverell, M.G. Gardiner, R.M. Guijt, T. Rodemann, J.A. Smith, and V.A. Tolhurst, Supported palladium catalysis using a heteroleptic 2-methylthiomethylpyridine-N,S-donor motif for Mizoroki-Heck and Suzuki-Miyaura coupling, including continuous organic monolith in capillary microscale flow-through mode. *Tetrahedron*, 2009. **65**(36), 7474-7481.
118. Fan, G.Z., H.J. Zhang, S.Q. Cheng, Z.D. Ren, Z.J. Hu, and Z.L. Wang, Lewis acid-promoted Suzuki reaction using palladium chloride anchored on a polymer as a catalyst. *Australian Journal of Chemistry*, 2008. **61**(8), 610-614.
119. Kim, J.W., J.H. Kim, D.H. Lee, and Y.S. Lee, Amphiphilic polymer supported N-heterocyclic carbene palladium complex for Suzuki cross-coupling reaction in water. *Tetrahedron Letters*, 2006. **47**(27), 4745-4748.
120. Altava, B., M.I. Burguete, E. Garcia-Verdugo, N. Karbass, S.V. Luis, A. Puzary, and V. Sans, Palladium N-methylimidazolium supported complexes as efficient catalysts for the Heck reaction. *Tetrahedron Letters*, 2006. **47**(14), 2311-2314.
121. Garcia-Bernabé, A., C.C. Tzschucke, W. Bannwarth, and R. Haag, Supramolecular immobilization of a perfluoro-tagged Pd-catalyst with dendritic architectures and application in Suzuki reactions. *Advanced Synthesis & Catalysis*, 2005. **347**(10), 1389-1394.
122. Phan, N.T.S., D.H. Brown, and P. Styring, A polymer-supported salen-type palladium complex as a catalyst for the Suzuki-Miyaura cross-coupling reaction. *Tetrahedron Letters*, 2004. **45**(42), 7915-7919.
123. Byun, J.W. and Y.S. Lee, Preparation of polymer-supported palladium/N-heterocyclic carbene complex for Suzuki cross-coupling reactions. *Tetrahedron Letters*, 2004. **45**(9), 1837-1840.
124. Bogdan, A.R., B.P. Mason, K.T. Sylvester, and D.T. McQuade, Improving solid-supported catalyst productivity by using simplified packed-bed microreactors. *Angewandte Chemie, International Edition*, 2007. **46**(10), 1698-1701.
125. Hodge, P., Synthesis of organic compounds using polymer-supported reagents, catalysts, and/or scavengers in benchtop flow systems. *Industrial & Engineering Chemistry Research*, 2005. **44**(23), 8542-8553.
126. Svec, F. and J.M.J. Fréchet, New designs of macroporous polymers and supports: From separation to biocatalysis. *Science*, 1996. **273**(5272), 205-211.
127. Peters, E.C., F. Svec, and J.M.J. Fréchet, Rigid macroporous polymer monoliths. *Advanced Materials (Weinheim, Germany)*, 1999. **11**(14), 1169-1181.
128. Kiwi-Minsker, L., Novel structured materials for structured catalytic reactors. *Chimia*, 2002. **56**(4), 143-147.
129. Buchmeiser, M.R., Metathesis-based monolithic supports: Synthesis, functionalization and applications. *Macromolecular Rapid Communications*, 2001. **22**(14), 1082-1094.

130. Svec, F. and D.M.J. Fréchet, Rigid Macroporous Organic Polymer Monoliths Prepared by Free Radical Polymerisation, in *Monolithic Materials - preparation, properties and applications*, F. Svec, T.B. Tennikova, and Z. Deyl, Editors. 2003, Elsevier. 19-50.
131. Buchmeiser, M.R., Polymeric monolithic materials: Syntheses, properties, functionalization and applications. *Polymer*, 2007. **48**(8), 2187-2198.
132. Izaak, T.I. and O.V. Vodyankina, Macroporous monolithic materials: synthesis, properties and application. *Russian Chemical Reviews*, 2009. **78**(1), 77-88.
133. Svec, F., My favorite materials: Porous polymer monoliths. *Journal of Separation Science*, 2009. **32**(1), 3-9.
134. Svec, F., Porous polymer monoliths: Amazingly wide variety of techniques enabling their preparation. *Journal of Chromatography A*, 2010. **1217**(6), 902-924.
135. Svec, F., Less common applications of monoliths: I. Microscale protein mapping with proteolytic enzymes immobilized on monolithic supports. *Electrophoresis*, 2006. **27**(5-6), 947-961.
136. Tomašić, V. and F. Jović, State-of-the-art in the monolithic catalysts/reactors. *Applied Catalysis a-General*, 2006. **311**, 112-121.
137. Vergunst, T., M.J.G. Linders, F. Kapteijn, and J.A. Moulijn, Carbon-based monolithic structures. *Catalysis Reviews-Science and Engineering*, 2001. **43**(3), 291-314.
138. Cybulski, A. and J.A. Moulijn, Monoliths in Heterogeneous Catalysis. *Catalysis Reviews-Science and Engineering*, 1994. **36**(2), 179-270.
139. Heck, R.M., S. Gulati, and R.J. Farrauto, The application of monoliths for gas phase catalytic reactions. *Chemical Engineering Journal*, 2001. **82**(1-3), 149-156.
140. Mair, D.A., T.R. Schwei, T.S. Dinio, F. Svec, and J.M.J. Fréchet, Use of photopatterned porous polymer monoliths as passive micromixers to enhance mixing efficiency for on-chip labeling reactions. *Lab on a Chip*, 2009. **9**(7), 877-883.
141. Hilder, E.F., F. Svec, and J.M.J. Fréchet, Polymeric monolithic stationary phases for capillary electrochromatography. *Electrophoresis*, 2002. **23**(22-23), 3934-3953.
142. Xie, S., R.W. Allington, J.M.J. Fréchet, and F. Svec, Porous polymer monoliths: an alternative to classical beads. *Advances in Biochemical Engineering/Biotechnology*, 2002. **76**(Modern Advances in Chromatography), 87-125.
143. Hilder, E.F., F. Svec, and J.M. Fréchet, Development and application of polymeric monolithic stationary phases for capillary electrochromatography. *Journal of Chromatography A*, 2004. **1044**(1-2), 3-22.
144. Svec, F., Organic polymer monoliths as stationary phases for capillary HPLC. *Journal of Separation Science*, 2004. **27**(17-18), 1419-1430.
145. Ro, K.W., R. Nayak, and D.R. Knapp, Monolithic media in microfluidic devices for proteomics. *Electrophoresis*, 2006. **27**(18), 3547-3558.
146. Svec, F., Less common applications of monoliths: Preconcentration and solid-phase extraction. *Journal of Chromatography B-Analytical Technologies in the Biomedical and Life Sciences*, 2006. **841**(1-2), 52-64.
147. Svec, F. and C.G. Huber, Monolithic materials - Promises, challenges, achievements. *Analytical Chemistry*, 2006. **78**(7), 2100-2107.

148. Eeltink, S. and F. Svec, Recent advances in the control of morphology and surface chemistry of porous polymer-based monolithic stationary phases and their application in CEC. *Electrophoresis*, 2007. **28**(1-2), 137-147.
149. Jungbauer, A. and R. Hahn, Polymethacrylate monoliths for preparative and industrial separation of biomolecular assemblies. *Journal of Chromatography A*, 2008. **1184**(1-2), 62-79.
150. Potter, O.G. and E.F. Hilder, Porous polymer monoliths for extraction: Diverse applications and platforms. *Journal of Separation Science*, 2008. **31**(11), 1881-1906.
151. Svec, F. and A.A. Kurganov, Less common applications of monoliths - III. Gas chromatography. *Journal of Chromatography A*, 2008. **1184**(1-2), 281-295.
152. Urban, J. and P. Jandera, Polymethacrylate monolithic columns for capillary liquid chromatography. *Journal of Separation Science*, 2008. **31**(14), 2521-2540.
153. Aoki, H., N. Tanaka, T. Kub, and K. Hosoya, Polymer-based monolithic columns in capillary format tailored by using controlled in situ polymerization. *Journal of Separation Science*, 2009. **32**(3), 341-358.
154. Krenkova, J. and F. Svec, Less common applications of monoliths: IV. Recent developments in immobilized enzyme reactors for proteomics and biotechnology. *Journal of Separation Science*, 2009. **32**(5-6), 706-718.
155. Vlakh, E.G. and T.B. Tennikova, Applications of polymethacrylate-based monoliths in high-performance liquid chromatography. *Journal of Chromatography A*, 2009. **1216**(13), 2637-2650.
156. Vázquez, M. and B. Paull, Review on recent and advanced applications of monoliths and related porous polymer gels in micro-fluidic devices. *Analytica Chimica Acta*, 2010. **668**(2), 100-113.
157. Hickey, A.M., L. Marle, T. McCreedy, P. Watts, G.M. Greenway, and J.A. Littlechild, Immobilization of thermophilic enzymes in miniaturized flow reactors. *Biochemical Society Transactions*, 2007. **35**, 1621-1623.
158. Mayr, M., B. Mayr, and M.R. Buchmeiser, Monolithic materials: New high-performance supports for permanently immobilized metathesis catalysts. *Angewandte Chemie-International Edition*, 2001. **40**(20), 3839-+.
159. Buchmeiser, M.R., S. Lubbad, M. Mayr, and K. Wurst, Access to silica- and monolithic polymer supported C-C-coupling catalysts via ROMP: applications in high-throughput screening, reactor technology and biphasic catalysis. *Inorganica Chimica Acta*, 2003. **345**, 145-153.
160. Nikbin, N., M. Ladlow, and S.V. Ley, Continuous flow ligand-free Heck reactions using monolithic Pd 0 nanoparticles. *Organic Process Research & Development*, 2007. **11**(3), 458-462.
161. Karbass, N., V. Sans, E. Garcia-Verdugo, M.I. Burguete, and S.V. Luis, Pd(0) supported onto monolithic polymers containing IL-like moieties. Continuous flow catalysis for the Heck reaction in near-critical EtOH. *Chemical Communications*, 2006(29), 3095-3097.
162. Bandari, R., W. Knolle, A. Prager-Duschke, H.-J. Gläsel, and M.R. Buchmeiser, Monolithic media prepared via electron beam curing for proteins separation and flow-through catalysis. *Macromolecular Chemistry and Physics*, 2007. **208**(13), 1428-1436.
163. Baumann, M., I.R. Baxendale, S.V. Ley, N. Nikbin, and C.D. Smith, Azide monoliths as convenient flow reactors for efficient Curtius rearrangement reactions. *Organic & Biomolecular Chemistry*, 2008. **6**(9), 1587-1593.

Chapter 2 Porous polymer monoliths

2.1 Introduction

As discussed in **Chapter 1** a porous polymer monoliths (PPM) is a single, continuous, rigid polymer structure containing numerous interconnected voids through which fluid can flow [1]. PPM's are typically prepared by filling a mould with a polymerisation mixture, consisting of a non-linking monomer, a crosslinking monomer and porogenic solvents, followed by initiation of the polymerisation. After the polymerisation reaction is complete, the porogens, unreacted material, and soluble oligomers are removed leaving behind the rigid porous monolithic structure. The mechanism of pore formation in PPM is well understood and has been thoroughly discussed in recent reviews [1-3]. An overview of the mechanism for PPM formation by free radical polymerisation will now be discussed as this is the method utilised in this work.

Polymerisation is triggered by the breakdown of an initiator to form free radicals, which undergo radical addition to the monomers in solution and begin to form polymer chains. As the highly-crosslinked polymer chains form they precipitate, or phase separate, to form nuclei due to their poor solubility in the porogenic solvents. The nuclei are solvated by unreacted monomers, which have a higher affinity for the nuclei than the porogenic solvents, causing polymerisation at the surface of the nuclei to be kinetically favoured over polymerisation in the bulk mixture. As the nuclei grow they continue to be preferentially solvated by the monomers in solution, which results in a continual back extraction of the monomers from solution. The growing nuclei capture polymer chains from the surrounding solution and near-by nuclei become linked to form clusters, which remain dispersed in the mixture and continue to grow. In the later stages of polymerisation these

clusters, or globules, become large enough to aggregate and form a continuous interconnected structure. This structure is reinforced by both interglobular crosslinking and capture of polymer chains from solution. The final structure is a system of interconnected microglobules with voids, or macropores, containing the porogenic solvents. The volume of the macropores, or the void volume fraction, is close to the volume fraction of the porogenic solvent in the initial polymerisation mixture [1].

The final porous structure of the monolith depends on many factors. Those with the greatest influence are initiator concentration and initiation rate, polymerisation temperature, the volume ratio of porogenic solvents, the polarity of the porogenic solvents, the crosslinking monomer (density of linking groups), the ratio of non-linking to crosslinking monomers and the chemical nature of the monomers (ie. polarity, sterics, etc.) [2, 3]. The effects of these parameters are discussed below.

A free radical initiator is a compound which fragments when exposed to an input energy to form radicals. This energy can be generated by thermal or photo effects depending on the chemical nature of the initiator. The rate at which a thermal initiator decomposes to form radicals is characterised by its thermal half-life, which is temperature dependent. For photoinitiators, the decomposition rate is dependent on the intensity and wavelength of the incident light. UV photoinitiators are preferred for preparation of monoliths as UV sources are relatively inexpensive and UV initiators are generally stable in the visible region which allows polymerisation mixtures to be prepared under ambient light.

The final porous structure of the PPM is significantly influenced by the concentration and decomposition rate of the free radical initiator. When the

decomposition rate of the initiator is high, more nuclei are formed simultaneously and are competitively solvated by the monomers in solution. A larger number of nuclei exhausts the supply of monomers faster, which limits the growth of the globules. Since a larger number of smaller globules are formed, the voids between them are also smaller which affords a monolith with smaller pores [1]. Using a high concentration of the initiator has the same effect as increasing the initiator decomposition rate. Conversely at lower decomposition rates, the number of nuclei formed simultaneously is lower and there is less competition for the monomers in solution, which allows the globules to grow larger resulting in a monolith with larger pores [1].

As discussed above, the porogenic solvents, or porogens, influence phase separation which is dependent on the affinity of the solvents towards the forming nuclei. If the porogens have a high affinity for the forming polymer, i.e. they are „good’ thermodynamic solvents, then they will compete with the free monomers in solvating the nuclei, resulting in smaller globules. If the affinity of the porogens is too high, then phase separation will not occur and a gel will be formed instead. Conversely porogens with low affinity for the polymer, i.e. „poor’ thermodynamic solvents, will not compete with the monomers, affording larger globules. Using a combination of a „poor’ thermodynamic solvent, referred to as the macroporogen, and a „good’ thermodynamic solvent, referred to as the microporogen, allows the globule size, and hence the pore size, to be tailored within the two extremes [1-3].

A porogenic solvent must be miscible with the polymerisation mixture and not participate in the radical polymerisation. While there are a large range of solvents that meet these requirements, proven porogen mixtures are more frequently utilised than explorations of new porogenic systems [3]. For both styrenic and acrylic/methacrylic systems, polar alcohols, such as methanol, make good

macroporogens and non-polar solvents, such as toluene, make good microporogens [2]. Porogenic solvent choice is significantly influenced by the solubility of the monomers as well as the initiation method. Bulky monomers with poor solubility may require specific macroporogens for the polymerisation mixture to be a single phase liquid. Thermal initiation requires elevated temperatures so only solvents with boiling points above the initiation temperature are generally used [4]. Since UV initiation is normally performed at room temperature, low boiling point non-UV absorbing alcohols are suitable. Predicting how particular solvents affect the pore size and morphology of monolith is difficult and is mainly based on experience rather than theoretical considerations [3].

The void volume, or porosity, of a PPM is determined primarily by the total volume of porogens present in the polymerisation mixture [1]. Early development of PPM's was based on suspension polymerisation of macroporous beads where a ratio of 40:60 monomers to porogens was shown to be optimal for most applications [5]. This ratio, or porogen concentration, is the most widely utilised for PPM's since it gives the best balance of permeability, surface area and mechanical stability in most applications. The porogen concentration not only controls porosity, but it also influences the pore size and the surface area of the PPM. It has been observed that at high porogen concentrations, both the pore size and porosity are considerably larger, however the surface area and mechanical strength are drastically reduced [6]. At high porogen concentrations the mechanical strength of the structure is insufficient to support itself and the PPM is destroyed upon removal of the porogens [6]. Conversely at low porogen concentrations the porosity and pore size are so low that the material becomes impervious to flow. Therefore, control over the porogen concentration can be used to directly influence the monolith's permeability, surface area, and mechanical strength.

PPM's are commonly prepared using a co-monomer system consisting of a non-linking monomer and a crosslinking monomer, however preparation using solely a crosslinking monomer is possible. The ratio of the non-linking to crosslinking monomers affects the amount of crosslinking in the forming polymer, which strongly influences its chemical and porous properties, morphology and mechanical stability [3]. At high crosslinker concentrations there is significantly more crosslinking in the forming polymer, causing the nuclei to precipitate earlier affording smaller globules and a smaller pore size [2]. Generally the ratio of non-linker to crosslinker is chosen to afford a monolith with sufficiently high surface area and reasonable permeability while being mechanical robust. For most methacrylic-based PPM this ratio is 60:40 non-linker to crosslinker, however it is highly dependent on the application and crosslinking monomer.

In development of a particular PPM, optimisation of all the different parameters would be far too time consuming so generally the pore size is controlled by varying the ratio of macroporogen to microporogen while keeping all the parameters fixed. This method allows the pore size to be varied over a wide range in order to maximise the surface area while having sufficiently high permeability for the particular application. The benefit of this approach is that only the pore size and surface area are altered, while the chemical properties of the monolith remain unchanged [7].

Control over the chemical properties of PPM by introduction of desired functional groups is vital for many applications, especially in bioreactors, affinity chromatography and supported catalysis. While several different approaches to introducing functionality to PPM's have been demonstrated, the most common approach is post-polymerisation chemical modification of PPM's prepared using non-linking monomers featuring reactive functional groups. This approach is relatively

simple and inexpensive, requires less development than other approaches, and also allows various functionalities to be introduced onto the same optimised PPM backbone [2]. While a variety of different functional monomers have been utilised, glycidyl methacrylate (GMA) and chloromethylstyrene (CMS) are the most prominently used due to their versatile chemistries. GMA-based PPM's are commonly prepared using ethylene glycol dimethylacrylate (EDMA) as the crosslinker as both are methacrylic monomers, giving the monolithic polymer backbone a homogeneous chemical structure. For the same reason, CMS-based monoliths are generally prepared using divinylbenzene (DVB) as the crosslinker. Both poly(GMA-*co*-EDMA) and poly(CMS-*co*-DVB) monoliths have been widely utilised for post-polymerisation chemical modification of the reactive functional groups in order to introduce a wide variety of functionalities. Chemically modified poly(GMA-*co*-EDMA) PPM's have been extensively used in separation science applications, such as affinity chromatography [8-10], ion chromatography [11, 12], capillary electrochromatography (CEC) [13], solid phase extraction [14], and pre-concentration [15, 16]. There have been fewer examples of chemically modified poly(CMS-*co*-DVB) PPM's, however some of the applications demonstrated have been in scavenging [17] and CEC [18].

For the supported homogeneous catalysis targeted here, the PPM must have the following properties:

- Thermal stability at temperatures used for catalysis.
- Chemically inert to the reaction solvents, reagents, catalyst, and reaction products.
- Contain reactive functional groups for catalyst immobilisation.
- High permeability to minimise flow-resistance.

The first three requirements all relate to the chemical properties of the monolith, which are determined by the choice of monomers. One particular polymer monolith that fulfils these requirements is poly(CMS-*co*-DVB), which has been proven to be suitable for supported catalysis [19]. Poly(CMS-*co*-DVB) monolith is chemically similar to Merrifield resins as both are synthesised from the same monomers. Since Merrifield resins have been used extensively for palladium supported catalysis in batch and flow-through applications, the use of poly(CMS-*co*-DVB) monolith allows for direct comparison with these existing systems. Another potential candidate is poly(GMA-*co*-EDMA) monoliths which have been extensively used as a support for affinity chromatography [9] and enzymatic bioreactors [20]. Poly(GMA-*co*-EDMA) is relatively less inert than poly(CMS-*co*-DVB) as the ester groups present within the polymer backbone form potentially reactive sites. Despite this, poly(GMA-*co*-EDMA) monolith is the preferred system as it can be synthesised by UV initiated polymerisation, making it suitable for use in microchips. Both PPM systems are thermally suitable for catalysis as methacrylic PPM's are known to be thermally stable up to 215°C and styrenic PPM's are stable up to 350°C [1].

Preparation of PPM was investigated within several different formats, including capillary, microchip, and column. The dimensions and physical properties of these different devices are discussed in **Chapter 5**. Bulk monolith was prepared by both thermal and UV initiation for porosimetry analysis and development of batch conditions.

2.2 Thermally initiated polymer monoliths

The most commonly used method for preparation of PPM is by thermally initiated radical polymerisation. The success of this approach lies in its simplicity as the only infrastructure required is a stable, homogeneous heat source such as a water

bath. The morphology and porous structure of the PPM's prepared are highly reproducible as the polymerisation is relatively slow, taking hours, or up to several days to reach completion. Minor fluctuations in temperature over this time scale will have negligible effect on the final porous structure.

Thermally initiated polymer monoliths were investigated, as optimised formulations for both poly(GMA-*co*-EDMA) and poly(CMS-*co*-DVB) PPM's with excellent flow-through properties are already well established [13, 18]. It should be pointed out that a PPM formulation is the liquid mixture that is the precursor to a PPM, but the final PPM is also dependent on the polymerisation method and conditions. As such the PPM should not be described as a formulation but rather the result of a particular formulation. These literature formulations prepared in capillaries provide a benchmark for which the back-pressure and other flow-properties of the photoinitiated PPM formulations can be compared. The thermally initiated poly(GMA-*co*-EDMA) monolith formulation used in this investigation was developed by Preinerstorfer *et al.* for the preparation of thiol-modified monolithic capillary columns for CEC [13]. This formulation consists of 24 wt% GMA, 16 wt% EDMA, 30 wt% cyclohexanol and 30 wt% dodecanol. The Preinerstorfer formulation was developed for use in 30 cm lengths of 100 μm ID capillary and had sufficiently low back-pressure to allow flushing at 30 $\mu\text{L h}^{-1}$ with solvent using a syringe pump and gas-tight syringes. The poly(CMS-*co*-DVB) monolith formulation used in this study was developed by Tripp *et al.* for the preparation of monolithic scavenger disks [17]. This formulation consists of 16 wt% CMS, 24 wt% DVB, 17.5 wt% toluene and 42.5 wt% dodecanol. The high crosslinking monomer content in this formulation affords a monolith with larger surface area and extra structural rigidity, while the high level of macroporogen gives the monolith sufficiently large

pores for low flow resistance. Greater structural rigidity was required as this formulation was developed for use as chromatographic disks and not in capillaries.

2.2.1 Thermally initiated polymer monolith in bulk

To enable discussion of the different monolith formulations used within this work, a naming strategy was developed. The first letter(s) refers to the type of initiation, T for thermal or UV for ultraviolet, the next three letters refer to the functional monomer, and the number allows distinguishing between formulations. The Preinerstorfer poly(GMA-*co*-EDMA) monolith formulation [13] will now be referred to as TGMA1 and the Tripp poly(CMS-*co*-DVB) monolith formulation [17] will be referred to as TCMS1.

These formulations were used to prepared PPM in bulk for characterisation by mercury intrusion porosimetry (MIP), which is further discussed in **Section 2.6**. The median pore diameter of the TCMS1 bulk monolith was found to be 0.99 μm , with a density of 0.38 g mL^{-1} and porosity of 70%. The porosity is moderately larger than the porogen volume in the polymerisation mixture, which is 61% of the total volume. The difference is unlikely to be due to incomplete polymerisation, but could possibly be due to the approximately 20 wt% content of ethylvinylbenzene isomers present in technical grade DVB source. This pore diameter correlates well with the previously reported mean pore diameter of 1.0 μm [17].

The median pore diameter of the TGMA1 bulk monolith was 0.76 μm , with a density of 0.43 g mL^{-1} , and of porosity of 63%. For this formulation, the porosity correlates closely to the volume of porogens in the polymerisation mixture, which was 62% of the total volume. The reported modal pore diameter for the TGMA1 formulation is 1.1 μm , however this monolith was prepared at 60°C [13]. It is expected that performing the polymerisation at a higher temperature will lead to

smaller macropores, as discussed above. The polymerisation of TGMA1 was conducted at 70 °C in order to keep the preparation conditions consistent with TCMS1.

2.2.2 Thermally initiated polymer monolith in fused-silica capillary

Both TCMS1 and TGMA1 formulations were used to prepare PPM in 25 cm length 250 μm ID polyimide coated fused-silica capillary using the same conditions used for preparation of bulk monolith. This relatively large ID was chosen to reduce the back-pressure from the monolithic columns, allowing for higher flow rates using the relatively low-pressure syringe pump system. The PPM was prepared in 30 cm lengths of vinylised capillary and then trimmed to 25 cm after polymerisation. This was done to ensure homogeneity of the PPM along the capillary length as voids were observed in the PPM formed near the ends of the capillary. The 25 cm column length was the longest length of capillary that could fit inside the column heaters used for heating without bending. Shorter column lengths were obtained by cutting these 25 cm long columns and initial quality control of the capillary columns was performed by observation of the capillary during the post-polymerisation solvent flush. Solvent leakage around the syringe plunger or from the fittings was used as an indicator for excessive back-pressure, which made the capillary unsuitable for subsequent reactor fabrication and testing. Both the TCMS1 and TGMA1 formulations afforded monolithic columns with excellent permeability and allowed flushing at flow rates up to 120 $\mu\text{L h}^{-1}$. At higher flow rates the back-pressure exceeded the pressure generated by the syringes resulting in leakage in the fittings and damage to syringes.

Cross-sections of the TGMA1 and TCMS1 capillary columns were imaged by SEM in order to analyse the monolith morphology as well as to compare the morphology with that obtained for bulk monolith. **Figure 2.1** shows SEM images for

bulk monolith and in capillary column prepared from the TGMA1 formulation at the same magnification. As can be seen from these images the morphology, which includes the globule size, globule density, and interglobular voids, are similar both in the bulk monolith and in capillary. The images obtained for bulk monolith and capillary column prepared from the TCMS1 formulation, shown in **Figure 2.2**, also show very similar morphology. No signs of radial changes in morphology can be observed in these images, implying a homogenous morphology in the capillaries.

As previously discussed, the amount of PPM prepared in capillary column is insufficient for MIP analysis. The PPM's density and porosity in 250 μm capillaries can be determined in capillary by weighing experiments, allowing for direct comparison with MIP analysis of bulk monolith. The mass of PPM in a capillary column was determined by weighing a known length of dried monolithic capillary column and subtracting the mass of the capillary. The mass of the capillary without the PPM could not be directly determined as the ends are trimmed after polymerisation, hence the average mass per length of capillary was determined and used to calculate the mass of capillary in the monolithic column. Fused-silica capillary is manufactured to a high standard and has only a few percent variation in its dimensions and mass. The density of the PPM in the capillary was determined by dividing its mass by the capillary volume. To determine the porosity of the PPM, a pre-weighed dry monolithic column was filled with ethanol, capped at the ends and re-weighed. Ethanol was used as it is less volatile than methanol, the solvent mainly used for PPM rinsing, and should not swell the monolith. Using the density of ethanol its volume was calculated, giving the void volume or porosity. This approach was used to determine the porosity and density of the TCMS1 formulation in 250 μm ID capillary. The density of TCMS1 in capillary was found to be $0.36 \text{ g mL}^{-1} \pm 3\%$ which is only 6% smaller than the value obtained from MIP of bulk monolith.

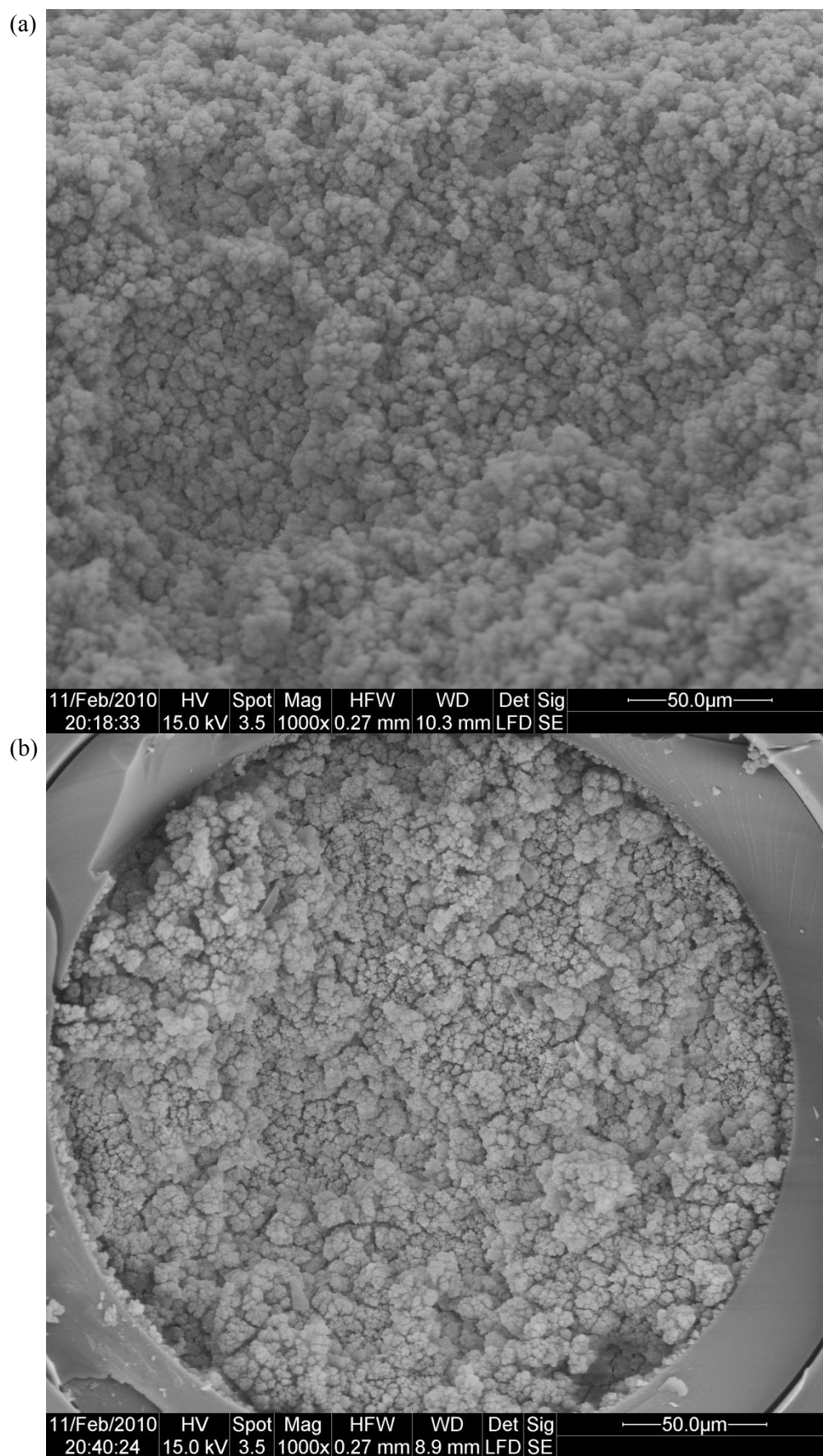


Figure 2.1 (a) Bulk GMA1 monolith and (b) TGMA1 formulation monolithic column cross-sections.

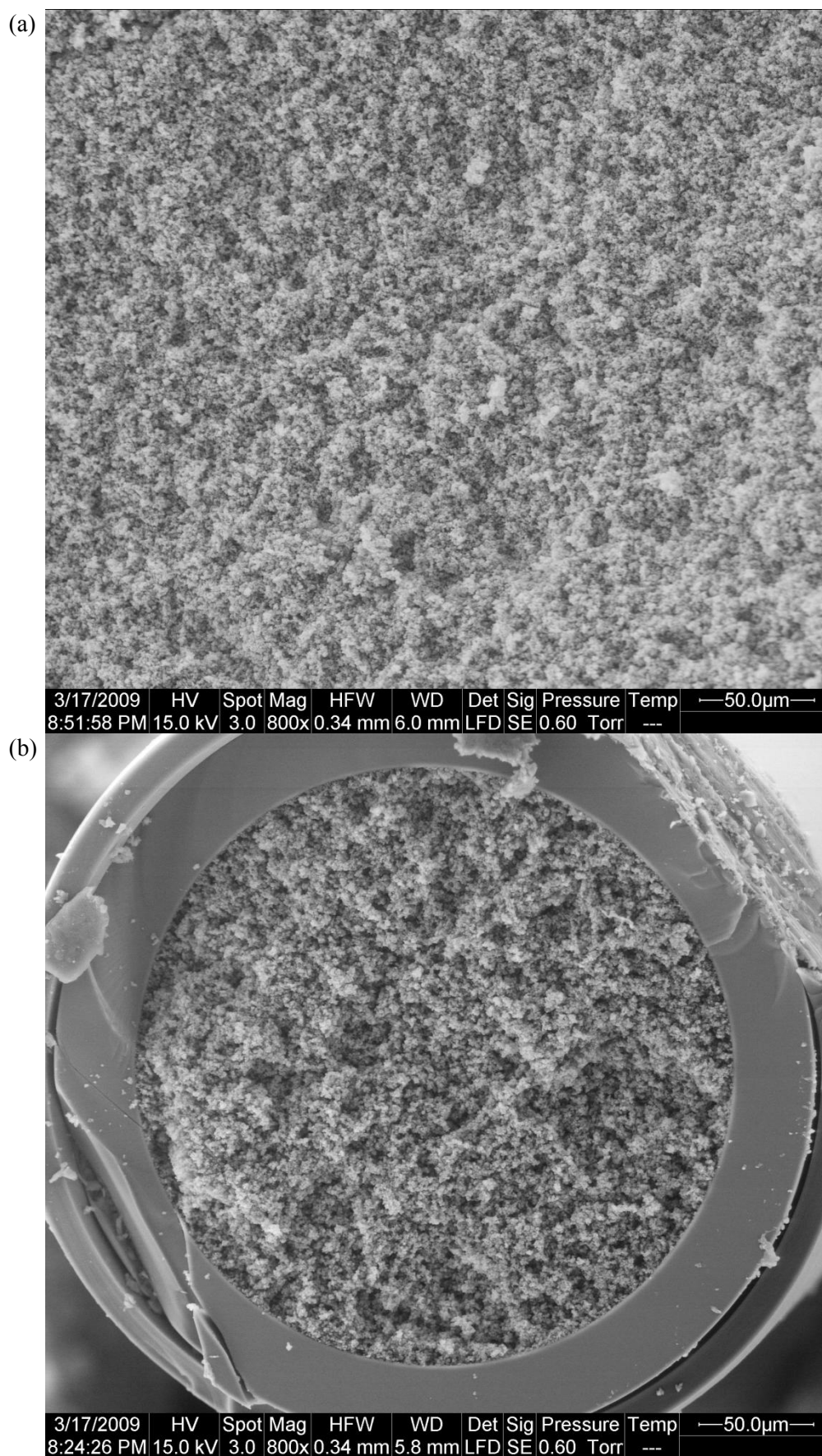


Figure 2.2 (a) Bulk TCMS1 monolith and (b) TCMS1 formulation monolithic column cross-sections.

The porosity measured was $79 \pm 4\%$, which is considerably higher than the 70% obtained for bulk monolith. This may imply that the PPM has a higher porosity in capillary compared to bulk. Minor differences between PPM prepared in bulk and capillary were expected, and the discrepancy in porosity between bulk and capillary was not explored in further detail. For subsequent calculations, the bulk values were taken as these were considered to give the best approximation for the porosity in the capillary columns used for flow-through catalysis.

2.3 Photoinitiated polymer monoliths

One of the major goals of this research was to explore, and hopefully demonstrate, that PPM's are a suitable catalyst support for the integration of microreactors in lab-on-a-chip devices, where it is vital to be able to restrict the region of monolith formation to the desired locations in the channel network [21]. Photoinitiated polymerisation, the second mostly commonly utilised method for preparation of PPM's, fulfils this requirement as polymerisation only occurs in the irradiated regions. This initiation method has been shown to be considerably faster than thermal initiation and can afford fully polymerised PPM in several minutes, rather than the 8-20 h typical of thermal initiation [22]. Complete polymerisation of the PPM is defined as complete consumption of the radical initiator, as some unbranched oligomers are expected even after the PPM growth has terminated. Photoinitiated polymerisation of PPM has almost exclusively been performed in the UV region of the spectrum, however the visible [23] and gamma [24] regions have also been exploited. The reason the UV region is frequently used is that UV curing is a common industrial technique, with well established exposure systems and free radical photoinitiators.

UV initiated polymerisation places several restrictions on suitable microdevice substrates, monomers, and porogens. The substrate must be at least partially transparent in the excitation region of the initiator, restricting the technique to optically transparent materials, such as glass, fused-silica, quartz, and certain polymers. As such, photoinitiated polymerisation of PPM has been demonstrated in glass columns [25], fused-silica capillaries (UV-transparent and polyimide coated) [4, 16, 22, 23, 26-33], glass microchips (including quartz and fused-silica) [8, 26, 34-38] and polymer microchips (including PMMA, COC/COP, and PDMS) [15, 39-48]. Initially glass microchips were investigated for the fabrication of microreactors as glass has excellent thermal and optical properties and is compatible with most solvents and reagents. Additionally, chemical modification of glass substrates for the introduction of vinyl groups for monolith anchoring is well established and has been demonstrated in capillary, column, and microchip [4, 25, 36]. Another goal of this research was to produce polymer microreactors, focussing this work on polymer-compatible photoinitiated PPM preparation conditions in an attempt to eliminate re-optimisation of the conditions when changing the microchip substrate.

In addition to the substrate, the porogens and monomers must be also transparent in the excitation region. Styrenic monomers and aromatic solvents absorb strongly in the UV region, rendering them unsuitable for UV-initiated polymerisation. This may be overcome by selecting an initiator that is active in a region of the spectrum where the monomers and porogens are transparent, as recently demonstrated by the photoinitiated polymerisation of styrenic monomers in the visible region [23]. Methacrylic monomers, such as GMA and EDMA, have been demonstrated to be compatible with UV photoinitiation [8, 15, 16, 49, 50].

Fused-silica capillary was used to model the glass microchips for formulation development as it is relatively inexpensive and it is well established for preparation

of monolithic columns. The largest commercially available ID UV-transparent capillary during this research has ID 100 μm , which unfortunately has a cross-sectional area 55% smaller than the glass microchips investigated. The length of capillary chosen for the preparation of monolithic columns was 30 cm, to model the microchip channel length. In terms of dimensions, the 100 μm ID capillary may not be a good model for the glass microchips as flow-resistance will be significantly higher in the capillary, but the capillaries represent a „worst-case scenario’. A PPM with sufficiently permeability for use in 100 μm ID capillary columns was expected to also be suitable for the $150 \times 150 \mu\text{m}$ microchannel of the glass microchips.

2.3.1 Photoinitiated PPM development in capillary

As discussed previously, the rate of radical generation has a significant effect on the morphology of a PPM and is dependent on several factors in photoinitiated polymerisation, including the source intensity and the molar absorptivity of the initiator. Basically, higher intensity light sources and/or higher molar absorptivity photoinitiators should give faster radical generation rates, which implies that changing the light source or the photoinitiator will likely result in a different radical generation rate, altering the morphology of the PPM. As a result any photoinitiated PPM formulation developed by one research group cannot be directly implemented by another without significant modification, unless using exactly the same light source, photoinitiator, and polymerisation conditions [31]. Therefore, the development of an original photoinitiated PPM formulation is generally required to suit the polymerisation conditions and application requirements, as illustrated in the following discussion.

The initial investigation of photoinitiated poly(GMA-*co*-EDMA) monolith used a formulation developed by Yu *et al.* which was reported to afford PPM with relatively low flow-resistance [4]. Yu *et al.* investigated the preparation of

poly(GMA-*co*-EDMA) monolith by photoinitiation using a large range of low boiling point solvents as porogens, amongst which a 1:1 combination of methanol and ethanol was found to afford a highly permeable monolith with a median pore size of 4.7 μm (pore size was obtained by MIP analysis of bulk monolith prepared in 6 mm ID quartz column) [4]. This formulation, hereafter known as UVGMA7, consisted of 24 wt% GMA, 16 wt% EDMA, 60 wt% porogens, and 1 wt% AIBN with respect to the monomers as the initiator and was prepared using a 365 nm UV tube source, with an intensity of 0.6 mWcm^{-2} and an exposure time of 16 h. This is an impractically long exposure time for the preparation of photoinitiated PPM, but is due to the relatively low molar absorptivity of AIBN and the low intensity of the light source [51]. In more recent literature, the use of DMPAP with a high intensity flood exposure lamp has been shown to give complete polymerisation within 100 μm ID fused-silica capillary in under 10 min [36]. Hence, in order to reduce the fabrication time, DMPAP was used with an OAI Model 30 flood exposure system, fitted with an Hg-Xe arc-lamp calibrated to 20 mW cm^{-2} at 260 nm. Using this combination of light source and initiator, 30 cm long monolithic columns were prepared in 100 μm ID capillary and rinsed with methanol at 60 $\mu\text{L h}^{-1}$. No effluent was collected after several hours indicating poor permeability, yet Yu *et al.* successfully rinsed their 37 cm long monolithic columns, with the same internal diameter, at 50 $\mu\text{L h}^{-1}$. This difference in permeability is likely a result of the significantly different exposure conditions and photoinitiator used between the investigated PPM and that reported by Yu *et al.*, which suggested that a novel PPM formulation would need to be developed to suit our polymerisation conditions.

Despite the existence of a large range of UV transparent solvents that are potential porogens, the most commonly utilised porogens for the preparation of poly(GMA-*co*-EDMA) monolith by photoinitiation are cyclohexanol and 1-

dodecanol [15, 49]. In this binary porogen system, the relatively non-polar 1-dodecanol acts as the microporogen and the more polar cyclohexanol as the macroporogen, hence the largest pore size and highest permeability is expected to result from using cyclohexanol as the sole porogen. To test the suitability of cyclohexanol as a porogenic solvent using the polymerisation under investigation, a formulation similar to UVGMA7 was prepared but using cyclohexanol as the porogen. This formulation, UVGMA1, was used to prepare a monolithic capillary column under the same conditions as previously used and rinsed with methanol at $60 \mu\text{L h}^{-1}$. While this monolithic column showed improved permeability over the column prepared from the UVGMA7 formulation, it was not sufficiently permeable as evidenced by leakage at the syringe and fittings. To determine if the addition of 1-dodecanol could improve the PPM's permeability, a series of formulations (UVGMA2 to UVGMA 6) were prepared in which the ratio of cyclohexanol to 1-dodecanol was systematically varied. These formulations are presented in **Table 2.1**.

Each of the UVGMA1-6 formulations were used to prepare monolithic columns in 30 cm long $100 \mu\text{m}$ ID capillary and were tested for relative permeability by flushing with methanol at $60 \mu\text{L h}^{-1}$. The effluent from the capillary columns was collected into sealed vials to allow the amount of solvent lost through leakage to be determined. The least leakage was observed for capillary column prepared using the UVGMA4 formulation, indicating the highest permeability of the six formulations investigated. This result was counter-intuitive as this formulation has relatively high microporogen content and should afford PPM with smaller pores than the UVGMA1 formulation. Cross-sectional SEM images for each of the monolithic capillary columns prepared are shown in **Figure 2.3-2.5** on pages 61-63. These images confirm that UVGMA1 results in the largest globules and hence the largest pores.

Formulation	GMA (wt%)	EDMA (wt%)	Cyclohexanol (wt%)	1-Dodecanol (wt%)	Porogen Percent Volume
UVGMA1	24	16	60	0	62.6
UVGMA2	24	16	48	12	63.3
UVGMA3	24	16	36	24	63.9
UVGMA4	24	16	24	36	64.6
UVGMA5	24	16	12	48	65.2
UVGMA6	24	16	0	60	65.7
UVGMA4-70	18	12	28	42	73.9
UVGMA4-80	12	8	32	48	82.9

Table 2.1 UV initiated poly(GMA-*co*-EDMA) formulations.

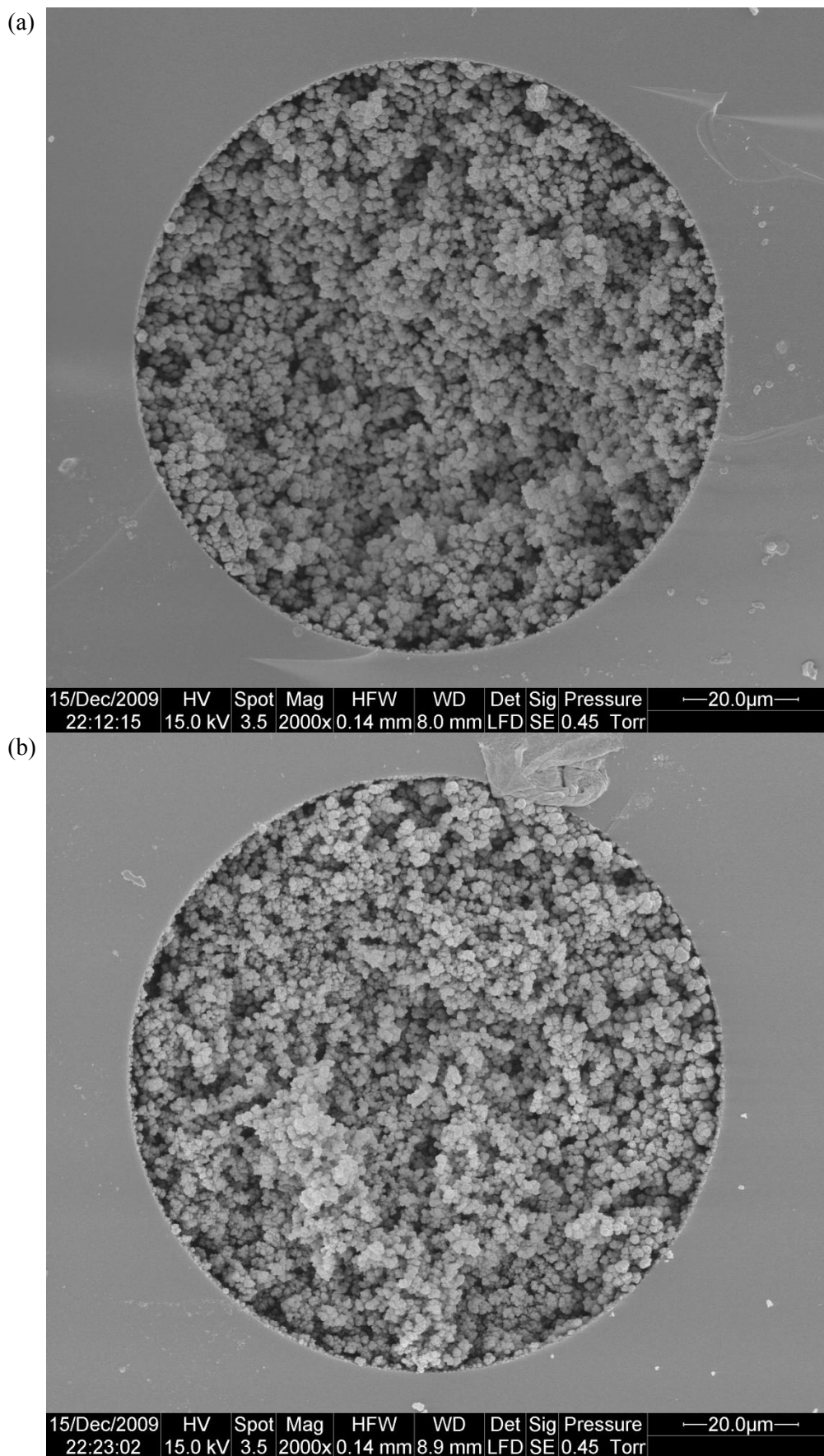


Figure 2.3 (a) UVGMA1 and (b) UVGMA2 formulation monolithic column cross-sections.

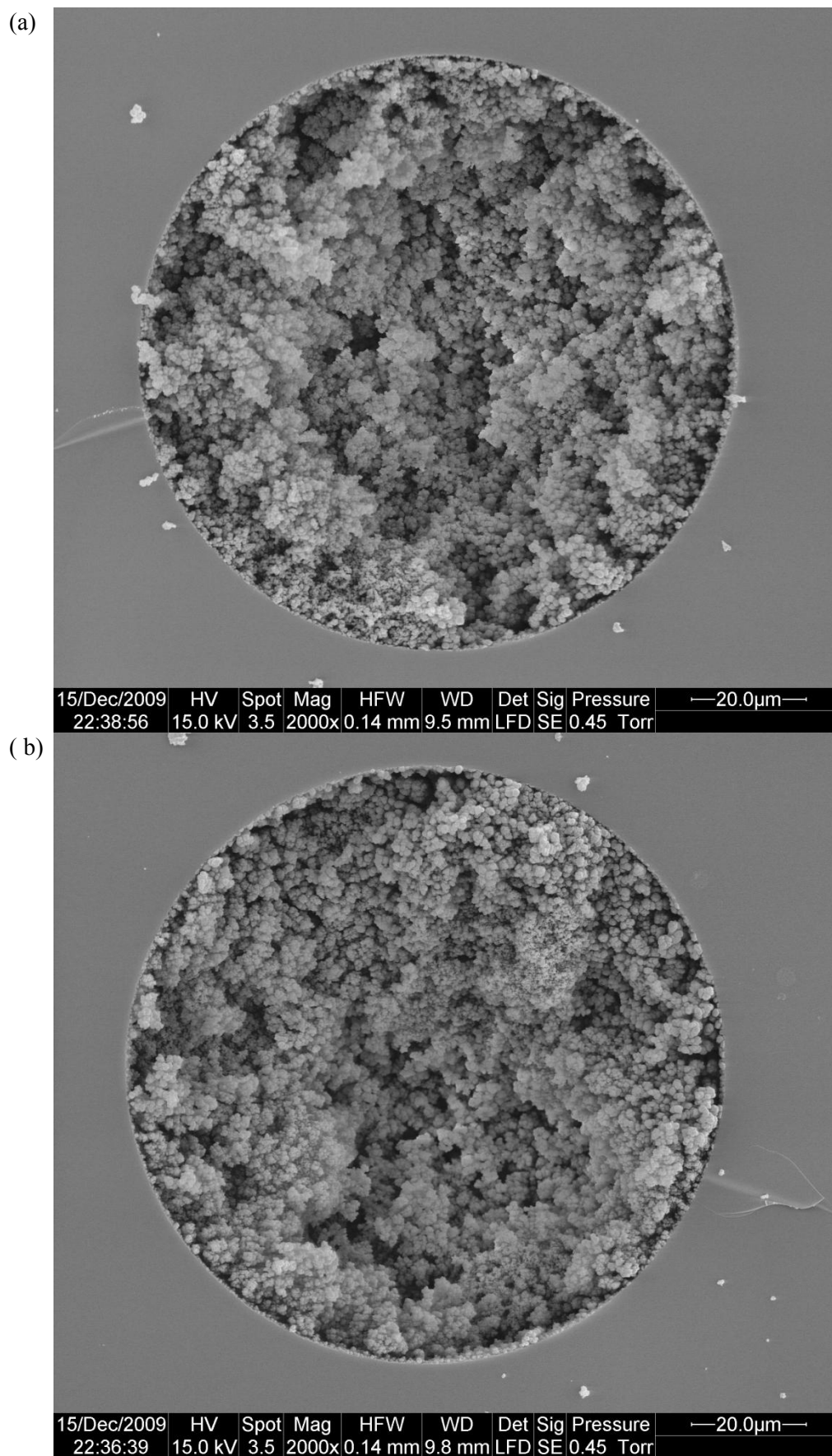


Figure 2.4 (a) UVGMA3 and (b) UVGMA4 formulation monolithic column cross-sections.

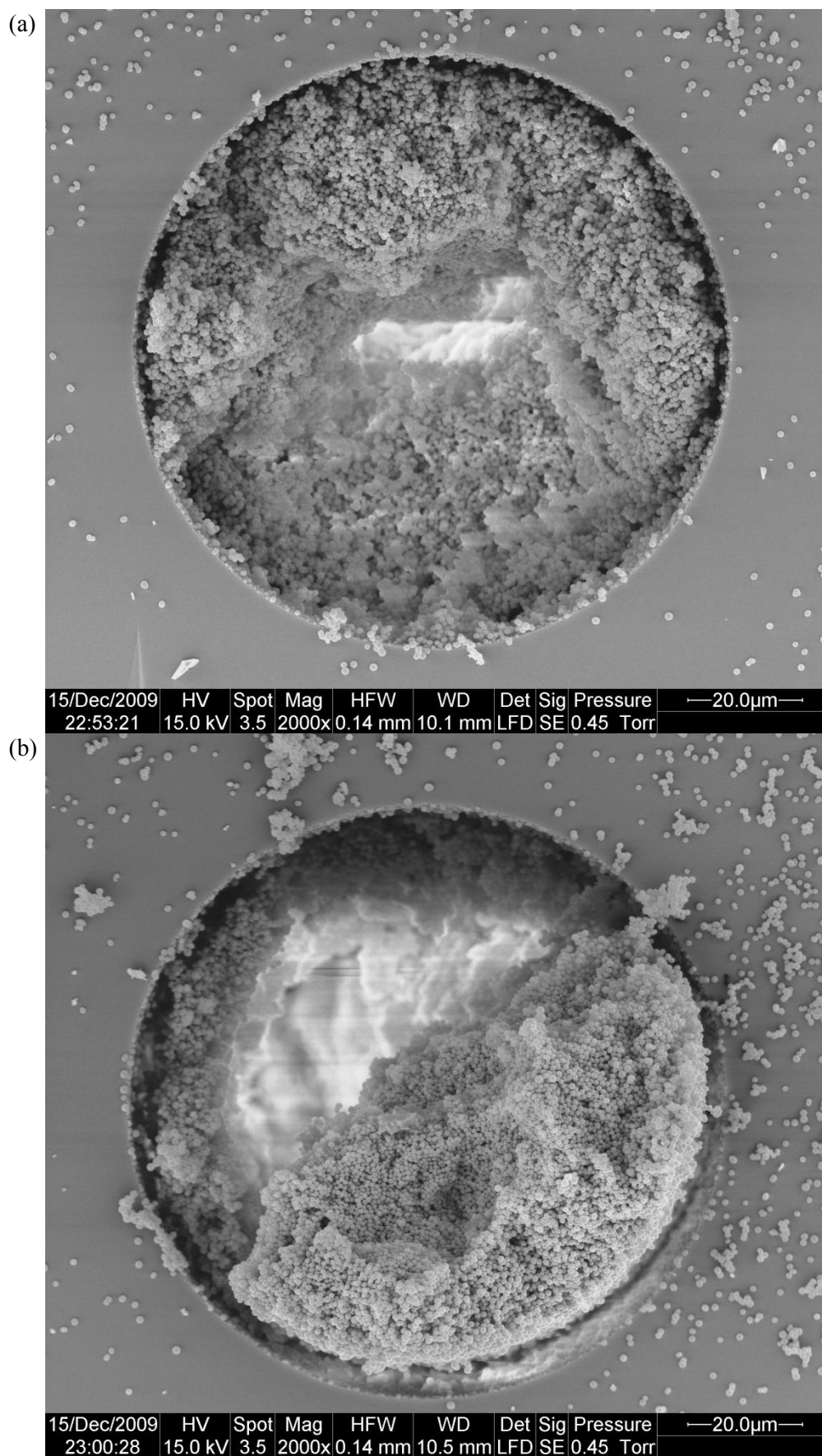


Figure 2.5 (a) UVGMA5 and (b) UVGMA6 formulation monolithic column cross-sections.

The images also confirm the expected trend of decreasing globule size with increasing microporogen content. Hence the pore size seems to have little effect on the permeability of the monolithic column in the formulations investigated.

The other property of PPM which directly affects flow and can be adjusted using the porogens is porosity, or total pore volume. **Table 2.1** also shows the percentage volume that the porogens occupy in the polymerisation mixture, calculated from the densities. As 1-dodecanol has a moderately higher density than cyclohexanol, the percentage porogen volume increases with higher 1-dodecanol content. While the difference between the percentage porogen volume of the UVGMA1 and UVGMA4 formulations is only 2%, the resulting increase in porosity seems to have a more significant effect on the permeability of the PPM than the decrease in pore size. This suggests that a more effective means to increase the permeability of a PPM may be to increase its porosity by increasing the formulation porogen content [6]. Interestingly, the high microporogen content formulations, UVGMA5 and UVGMA6, seem to afford PPM with reduced inter-globular linking to the point where the structure is not mechanically stable and falls apart into individual globules or beads, as can be seen in **Figure 2.5**. These individual globules may block the pore of the fixed structure, reducing permeability. Hence why the capillary columns prepared from formulations UVGMA5-6 were found to be less permeable than those prepared from the UVGMA4 formulation during flow testing.

Despite its superior permeability, monolithic columns prepared from the UVGMA4 formulation were still not sufficiently permeable for microreactor fabrication, this is further discussed in **Chapter 3, Section 3.2.3**. To further improve permeability the effect of increasing the porogen content was investigated. One should keep in mind that while an increase in porogen content improves permeability, it also reduces the surface area and mechanical stability of the PPM

[6]. The reduced surface area may lead to lower catalyst loading within the final microreactors, but the ability to pump liquid through the reactor without leakage was considered to be of greater concern than catalyst loading. Based on UVGMA4, two formulations were prepared by increasing the porogen content from 60 wt% to 70 wt% and 80 wt% respectively. These formulations are known as UVGMA4-70 and UVGMA4-80, details of which are given in **Table 2.1**. Monolithic capillary columns were prepared using these high porosity formulations and tested for flow as previously described. The mechanical strength of PPM prepared from the UVGMA4-80 formulation was too low and it was flushed out of the capillary during the post-polymerisation solvent flush.

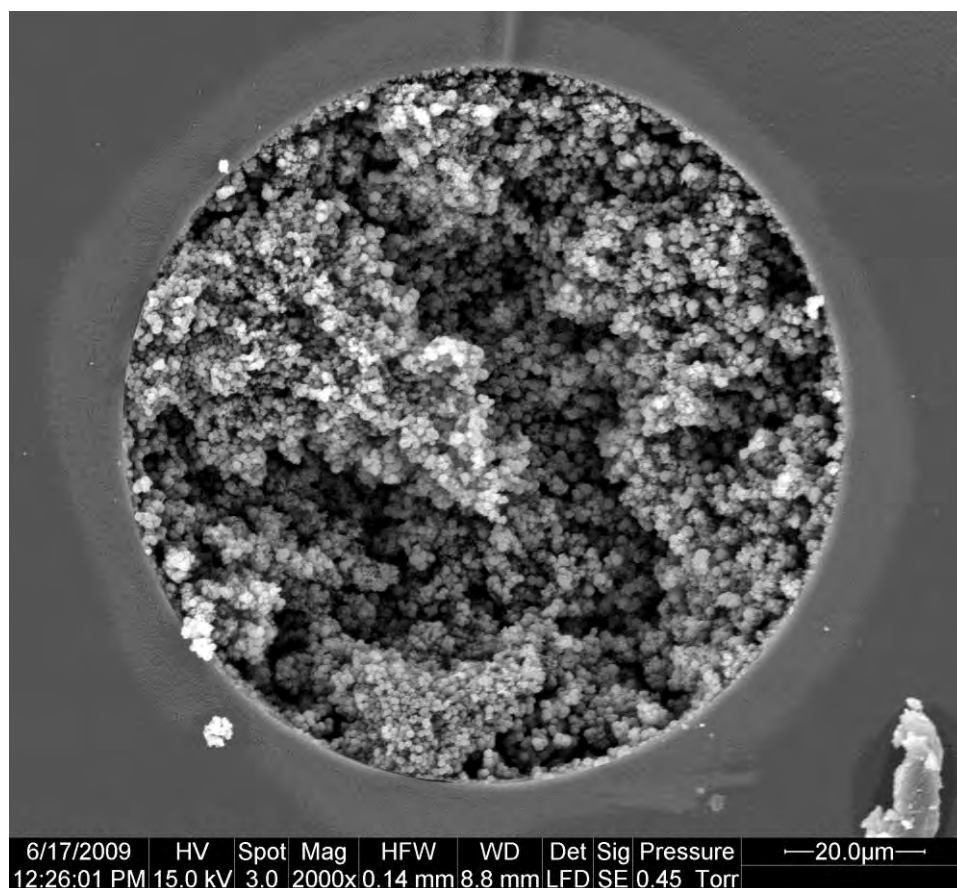


Figure 2.6 UVGMA4-70 formulation monolithic column cross-section.

PPM prepared from the UVGMA4-70 formulation was retained within the capillary column and showed greatly improved permeability over monolithic columns

prepared from the UVGMA4 formulation. A cross-sectional SEM image of a monolithic column prepared from the UVGMA4-70 formulation is shown in **Figure 2.6**, also indicates a more porous PPM than in **Figure 2.4(b)**.

2.3.2 Photoinitiated PPM in glass microchip

In flow-through microreactors, the residence time is similar to the reaction time for conventional reactions. In order to calculate the residence time, the length, the porosity of the PPM and the flow rate are required, discussed in more detail in **Chapter 4**. This requires relatively accurate control over the length of the monolithic column within the microchips. The monolith length is controlled by exposing the microchip through a photomask which only allows irradiation of the desired regions of the microchannel. In order to test the effectiveness of masking to control the region of PPM formation in the glass microchips, a microchip was masked according to the diagram in **Figure 2.7(a)** exposing approximately 60% of the channel length. PPM was formed within the masked microchip using the same polymerisation conditions as described in the previous section. PPM not only formed in the unmasked region, but also partially formed in the masked sections of the microchannel immediately adjacent to the exposed section. The PPM formation extended for just over 0.8 mm outside the masked regions. In order to reduce the extent of partial PPM formation in the masked regions, the masking positions were altered to that shown in **Figure 2.7(b)**. Partial PPM formation was still observed in the masked regions, including in the wells, most likely due to light scattered from the rough microchannel surface which was etched by powder blasting, see **Section 2.4.5**. Reducing the exposure time from 10 min to 1 min resulted in no PPM formed within the masked regions, but such a short exposure time is unlikely to be sufficient for complete polymerisation of the PPM within the exposed region.

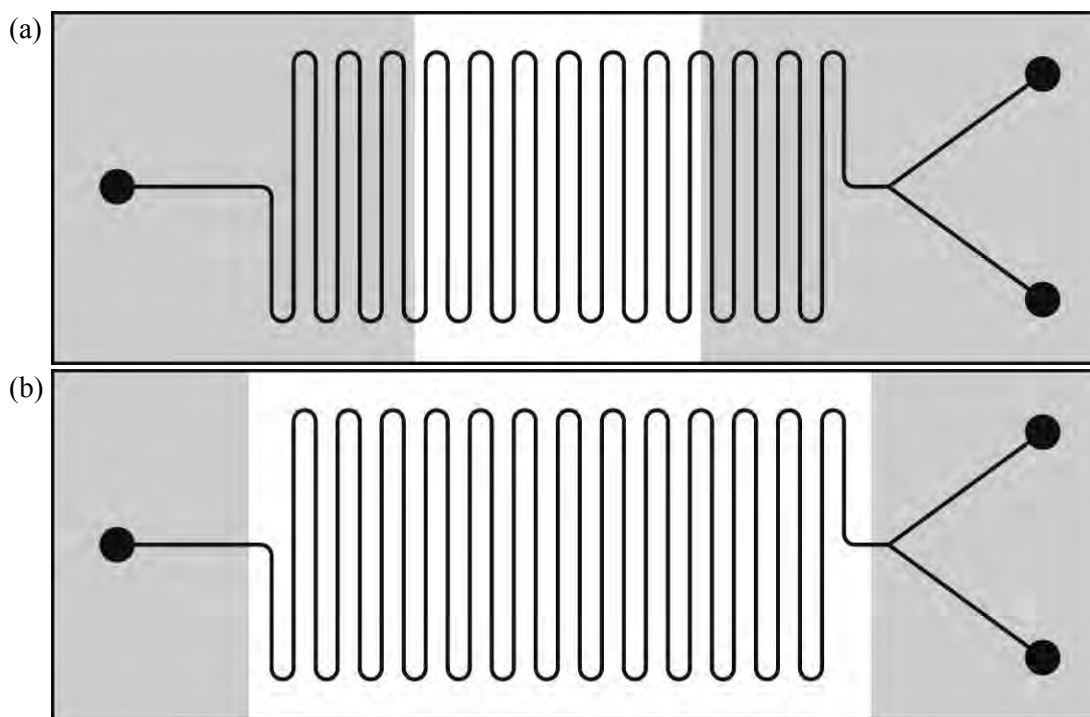


Figure 2.7 (a) Glass microchip short and (b) long (normal) masking.

To explore the effect of exposure time on the polymerisation, monolithic columns were prepared in 100 μm ID capillary using exposure times of 1, 2, 5, and 10 min. UVGMA1 was used for this study since no further optimisation of the formulation had been conducted at the time. The monolithic capillary columns prepared using different exposure times were tested for flow and imaged under SEM, as previously discussed in **Section 2.3.1**. Both the 1 min and 2 min exposures afforded monolithic columns with significantly improved permeability, which was likely due to increased porosity from incomplete polymerisation of the PPM. The SEM images for each of the monolithic columns prepared, shown in **Figure 2.8** and **Figure 2.9**, also reflect this trend as the PPM in **Figure 2.8(a)** (1 min exposure) is considerably more porous when compared to **Figure 2.9(b)** (10 min exposure). Limiting the polymerisation to improve PPM permeability has been demonstrated [52], however this can lead to significant inter-monolithic column variation as the short polymerisation time highlights the effects of subtle changes in the polymerisation conditions.

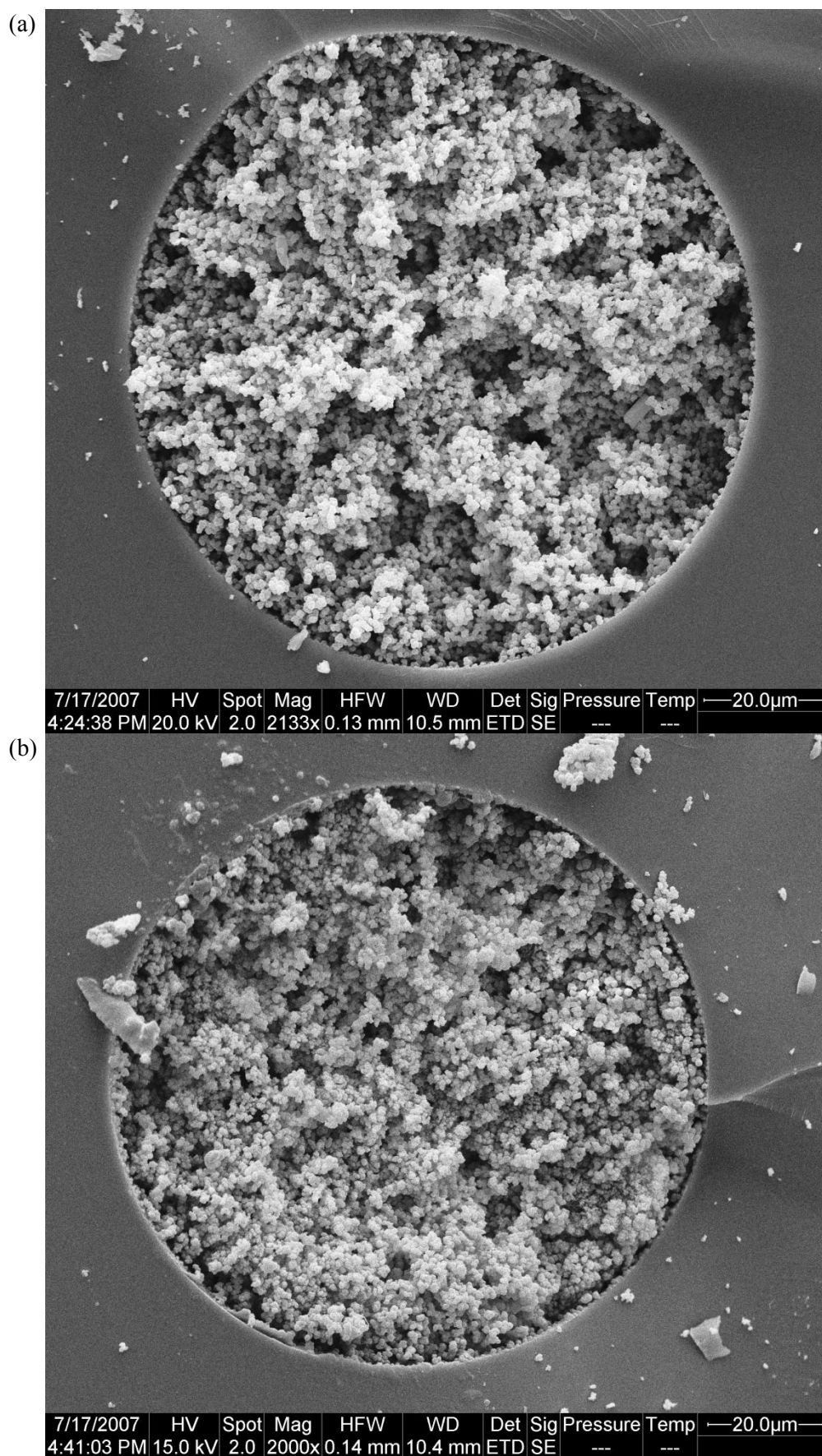


Figure 2.8 (a) UVGMA1 formulation monolithic column cross-section formed using 1 min exposure, (b) and 2 min exposure.

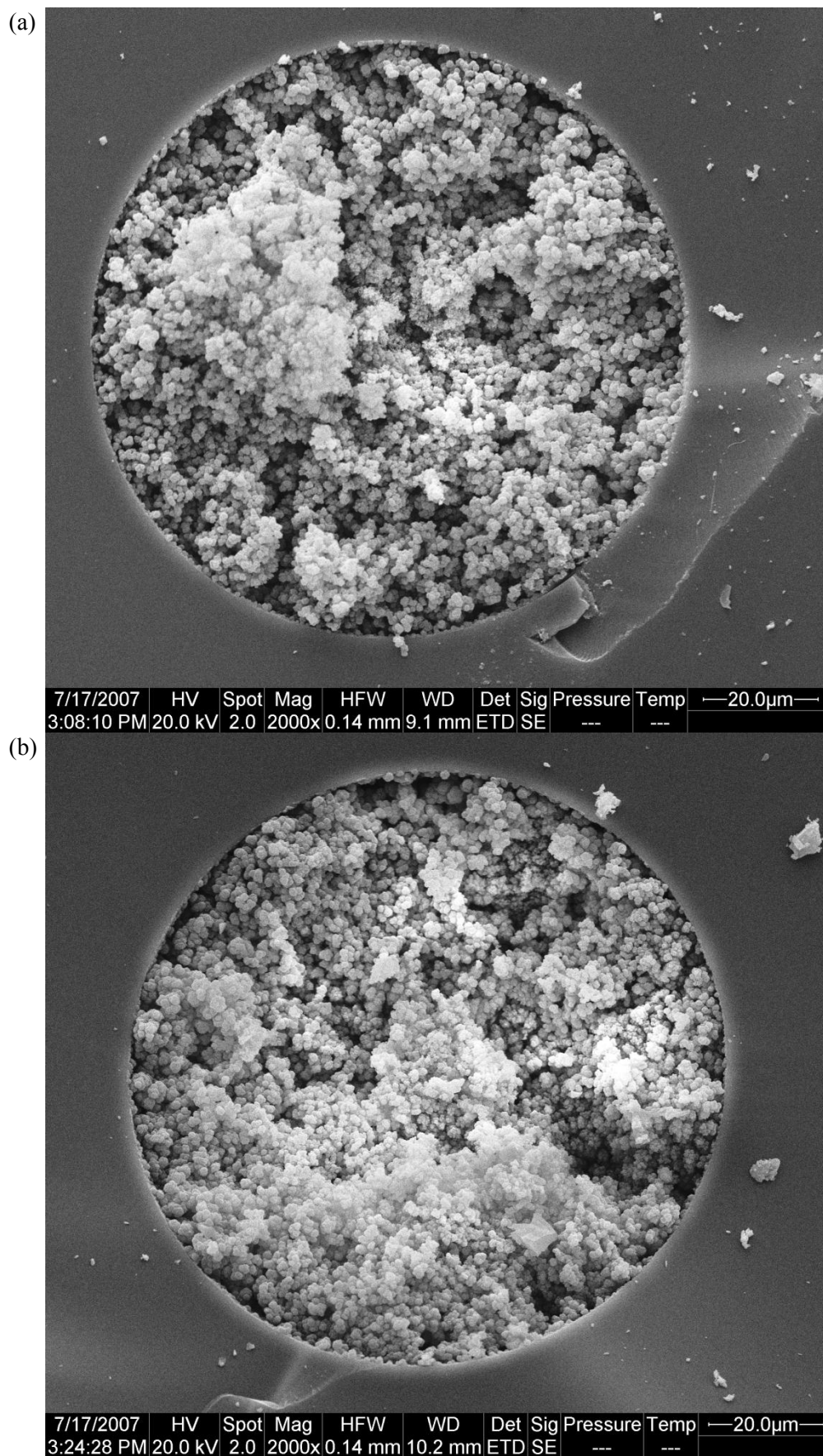


Figure 2.9 (a) UVGMA1 formulation monolithic column cross-section formed using 5 min exposure, (b) and 10 min exposure.

Another disadvantage of this approach is that the porosity and density of the PPM, required for determining microreactor loading and performance, cannot be easily quantified, this is further discussed in **Chapter 4**. The use of short exposure times to improve the masking was therefore not further pursued. Alternative methods for controlling the region of PPM formation were explored using the optimised UVGMA4-70 formulation.

A method commonly used to control the region of PPM formation for thermally initiated polymerisation of monolithic columns for CEC is by partial filling [13], where the capillary is only partially filled with polymerisation mixture. A potential problem with this approach is heterogeneous monolith formation at the interface between the filled and empty regions of the capillary. Depending on the choice of monomers and porogens, evaporation can occur in this region during polymerisation, resulting in different morphology from the main section of PPM. This should be insignificant when using photoinitiation with high boiling-point porogens, as the polymerisation is fast and performed at room temperature. This partial filling method was successfully used in the glass microchips to control the region of monolith formation in the microchip without the need for masking and prevented PPM formation in wells and in the Y-section of the microchannel. SEM cross-sectional images of the glass microchip monolithic columns are shown **Figure 2.20(b)**, **Figure 2.21** and **Figure 2.22** on pages 90-92. This approach has several limitations. Firstly, the ends of the polymerisation mixture are exposed to air, which may result in heterogeneous morphology in this region due to oxygen quenching of the polymerisation. Secondly, if the wells are not perfectly sealed the polymerisation mixture can move during polymerisation, which may adversely affect the homogeneity of the monolith. Clearly these powder blasted glass microchips are not suited for preparation of PPM's as scattering prohibited the use of photo-masking.

Devices with smoother channel walls may be more suitable due to reduced light scattering.

2.3.3 Alternative light sources for photopolymerisation of PPM

In this study, three different types of light sources were compared for photopolymerisation of PPM. The sources investigated were an OAI Inc. Model 30 flood exposure system, a Spectrolinker™ XL-1500 UV tube system, and an Opto Tech Corp. Shark Series™ UV-LED array. A summary of the basic properties of these sources is shown in **Table 2.2**.

	Model 30	XL-1500	UV-LED
Peak wavelength (nm)	N/A	365 or 254	365
Intensity (mW cm ⁻²)	20 @ 260 nm	5.5-6.5 @ 254 nm 4.4-5.0 @ 365 nm	0.76 @ 365 nm
Exposure area (cm ²)	452	1476	452
Power usage (W)	500	90	6
Cost (AUD)	\$25,000	\$5,000	\$750

Table 2.2 Properties of the different light sources investigated

As can be seen in **Table 2.2**, these light sources differ significantly in their output intensities, which in turn will affect the PPM formation. One of the goals of this section of research was to explore, and hopefully demonstrate the suitability of inexpensive light sources, such as LEDs, for preparation of monolithic columns in microchip.

The light source is the most crucial component in a photoinitiated polymerisation system as it determines the choice of photoinitiator and significantly

affects the choice of substrate. The light source discussed thus far is an OAI Inc. Model 30 arc-lamp flood exposure system, which is specifically designed for photolithography.

Arc-lamps are generally incorporated into flood exposure systems, but they are also often used just as point sources. These sources are characterised by a broad spectral range with narrow bands of high intensity dependent on the lamp material, as shown in **Figure 2.10**.

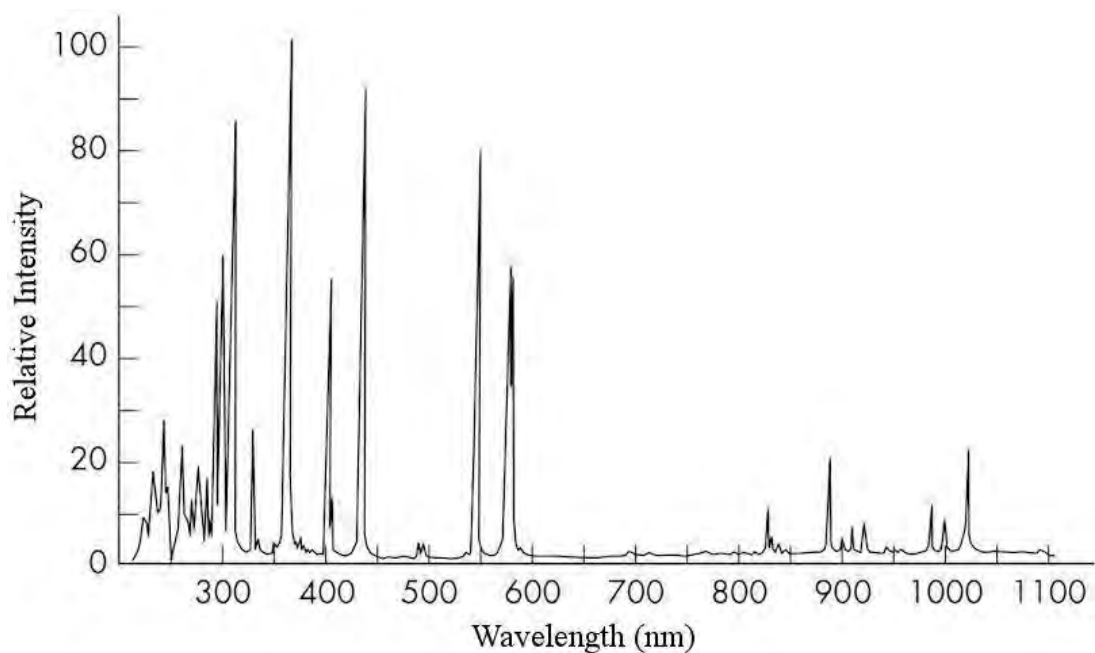


Figure 2.10 Mercury-xeon arc-lamp output spectrum, supplied by Ushio Inc.

Mercury lamps are used for near UV applications and mercury-xeon lamps for deep UV applications. The optics of a general exposure system includes a reflector, which focuses the light from the lamp into a beam homogeniser to ensure uniform intensity across the light beam, which then is finally passed through a collimating lens so that the light pencils are parallel. Flood exposure systems feature specialised power supplies that are able to automatically regulate the lamp power to maintain a constant intensity. As the lamp can take several minutes to reach stable operating conditions after ignition, an electronically controlled shutter is used to control the exposure. Arc

lamps have high power requirements and relatively short lifetimes, in the order of 200-2000 h. They also require large currents during operation and high voltages during ignition of the lamp which makes the operation of these lamps potentially hazardous. Mercury arc-lamps have been utilised for near UV photopolymerisation of PPM both as point sources [15, 25, 31, 37, 49] and integrated in dedicated flood exposure systems [8, 53]. Flood exposure systems using Hg-Xe arc-lamps have also been used for deep UV photopolymerisation of PPM [36, 47]. While arc-lamps are excellent UV sources for photoinitiated PPM, they are not commonly used due to their associated costs. The setup cost of a flood exposure system is \$20,000-\$25,000 AUD and replacement lamps are \$500-\$1000 AUD each. The most frequently used light source for photoinitiated polymerisation of PPM are UV tubes, in both the near UV [4, 16, 22, 27, 28, 32, 34, 35, 38, 40, 44, 50, 54-56] deep UV regions [29, 30, 42, 57].

UV tube sources have been primarily developed for UV curing of polymer coatings in industrial applications. They can be incorporated into a range of different exposure systems, ranging from microprocessor controlled exposure chambers, such as the Spectrolinker™ XL-1500 UV crosslinker investigated, to hand held devices. These tubes are characterised by three different peak spectra regions, 365 nm for UVA, 310 nm for UVB, and 254nm for UVC. UVA and UVB tubes are fluorescent, whereas the UVC tubes are discharge lamps. The UVA and UVB tubes make use of a fluorescent coating to produce the desired spectral output from the discharge output, which causes the output to be relatively broad. The output from the UVC tubes is comparatively narrow. The XL-1500 was fitted with either UVA or UVC tubes, the spectra for which are shown in **Figures 2.11** and **2.12**, respectively. UV tube sources are characterised by long warm-up times, diffuse output, irreproducible

and fluctuating intensity. For curing of thin films, only the total exposure energy is important and fluctuating intensity is not detrimental to the curing process.

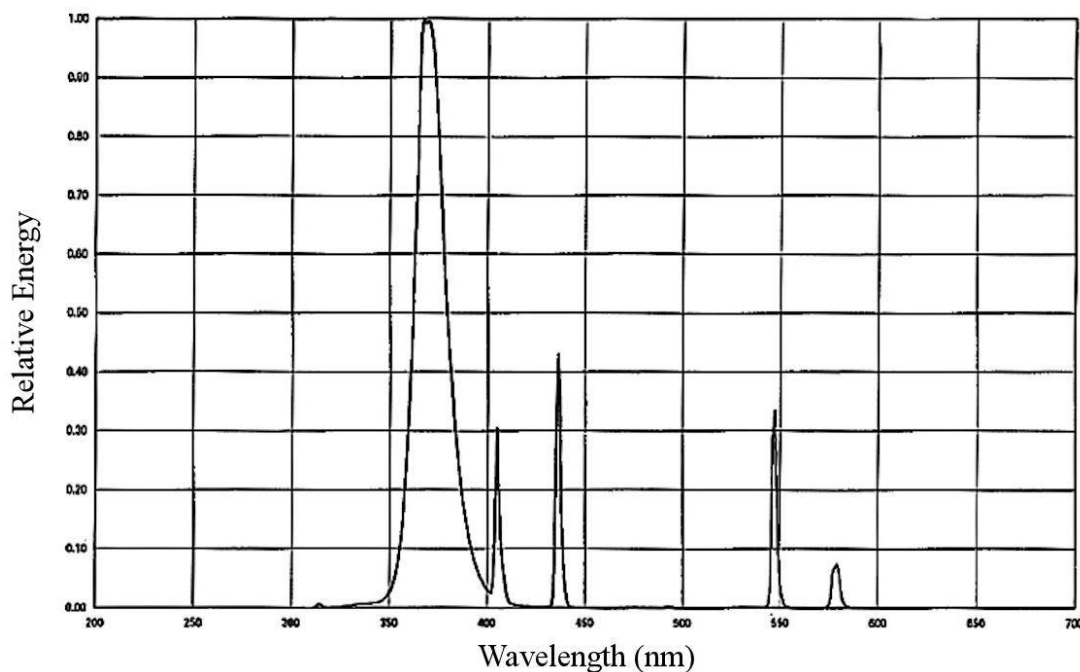


Figure 2.11 Spectrolinker XL-1500 UVA (365 nm) UV tube output spectrum, supplied by Spectroline Corporation.

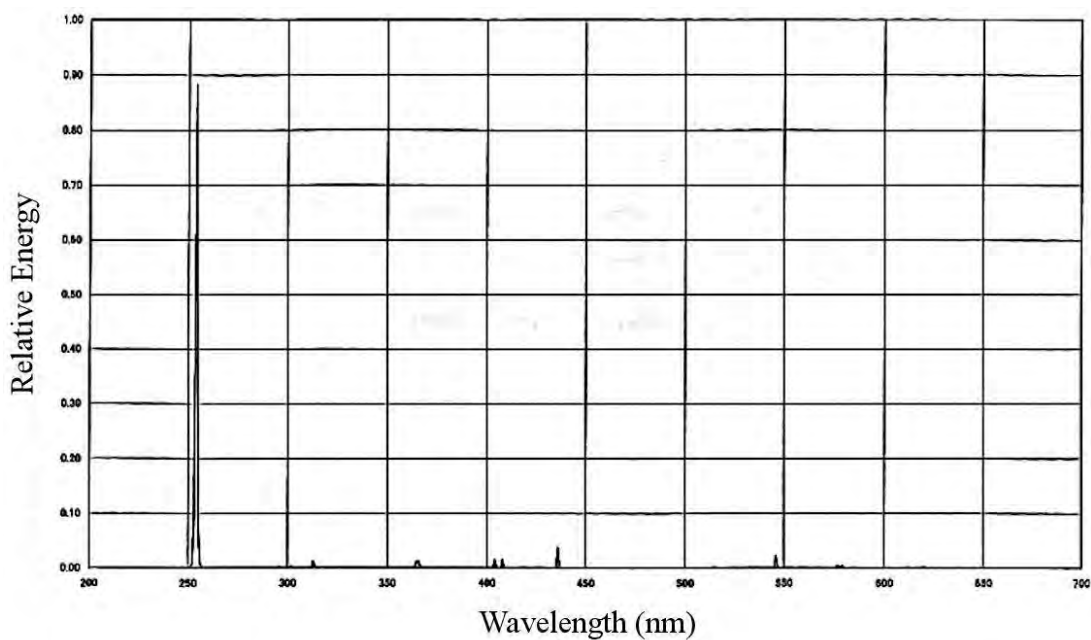


Figure 2.12 Spectrolinker XL-1500 UVC (254 nm) UV tube output spectrum, supplied by Spectroline Corporation.

The setup cost of UV tube sources are relatively low, \$1,000-\$5,000 AUD depending on the intensity and exposure area required. The lifetime of the tubes ranges from 500-5000 h, however the output intensity moderately decreases as the tubes age. Replacement tubes cost approximately \$30 AUD each. UV tube sources have only moderate power requirements and are quite safe to use. For PPM formation, the fluctuating intensity can potentially lead to poor inter-monolithic column reproducibility and the diffuse output reduces the effectiveness of masking to control the region of PPM formation.

An alternative light source that has recently been applied to UV curing and photochemistry in industrial and research applications are Light Emitting Diodes (LEDs). LEDs are solid state light sources which have been used in consumer electronics for decades in the visible region. It has been only in recent years that high intensity LEDs in the UV region have been developed, and wavelengths down to 254 nm are now commercially available. LEDs have many benefits over traditional light sources, including virtually no warm-up time, highly reproducible intensity, narrow output spectrum, low heat generation, high efficiency, very long lifetimes of 10,000-100,000 h, and low setup and operational costs. One limitation of LEDs is their size and limited scalability. Typically LEDs are relatively small with a light emitting area less than 1 mm² with output of approximately 30 mW. For large scale exposures, the limited output area and intensity is generally overcome by using arrays of LEDs which can be either a number of individual components in close proximity or a number of components integrated into a single component. LED exposure units typically cost \$500-\$5000 AUD, depending on intensity and area (i.e. array size). An example of such a LED array in the near UV region is the Opto Tech Corp. Shark Series™ UV-LED, which is an array of 50 365 nm LEDs on a single die. The output spectrum for this light source is shown in **Figure 2.13**. Common

LEDs have built-in optics that control the angle of the output light cone, which is typically 30 ° for LED arrays.

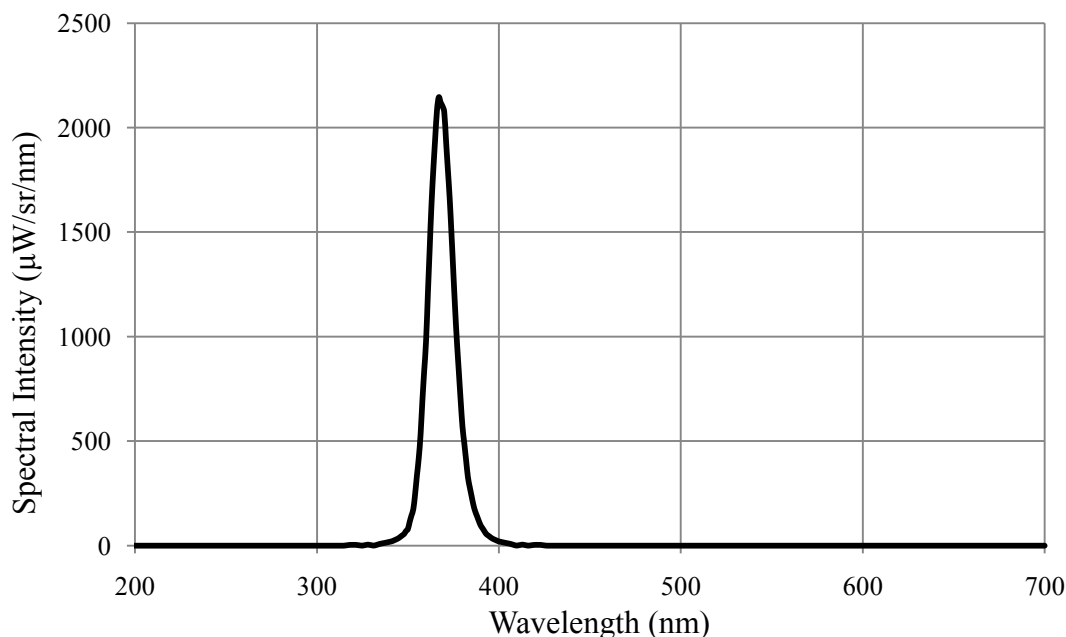


Figure 2.13 Optotech Shark Series™ UV-LED output spectrum, supplied by Optotech Corporation.

While the light produced is not collimated, the light angles are sufficiently small to be effective for photolithography [58]. Recently, photoinitiated polymerisation of PPM using LEDs has been demonstrated in both the visible [23, 33] and UV [45] regions. Abele *et al.* were able to form poly(GMA-*co*-EDMA) monolithic columns in fused-silica capillary and polymer microchips using a single 370 nm LED with dimethylaminobenzophenone (DMABP), also known as Michler's ketone. A major problem with this initiator is that the chromophore remains intact after radical generation, which stains the polymer yellow and reduces the penetration of light into the polymerisation mixture.

While light source choice is very important for photopolymerisation of thick film polymers and PPM, it is also equally important to choose an appropriate initiator that complements the source spectrum [59]. Photoinitiators are divided into two

types, type I and type II, depending on the mechanism by which they generate radicals. Type I photoinitiators are photosensitive molecules that undergo a unimolecular direct fragmentation process, typically α -cleavage, upon the absorption of light to form radicals. The fragmentation of the molecule often destroys the chromophore and forms fragments with lower molar absorbance, known as photobleaching. This allows the incident light to penetrate further into the polymerisation mixture and improves the homogeneity of the radical generation rate with depth. In the opposite case, the fragments have higher molar absorbance than the parent molecules and greatly diminish light penetration. Common type I initiators include benzyl ketals (such as DMPAP), α,α -dialkoxyacetophenones, α -hydroxy alkylphenones, α -aminoalkylphenones, and acylphosphine oxides (such as BAPO) [60]. Unlike type I, type II photoinitiators, which are generally benzophenone derivatives [60], do not directly fragment to form radicals. Absorption of light energy results in an excited state leading to a bimolecular reaction, typically hydrogen abstraction, with a co-synergist, usually a tertiary amine, to generate radicals. The co-synergist is incorporated in the initiator molecule with some type II initiators, such as with DMABP. Generally photoinitiators with high molar absorptivities within the exposure region are preferred, however in some applications a high molar absorptivity can actually be detrimental to the polymerisation as it greatly reduces the exposure depth. Type I photoinitiators are preferred for free radical polymerisation as they have higher activities.

For preparation of PPM, a photoinitiator must fulfil the following requirements:

1. Rapid generation of radicals upon exposure to improve morphology homogeneity and give complete polymerisation in a reasonable time.

2. Moderate molar absorptivity in the exposure region as a high molar absorptivity will reduce the penetration of the light leading to heterogeneous morphology.
3. The photodecomposition products are transparent in exposure region.

The development of the UVGMA4-70 formulation was performed using the Model 30 with DMPAP as the initiator, which has been shown to be a good match of source and initiator [36, 47]. DMPAP is a commonly used initiator for the preparation of PPM, due to its relatively high activity because of its ability to undergo a secondary fragmentation to generate four radical fragments instead of the typical two generated by initiators such as AIBN [51]. DMPAP was also investigated for use with the XL-1500 UVC since it is also a deep UV source and is also known to be an effective combination for PPM formation due to its complementary spectrum [30].

For near UV sources, AIBN is by far the mostly commonly used photoinitiator [4, 16, 22, 28, 35-38, 56], despite having relatively low molar absorptivity and low activity [51]. DMPAP has also been used with near UV sources for the preparation of PPM [31, 49], however it was not investigated for near UV photopolymerisation because it is known to photodarken in this region which could potentially lead to poor morphology [59]. Bis(2,4,6-trimethylbenzoyl)phenylphosphine oxide (BAPO or Irgacure® 819) has been successfully utilised for polymerisation of thick polymer films using LED sources [59] and has been reported for the preparation of photo-polymerised sol-gel monolith [61] but not for the preparation of PPM. BAPO is a highly active photoinitiator with a wide absorbance range extending from the deep UV into the visible region. Its high activity arises from the high molar absorptivity and generation of four radicals during

photolysis, like DMPAP. Unlike DMPAP, BAPO photobleaches in the near UV, making it suitable for PPM preparation in this region.

The UV-LED was used for the investigation of near-UV photopolymerisation as initiators active enough to give complete polymerisation with the UV-LED were expected to also yield a fully formed PPM when using the higher intensity XL-1500 UVA. PPM was prepared in 100 μm ID fused-silica capillary at various exposure times using either AIBN or BAPO. Using AIBN as the initiator with the UVGMA4 formulation, PPM was prepared in fused-silica capillary using exposure times of 40, 60 and 180 min. SEM images, shown in **Figures 2.14** and **2.15(a)** respectively, of the capillaries cross-sections were used to assess the degree of polymerisation and to analyse the PPM morphology. After 40 min exposure with AIBN as the initiator, monolith had only formed on the capillary walls, **Figure 2.14(a)**. PPM formed in the centre of the capillary may have been flushed out during the solvent flush. At 60 min exposure there was significantly more PPM formed, however the polymerisation did not extend across the capillary cross-section, leaving the centre of the capillary devoid of polymer, see **Figure 2.14(b)**. Even at 180 min exposure a significant void between the capillary wall and PPM in the centre was observed, as shown in **Figure 2.15(a)**. BAPO was initially trialled with UVGMA4 using an exposure time of 60 min, during which complete polymerisation was achieved, as shown in **Figure 2.15(b)**. The PPM formed had excellent morphology, which suggests that BAPO is highly suitable for PPM formation using low intensity near UV sources. The exposure time required to achieve complete polymerisation with BAPO was investigated using the UVGMA4-70 formulation in 100 μm ID capillary by using exposure times of 5, 10, 20, and 40 min. After only 5 min of exposure, significant PPM was found, as shown in **Figure 2.16(a)**. Despite the severe charging in **Figure 2.16(a)**, a radial gradient of globule sizes can be observed, indicating incomplete

polymerisation. At exposure times of 10 min and 20 min, the radial uniformity of the globule sizes were improved, but the porosity of the 10 min exposure, **Figure 2.16(b)**, appears to be greater than the 20 min exposure, **Figure 2.17(a)** which may indicate incomplete polymerisation at 10 min exposure. While minor differences could be observed between the 20 min and 40 min exposures, **Figure 2.17**, little difference was observed between the 40 min and 60 min exposures, implying that polymerisation was complete at 40 min. Therefore, 40 min was adopted as the preferred exposure time for BAPO based polymerisation mixtures with the UV-LED.

The exposure time required to achieve complete polymerisation with BAPO using the XL-1500 UVA was investigated using the UVGMA4-70 formulation in 100 μm ID capillary. The exposure times investigated were 5, 10, 20, and 30 min as significantly shorter exposure times than required for the UV-LED were expected based on the increased intensity. The SEM images of the capillaries cross-sections obtained are shown in **Figures 2.18 and 2.19**. After 5 min exposure PPM had only formed on the capillary walls, as shown in **Figure 2.18(a)**. This result was highly unexpected as the same exposure time using the UV-LED afforded a significantly further polymerised PPM. Intuitively, the higher intensity should yield a higher radical generation rate and therefore faster PPM formation. At 10 min exposure the PPM was still not completely polymerised as illustrated by the radial gradient in globule size seen in **Figure 2.18(b)**. Very little difference between the radial globule sizes and porosity was observed between 20 and 30 min exposure, **Figure 2.19**, implying that the polymerisation reaches completion before 20 min. This exposure time was used for photo-polymerisation of PPM when using the XL-1500 UVA with BAPO. Upon close inspection of the capillary monolithic columns prepared using the XL-1500 UVA with BAPO, small regions devoid of PPM at irregular intervals along the length of the capillary were observed.

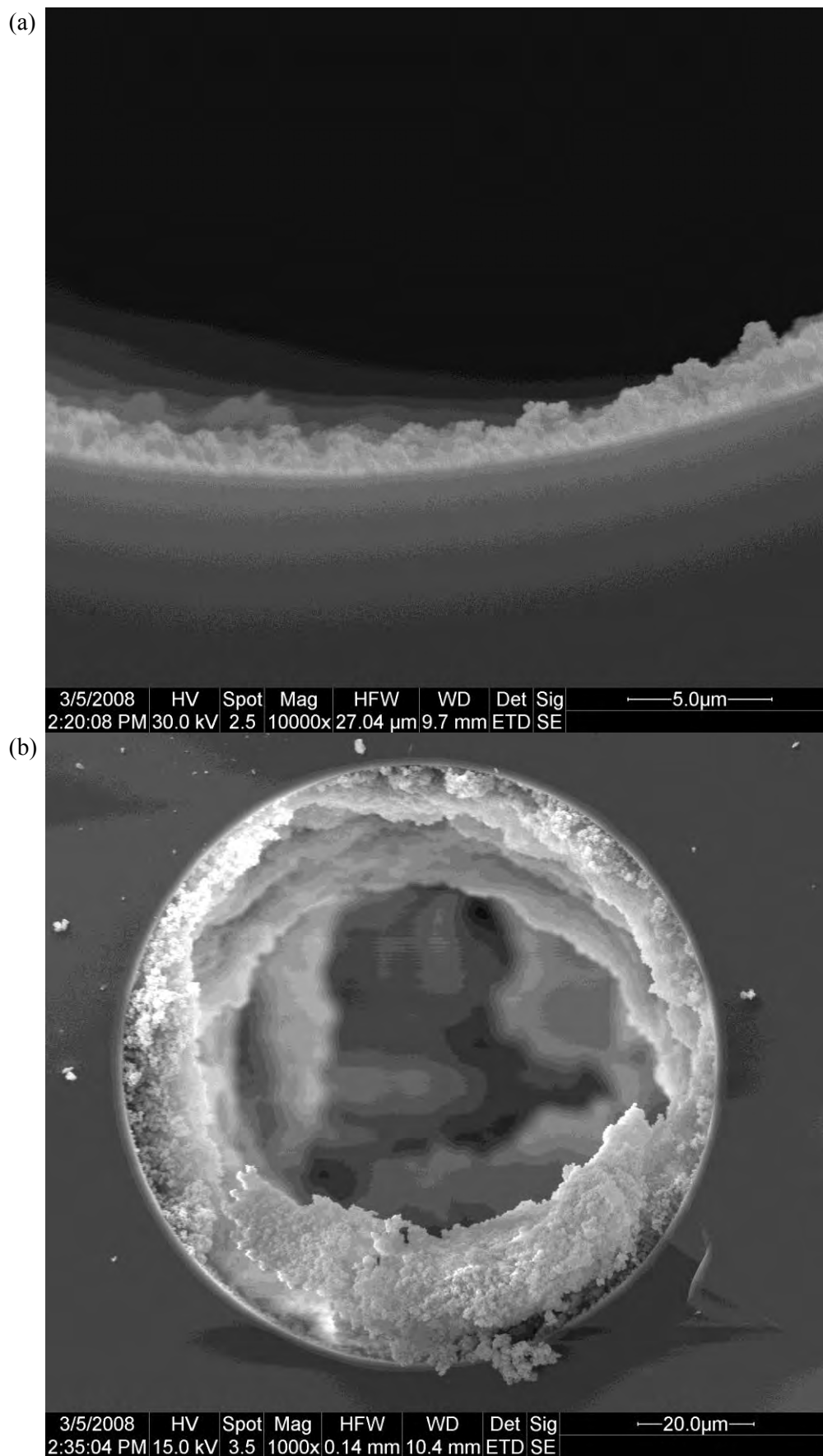


Figure 2.14 (a) Monolithic column cross-section formed with the UV-LED and AIBN using a 40 min exposure, (b) 60 min exposure.

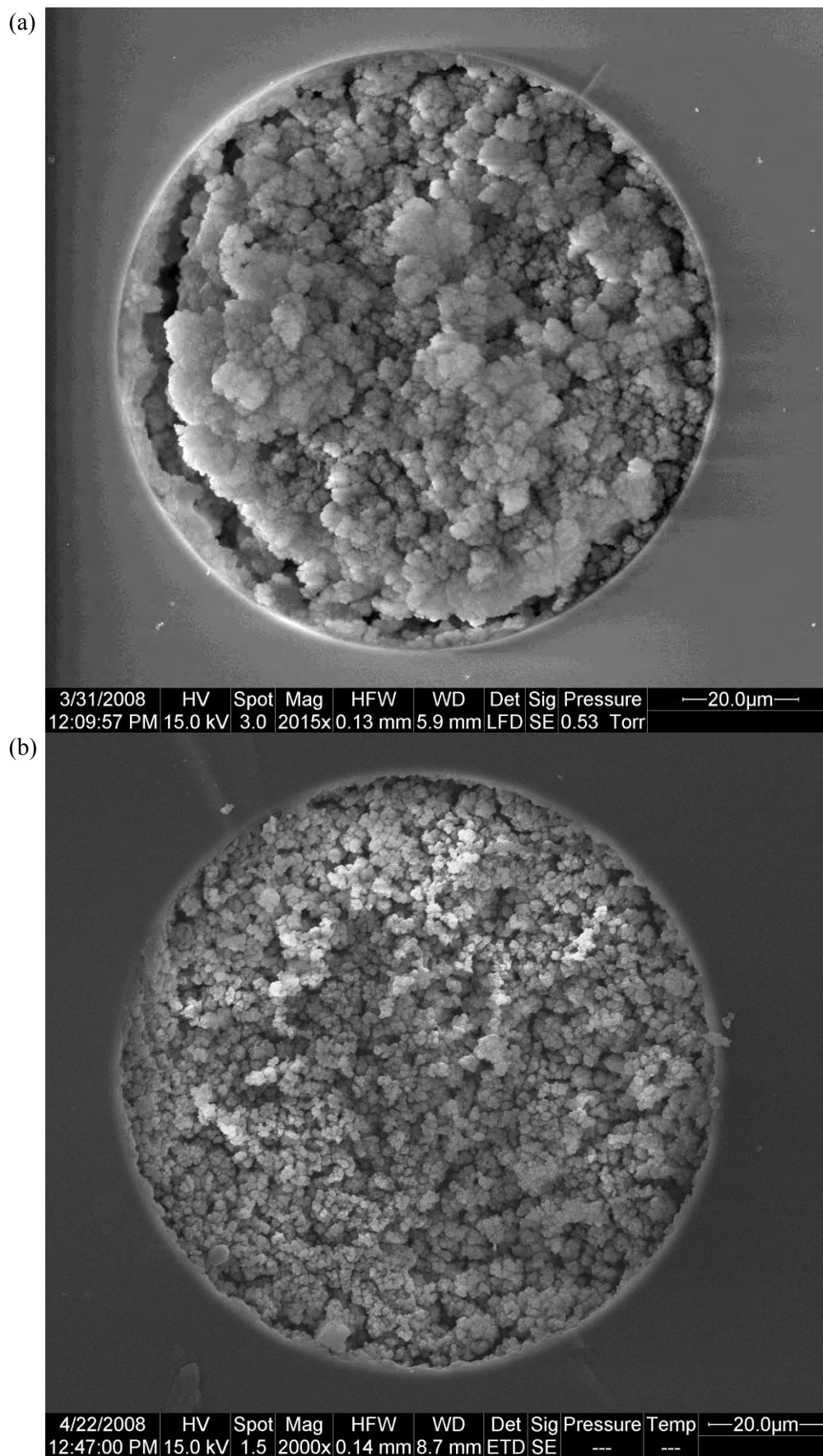


Figure 2.15 (a) Monolithic column cross-section formed with the UV-LED and AIBN using a 180 min exposure, (b) 60 min exposure with BAPO.

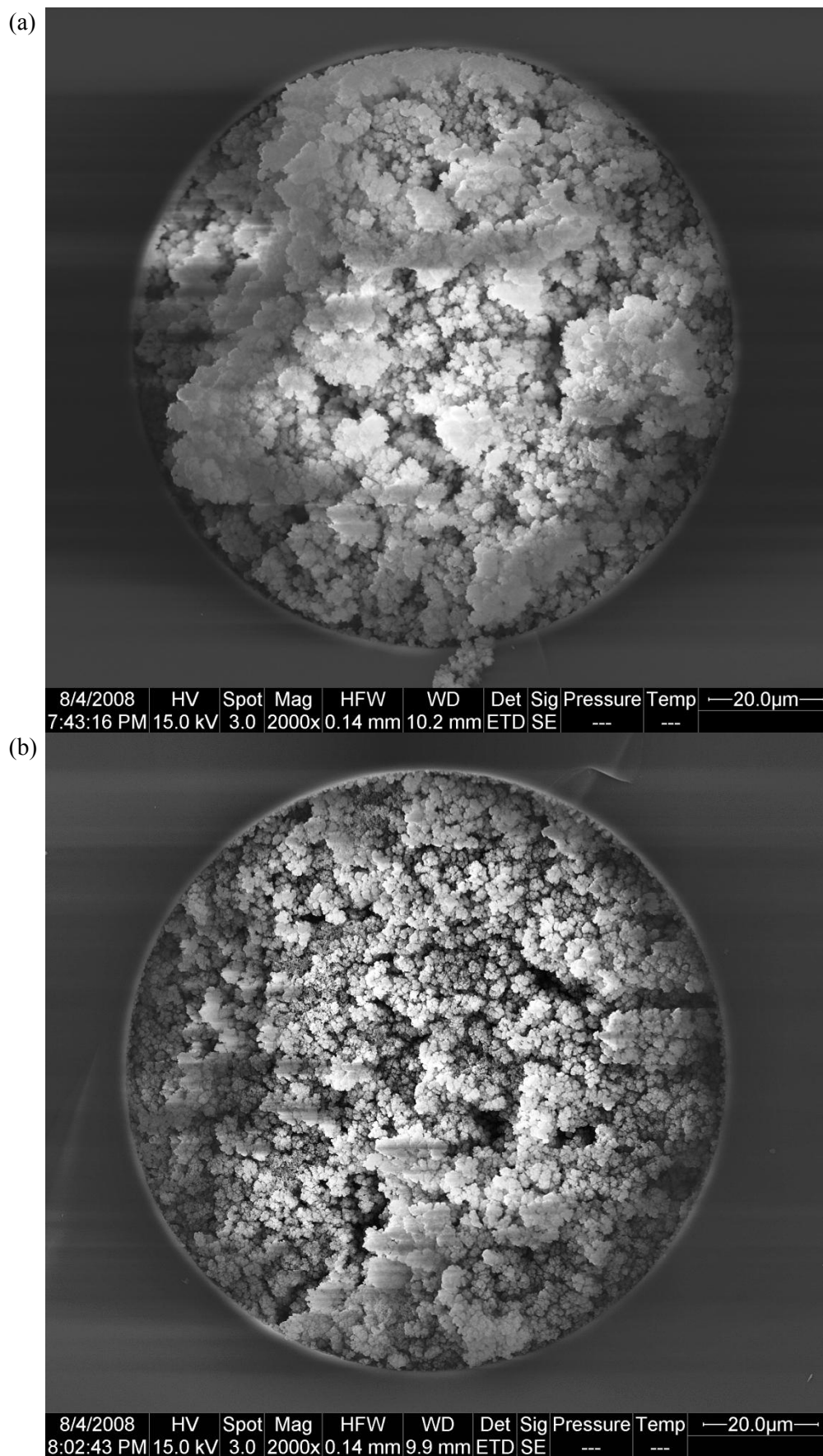


Figure 2.16 (a) Monolithic column cross-section formed with the UV-LED and BAPO using a 5 min exposure, (b) a 10 min exposure.

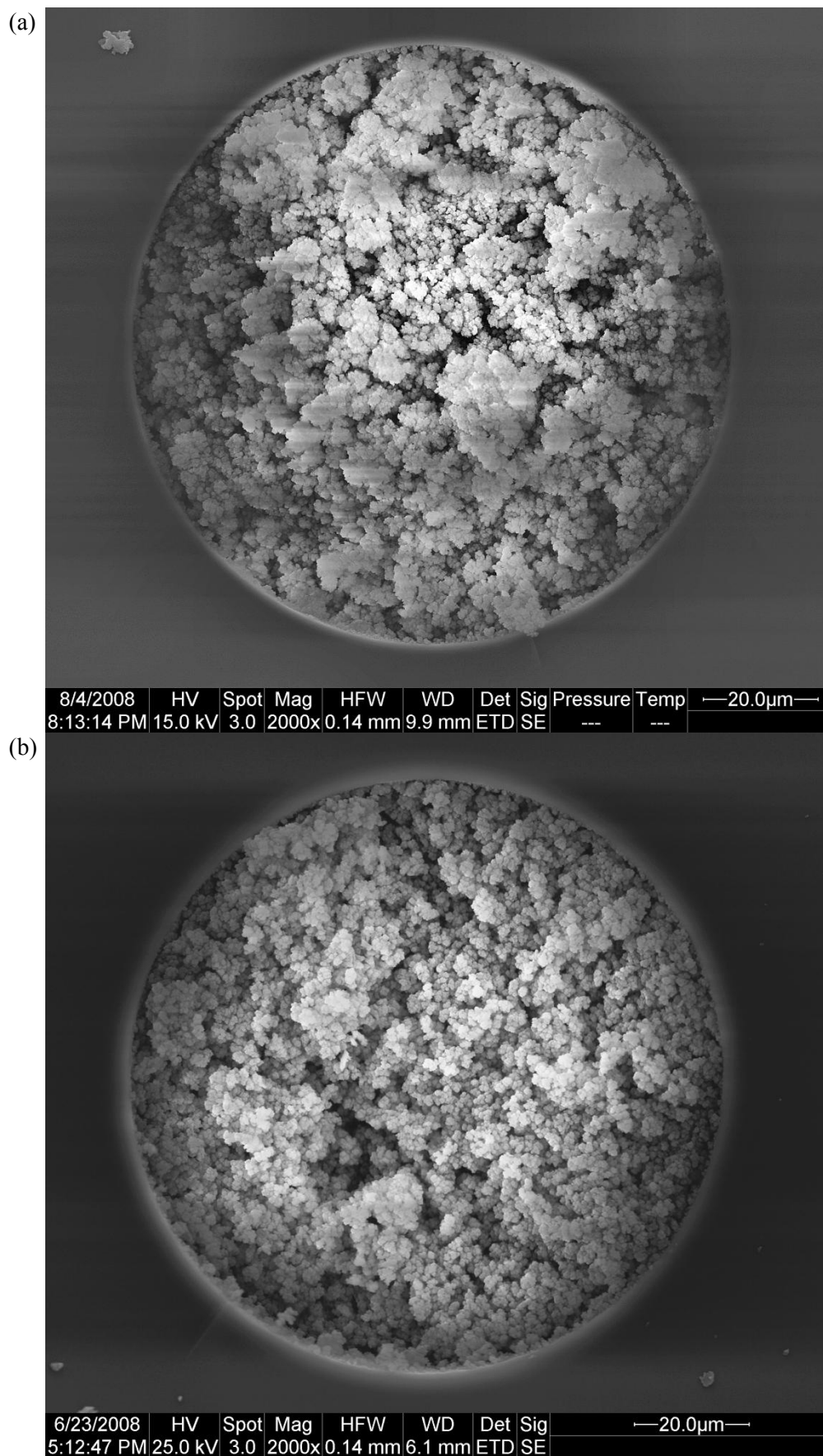


Figure 2.17 (a) Monolithic column cross-section formed with the UV-LED and BAPO using a 20 min exposure, (b) 40 min exposure.

The voids were also observed when using the Model 30 or XL-1500 UVC with BAPO. They were not present when using the UV-LED as the light source, and using different batches of surface treated capillary and polymerisation mixtures made no difference to the formation of the voids. This suggests that either there is significant spatial intensity variation within the XL-1500, or that BAPO does not function as a radical initiator when the exposure intensity is above a certain threshold. Intensity measurements taken at 365 nm within the XL-1500 UVA, using an OAI Inc. Model 306 intensity meter, at different locations in the exposure area, showed no significant variation. To test if the void formation was dependent on intensity, PPM was formed in 100 μm ID fused-silica capillary through several sheets of borosilicate glass to attenuate the light. The intensity was reduced to 2 mW cm^{-2} using a 2 cm depth of glass, which was still much higher than the 0.7 mW cm^{-2} UV-LED. Forming PPM by exposing through the glass reduced the formation of the voids, but it did not eliminate them entirely. BAPO was found to be only suitable as a photoinitiator for preparation of capillary monolithic columns when using the UV-LED.

Preparation of PPM using XL-1500 UVC with DMPAP was investigated using the UVGMA4-70 formulation in 100 μm ID capillary. As DMPAP has similar activity to BAPO, a 20 min exposure was used. This was found to be sufficient to give complete polymerisation when using the XL-1500 UVA. The SEM cross-section of the monolithic column in **Figure 2.20(a)** shows uniform globule sizes across the capillary and similar porosity to previously obtained images of fully polymerised UVGMA4-70, **Figure 2.6** on page 65. Exposure times developed for 100 μm ID capillary were applied for the preparation of monolithic columns in borosilicate microchips using the various combinations of light sources and initiators, using the UVGMA4-70 formulation.

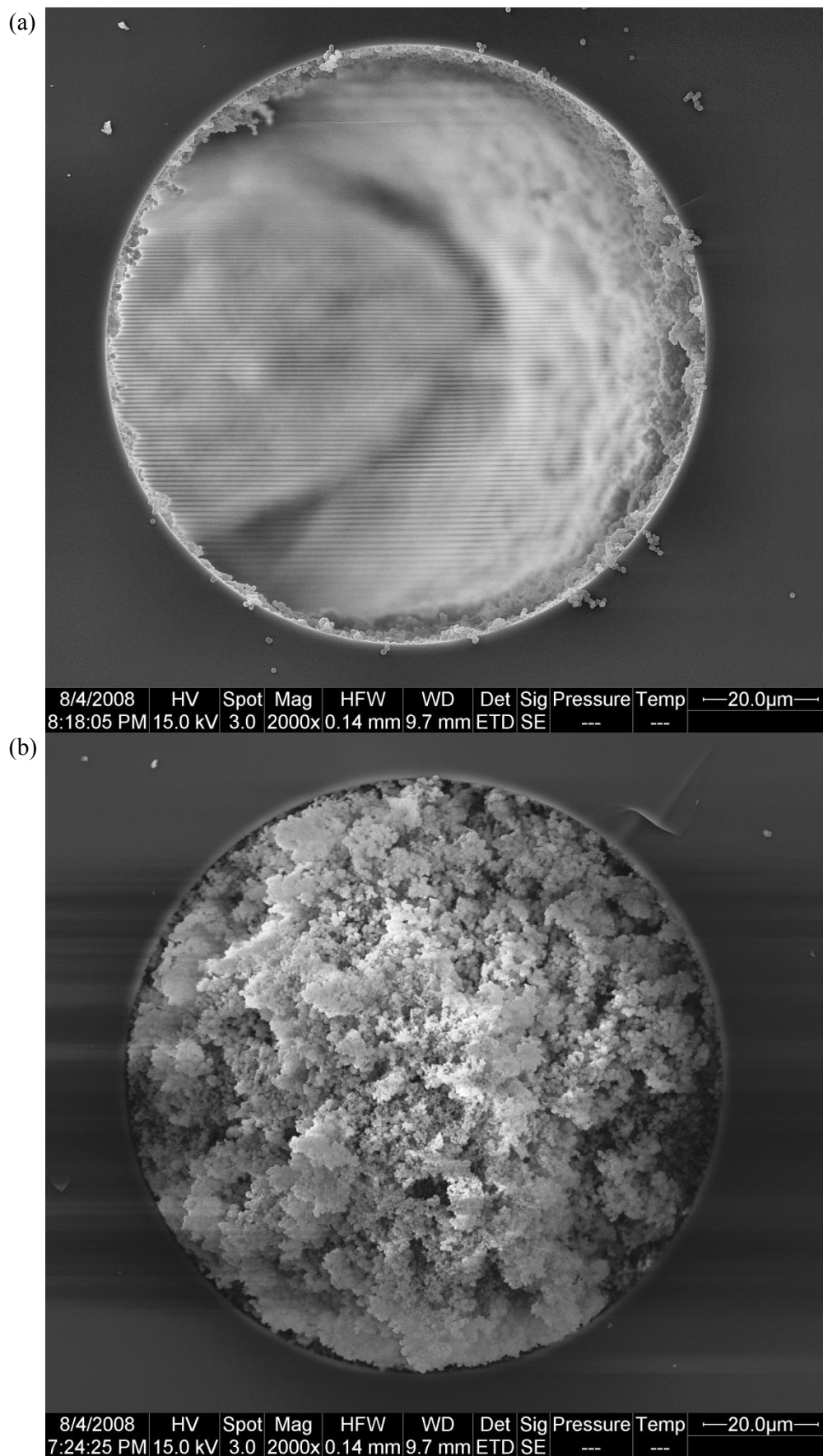


Figure 2.18 (a) Monolithic column cross-section formed with the XL-1500 UVA and BAPO using a 5 min exposure, (b) 10 min exposure.

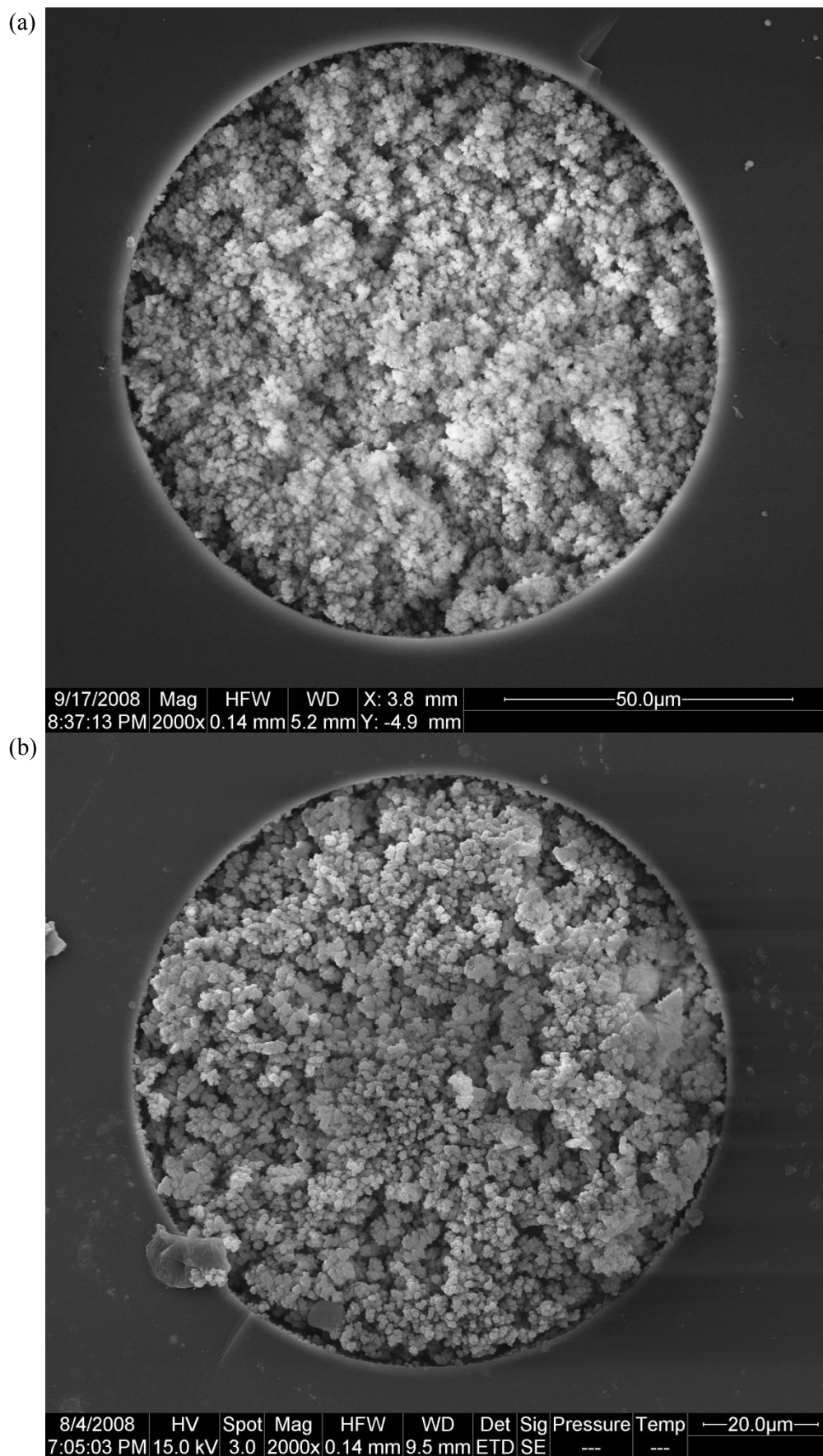


Figure 2.19 (a) Monolithic column cross-section formed with the XL-1500 UVA and BAPO using a 20 min exposure, (b) 30 min exposure.

SEM images of the microchip monolithic column cross-sections obtained for each combination are shown in **Figures 2.20(b) to 2.22**. With the exception of PPM formed using DMPAP with the XL-1500 UVC, all of the monolithic columns formed in borosilicate microchips showed excellent morphology and appeared to be fully polymerised. Each of these microchips had excellent flow-through properties and were easily flushed with methanol at $60 \mu\text{L h}^{-1}$. As expected the morphologies of the monolithic columns in the microchips are dissimilar due to differences in the polymerisation conditions. The microglobular sizes for PPM prepared using BAPO, in **Figures 2.21 and 2.22(a)**, were considerably smaller than for PPM prepared using DMPAP, **Figures 2.20(a) and 2.22(b)**, which is likely due to faster polymerisation kinetics. These SEM images also reveal the considerable variation in the channel dimensions of the borosilicate microchips, which is further discussed in **Chapter 5**. When using DMPAP with the XL-1500 UVC, the PPM failed to completely polymerise, as depicted in **Figure 2.22**. While the PPM formed normally near the top of the microchannel, the region closest to the exposure source, considerably less PPM formation was found in the regions further away from the source. This suggests that the light was not able to penetrate the full depth of the microchannel, which may result from poor transmission of the 254 nm radiation through the borosilicate microchip and/or the photodarkening of DMPAP, preventing penetration beyond the surface layer. If the light was being moderately attenuated by the borosilicate, then an increase in the exposure time should result in a greater degree of polymerisation. To test this, PPM was formed while increasing the exposure time to 40 min, which resulted in the same degree of polymerisation as observed for the 20 min exposure, as assessed by SEM imaging. This suggests that photodarkening of DMPAP is most likely limiting the monolith formation. This problem was not observed when using the Model 30 as the light source as its output spectrum is comparatively broad and is

approximately four times greater in intensity. DMPAP was found to be unsuitable as a photoinitiator for the photo-polymerisation of PPM in glass microchips using the XL-1500 UVC as the exposure source. The voids that formed when monolithic columns were prepared in capillary using the XL-1500 were not observed when the equivalent monolithic columns were prepared in borosilicate microchips. This could be due to intensity attenuation by the borosilicate provided the rough channel surface did not disable visualisation of the voids.

The successful combinations of light source and initiator for 100 μm ID fused-silica capillary were the Model 30 and XL-1500 UVC with DMPAP, and the UV-LED with BAPO. The successful combinations for glass microchips were the Model 30 with DMPAP, the XL-1500 (both UVA and UVC) and UV-LED with BAPO. Due to problems incurred with the XL-1500, the Model 30 with DMPAP and the UV-LED with BAPO were used for the remainder of this work.

2.4 Photopolymerised PPM in plastic devices

Plastic microreactors are attractive for several reasons, as discussed in **Chapter 1**, including relatively easy and rapid fabrication, excellent reproducibility, and low cost. Generally, plastic substrates are employed to fabricate microdevices rather than pure polymers as plastics contain additives which alter the material's physical properties and improve stability [62]. These additives may include fillers, plasticisers, heat stabilisers, antioxidants, and UV stabilisers which improve the material's machinability and shelf-life. Common plastics such as polymethylmethacrylate (PMMA), polycarbonate (PC), polyester, polystyrene, polyvinylchloride (PVC), and PDMS have been utilised for microdevice fabrication [62].

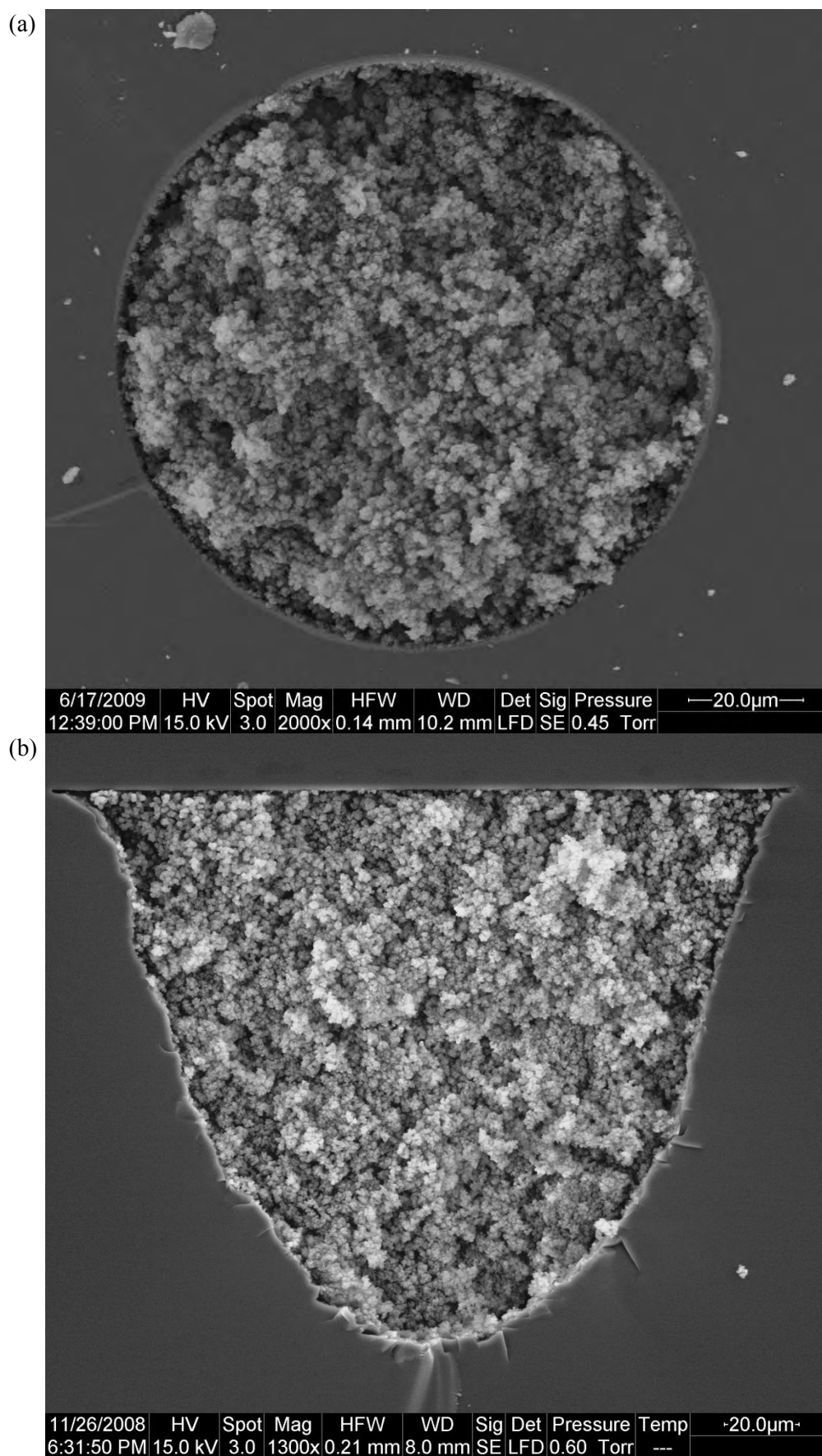


Figure 2.20(a) Cross-section of PPM formed in capillary with the XL-1500 UVC and DMPAP, **(b)** PPM formed in microchip with the Model 30 and DMPAP.

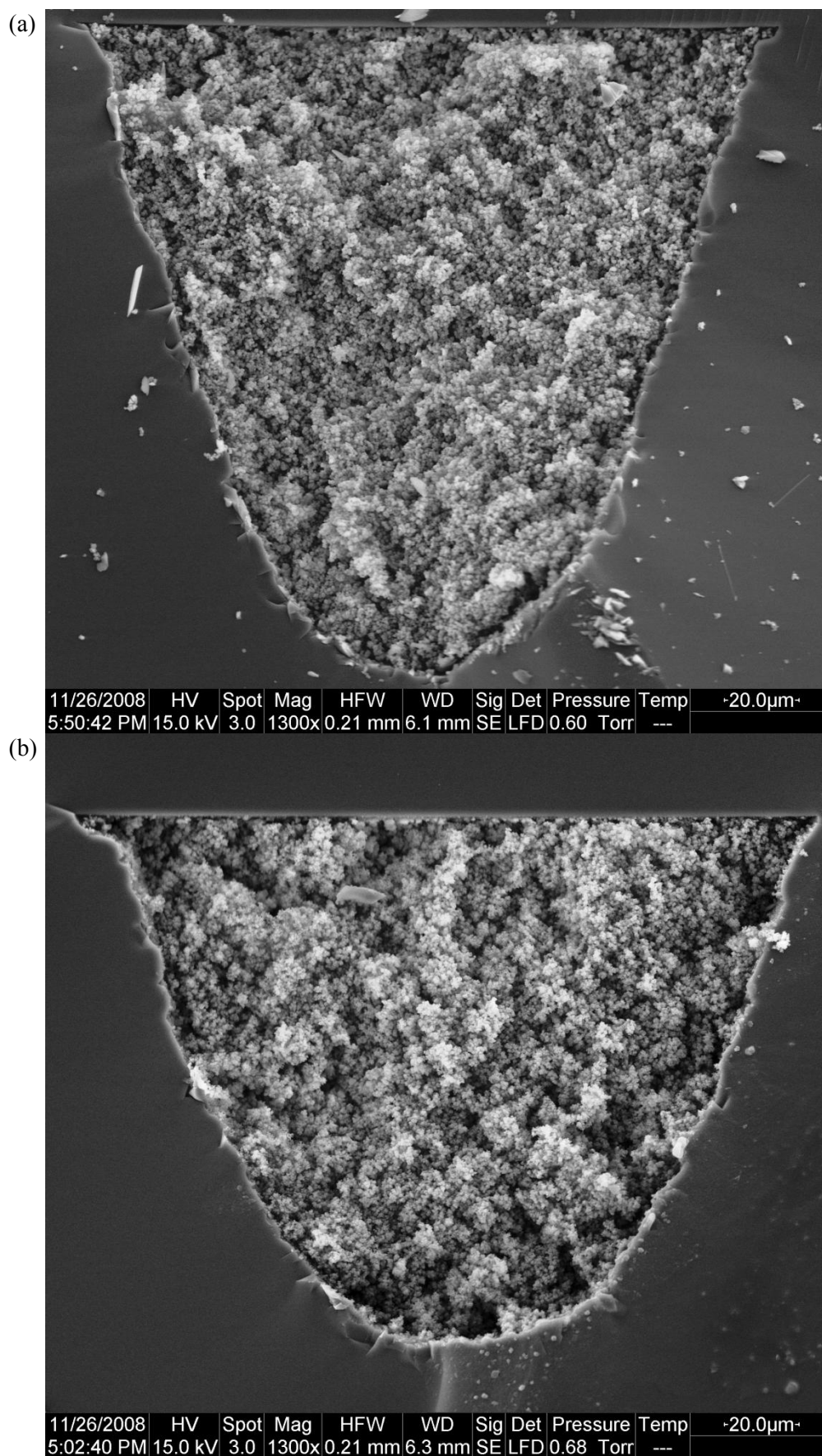


Figure 2.21(a) Cross-section of PPM formed in microchip using BAPO with the UV-LED **(b)** using BAPO using with the XL-1500 UVA.

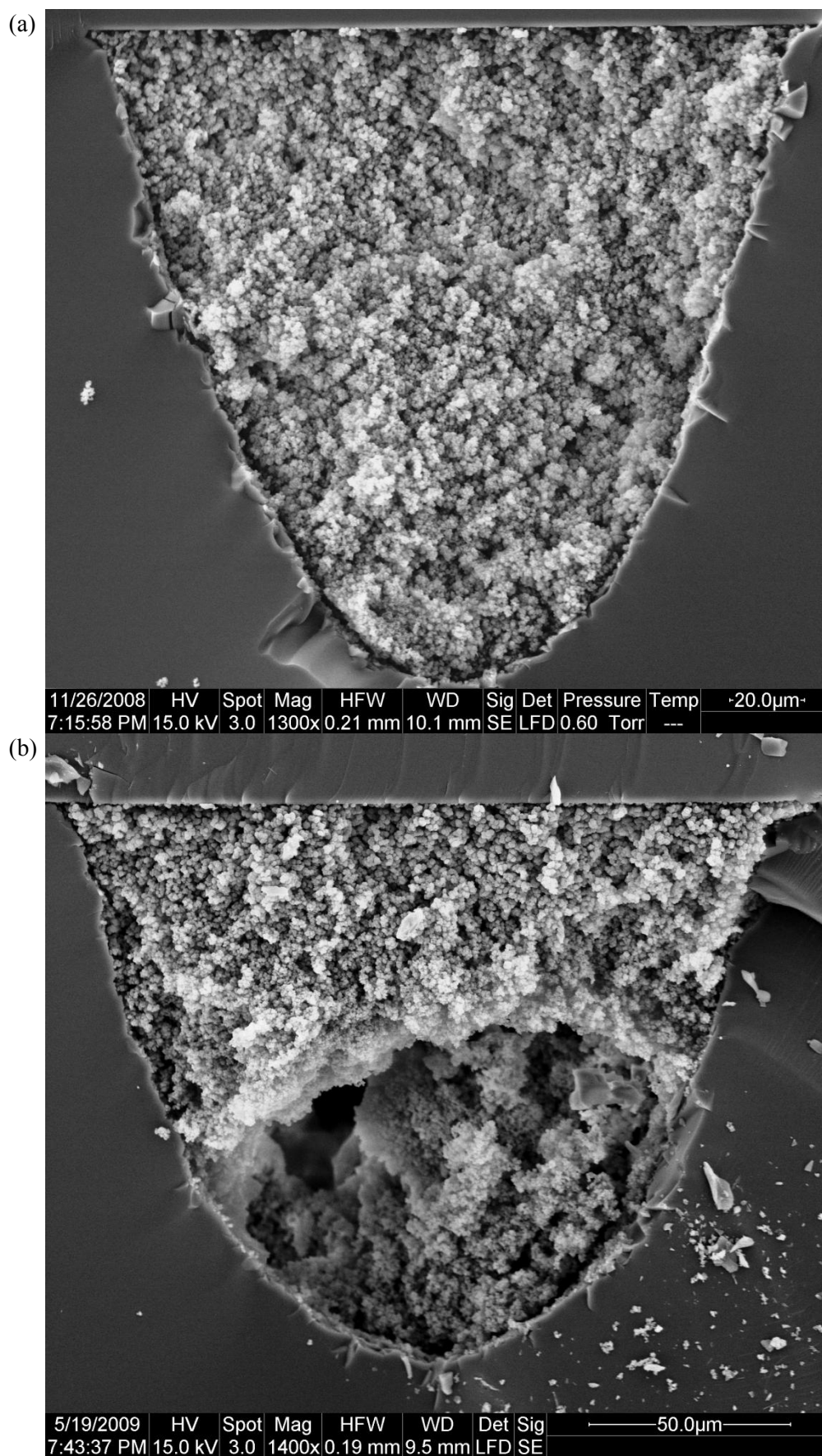


Figure 2.22(a) Cross-section of PPM formed in microchip using BAPO with the XL-1500 UVC **(b)** using DMPAP with the XL-1500 UVC.

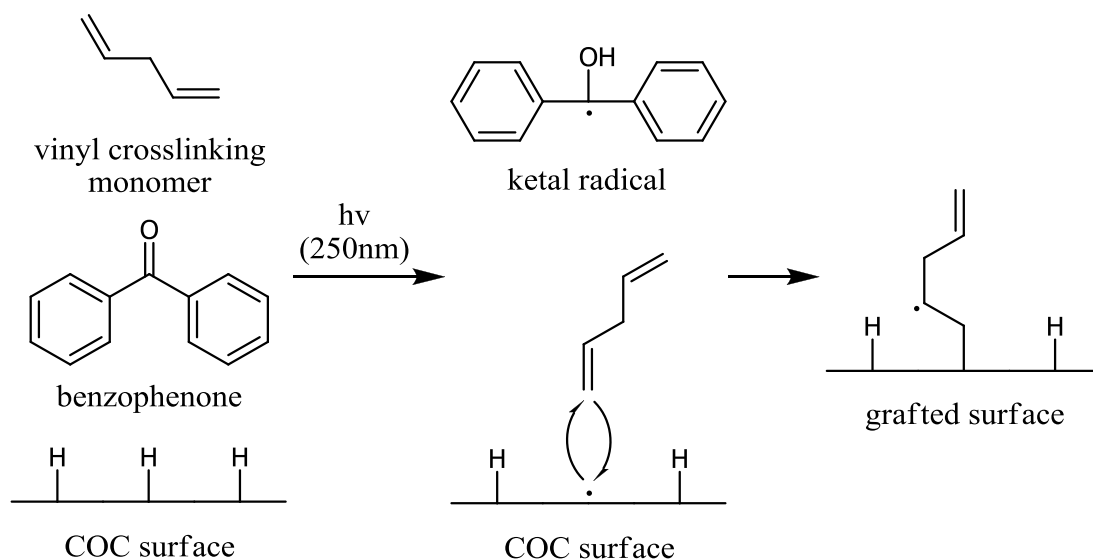
However many of these substrates are not suitable for preparation of PPM-based microreactors due to solvent and chemical incompatibility, low melting points, or poor optical transmission properties [62]. Rohr *et al.* investigated a range of different plastics for UV initiated polymerisation of monolithic columns and found that the most suitable plastic was cyclic olefin copolymer/cyclic olefin polymer (COC/COP) due to its excellent chemical compatibility, optical properties, and relatively high thermal stability [63]. COC was investigated here as plastic substrate for microreactors as it has excellent deep UV transmission and only contains an antioxidant additive, whereas COP generally contains several additives which may interfere with microreactor fabrication and performance [43]. The goal of this work was to create the first plastic microchips for flow-through supported palladium catalysis using PPM's for catalyst immobilisation. Since the Suzuki-Miyaura reaction performed at 80 °C was targeted as a model reaction (**Chapter 4**), the devices need to be fully functional at this temperature.

2.4.1 Choice of COC grade

COC is a co-polymer formed by addition polymerisation of norbornene and ethylene and is produced commercially by Ticona under the trade name TOPAS®. COC is relatively chemically inert and is compatible with a wide range of solvents, except for non-polar aromatic solvents like toluene. Several different grades with varying thermal and optical properties are available, based on different ratios of the two monomers.

Due to its relative inertness, modification of the surface chemistry of COC-based devices is difficult by chemical means as the polymer does not contain reactive functional groups. The introduction of vinyl groups to the microchannel surface, required for PPM adhesion, has been achieved via photografting of monomers onto the COC surface using benzophenone (BP) [39]. This method was developed by

Stachowiak *et al.* and is based on using BP as a hydrogen abstracting photoinitiator to create radicals on the surface of the COC, enabling reaction with the vinyl monomers. A simplified reaction scheme for the photografting of COC with a vinyl crosslinking monomer is shown in **Scheme 2.1**.



Scheme 2.1 Photografting of COC surface with a vinyl crosslinking monomer.

The grafting mechanism works as follows: upon irradiation BP abstracts hydrogen from a secondary or tertiary carbon on the surface of the polymer, forming a surface bound radical and a ketal radical. The surface bound radical adds across one of the double bonds of vinyl crosslinking monomer in solution, forming a bond and the radical moves to the second carbon of the vinyl group, as shown in **Scheme 2.1**. The ketal radical is unable to initiate polymerisation with vinyl monomers due to its stability and steric bulk. Chains are formed from the polymer surface by radical polymerisation, which continue to grow until terminated by a ketal radical or by an adjacent polymer chain. As terminal ketal groups can be photolytically cleaved off to continue the polymerisation, the polymerisation continues while irradiated until all the monomers are consumed. This provides limited control over the grafted chain

length by limiting the exposure time. The photografting results in polymer chains containing vinyl groups covalently bound to the COC surface.

The most important step of the photografting procedure is the initial generation of the surface radical by hydrogen abstraction. The mechanism for this process was elicited by Rånby *et al.* [64]. Upon irradiation BP becomes excited and forms a singlet state, which itself is unable to abstract hydrogen. The excited molecule transfers some of its energy to the substrate and transitions from a singlet to a „superheated’ state. The molecule then undergoes intra-system crossing to form the triplet state which can abstract hydrogen from the excited substrate. Rånby *et al.* found that ~250 nm radiation is necessary to generate the initial singlet and that hydrogen abstraction does not occur in its absence [64]. In-channel photografting with BP therefore requires the polymer substrate to be at least partially transparent around 250 nm. Other examples of hydrogen abstracting photoinitiators are mostly based on benzyl ketones and have the same mechanism as BP, requiring deep UV radiation to achieve photografting [65, 66]. Currently, no near UV hydrogen abstracting photoinitiators suitable for photografting appear to have been reported.

Three grades of COC have been investigated as potential substrates for microreactors, namely 5013S-04, 6013S-04, and 6015-04 which have glass transition temperatures of 134 °C, 138 °C, and 158 °C, respectively. The glass transition temperature is the temperature at which the plastic deforms, not its melting temperature. Since the glass transition temperatures are above 80 °C, microreactors fabricated from these grades should not deform under the reaction conditions proposed.

Plates (1 mm thickness) of the three grades were obtained and tested for thermal resistance, deep UV transmission, and suitability for photografting. UV

transmission spectra were obtained between 200-400 nm for each of the three grades, which are shown in **Figures 2.23-2.25**.

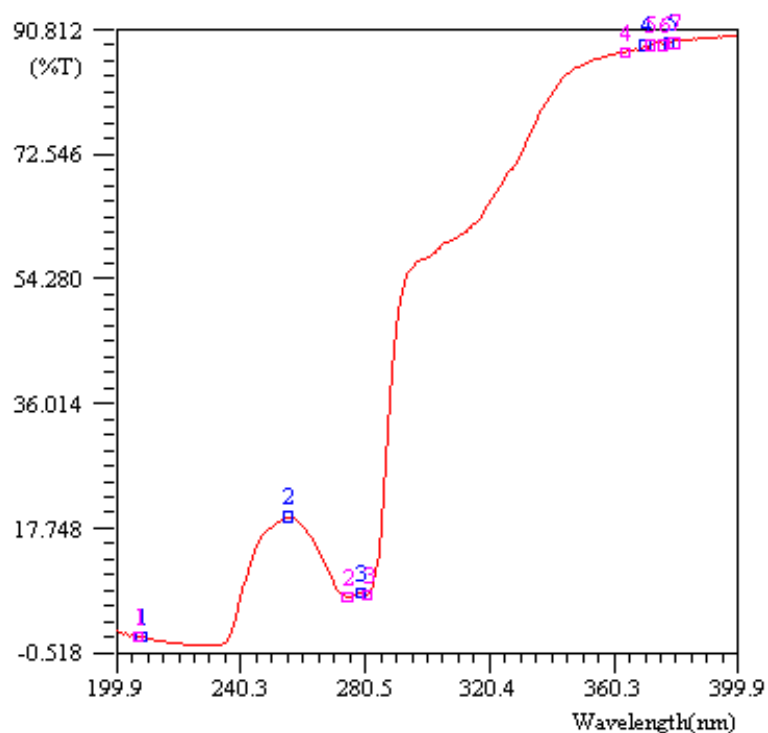


Figure 2.23 200-400 nm transmission spectrum for 5013S-04 COC.

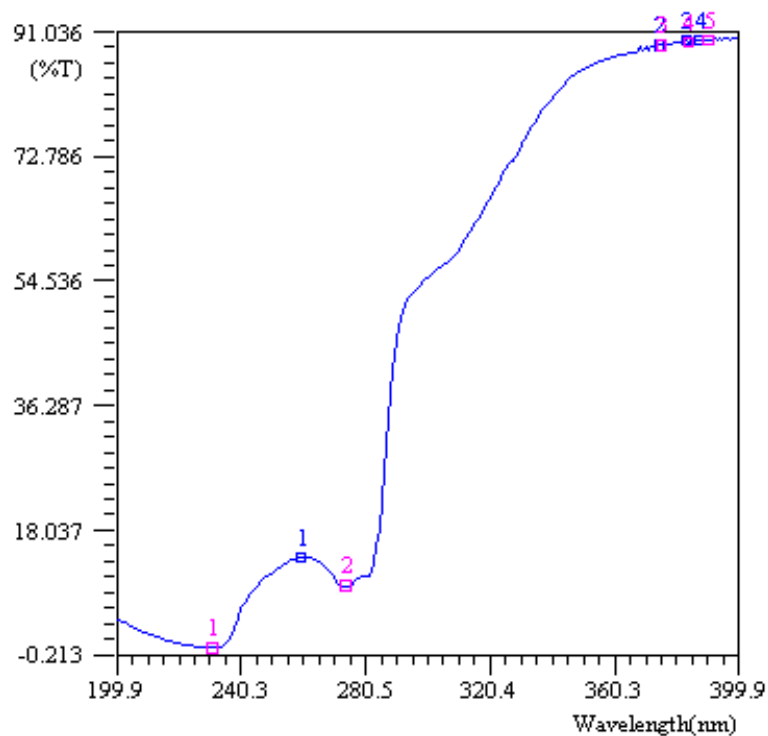


Figure 2.24 200-400 nm transmission spectrum for 6013S-04 COC.

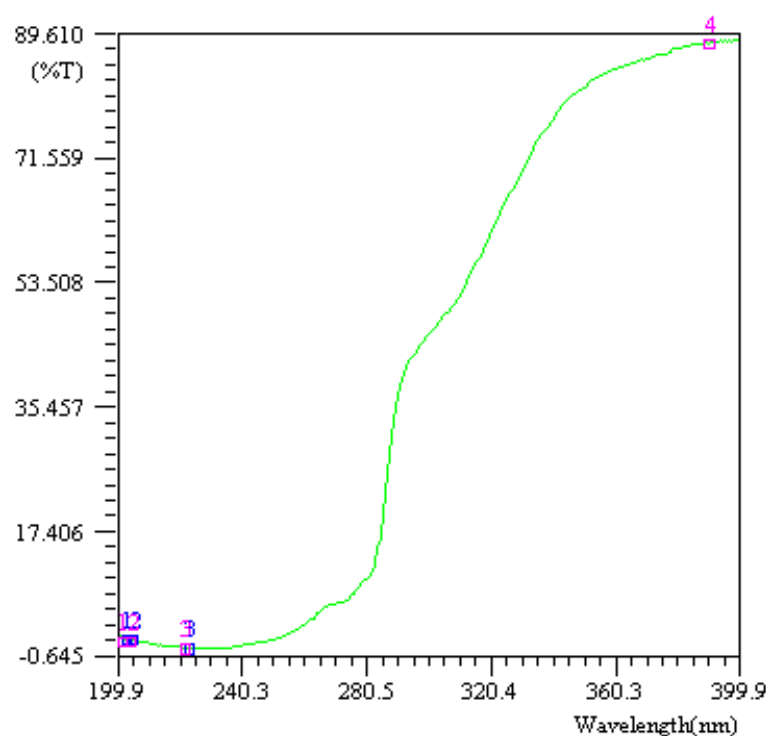


Figure 2.25 200-400 nm transmission spectrum for 6015S-04 COC.

All three grades have relatively poor deep UV transmission compared to the 8007x10 grade, which has approximately 60% transmission at 250 nm [43]. This excellent transmission in the deep UV was why Stachowiak *et al.* chose 8007x10 over other grades for developing their photografting procedure [39]. Grade 8007x10 was not considered for microreactor fabrication as it has a glass transition temperature of 78°C. The transmission of both the 5013S-04 and 6013S-04 grades was less than 20% at 250 nm, while the transmission of the 6015 grade was less than 5%. Plates of the different COC grades were photografted with monomers to determine if the 250 nm transmission of these grades was sufficient for photografting. The success of photografting is generally determined by SEM or by FT-IR of the plastic surface [53], although this is relatively time consuming and requires specialist instrumentation. A quick and easy method for determining the success of grafting conditions was developed. A grafting mixture consisting of trimethylpropyltriacylate (TMPTA) and BP was sandwiched between two plates of

COC and exposed. The XL-1500 UVC was used because of its narrow output in the spectral region required for BP hydrogen abstraction. It is also cheaper and safer to operate than the Model 30. TMPTA was used because of its lower cost compared to the more commonly used ethylene glycol diacrylate (EDA). If the grafting was successful, the two plates become bound together and the strength of the bond gives a crude estimate of the level of grafting. Plates of 8007x10 were strongly bound together after only 10 min exposure. Each of the three grades of COC proposed for use in this project were tested using this method and even after 40 min of exposure none of the plates were bound together. If one side of the plate sandwich was exposed for 20 min followed by a second 20 min exposure of the other side, the grafting was successful for all three grades. This may indicate that the radiation is unable to penetrate deep enough through the graft mixture to reach the opposite surface of the bottom plate of COC. The 5013S-04 and 6013S-04 plates could not be separated after bonding, while the 6015S-04 plates could with sufficiently large force, suggesting that the 5013S-04 and 6013S-04 grades may be suitable for in-channel photografting.

Plates of the four different grades were tested for thermal deformation at 80 °C. Both 6013S-04 and 6015S-04 showed no deformation, 5013S-04 showed minor deformation and 8007x10 was severely deformed. From these experiments, the 6013S-04 grade was determined to be the most suitable for the fabrication of polymer microreactors at the targeted temperature. Microchips in this grade were ordered from the Microfluidic ChipShop GmbH while custom-fabricated capillary was ordered from Paradigm Optics Inc.

2.4.2 COC capillary grafting

The development of photografting conditions and PPM formulations for COC microchips were performed using COC capillary from the same grade. It was considerably cheaper to use COC capillary than to use COC microchips (\$220 AUD each) at approximately \$32 AUD per metre. The 276 μm ID 723 μm OD capillary was used for development of grafting conditions as the cross-sectional area was the closest to that of the COC microchips, and fittings to interface with the capillary were commercially available.

The COC capillary was very brittle making it challenging to work with. If a length of capillary was excessively strained, microscopic cracks would form in the capillary wall which would leak when pumping liquid through the capillary. Special care was taken to prevent bending or twisting of the capillary during the grafting and PPM preparation. Initial testing was performed using 154 μm ID 370 μm OD capillary but was found to be too fragile for monolithic column fabrication.

The light source used for all photografting experiments was the XL-1500 UVC as its output spectrum matches the wavelength required for BP photografting, although the intensity variation of this source may lead to irreproducible thickness of the grafted polymer layer. While the output intensity of the Model 30 is more stable, the use of the cheaper and safer XL-1500 was preferred.

Initially the grafting procedure developed by Stachowiak *et al.* was trialled in 276 μm ID capillary using 1:1 methyl methacrylate/ethylene glycol diacrylate (MMA/EDA) with 3 wt% BP [39]. Lengths of 276 μm ID COC capillary were filled with the grafting mixture and exposed under the XL-1500 UVC at time intervals increasing from 5 to 15 min after which they were flushed with methanol. If flow through a grafted capillary could not be achieved, then it was assumed that the

capillary was blocked due to excessive polymer formation. It was found that a 15 min exposure lead to capillary blockage, so a grafting time of 10 min was adopted. Inspection of the grafted COC cross-section under SEM did not reveal any differences between the grafted and non-grafted capillary. PPM was formed in the grafted capillary to visualise the grafted and non-grafted regions of the capillary. An SEM image of the cross-section of the monolithic COC capillary, prepared from a grafted capillary using the UVGMA4 formulation with BAPO as the initiator and the UV-LED as the source, is shown in **Figure 2.26**. The PPM was only bound to a small section of the capillary wall, indicating that the grafting did not completely cover the inner capillary radius. This may be the result of insufficient intensity due to poor 254 nm transmission of the 6013S-04 COC and/or light absorption by the graft mixture.

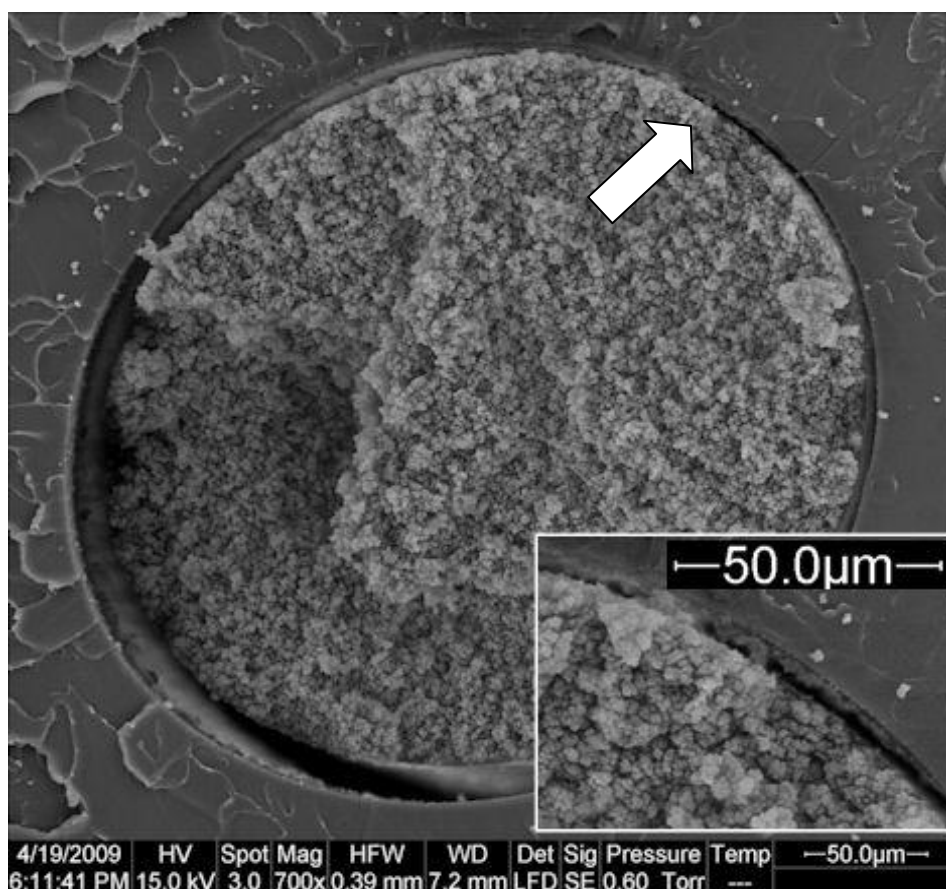


Figure 2.26 PPM in 10 min grafted 276 μm ID COC capillary. The arrow indicates the grafted surface region, which is also shown as an insert at the bottom left.

Increasing the exposure time to 11 and 12 min did not improve the radial homogeneity of the grafting and homopolymer formation blocked the capillary when the exposure time was increased to 15 min. It was anticipated that rotation of the capillary during the exposure might address this problem, as the entire wall of the capillary would receive a similar exposure dose. Thus the capillary was grafted for a set time and then rotated 180° along its axis and exposed again for the same period of time. Two 10 min exposures led to blockage of the capillary. To prevent blockage the exposure time was reduced to 9 min. PPM was formed in the 2×9 min grafted capillary, using the UVGMA4-70 formulation with BAPO and the UV-LED, as illustrated in the SEM image shown in **Figure 2.27**.

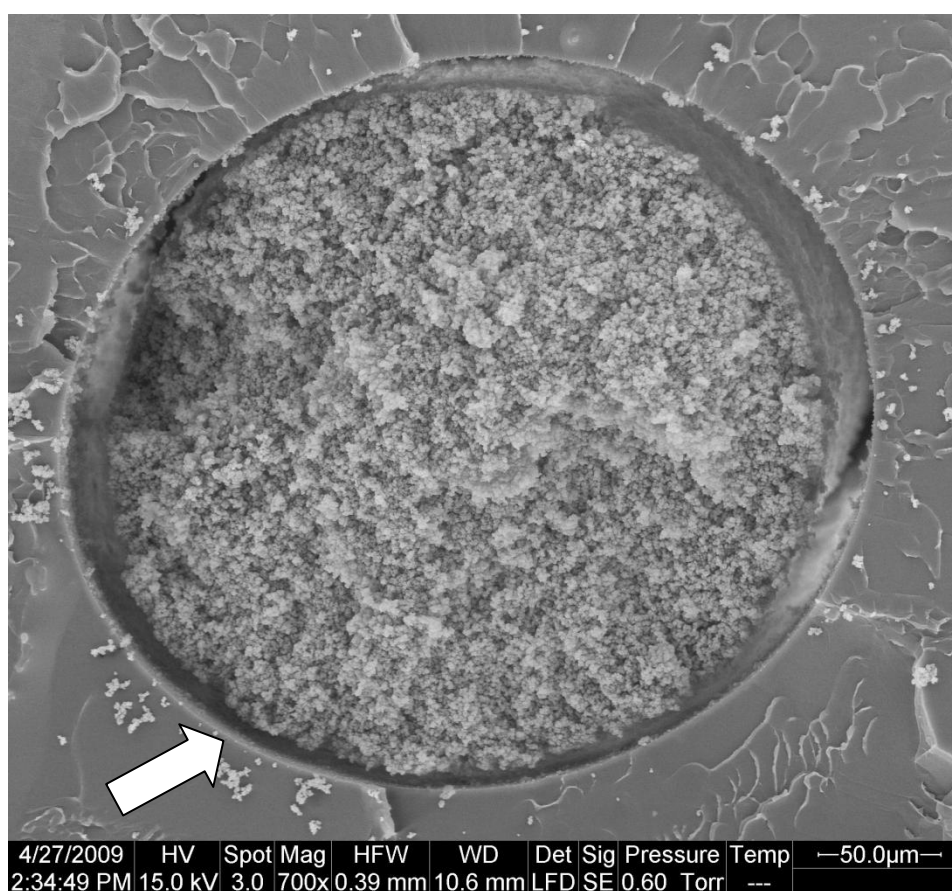
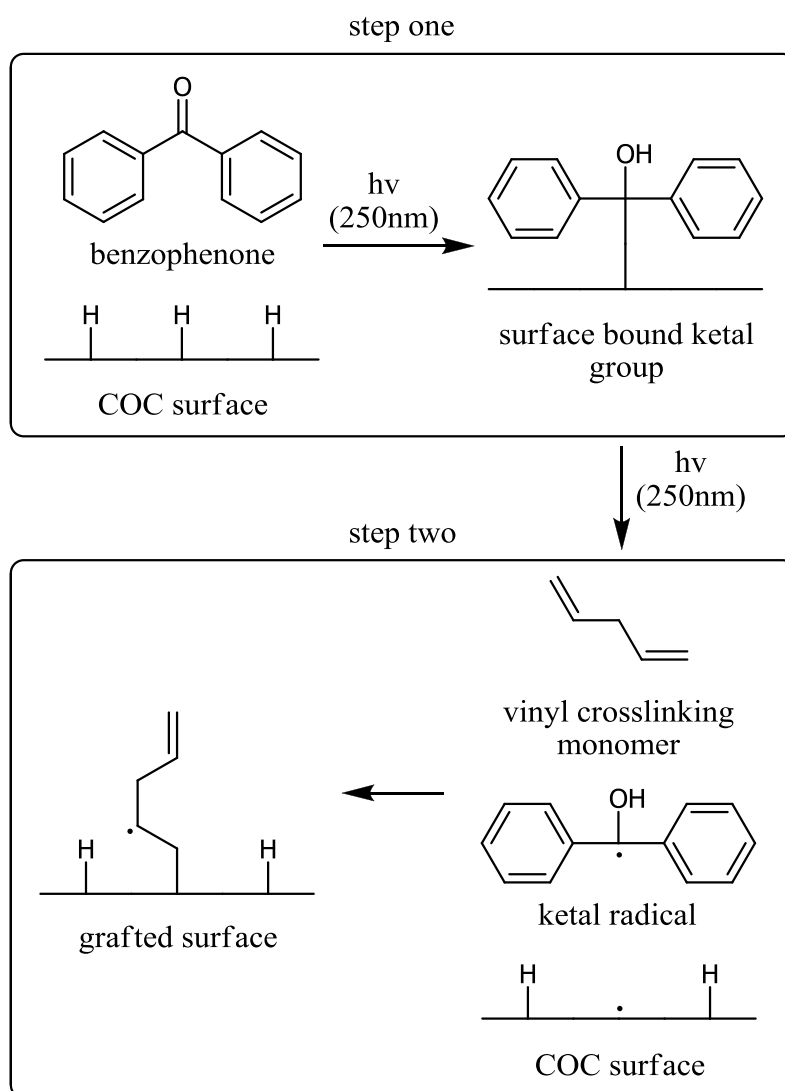


Figure 2.27 PPM in 2×9 min grafted 276 µm ID COC capillary. The arrow indicates a region devoid of grating.

The grafting was improved by exposing both sides of the capillary, however, the side regions which were not directly exposed were not grafted as indicated in **Figure 2.27**. This exposure time would occasionally lead to blockage of the grafted capillary due to fluctuations in the intensity of the XL-1500 UVC.

An alternative photografting method, also developed by Stachowiak *et al.*, uses a sequential grafting procedure that eliminates homopolymer formation [67].



Scheme 2.2 Two-step photografting of COC with a vinyl crosslinking monomer.

In this method, detailed in **Scheme 2.2**, the first step is to photograft the polymer surface with BP in a solvent. When exposed to UV radiation the BP abstracts hydrogen from the COC surface, and the surface radical combines with the ketal

radical to produce a surface-bound ketal group. The exposure can be continued for as long as desired until a complete monolayer of surface-bound ketal group is obtained. The graft solution is removed and the microchannel rinsed to remove any unbound BP. Next, the channel is filled with a mixture containing only monomers or a mixture of solvent and monomers. Upon exposure to deep UV radiation, the surface bound ketal groups are cleaved off regenerating the surface-bound radicals and initiating the grafting polymerisation with the vinyl monomers. The benefit of this approach is that there is no photoinitiator in the monomer mixture, avoiding homopolymer formation initiated by hydrogen abstraction from the monomers. Additionally, the graft polymerisation starts from the microchannel wall with much greater density of surface groups than the single step approach.

The two-step photografting procedure was trialled for photografting 6013S-04 COC capillary. The 314 μm ID COC capillary was grafted with a solution of 3 wt% BP in methanol using the XL-1500 UVC for 20 min on both sides of the capillary. This excessive exposure time was chosen to ensure complete coverage of the inner capillary wall. In the next step after rinsing the capillary, it was filled with a mixture of 1:1 MMA/EDA and 2.5 wt% hydroquinone. Hydroquinone is a strongly UV absorbing radical inhibitor commonly used to reduce oligomer formation in storage of monomers. It was added to slow down the grafting reaction, to reduce the penetration of 254 nm radiation into the central region of the capillary and to improve the storage lifetime of the monomer grafting mixture. The semipinacol radical is the chain terminating group during grafting, which is cleaved off due to the input of deep UV radiation. If the deep UV radiation can be prevented from penetrating into the monomer mixture, only a thin graft layer is expected at capillary walls regardless of the exposure time. The grafting time for the monomer mixture was increased incrementally in 2×5 min steps until the capillary became blocked,

indicating excessive grafting. Blockage was incurred at 2×15 min exposure, so the exposure time was reduced to 2×10 min. This may indicate that the addition of hydroquinone has only a negligible effect on the formation of the grafted polymer. PPM was prepared in the two-step grafted capillary using the UVGMA4-70 formulation, with DMPAP using the Model 30, and imaged under SEM as shown in **Figure 2.28**. The image obtained shows complete coverage of the capillary wall with a thick grafted layer of polymer. The detachment of the PPM from the capillary wall was due to other reasons which are discussed later in **Section 2.4.4**. Hence the two-step procedure was adopted as the preferred method for grafting 6013S-04 COC.

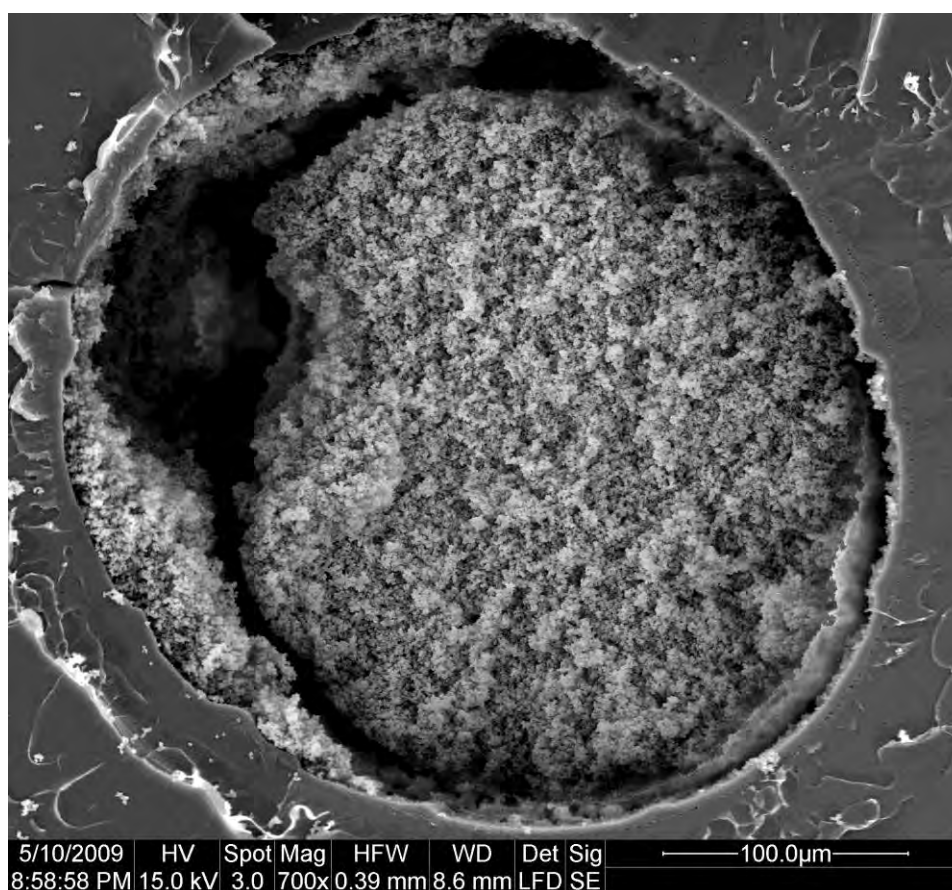


Figure 2.28 PPM in two-step grafted 314 µm ID COC capillary.

2.4.3 COC microchip machining and grafting

The microchips purchased from the Microfluidic ChipShop were fabricated from two plates of 6013S-04 COC. The top plate containing the microchannel and wells was

1.67 mm thick and the bottom sealing plate was 1.14 mm thick. Photografting conditions were developed using 276 μm ID and 723 μm OD capillary with a wall thickness of 447 μm . The thickness of COC that the radiation needs to penetrate for grafting is 2-3 times greater for the microchips, and thus a correspondingly longer exposure time was expected to obtain the same level of grafting as achieved in the COC capillary. To compensate for the intensity attenuation, the initial exposure time trialled in microchip was doubled and, using the two-step graft procedure, a COC microchip was grafted for 2×40 min with BP followed by 2×20 min with the monomer mixture. PPM was formed in the microchip, however this PPM was not wall attached and was pushed out of the channel during the post-polymerisation solvent flush. The exposure times were increased to 2×1 h for the BP graft and 2×40 min for the monomer graft, however the PPM still did not attach to the channel walls. This indicates that insufficient 254 nm radiation is able to penetrate through the COC for grafting to occur. To examine the amount of radiation able to penetrate the entire depth of the microchips, the UV transmission between 200-400 nm was measured, indicating no transmission of 250 nm radiation, as shown in **Figure 2.29**. The spectrum obtained for the 1 mm thick plates of this grade of COC, **Figure 2.24** on page 96, showed sufficient transmission to allow grafting, thus the additional thickness of the microchip layers was suspected to prevent grafting from occurring. Due to substantial cost of these custom fabricated microchips, ordering additional microchips fabricated from thinner plates was not feasible. Instead, the existing microchips were machined thinner so that the top and bottom plates were 0.9 mm thick, reducing the overall chip thickness by 1 mm. The UV spectrum of the machined microchips showed improved transmission at 250 nm, **Figure 2.30**, however the optical transparency of the microchips was drastically reduced by the rough surface resulting from the machining.

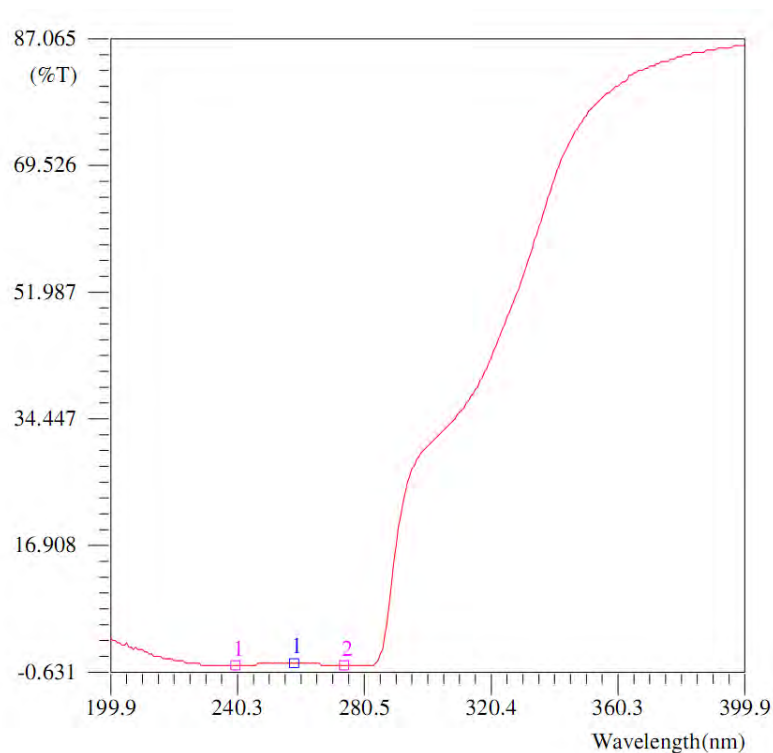


Figure 2.29 UV transmission spectrum of 6013S-04 COC microchip.

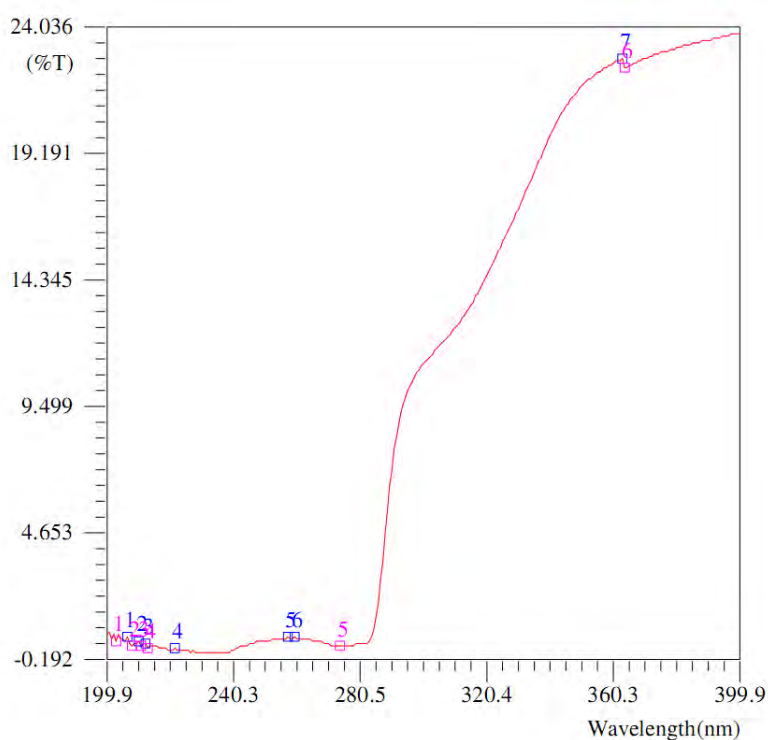


Figure 2.30 UV transmission spectrum of machined 6013S-04 COC microchip.

The machined microchips were polished to restore their optical transmission properties and reduce scattering. The UV spectrum of the polished microchips

showed significantly improved 250 nm transmission and similar optical transparency to the unprocessed microchips, as shown in **Figure 2.31**. The machined microchips were photografted using the two-step procedure with exposure times double those developed for capillary, and then PPM formed in the grafted microchip. The PPM was successfully retained during the post-polymerisation solvent flush, indicating that the grafting was successful. SEM images of the microchip cross-section, shown in **Figure 2.32(a)**, revealed a graft layer approximately 10 μm thick, so the monomer graft time was reduced to 2×15 min.

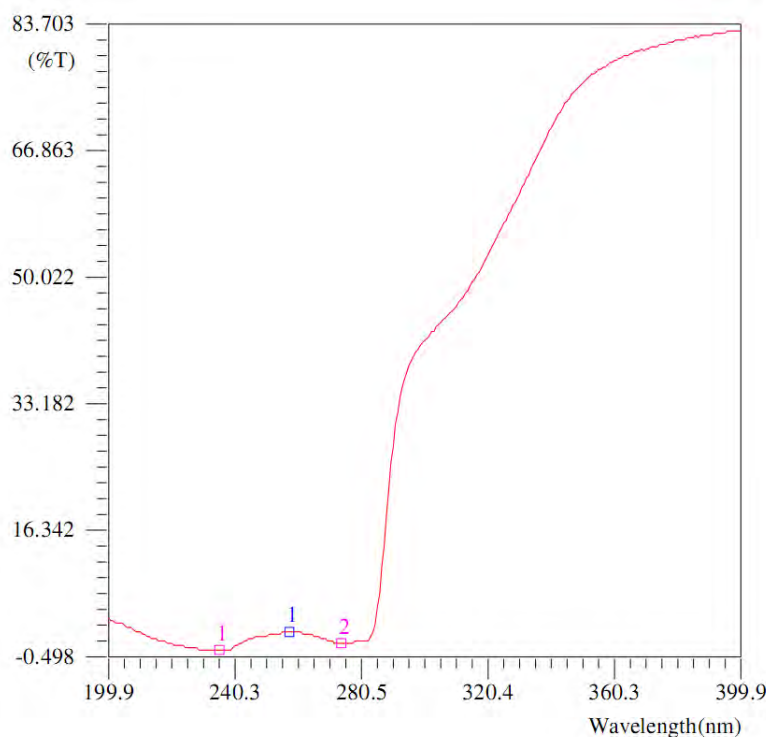


Figure 2.31 UV transmission spectrum of machined and polished 6013S-04 COC microchip.

The reduced monomer graft time was sufficient for all of the microchannel wall to be grafted while only forming a graft layer a few micrometres thick, as shown in **Figure 2.32(b)**. This grafting procedure was adopted for preparation of monolithic columns within the 6013S-04 COC microchips.

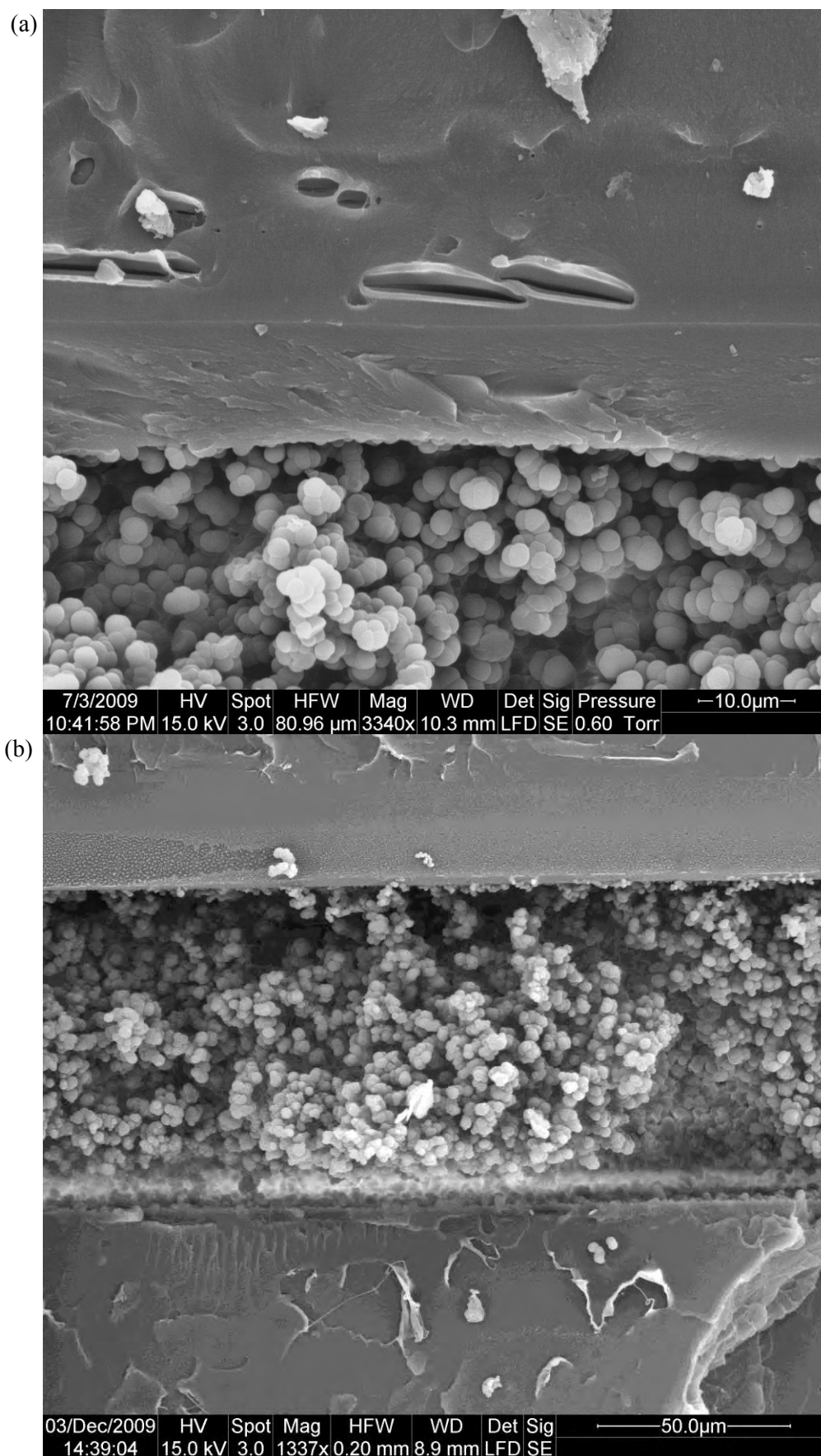


Figure 2.32(a) PPM in COC microchip showing an excessively thick grafted layer,
(b) PPM in COC microchip showing monolith adhesion and reduced graft layer.

2.4.4 PPM formulation development for COC devices

During the development of photografting conditions in 276 μm ID COC capillary, PPM prepared from both the UVGMA4 and UVGMA-70 formulations was used to test the grafting. The SEM images of the capillary cross-sections, such as **Figure 2.28** on page 104, show severe detachment of the main PPM body from the PPM adhered to the capillary wall. As these formulations were developed for 100 μm ID capillary, this detachment may result from shrinkage of the PPM in the larger internal dimension COC capillary. To test this hypothesis, PPM was prepared using the UVGMA4-70 formulation in the tips of surface treated Pasteur pipettes (ID ≥ 1 mm), which were treated using the same procedure as used for fused-silica capillary. Using glass as the substrate with chemical vinylisation should eliminate any potential effects such as non-homogeneous photografting observed in COC capillary. Also, the larger ID should significantly increase the effect of any shrinkage of the PPM. SEM images obtained of the PPM filled Pasteur pipette cross-sections showed that the inner wall of the pipette was completely covered with PPM, however breakages were observed in the PPM directly attached to the wall, as illustrated in **Figure 2.33**. The homogeneity of the PPM formed as well as the presence of wall-bound PPM makes it highly unlikely that this gap formed during polymerisation. Instead the PPM probably shrunk after formation, breaking off the wall. Since the PPM appears to break preferentially near the directly wall-attached monolith, this suggests that the PPM is structural weak in this region [68], which may be understood by considering how PPM formation at the wall differs from that in the main PPM body. At the wall there is a higher density of vinyl groups as a result of the surface modification, causing the polymerisation to proceed faster and deplete the monomers from the polymerisation mixture more rapidly in the vicinity of the wall than in the remainder of the capillary [69]. The reduced concentration of monomers

causes the formation of PPM with lower density that either the PPM at the wall or in the bulk of the capillary, making this region structural weaker and hence more likely to fracture when under stress. From the SEM image in **Figure 2.33**, the shrinkage of the PPM prepared using the UVGMA4-70 formulation was estimated to be 8% of the cross-sectional area.

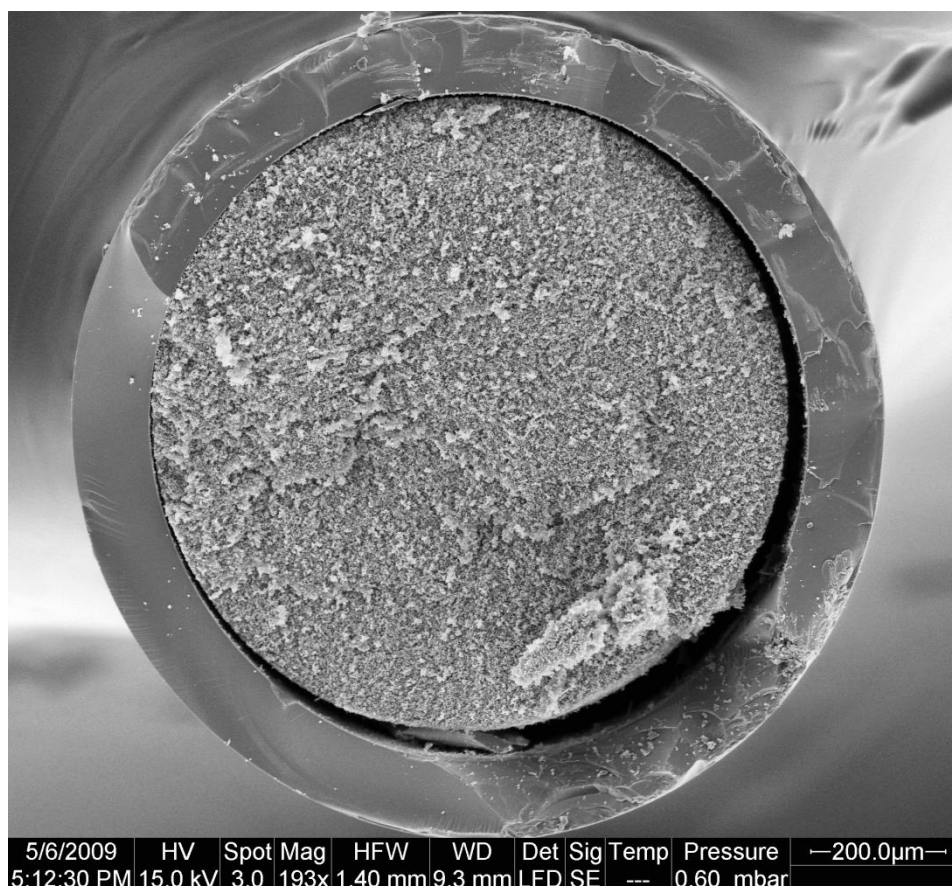


Figure 2.33 PPM formed using UVGMA4-70 formulation in Pasteur pipette.

To determine if the observed PPM shrinkage was formulation specific, three different poly(GMA-*co*-EDMA) formulations from the literature were prepared in grafted 276 μm ID COC capillary [4, 8, 49]. The basic properties of these formulations are shown in **Table 2.3**. Cross-sectional SEM images were obtained for each monolithic capillary prepared from these formulations and in each sample severe wall-detachment of the PPM was observed. PPM shrinkage was significantly less for all three literature formulations compared to the UVGMA4-70 formulation. Based on the low levels of shrinkage in the UVGMA7 and UVGMA8 formulations,

the extent of the shrinkage of these two formulations was further investigated by using them to prepare PPM in Pasteur pipette tips, as these were previously found to successfully exaggerate any shrinkage. The SEM images of the PPM filled pipette cross-sections obtained are shown in **Figure 2.34**, neither of which shows any indication of shrinkage nor wall-detachment of the PPM. Additionally, these images show that PPM prepared from the UVGMA7 formulation forms much larger globules, indicating a larger pore size than PPM prepared from either the UVGMA8 or UVGMA4-70 formulations. Interestingly, the pipette monolithic column prepared from the UVGMA7 formulation had exceptionally high permeability, but the same formulation prepared in 30 cm long 100 μm ID capillary, discussed in **Section 2.3.1**, could not be flushed due to excessively high back-pressure.

While the UVGMA8 formulation uses the same porogens as the UVGMA4 and UVGMA4-70 formulations, they each have different porogen-to-monomer ratios. The porogen-to-monomer mass ratio for the UVGMA4 and UVGMA4-70 formulations are 1.5 and 2.33 respectively, while this ratio for the UVGMA8 formulation is 1. The trend observed in the shrinkage for PPM prepared from these three formulations may indicate that the shrinkage is proportional to the porogen concentration, with lower concentrations resulting in less shrinkage. The UVGMA7 formulation features the same porogen-to-monomer ratio as the UVGMA4 formulation, however the porogens are low molecular weight alcoholic solvents which implies that the solvation properties of the porogens may also significantly affect PPM shrinkage.

Research group	Formulation ID	GMA/EDMA mass ratio	Porogens and mass ratio	Porogen/monomer mass ratio
Yu <i>et al.</i> [4]	UVGMA7	1.5	Methanol, ethanol (1:1)	1.5
Yang <i>et al.</i> [49]	UVGMA8	0.67	Cyclohexanol, 1-dodecanol (3:7)	1
Mao <i>et al.</i> [8]	UVGMA9	1.6	1-Dodecanol	1.5

Table 2.3 Reported photoinitiated poly(GMA-*co*-EDMA) formulations.

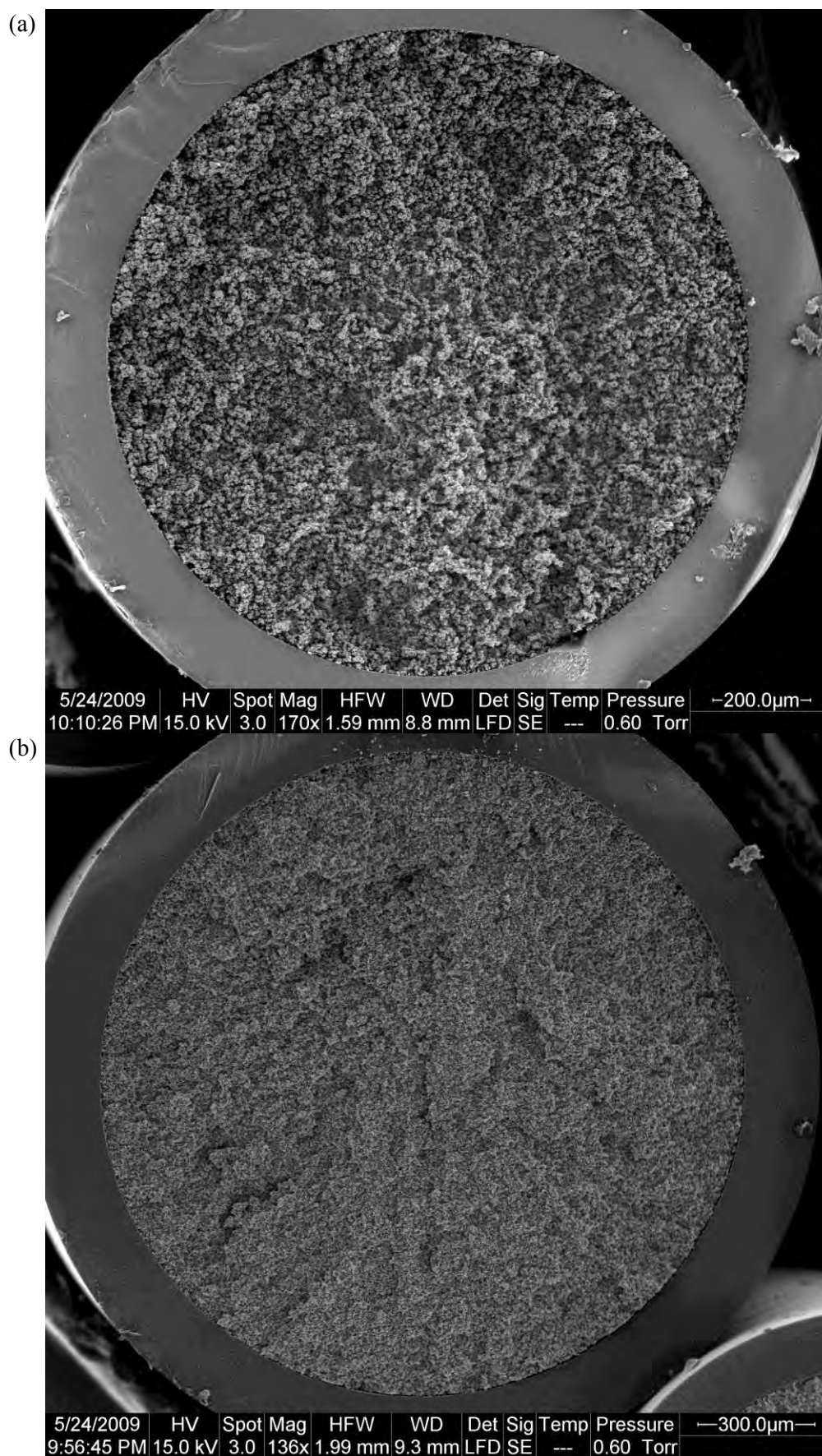


Figure 2.34(a) PPM in Pasteur pipette prepared using the UVGMA7, (b) and UVGMA8 formulations.

This shrinkage can be explained by considering the mechanism for PPM pore formation. As previously discussed in **Section 2.1**, „poor’ thermodynamic solvents cause the polymer nuclei formed during PPM polymerisation to be preferentially solvated with the monomers leading to the formation of large globules, whereas „good’ thermodynamic solvents compete with the monomers in solvating the nuclei and restrict the growth of the microglobules. These „good’ thermodynamic solvents continue to solvate the PPM even after polymerisation is complete. This means that PPM is formed in a swollen state and once the porogenic solvents are removed by rinsing with a „poor’ thermodynamic solvent, such as methanol, the microglobules collapse causing the PPM to shrink. The extent of this shrinkage is directly related to the porogen concentration and the thermodynamic properties of the solvent. Macroporogens, such as 1-dodecanol, are relatively non-polar and should significantly swell the monolith. Indeed, UVGMA4-70 has a high concentration of 1-dodecanol and this formulation resulted in severe shrinkage, as shown in **Figure 2.33** on page 110. As greater shrinkage is expected at higher porogen concentrations, the PPM prepared from the UVGMA4-70 formulation shrank more than PPM prepared from the UVGMA8 formulation despite using similar porogens. A good macroporogen, such as methanol, is not expected to significantly swell the polymer, and no shrinkage was observed for PPM formed using the UVGMA7 formulation in Pasteur pipette.

Based on these results, shrinkage may be due to contraction of the PPM after the porogenic solvents are removed during the post-polymerisation solvent flush. If the porogens used to form the PPM swell the formed polymer, their removal will result in contraction or shrinkage in both radial and lateral directions. As the PPM contracts, a strain is put between the wall-bound monolith and the main PPM body, the force of which will depend on the surface area to volume ratio of the column. At

small column dimensions, the surface area to volume ratio is higher and the relative strain on the contracting PPM is less, which explains why no contraction was observed in the 100 μm ID capillary. However in large capillaries/channels, the surface area to volume ratio is lower and force caused by the contraction may cause the PPM to fracture near the wall where it is structurally weakest.

Even though no shrinkage was observed for PPM prepared using either the UVGMA7 and UVGMA8 formulations in Pasteur pipette tips, severe wall-detachment was observed for the same PPM prepared in COC capillary. In an attempt to further reduce any shrinkage of the PPM, the ratio of porogens-to-monomers for the UVGMA7 formulation was lowered from 1.5 to 1 (UVGMA7-50). This formulation was used to prepare PPM in grafted 276 μm COC capillary, the SEM images of which indicated reduced, but not eliminated, wall-detachment of the PPM, as shown in **Figure 2.35(a)**. Nevertheless this formulation was adopted as the preferred formulation for use in COC devices due to excellent flow-through properties and further reduced shrinkage. As wall-detachment was not observed when the PPM was formed in Pasteur pipette, it was hypothesised that COC capillary sample preparation for SEM may be responsible for the observed wall-detachment. The COC capillary cross-sections were prepared by cutting a score around the outside of the capillary using a razor blade and then snapping the capillary at the score. Initially the capillary was simply cut with a razor blade, but this was found to crush the PPM. SEM imaging of a length-ways cross-section of a monolithic COC capillary, shown in **Figure 2.35(b)**, revealed that the COC capillary was significantly stretched where it was snapped. This image also shows that the monolithic column is wall-attached in the regions where the COC has not been stretched. To prevent the COC capillary from stretching during SEM sample preparation, the capillary was lightly scored using a razor blade and then placed in liquid nitrogen to make the

COC brittle. The COC was found not to be brittle enough to snap after freezing and instead stretched more severely than with the original method. In a last attempt, the monolithic capillary was set in at least 5 mm thick epoxy resin immediately after polymerisation of the PPM to prevent any expansion of the capillary during the solvent flush. After the post-polymerisation solvent flush and drying, a deep score was made all around the resin to 1-2 mm from the capillary and the assembly was frozen in liquid nitrogen. When the capillary was removed from liquid nitrogen and snapped at the score, the resin broke but the COC capillary stretched, which resulted in the PPM detaching from the capillary wall. It was concluded that SEM images of cross-sections of monolithic COC capillary columns could not be prepared without capillary stretching.

Monolithic COC capillary columns were prepared using the different light-source/photoinitiator combinations to test their suitability for monolith preparation in COC microchips. PPM using the UVGMA7-50 formulation was prepared in grafted 276 μm ID COC capillary with the following light-source/initiator combinations: Model 30 with DMPAP, XL-1500 UVC with DMPAP, and the UV-LED with BAPO. The exposure times used were the same as used for 100 μm ID fused-silica capillary. SEM images of the capillary cross-sections were used for analysis of the morphology of the PPM. PPM was successfully formed using the Model 30 and UV-LED, however complete polymerisation was not obtained using the XL-1500 UVC where the monolith was only formed close to the capillary wall. Doubling of the exposure time to 40 min did not improve the PPM formation, possibly due to the limited deep UV transmission of the 6013S-04 COC and/or photodarkening of DMPAP.

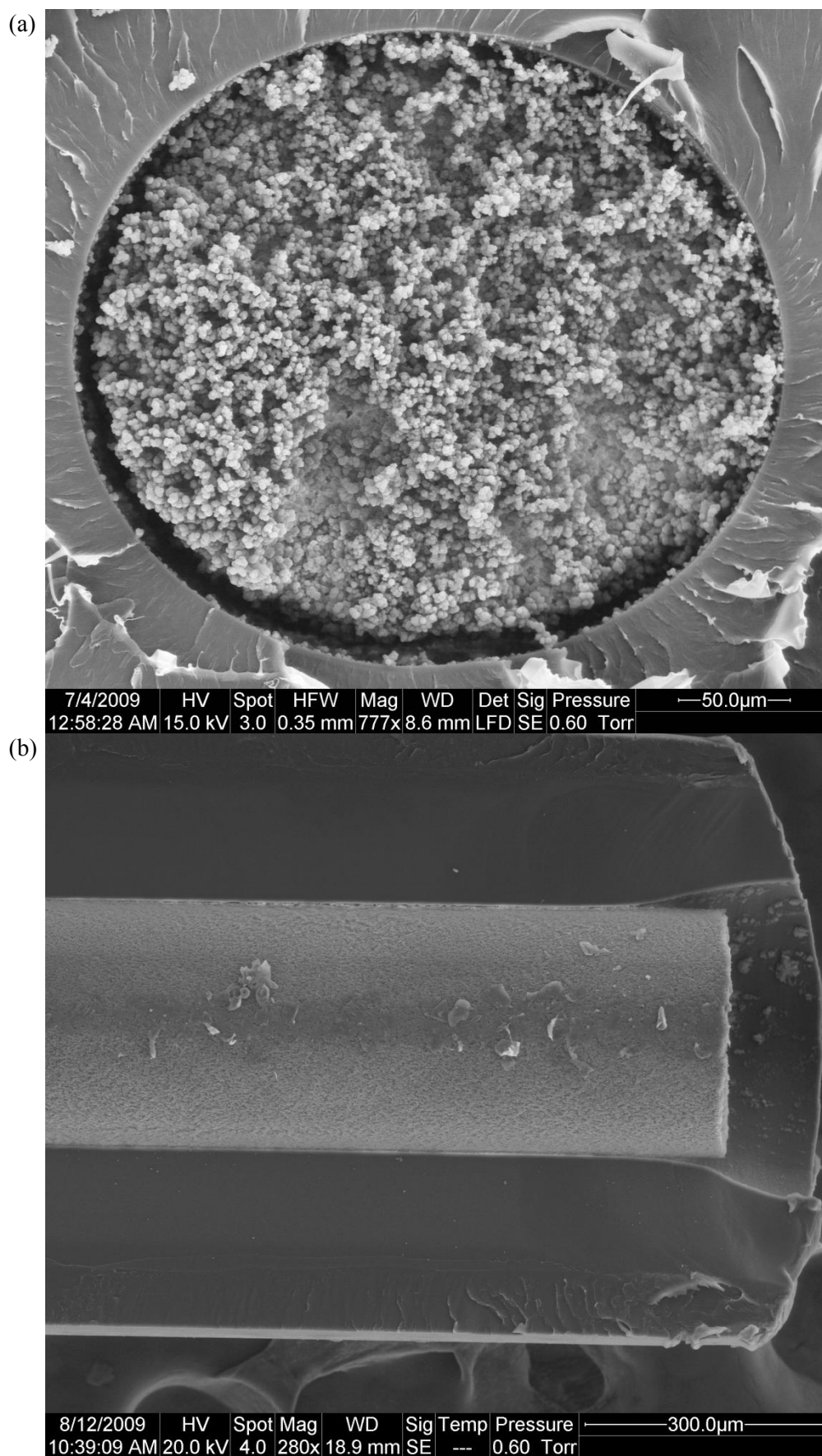


Figure 2.35(a) PPM prepared from the UVGMA7-50 formulation in COC capillary, **(b)** a length-wise cross-section of PPM in COC capillary.

When using the Model 30 with DMPAP, photografting of the COC capillary was not required for PPM wall-adhesion. DMPAP may not be only acting as type I photoinitiator, but also as a hydrogen abstracting type II photoinitiator, grafting the COC surface with the monomers in solution [65]. This bond strength of the *in-situ* grafted PPM was found to be considerably lower than for grafted capillary, which is likely to result from DMPAP's poor hydrogen abstracting performance and also the lower reactivity of methacrylates towards surface bound radicals compared to acrylates [63]. Experimentally, PPM formed using this approach was found to detach from the wall during reactor fabrication, making it unsuitable for the fabrication of flow-through devices.

2.4.5 PPM in COC microchips

The 276 μm ID COC capillary was chosen for the development of grafting and PPM photopolymerisation conditions as its cross-sectional area is similar to that of microchannel in the COC microchips, which are described in detail in **Chapter 5**. However the microchannel within the microchips is trapezoidal with a height to width ratio of approximately six, which means that the channel depth, and hence the exposure depth, is considerably less than that of the channel in the capillary. The reduced exposure depth could result in PPM with significantly different morphology being formed. Additionally, the substrate thickness is larger for the microchips, which could also affect the PPM formation. Above 300 nm, the 6013S-04 COC has high transparency and the thickness of the substrate should have a negligible effect on the light intensity in the microchannel. The 365 nm peak output of the UV-LED is therefore ideal for photopolymerisation of PPM in this grade of COC. The Model 30 is calibrated at 260 nm which is significantly attenuated by this grade of COC, but its broad output spectrum extends into the near UV and visible ranges, which enabled photopolymerisation of PPM in borosilicate microchips. From the capillary studies,

the best combinations of light source and initiator were the Model 30 with DMPAP and the UV-LED with BAPO. Both of these systems were used to prepare PPM in grafted COC microchips using the UVGMA7-50 formulation. The microchips were masked according to the diagram in **Figure 2.36** to prevent PPM formation in the wells.



Figure 2.36 COC microchip masking diagram.

Masking effectively prevented PPM formation in the masked regions with a sharp cut-off of polymerisation at the edge of the mask. Issues reported for masking in borosilicate microchips, **Section 2.3.2**, were likely due to the high surface roughness of the powder blasted microchannels, as the refractive index of borosilicate and 6013-S04 COC are similar. Cross-sections of the microchips were prepared for SEM imaging by scoring the top layer of the microchip approximately 0.2 mm deep using a razor blade, freezing the chips in liquid nitrogen for 30 min, and breaking the microchip at the score mark quickly after removal from liquid nitrogen. The images of PPM formed in COC microchips using both light source/initiator systems are shown in **Figure 2.37**. While the microchips generally broke cleanly at the score, a minor amount of PPM detachment from the microchannel walls occurred, most likely due to flexing of the microchip during the sample preparation for SEM.

Thanks to the improved masking, the COC microchips were found to be more suitable for the preparation of photopolymerised PPM than the powder blasted borosilicate microchips. As the surface roughness is an artefact of the microchip fabrication process, this should be taken into account when selecting devices for PPM preparation.

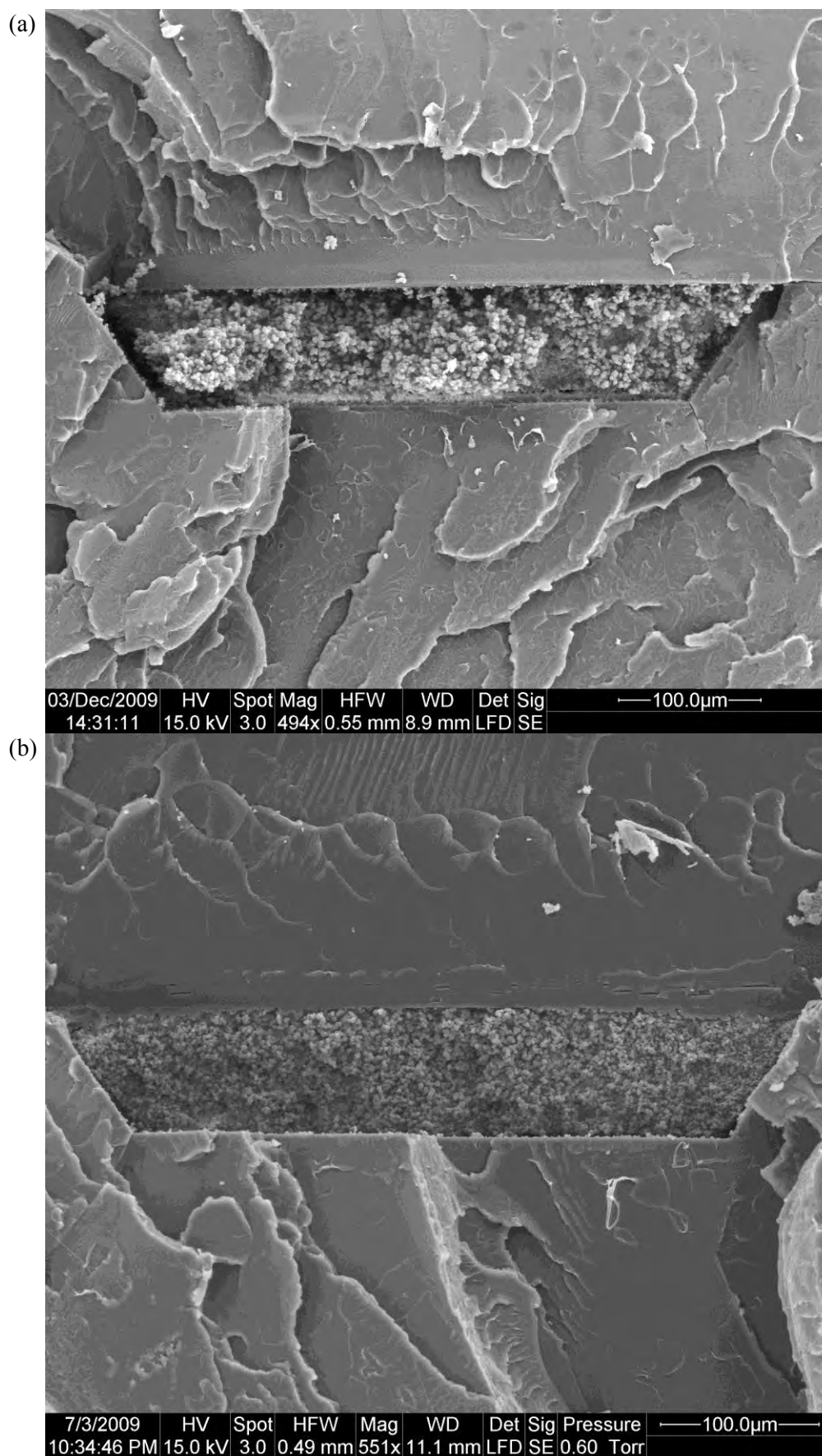


Figure 2.37(a) PPM formed using the Model 30 with DMPAP in COC microchip,
(b) using the UV-LED with BAPO in COC microchip.

2.5 Photopolymerised PPM in large ID glass columns

Based on the success of low shrinkage photopolymerised PPM prepared in >1 mm ID Pasteur pipettes, PPM preparation was also investigated in 2 mm and 4 mm ID borosilicate columns. The goal of this section of work was to determine the limits of the light source/initiator combinations used for PPM preparation in microchip and also to investigate the scalability of the PPM-based reactors. Large ID photo-polymerised PPM columns have been demonstrated by Yu *et al.* and Sirc *et al.* both of whom claim they obtained PPM with homogeneous morphology in 4 mm and 3.3 mm ID columns respectively [25, 28]. At these dimensions PPM shrinkage is a significant problem which may be overcome by compressing the polymerisation mixture during polymerisation [25]. The investigation of Pasteur pipettes and COC capillary showed that the shrinkage can be significantly reduced by careful choice of the porogenic solvents and the porogen concentration. Using the UVGMA7-50 formulation, a homogeneous, wall-attached PPM was successfully prepared in a column of >1 mm ID without the need for compression. In this work, 2 mm and 4 mm ID borosilicate tubes were selected as columns of these dimensions are commonly used in LC. The glass tubing was cut into approximately 10 cm lengths and the inner wall vinylised by scaling up the procedure described for fused-silica capillary.

PPM columns (2 mm ID) were prepared using the UVGMA7-50 formulation with both the Model 30/DMPAP and the UV-LED/BAPO light source/initiator combinations. The exposure time used for the Model 30 with DMAPAP was 1 h as this time is used for the formation of PPM in 4 mm ID quartz tubes for the preparation of bulk monolith. The 40 min exposure time developed for preparation of PPM in 100 μ m ID capillary using the UV-LED/BAPO was found to yield a completely polymerised PPM in ≥ 1 mm ID Pasteur pipette. Initially this exposure

time was also used for the 2 mm ID columns, even though it may not yield a complete polymerisation, to determine the feasibility of this combination of light source and initiator for large ID systems. These monolithic columns were prepared for SEM imaging by scoring around the outside of the column with a capillary cutter and snapping at the score. The SEM image obtained for the column prepared using the UV-LED with BAPO, in **Figure 2.38(a)**, shows that the morphology of this PPM is inhomogeneous, with the globule density decreasing from the column wall towards the region indicated with an arrow. The trend of decreasing globule size towards this region is likely an illustration of the decreasing intensity of the UV light as it penetrates the polymerisation mixture, since the globule size is proportional to intensity. This behaviour is expected as radical generation does not occur simultaneously across the column, but rather as a wave front that propagates from the directly exposed regions and diminishes in magnitude as it penetrates deeper into the polymerisation mixture [59]. This inevitably results in a PPM with a gradient morphology, with larger globules at the edge and smaller near the centre. In most cases however, this gradient is so shallow that the PPM cross-section appears completely homogeneous.

The SEM image obtained for the column prepared using the Model 30 with DMPAP, in **Figure 2.38(b)**, shows homogeneous PPM morphology, which may suggest that the combination of greater exposure intensity and time is beneficial for PPM formation. Increasing the exposure time for PPM formation using the UV-LED with BAPO was found to significantly improve the morphology, as shown in **Figure 2.39**. The images in **Figure 2.38(b)** and **Figure 2.39** also reveal severe detachment of the PPM from the column wall, not seen in **Figure 2.38(a)**. As these PPM's were prepared in glass columns, visual inspection of the columns was possible during all stages of fabrication of the monolithic column.



Figure 2.38(a) PPM in 2 mm ID column formed using UV-LED/BAPO with a 40 min exposure, **(b)** using Model 30/DMPAP.

There were no visible gaps between the PPM and the column wall before or after the post-polymerisation solvent flush, but such gaps appeared after drying the PPM for SEM analysis. Hence this detachment may result from minor shrinkage of the PPM in its dry state [7].

Monolithic columns (4 mm ID) were prepared using the optimised exposure conditions used for the 2 mm ID columns, from which cross-sections were imaged by SEM (**Figure 2.40**). The cross-sectional SEM image obtained for the monolithic column formed using the UV-LED in **Figure 2.40(a)** clearly indicates incomplete formation of the PPM. Complete formation was achieved for the monolith column formed using the Model 30 however, as indicated in **Figure 2.40(b)**. Rather than pursuing longer exposure times with the UV-LED, it was concluded that the UV-LED is not suitable for preparation of monolithic columns with diameters larger than 2 mm within reasonable exposure times. Close inspection of the SEM image in **Figure 2.40(b)** reveals the same radial variation in the PPM morphology observed in **Figure 2.38(a)**, albeit less pronounced.

In both 2 mm and 4 mm ID columns the formation of a thick surface layer of polymer on the surface of the inner column wall was observed for PPM formed from the UVGMA7-50 formulation, as shown in **Figure 2.41(a)**. This layer is more clearly visible in **Figure 2.41(b)** where the column was not surface treated before PPM formation. Known as the fluid impervious layer, or the sheath, the formation of this layer has been recently discussed [26, 68, 69]. The formation of the sheath layer can be desirable in certain applications, such as in CEC, where it prevents analytes from interacting with the inner capillary surface. It can also be detrimental in other applications, especially in small dimension columns as this layer can occupy a considerable amount of the cross-section resulting in higher back-pressures.

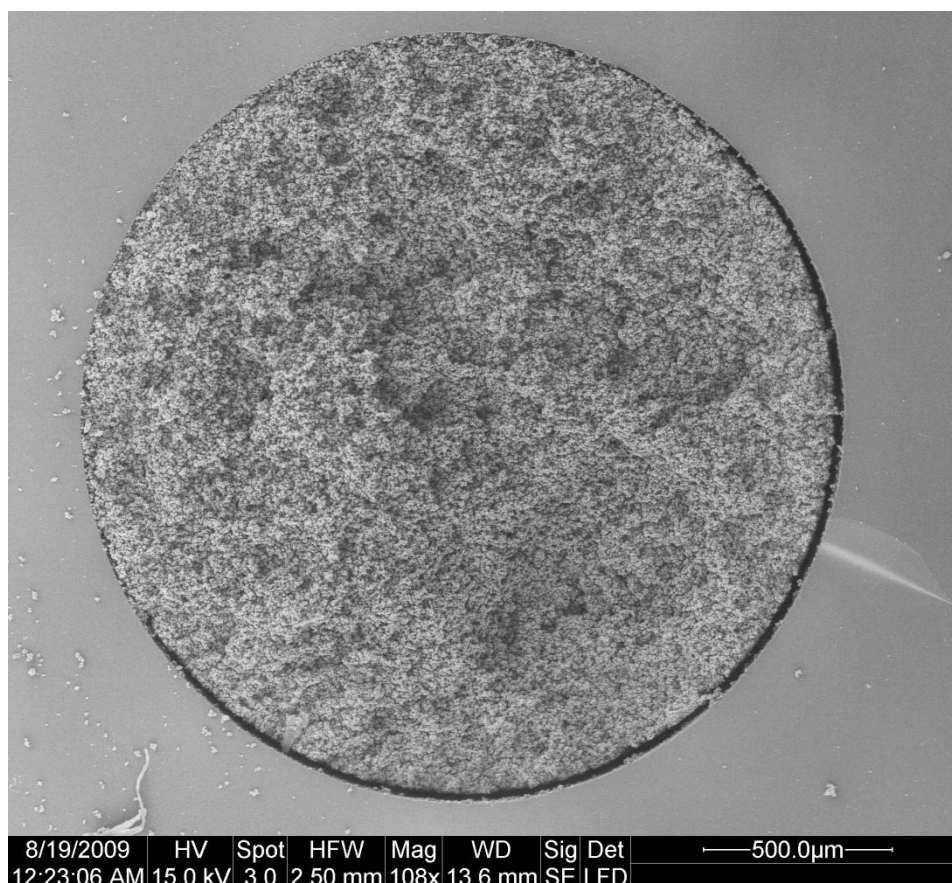


Figure 2.39 PPM in 2 mm ID column formed using UV-LED/BAPO with a 2 h exposure.

Nischang *et al.* have attributed the formation of the sheath layer to accelerated polymerisation close to the wall due to a higher density of vinyl groups as a result of the surface modification [69]. The thickness of the sheath could be controlled by varying the surface vinyl group density and polymerisation rate. Gibson *et al.* have attributed the formation of the sheath layer to hydrophobic van der Waals interactions between the monomers and the surface of the column [68]. In this model, the non-polar vinyl groups at the surface are proposed to create a hydrophobic layer for which the relatively non-polar vinyl groups have a strong affinity. This effect results in an increase in the concentration of monomers close to the wall resulting in the formation of the sheath. Neither research group investigated the potential effect of the interaction of the porogens with the surface.

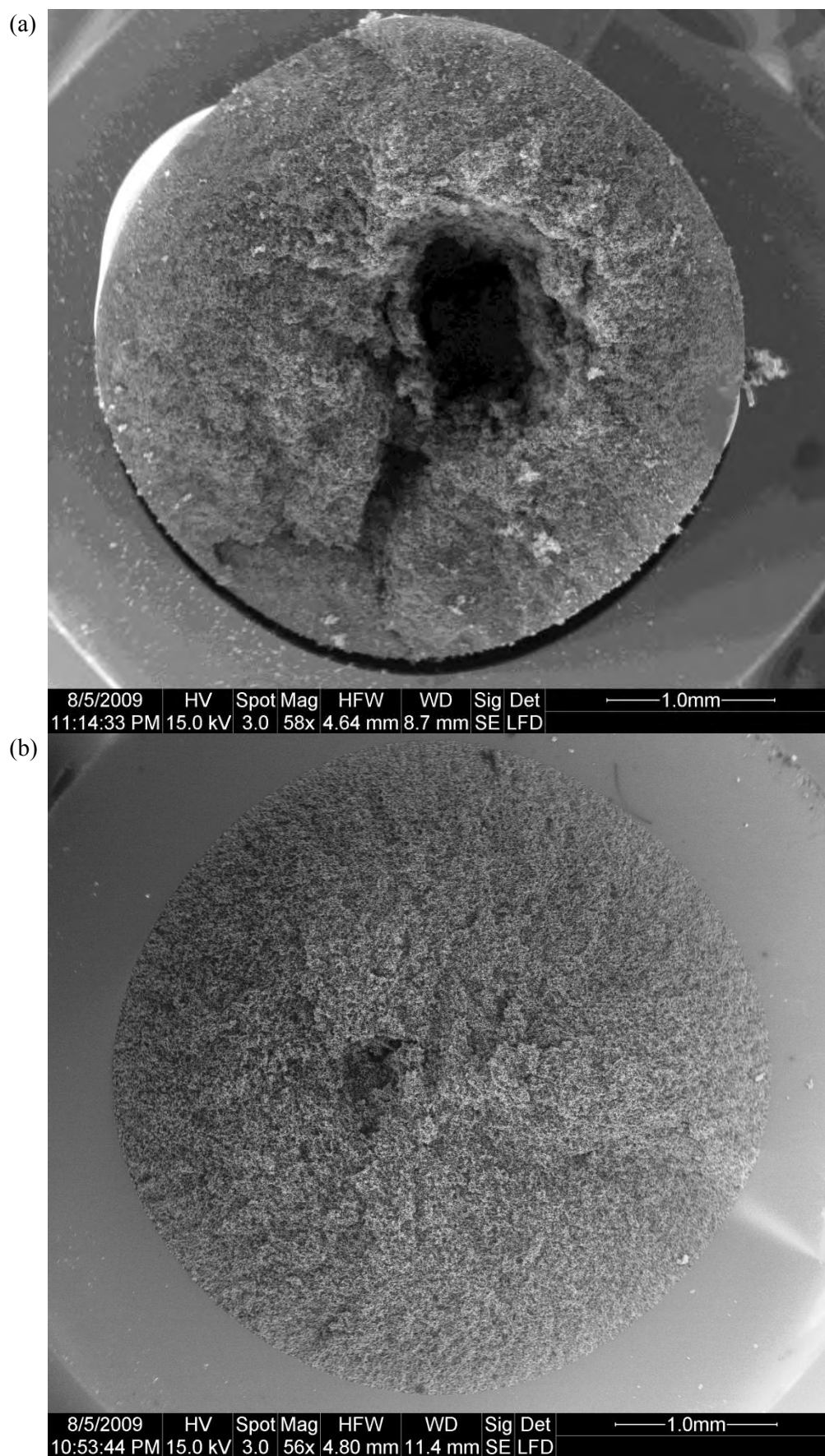


Figure 2.40(a) PPM in 4 mm ID column using UV-LED/BAPO with 2 h exposure,
(b) PPM in 4 mm ID column using Model 30/DMPAP with 1 h exposure.

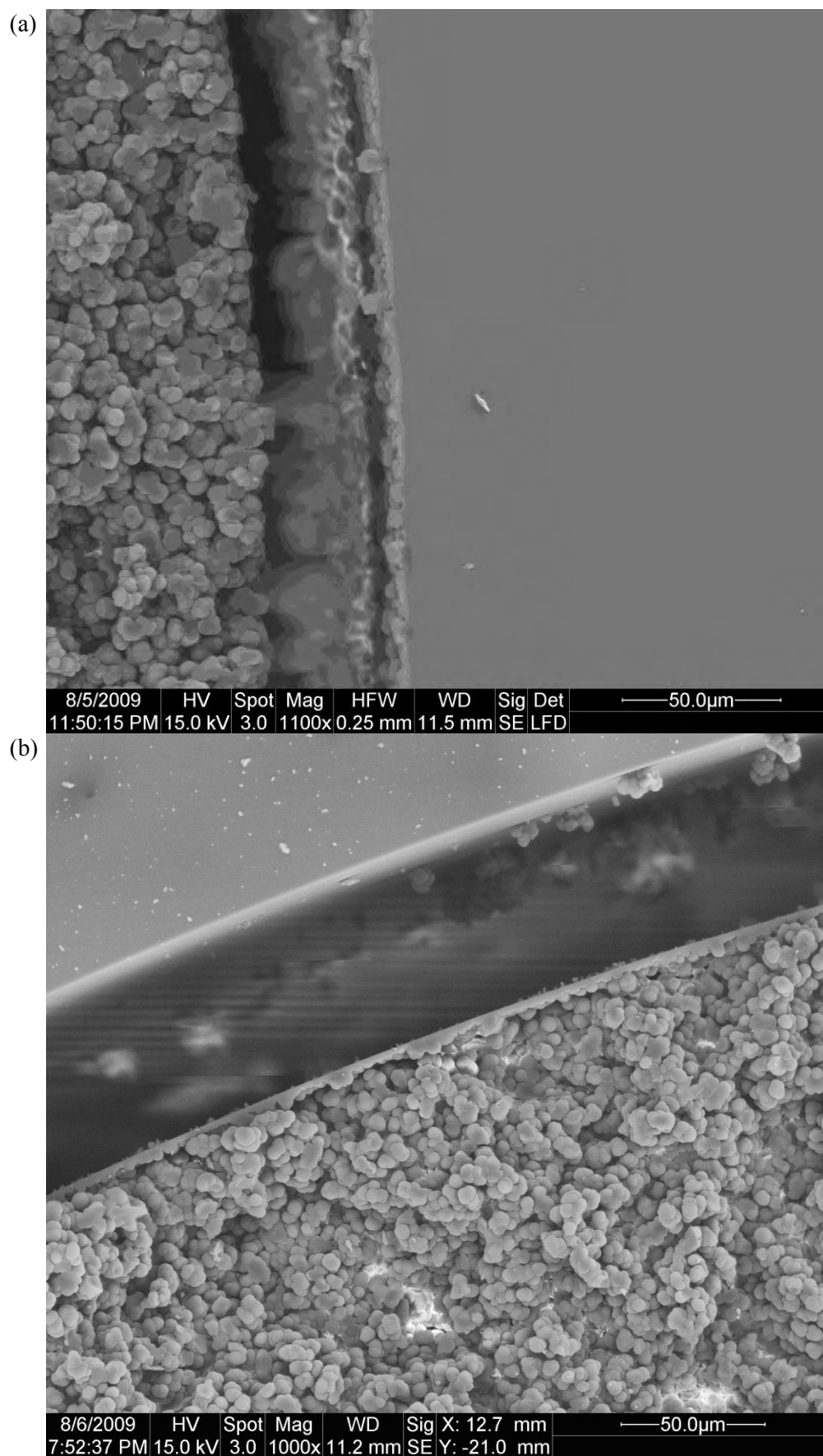


Figure 2.41(a) Main PPM body broken off from sheath layer. (b) PPM in un-treated column showing sheath layer .

In our work, the UVGMA4-70, and UVGMA7-50 formulations are based on fairly different porogenic solvent systems (cyclohexanol/1-dodecanol and methanol/ethanol respectively). The formation of a sheath layer was not observed for PPM prepared using the UVGMA4-70 monolith while a thick sheath layer was formed when using the UVGMA7-50 formulation. This indicates that the porogenic solvents and their concentration play an important role in sheath formation, which can be understood by considering the interactions between the column surface, monomers, and porogens. Near the surface of a vinylised or grafted column, the environment is relatively non-polar due to the presence of the vinyl groups and will have an affinity for non-polar molecules. For the UVGMA4-70 formulation, the porogens are relatively non-polar and will compete with the monomers to solvate the surface. In the UVGMA7-50 formulation, the porogens are highly polar and are hydrophobically repelled from the surface leaving a higher concentration of monomers close to the surface. This monomer-rich region results in the formation of the dense sheath. Based on the hydrophobic repulsion, a thick sheath is expected when using more polar porogens and more apolar monomers.

Both 2 mm ID and 4 mm ID monolithic columns were successfully prepared using photoinitiated polymerisation and used to prepared reactors, further discussed in **Chapter 4**. Monolithic columns prepared using the UVGMA7-50 formulation demonstrated remarkably low backpressures and were capable of flow rates of 0.5 mL min^{-1} using plastic syringes.

2.6 Preparation and characterisation of photopolymerised bulk monolith

Characterisation of PPM morphology, porous properties and surface area is vital for development and optimisation in most applications [70], for which a variety

of techniques have been employed, including inverse size-exclusion chromatography (ISEC) [7], atomic force microscopy [71], transmission electron microscopy (TEM) [72], conductivity [18, 23], volumetric flow-through [18], and three-dimensional laser scanning confocal microscopy (LSCM) [26]. However the most commonly used techniques are mercury intrusion porosimetry (MIP) [4, 6, 28, 43], nitrogen adsorption-desorption isotherms [5, 6, 10, 73], and scanning electron microscopy (SEM) [12, 17, 43, 54]. The major limitations of these three techniques are that they require completely dry PPM for analysis which alters the monolith's porous properties [7], and both MIP and nitrogen isotherm analysis require significantly more material than is produced in either microchip or capillary format. Analysis by MIP or nitrogen isotherms requires preparation of PPM on a scale large enough to yield greater than 100 mg of material in a container where the PPM is easily removed after polymerisation. PPM prepared in this manner for the purpose of characterisation is referred to as bulk monolith, the use of which is based on the assumption that the dimensions of the container have little effect of the porous properties of the PPM and hence PPM prepared in a large container should be the same as PPM prepared in capillary under the same polymerisation conditions. Recently Bystroem *et al.* were able to show that this is not the case and that the container dimensions significantly affect PPM porous properties [70]. Bystroem *et al.* prepared styrenic PPM in different volume vials and also fused-silica capillary using nitroxide-mediated controlled polymerisation, which eliminates temperature gradient effects. They found significant differences between PPM prepared in all formats investigated, both in their mesoporous and macroporous properties. When the container dimensions were reduced from conventional glass vial size to fused-silica capillary size, they found that the specific surface area decreased by 34% and the median pore diameter increased by 45%. Despite these significant changes in the

PPM porous properties, no differences were obvious from SEM images obtained for each sample type. Hence Bystroem *et al.* concluded that analysis of bulk monolith does not afford significant insight into the porous properties of monolith formed within flow-through devices. However, analysis of bulk monolith can be useful for investigating the trends in the porous properties of a series of different monoliths prepared for formulation development.

The development of the various PPM formulations reported in this chapter was mainly based on the permeability of the monolithic columns, in conjunction with SEM analysis for morphological analysis and estimation of the polymerisation end point. The MIP analysis of bulk monolith was performed after formulation development as access to an instrument for analysis was not available until after completion of laboratory experiments. MIP analysis was performed to determine PPM porosity and density for each of the formulations in order to calculate reaction contact times and palladium loadings, discussed in **Chapters 3 and 4**.

The basis of MIP is submersion of a porous solid in mercury, a non-wetting liquid, within a sealed chamber and placing the chamber under pressure to force mercury into the pores of the sample [7]. The volume of mercury in the chamber is measured by capacitance between the conducting mercury and a metal layer on the exterior of the probe. Thus the instrument measures the volume of mercury versus the applied pressure to determine the porous properties of the sample, including pore size distribution, cumulative pore volume, bulk density, total porosity, and surface area. MIP covers the range of flow-through pore sizes and mesopore sizes down to 4 nm in diameter, thus is well suited for studying the macroporous structure of PPM's.

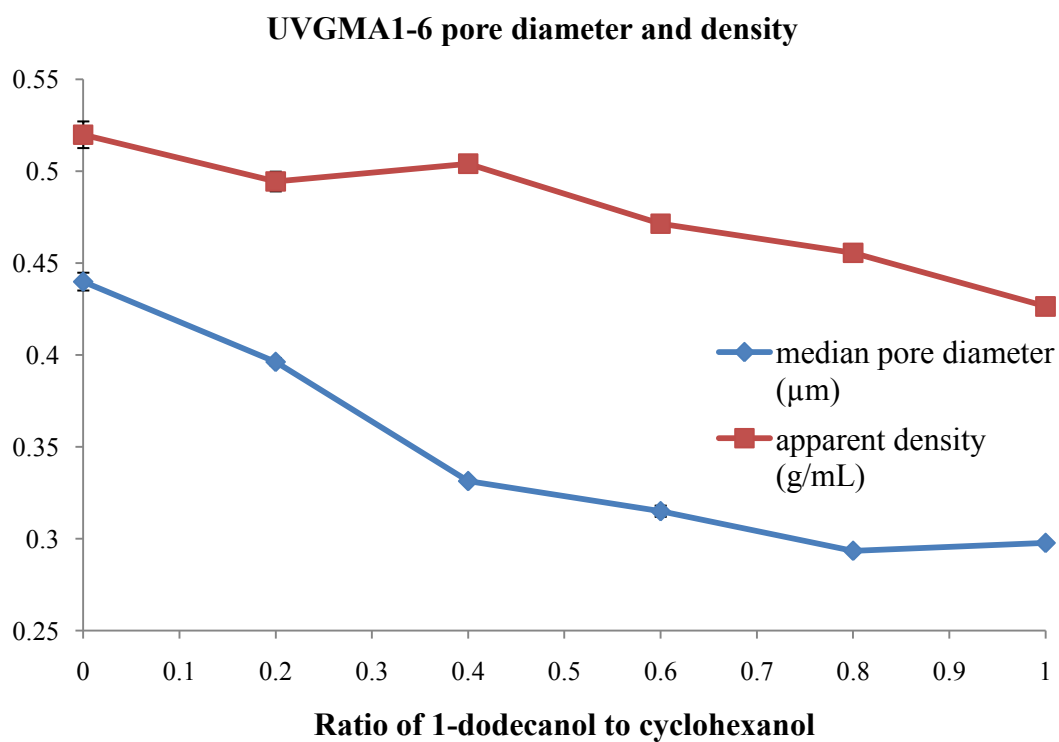
Thermally initiated bulk monolith was prepared using the TCMS1 and TGMA1 formulations in 4 mL glass vials, which is the method most commonly utilised [7, 74]. This affords several grams of material, which is more than sufficient for MIP analysis. The benefit of this approach is that it can be easily scaled up if more material is required. The results of the MIP analysis of thermally initiated PPM was discussed earlier in **Section 2.2.1**.

Preparation of photoinitiated PPM is considerably more difficult since, as discussed in **Section 2.3**, the polymerisation rate is partially dependent on the exposure depth. Hence using a mould with a large depth in order to produce sufficient material for analysis inevitably results in PPM with different morphology than in the target device. Despite this, relatively large exposure depth containers have been used to prepare photoinitiated PPM, such as glass vials [26, 32] and quartz tubes [4, 27]. As the majority of PPM applications use channel depths of 100 μm or less, the PPM prepared in such large dimension containers should not even be closely representative of the channel PPM in terms of morphology and porous properties. Realising this problem, Rohr *et al.* developed a container designed specifically for preparation of photoinitiated PPM which had a large flat disc-like cavity with an optically transparent window. The idea behind using such a device is to have a uniform exposure depth and large exposure area in order to produce enough material for characterisation. Based on the design used by Rohr *et al.*, a bulk polymerisation container was designed with an exposure depth of 2 mm, discussed in detail in **Chapter 5**.

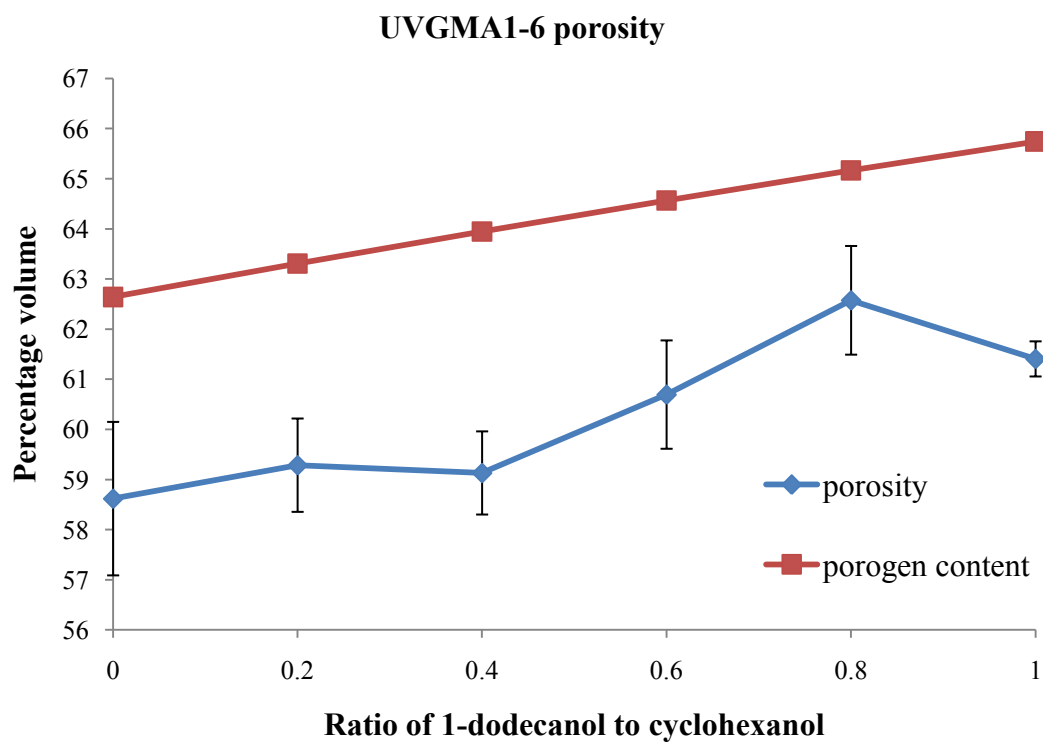
Bulk monolith was prepared from the UVGMA1-6 formulations using this container with the Model 30 as the source and DMPAP as the initiator. Samples of the bulk monolith were analysed by MIP in duplicate for median pore size (by volume), apparent density, and porosity. This pore size is the median for the total

pore volume measured, which gives a measure of the size of the macropores. The apparent density is determined from the initial introduction of mercury under vacuum, which should be before intrusion into the pores. All MIP data collected for bulk photoinitiated PPM is summarised in **Table 2.4**. Only the ratio of the porogenic solvents, cyclohexanol and 1-dodecanol, was varied in these six formulations and all other parameters were held constant. The variation in pore size and density with increasing the amount of 1-dodecanol observed is represented by **Plot 2.1**, which shows the expected trend towards smaller pores with increasing macroporogen content. The overall change in pore diameter is 0.142 μm , which suggests that these two porogens have similar solvating properties in this system. **Plot 2.2** shows the porogen content as a percentage of the total polymerisation mixture volume and measured porosity with increasing 1-dodecanol content. It was expected that the change in porosity would closely match the percentage porogen content, but significant error in the measured porosity values made assigning any trend difficult. The measured porosities are considerably lower than the percentage porogen content, which may indicate significant shrinkage of the bulk PPM after drying. Bulk monolith prepared from the UVGMA6 formulation appears to deviate from the expected trends for pore diameter and porosity. This may result from incomplete phase separation due to the high macroporogen content, however without further investigation this is speculative.

Next, the UVGMA4-70 formulation was used to prepare bulk monolith using both the Model 30 with DMPAP and UV-LED with BAPO. Again, an exposure time of 1 h was used for the Model 30, which successfully afforded fully polymerised bulk monolith. Starting with 1 h, increasingly longer exposure times were used in an attempt to fully polymerise bulk monolith inside the container using the UV-LED, but even after 2 h complete conversion was not realised.



Plot 2.1 Median pore diameters and apparent densities for bulk monolith prepared from the UVGMA1-6 formulations.



Plot 2.2 Porosities and porogens contents for bulk monolith prepared from the UVGMA1-6 formulations.

The polymerisation mixture in the base of the container did not polymerise and remained liquid after exposure. This suggested that the exposure depth of the polymerisation container was too large to prepare bulk monolith using the UV-LED/BAPO combination.

A second container was designed with the minimum possible exposure depth that could be reliably machined, at 200 μm . The full details of this second container are discussed in **Chapter 5**. This container, known hereafter as container 2, has an exposure depth closer to that of the microchips and capillaries investigated, thus should afford bulk monolith with porous properties closer to those found within those devices. This container was used to prepare bulk monolith using the UVGMA4-70 formulation with the Model 30/DMPAP combination for comparison with bulk monolith prepared in the first container, known hereafter as container 1. Initially an exposure time of 10 min was used as this is the time used for preparation of PPM within microchips and capillaries. This exposure time was found not to afford fully polymerised PPM and so was increased to 30 min. The bulk PPM formed in container 2 had a pore diameter 35% larger, 16% lower density and approximately the same porosity as PPM formed in container 1, as shown in **Table 2.4**. It was expected that decreasing the exposure depth would significantly affect pore formation, as this is mainly dependent of the polymerisation rate, and have less of an effect on the density and porosity as they are mainly dependent on the porogen concentration. Container 2 was used to prepared bulk monolith with the same formulation, but using the UV-LED/BAPO combination, which afforded fully polymerised PPM using as exposure time of 40 min, as used for PPM formation in capillary and microchip. The bulk monolith produced had a 4% smaller pore diameter, 20% higher density and a similar porosity to the bulk monolith formed using the Model 30/DMPAP combination.

Container 2 was used to prepare bulk monolith using the UVGMA7-50 formulation with the Model 30/DMPAP and UV-LED/BAPO combinations, utilising the same exposure times as used with the previous bulk monolith preparation. This formulation affords bulk monolith with very large pores, over 2 μm in diameter. In this case, the UV-LED/BAPO combination gave PPM with 9% larger pores, 26% higher density, and 6% lower porosity than the Model 30/DMPAP combination. The difference observed in porous properties of bulk monolith prepared from the two different light source/initiator combinations may result from differences in the polymerisation conditions, such as small variations in reagent concentrations. Inter-sample variation was not investigated, and is required before a true comparison can be made.

Finally, bulk monolith was prepared in container 1 using the UVGMA7-50 formation as this container has an exposure depth similar to the dimensions of the 2 mm and 4 mm ID columns, thus the bulk monolith prepared using this container should have closer porous properties to those monolithic columns. Only the Model 30/DMPAP combination was used with this container. The median pore diameter and porosity for this bulk monolith were similar to the other samples prepared using container 2, probably due to the low shrinkage of this formulation. However, the density obtained was in between the two previous samples.

2.7 Conclusions

Poly(GMA-*co*-EDMA) monolith formulations were developed for photopolymerisation of highly permeable monolithic columns in both smaller ID formats (100 - 150 μm) and larger ID formats (0.25 - 4 mm). This investigation highlighted the necessity of tailoring the PPM formulation to suit the format of interest when utilising photopolymerisation.

Conditions for producing poly(GMA-*co*-EDMA) monolith with excellent morphology by photopolymerisation utilising different light sources, in particular a LED source, in different formats and substrates were successfully developed. Interestingly, despite it being the most commonly utilised source type, the XL-1500 was found to be unsuitable for photopolymerisation of PPM within the devices investigated. The UV-LED/BAPO source/initiator combination developed here should enable greater access to photopolymerisation of PPM by greatly reducing the infrastructure expense of this technique. This combination was successfully used to produce PPM columns up to 2 mm in diameter.

Of the two microchip substrates investigated, borosilicate and COC, the COC devices allowed greater control over the region of PPM formation and hence are more suitable for integrating this type of microreactor with other microfluidic devices. Photografting of COC grades with poor deep UV transmission was achieved in order to allow anchoring of PPM to the polymer surface, also enabling localisation of the surface modification, through use of a photomask, which is also desirable for integration.

The understanding gained during the investigation of poly(GMA-*co*-EDMA) monolith formulations for larger ID formats allowed the production of 4 mm ID monolithic columns without the need for compression to prevent shrinkage. Also highlighted was an alternative explanation of sheath layer formation and its dependence on the porogenic solvents.

Formulation	Source/initiator	Container	Median pore diameter (μm)	Apparent density (gmL^{-1})	Porosity (%)
UVGMA4-70	Model 30/DMPAP	Container 1	0.305 ± 0.005^a	0.363 ± 0.006^a	71.6 ± 0.6^a
UVGMA4-70	Model 30/DMPAP	Container 2	0.468 ± 0.003^a	0.306 ± 0.003^a	73.8 ± 2.3^a
UVGMA4-70	UV-LED/BAPO	Container 2	0.450^b	0.384^b	72.1^b
UVGMA7-50	Model 30/DMPAP	Container 2	2.011 ± 0.035^a	0.337 ± 0.004^a	69.9 ± 2.0^a
UVGMA7-50	UV-LED/BAPO	Container 2	2.219 ± 0.010^a	0.456 ± 0.0016^a	63.2 ± 2.0^a
UVGMA7-50	Model 30/DMPAP	Container 1	2.260 ± 0.018^a	0.397 ± 0.0084^a	65.4 ± 2.4^a

Table 2.4 Photoinitiated bulk PPM MIP analysis results for the UVGMA4-70 and UVMGA7-50 formulations. (a) measurements performed in-house, (b) measurements performed by Particle and Surface Sciences Pty. Ltd.

Formulation	Non-linking monomer	Crosslinking monomer	Porogen 1	Porogen 2
TGMA1	GMA (0.60 g)	EDMA (0.40 g)	Cyclohexanol (0.75 g)	1-dodecanol (0.75 g)
TCMS1	CMS (0.40 g)	DVB (0.60 g)	Toluene (0.44 g)	1-dodecanol (1.06 g)
UVGMA1	GMA (0.60 g)	EDMA (0.40 g)	Cyclohexanol (1.50 g)	
UVGMA2	GMA (0.60 g)	EDMA (0.40 g)	Cyclohexanol (1.20 g)	1-dodecanol (0.30 g)
UVGMA3	GMA (0.60 g)	EDMA (0.40 g)	Cyclohexanol (0.90 g)	1-dodecanol (0.60 g)
UVGMA4	GMA (0.60 g)	EDMA (0.40 g)	Cyclohexanol (0.60 g)	1-dodecanol (0.90 g)
UVGMA5	GMA (0.60 g)	EDMA (0.40 g)	Cyclohexanol (0.30 g)	1-dodecanol (1.20 g)

Table 2.5 Summary of PPM formulations investigated.

Formulation	Non-linking monomer	Crosslinking monomer	Porogen 1	Porogen 2
UVGMA6	GMA (0.60 g)	EDMA (0.40 g)	1-dodecanol (1.50 g)	
UVGMA4-70	GMA (0.60 g)	EDMA (0.40 g)	Cyclohexanol (0.93 g)	1-dodecanol (1.40 g)
UVGMA4-80	GMA (0.60 g)	EDMA (0.40 g)	Cyclohexanol (1.60 g)	1-dodecanol (2.40 g)
UVGMA8	GMA (0.60 g)	EDMA (0.40 g)	Cyclohexanol (0.30 g)	1-dodecanol (0.70 g)
UVGMA9	GMA (0.61 g)	EDMA (0.39 g)	1-dodecanol (1.37 g)	
UVGMA7	GMA (0.60 g)	EDMA (0.40 g)	Methanol (0.75 g)	Ethanol (0.75 g)
UVGMA7-50	GMA (0.60 g)	EDMA (0.40 g)	Methanol (0.50 g)	Ethanol (0.50 g)

Table 2.6 Continued Summary of PPM formulations investigated.

2.8 Experimental

2.8.1 Inner-capillary wall vinylisation

This procedure was modified from the one developed by Rohr *et al.* [75]. A length of fused-silica capillary was rinsed by flushing with acetone followed by water. Controlled fluid pumping was performed using Hamilton Gastight® syringes and Harvard Apparatus model PHD 2000 syringe pumps. The capillary was flushed with a 0.2M NaOH solution until a basic pH was detected at its terminus, after which flushing was continued for 30 min at $15 \mu\text{L h}^{-1}$. The capillary was rinsed with water until a neutral pH was detected, then flushed with a 0.2M HCl solution until an acidic pH was detected, after which flushing was continued for 30 min at $15 \mu\text{L h}^{-1}$. The capillary was rinsed with water until a neutral pH was detected, followed by a rinse with ethanol. A solution of 20% w/w 3-(trimethoxysilyl)propyl methacrylate in ethanol adjusted to pH 5 with acetic acid was prepared and flushed through the capillary at $15 \mu\text{L h}^{-1}$, after which it was rinsed with acetone, dried with compressed nitrogen, and stored for at least 24 h before use.

2.8.2 PPM polymerisation mixture preparation

Each polymerisation mixture was prepared in the same way. The following description is for the UVGMA4-70 formulation with BAPO. The reagents used for the other formulations investigated can be found in **Table 2.5** on pages 138 and 139. All polymerisation mixtures were prepared using 1 wt% initiator with respect to the monomers. The following reagents were weighed into an amber vial in the order listed: phenylbis(2,4,6-trimethylbenzoyl)phosphine oxide (10 mg), glycidyl methacrylate (0.6 g), ethylene glycol dimethacrylate (0.4 g), cyclohexanol (0.932 g), 1-dodecanol (1.398 g). This mixture was ultrasonicated for 5 min to dissolve the

initiator, and purged with nitrogen for 10 min. After usage the mixture was stored at -18 °C freezer.

2.8.3 Thermally initiated PPM preparation in fused-silica capillary

Vinylised capillary (250 μm ID) was cut into 30 cm lengths and flushed with polymerisation mixture until no air bubbles were observed. The ends of the capillary were sealed with rubber septa and placed in a 70 °C water bath for 16 h. After removal from the water bath, the capillary was trimmed to 25 cm by cutting equally from both ends and flushed with methanol at 120 $\mu\text{L h}^{-1}$ for 2 h.

2.8.4 Photoinitiated PPM preparation in fused-silica capillary

Vinylised capillary (100 μm ID) was cut into 35 cm lengths, flushed with polymerisation mixture until no air bubbles were observed, and the ends of the capillary were sealed with rubber septa. For both the OAI Inc. Model 30 and Opto Tech Corp. Shark SeriesTMUV-LED sources, the capillary was coiled up to fit within the exposure area, for the SpectrolinkerTM XL-1500 the capillary was straight. The capillary was exposed using either the Model 30, UV-LED, or XL-1500, after which it was flushed with methanol at 30 $\mu\text{L h}^{-1}$ for 8 h. Finally the capillary was trimmed to 30 cm by cutting equally from both ends.

2.8.5 Photoinitiated PPM preparation in glass microchips

The microchannel wall of the microchips was vinylised using the same procedure as used for capillary. The microchip was filled with polymerisation mixture by pipetting the mixture into both Y wells and putting a minor vacuum on the opposite well using a plastic syringe. Once the channel was full, the single well was sealed using a rubber septa and the mixture in the Y section of the microchannel was removed by placing one of the wells under vacuum using a plastic syringe. Pressure was applied to the single sealed well to move the mixture into the Y section,

and the removal process repeated. The result was a section of the microchannel at both ends of the chip devoid of polymerisation mixture. All three wells were sealed with rubber septa and tape. The microchip was exposed using either the Model 30, UV-LED, or XL-1500, after which it was placed in a chip holder (described in **Chapter 5, Section 5.2**) and flushed with methanol at $60 \mu\text{L h}^{-1}$ for 4 h.

2.8.6 COC plate grafting adhesion testing

COC plates ($75.5 \times 25.5 \times 1 \text{ mm}$) were cut into two equal pieces and cleaned with acetone and tissue. A mixture of TMPTA (0.5 g) and 3 wt% BP (15 mg) was prepared and purged with nitrogen for 10 min. The mixture was pipetted onto one of the slides until it was covered. A second plate was placed on top of the first then the two plates were clamped together with bull clips along opposite edges of the plates. The plates were exposed for 20 min in the XL-1500 UVC on each face.

2.8.7 COC capillary one-step grafting

A grafting mixture was prepared by weighing MMA (0.5 g), EDA (0.5 g), and BP (30 mg) into a vial, followed by sonication to dissolve the BP. A 12 cm length of COC capillary was filled with the grafting mixture and sealed at both ends using rubber septa. The capillary was exposed in the XL-1500 UVC for 8 min, rotated 180° along the capillary length and exposed again for the same time. Finally the capillary was flushed with methanol and dried with compressed nitrogen.

2.8.8 COC capillary two-step grafting

Two solutions were prepared, an initiator solution consisting of BP (30 mg) in methanol (1.0 g), and a monomer mixture consisting of MMA (0.5 g), EDA (0.5 g), and hydroquinone (25 mg). A 40 cm length of COC capillary was cut and filled with the BP solution, then sealed with rubber septa. The capillary was exposed in the XL-1500 UVC for 20 min, rotated 180° along the capillary length and then

exposed again for the same time. The capillary was then flushed with methanol, dried with compressed nitrogen, filled with the monomer mixture and sealed with rubber septa. The capillary was exposed in the XL-1500 UVC for 10 min, rotated 180°, and exposed again for the same time. Finally the grafted capillary was flushed with methanol and dried with compressed nitrogen.

2.8.9 Photoinitiated PPM preparation in COC capillary

Grafted COC capillary was cut into 12 cm lengths, flushed with polymerisation mixture until no air bubbles were observed, and sealed with rubber septa. The capillary was exposed using either the Model 30, UV-LED, or XL-1500, after which it was flushed with methanol at $60 \mu\text{L h}^{-1}$ for 4 h. Finally the capillary was trimmed to 10 cm by cutting equally from both ends.

2.8.10 Pasteur pipette inner-wall vinylisation

The method used was adapted from that described in **Section 2.8.1**, scaled up for the larger dimensions using flow rates of 0.1 mL min^{-1} . Three long Pasteur pipettes were placed inside each other such that the tips of each entered the inner neck of the pipette below. Tefzel tubing (1.6 mm ID) was placed in the neck of the top pipette and connected to a syringe.

2.8.11 Photoinitiated PPM preparation in Pasteur pipette

Polymerisation mixture was drawn into a vinylised pipette up to the tapered neck and held in place by sealing the other end of the pipette. The tip of the pipette was sealed with rubber septa. The pipette was placed under the light source at a slight angle, to keep the polymerisation mixture from draining into the main chamber of the pipette, and then exposed to form the PPM. Once the exposure was complete, the pipette was placed in a stoppered Büchner flask with only the PPM filled tip inside the flask. The empty top section of the pipette was filled with methanol and a

vacuum applied to the flask to draw the methanol through the PPM. The pipette was filled with methanol repeatedly until the effluent exiting the pipette tip was clear. The pipette was left in the flask under vacuum for 4 h to dry.

2.8.12 COC microchip machining

Milling of the COC microchips was performed by Peter Dove of the Central Science Laboratory, University of Tasmania. The microchips were milled using a flycutter in a vertical milling machine in order to reduce the plate thickness to 0.9 mm for the top and bottom plates. Polishing of the COC microchips was performed by Simon Stephens of the School of Earth Sciences, University of Tasmania. The polishing was done in a two stage process. The first stage involved fine grinding to remove the machining marks and smooth the surface for polishing. A sheet of 1200 wet and dry Silicon Carbide paper was laid out flat on a glass plate wet with water. The chip was laid face down on the abrasive paper and with moderate pressure moved straight back and forth across a small area. Clean water was added frequently to wash away the cuttings. Every 30 sec the chip was rotated though 90° so that the scratches from the abrasive were across one another in order to keep the surface relatively flat. This was continued until the curved machine marks were removed. The second stage of polishing was done with 0.3 µm alumina mixed with clean water on a Pan-W cloth disc. Pressure was approximately 0.5 kg for 3 min at 200 rpm or until the microchip surface appeared shiny. Finally, the polished microchips were cleaned by first rinsing with water, then flushing 1 mL of a mixture of detergent and water through the microchannel and then sonicating the microchip in the detergent solution for 5 min. The microchip was rinsed and flushed with Milli-Q water, followed by methanol, then dried with compressed nitrogen.

2.8.13 COC microchip grafting

Photografting the COC microchips was performed using a method adapted from that described in **Section 2.8.8**, using longer exposure times and photomasking. A COC microchip was filled with a BP solution by capillary action and the wells sealed with rubber septa and black electrical tape. The microchannel was also masked with black electrical tape, leaving 4.9 cm of the channel exposed. The microchip was exposed in the XL-1500 UVC for 40 min, flipped over and then exposed again for the same time. Next, the microchip was flushed with methanol, dried with compressed nitrogen, then filled with the monomer mixture and sealed with rubber septa. The microchip was exposed in the XL-1500 UVC for 15 min, flipped over and exposed again for the same time. Finally the microchip was flushed with methanol and dried with compressed nitrogen.

2.8.14 Photoinitiated PPM preparation in COC microchip

The grafted COC was filled with polymerisation mixture by capillary action and the wells were sealed with rubber septa and black electrical tape. The ends of the microchip were masked with black electrical tape, leaving 4.9 cm of the microchannel exposed. The microchip was exposed using either the Model 30, UV-LED, or XL-1500, after which it was flushed with methanol at $60 \mu\text{L h}^{-1}$ for 4 h.

2.8.15 Glass column preparation and inner-wall vinylisation

Approximately 11 cm lengths of 2 mm and 4 mm ID, 6 mm OD borosilicate glass tubing were cut and the ends rounded using a blow torch. Once cooled, the inner-wall of the columns were vinylised by adapting the method described in **Section 2.8.1** for the larger dimensions, using flow rates of 0.1 mL min^{-1} . To increase through-put, four lengths of glass column of the same ID were joined together with 3 cm lengths of 5 mm ID polyethylene tubing.

2.8.16 Photoinitiated PPM preparation in glass column

A vinylised glass column was sealed at one end using parafilm and PTFE tape, filled with polymerisation mixture, and then the other end sealed. The column was exposed under the desired light source for the required time. After exposure, the end seals were removed and the column was connected to a 60 mL plastic syringe using 5 mm ID polyethylene tubing. The other end of the column was placed in a 100 mL conical flask filled with methanol. The syringe was used to apply a vacuum to one end of the column in order to draw methanol through it.

2.8.17 SEM sample preparation

SEM stubs were prepared by cutting 2 mm thick aluminium sheet into 2×1 cm pieces which were bent into right-angle brackets, glued onto 12.7 mm diameter SEM stubs using Araldite™, and allowed to dry overnight. Fused-silica capillary monolithic columns were cut into 5-9 mm lengths from different sections, while COC capillary monolithic columns were scored around the outside at 1 cm intervals using a razor blade and snapped at the score. In a similar fashion, Pasteur pipette monolithic columns were scored around the outside at 1 cm intervals using a ceramic capillary cutter and snapped at the score. Samples were adhered to the upright part of a bracketed stub using carbon tape such that the 4-5 samples were vertical with the tips ~1 mm above the tip of the bracket. Borosilicate microchip monolithic columns were scored down the centre using a ceramic capillary cutter and then snapped in two using two sets of pliers. COC microchip monolithic columns were scored 0.5 mm deep across the width of the top plate of the microchip at 1 cm intervals using a box cutter. The COC microchip was placed in liquid nitrogen for 30 min, after which it was quickly removed and snapped at the score marks using pliers. Parts with clean cross-sections of the monolithic column were broken into smaller pieces and mounted onto bracketed SEM stubs with carbon tape such that the

cross-sections were facing vertical. These mounted stubs were dried under vacuum for 4-6 h before being sputter coated with gold or platinum.

2.8.18 Glass column SEM sample preparation

SEM stubs for mounting glass column sections were prepared in a similar manner as described in **Section 2.8.17** except, instead of using aluminium brackets, plungers of 3 mL plastic syringe trimmed to 2 cm from the thumb grip were glued on. This provided a cross-shaped structure to which 3 cm long samples of the 6 mm OD glass monolithic columns were mounted with Araldite™. The column samples were prepared by placing the column in a cordless drill and scoring the outside around the rotation axis with a ceramic capillary cutter at 3 cm intervals, after which the columns were wrapped in paper towel and snapped to the scores.

2.8.19 SEM imaging

Scanning electron micrographs were acquired using a FEI Quanta 600 MLA ESEM either in high vacuum or low vacuum mode (0.45-0.6 Torr). Initial micrographs showed severe charging, **Figure 2.16** for example, which is denoted by regions of elevated brightness. Charging is caused by the accumulation of charge on the surface of the polymer which reflects the electron beam through electrostatic repulsion and makes the charged region appear brighter, resulting in a loss of contrast in the image. This was overcome by using the SEM in low vacuum mode where the vacuum is reduced and water vapour introduced into the chamber, which helped reduce the charge accumulation. Most of the SEM micrographs shown were acquired in low vacuum mode at 0.6 Torr with 15-20 kV acceleration voltage and a 3.0 spot size.

2.8.20 Preparation of thermally initiated bulk monolith

Screw thread glass vials (15 × 45 mm) were filled with polymerisation mixture, sealed, and then placed in a 70°C water bath for 16 h. The vials were broken open to remove the bulk monolith, which was transferred into cellulose thimbles and rinsed with hot methanol in a soxhlet overnight. The thimbles were removed from the soxhlet and dried in a vacuum oven at 60 °C for 4 h, after which the bulk monolith was transferred into 20 mL glass vials.

2.8.21 Preparation of photoinitiated bulk monolith using container 1

Container 1 was thoroughly cleaned with methanol and tissue, and then allowed to dry. The container was assembled and polymerisation mixture injected into the chamber through the rubber o-ring using a 25 gauge syringe needle and glass syringe. The container was exposed using either the Model 30 or UV-LED. After exposure, the container was disassembled and the bulk monolith was transferred into a cellulose thimble and rinsed and dried as described in **Section 2.8.20**.

2.8.22 Preparation of photoinitiated bulk monolith using container 2

Container 2 was thoroughly cleaned with methanol and tissue, and then allowed to dry. The quartz disc was placed in a 1M sodium hydroxide bath for 1 h, rinsed with water, placed in a 1M hydrochloric acid bath for 1 h, then rinsed with water and dried. The quartz disc was then placed in a vacuum desiccator with an open vial of trichloro(1*H*,1*H*,2*H*,2*H*-perfluorooctyl)silane, evacuated and left overnight. The assembled container was filled with excess polymerisation mixture and then a treated quartz disc was placed in the container. The disc was held in place with the sealing ring and the excess polymerisation mixture removed. The container was exposed using either the Model 30 or UV-LED. After exposure, the container

was disassembled and the bulk monolith was transferred into a cellulose thimble and rinsed and dried as described in **Section 2.8.20**.

2.8.23 MIP analysis of bulk monolith

Porosimetry analysis was performed using a Micromeritics® AutoPore™ IV 9500 mercury intrusion porosimeter. The dry bulk monolith was broken into pieces small enough to fit into the 3 mL penetrometers, then 0.1 g of sample was placed inside and sealed. Automated analysis was performed on the sample with equalisation by rate, using 1 to 33,000 psi for intrusion and 33,000 psi to atmospheric for extrusion.

2.8.24 Capillary weighing experiment

Monolithic capillary column was prepared using the TCMS1 formulation as described in **Section 2.8.3**. The monolithic column was dried by attaching the capillary to a compressed 60 mL plastic syringe, and forcing air through the capillary overnight. The dried capillary was placed in a glass Petri dish and weighed on an analytical balance. Next, the capillary was flushed with ethanol for 30 min at $120 \mu\text{L h}^{-1}$, quickly sealed at both ends with rubber septa, and then reweighed. Finally, the mass of the rubber septa was recorded. This procedure was repeated another two times to the same capillary.

2.9 References

1. Svec, F. and D.M.J. Fréchet, Rigid Macroporous Organic Polymer Monoliths Prepared by Free Radical Polymerisation, in *Monolithic Materials - preparation, properties and applications*, F. Svec, T.B. Tennikova, and Z. Deyl, Editors. 2003, Elsevier. 19-50.
2. Buchmeiser, M.R., Polymeric monolithic materials: Syntheses, properties, functionalization and applications. *Polymer*, 2007. **48**(8), 2187-2198.
3. Svec, F., Porous polymer monoliths: Amazingly wide variety of techniques enabling their preparation. *Journal of Chromatography A*, 2010. **1217**(6), 902-924.
4. Yu, C., M.C. Xu, F. Svec, and J.M.J. Fréchet, Preparation of monolithic polymers with controlled porous properties for microfluidic chip applications using photoinitiated free-radical polymerization. *Journal of Polymer Science Part a-Polymer Chemistry*, 2002. **40**(6), 755-769.
5. Viklund, C., F. Svec, J.M.J. Fréchet, and K. Irgum, Monolithic, "Molded", Porous Materials with High Flow Characteristics for Separations, Catalysis, or Solid-Phase Chemistry: Control of Porous Properties during Polymerization. *Chemistry of Materials*, 1996. **8**(3), 744-50.
6. Danquah, M.K. and G.M. Forde, Preparation of macroporous methacrylate monolithic material with convective flow properties for bioseparation: Investigating the kinetics of pore formation and hydrodynamic performance. *Chemical Engineering Journal*, 2008. **140**(1-3), 593-599.
7. Urban, J., S. Eeltink, P. Jandera, and P.J. Schoenmakers, Characterization of polymer-based monolithic capillary columns by inverse size-exclusion chromatography and mercury-intrusion porosimetry. *Journal of Chromatography A*, 2008. **1182**(2), 161-168.
8. Mao, X.L., Y. Luo, Z.P. Dai, K.Y. Wang, Y.G. Du, and B.C. Lin, Integrated lectin affinity microfluidic chip for glycoform separation. *Analytical Chemistry*, 2004. **76**(23), 6941-6947.
9. Luo, Q.Z., H.F. Zou, X.Z. Xiao, Z. Guo, L. Kong, and X.Q. Mao, Chromatographic separation of proteins on metal immobilized iminodiacetic acid-bound molded monolithic rods of macroporous poly(glycidyl methacrylate-co-ethylene dimethacrylate). *Journal of Chromatography A*, 2001. **926**(2), 255-264.
10. Pan, Z., H. Zou, W. Mo, X. Huang, and R. Wu, Protein A immobilized monolithic capillary column for affinity chromatography. *Analytica Chimica Acta*, 2002. **466**(1), 141-150.
11. Sýkora, D., F. Svec, and J.M.J. Fréchet, Separation of oligonucleotides on novel monolithic columns with ion-exchange functional surfaces. *Journal of Chromatography A*, 1999. **852**(1), 297-304.
12. Ueki, Y., T. Umemura, J. Li, T. Otake, and K. Tsunoda, Preparation and Application of Methacrylate-Based Cation-Exchange Monolithic Columns for Capillary Ion Chromatography. *Analytical Chemistry*, 2004. **76**(23), 7007-7012.
13. Preinerstorfer, B., W. Bicker, W. Lindner, and M. Lämmerhofer, Development of reactive thiol-modified monolithic capillaries and in-column surface functionalization by radical addition of a chromatographic ligand for capillary electrochromatography. *Journal of Chromatography, A*, 2004. **1044**(1-2), 187-199.
14. Wen, Y. and Y.-Q. Feng, Preparation and evaluation of hydroxylated poly(glycidyl methacrylate-co-ethylene dimethacrylate) monolithic capillary

- for in-tube solid-phase microextraction coupled to high-performance liquid chromatography. *Journal of chromatography. A*, 2007. **1160**(1-2), 90-8.
15. Sun, X.H., W.C. Yang, T. Pan, and A.T. Woolley, Affinity monolith integrated poly(methyl methacrylate) microchips for on-line protein extraction and capillary electrophoresis. *Analytical Chemistry*, 2008. **80**(13), 5126-5130.
16. Faure, K., N. Delaunay, G. Alloncle, S. Cotte, and J.-L. Rocca, Optimization of in-situ monolithic synthesis for immunopreconcentration in capillary. *Journal of Chromatography, A*, 2007. **1149**(2), 145-150.
17. Tripp, J.A., F. Svec, and J.M.J. Fréchet, Grafted macroporous polymer monolithic disks: A new format of scavengers for solution-phase combinatorial chemistry. *Journal of Combinatorial Chemistry*, 2001. **3**(2), 216-223.
18. Gusev, I., X. Huang, and C. Horváth, Capillary columns with in situ formed porous monolithic packing for micro high-performance liquid chromatography and capillary electrochromatography. *Journal of Chromatography A*, 1999. **855**(1), 273-290.
19. Karbass, N., V. Sans, E. Garcia-Verdugo, M.I. Burguete, and S.V. Luis, Pd(0) supported onto monolithic polymers containing IL-like moieties. Continuous flow catalysis for the Heck reaction in near-critical EtOH. *Chemical Communications*, 2006(29), 3095-3097.
20. Ma, J., L. Zhang, Z. Liang, W. Zhang, and Y. Zhang, Monolith-based immobilized enzyme reactors: Recent developments and applications for proteome analysis. *Journal of Separation Science*, 2007. **30**(17), 3050-3059.
21. Ro, K.W., R. Nayak, and D.R. Knapp, Monolithic media in microfluidic devices for proteomics. *Electrophoresis*, 2006. **27**(18), 3547-3558.
22. Geiser, L., S. Eeltink, F. Svec, and J.M.J. Fréchet, Stability and repeatability of capillary columns based on porous monoliths of poly(butyl methacrylate-co-ethylene dimethacrylate). *Journal of Chromatography, A*, 2007. **1140**(1-2), 140-146.
23. Walsh, Z., P.A. Levkin, V. Jain, B. Paull, F. Svec, and M. Macka, Visible light initiated polymerization of styrenic monolithic stationary phases using 470 nm light emitting diode arrays. *Journal of Separation Science*, 2010. **33**(1), 61-66.
24. Safrany, A., B. Beiler, K. Laszlo, and F. Svec, Control of pore formation in macroporous polymers synthesized by single-step gamma-radiation-initiated polymerization and cross-linking. *Polymer*, 2005. **46**(9), 2862-2871.
25. Širc, J., Z. Bosáková, P. Coufal, J. Michálek, M. Pěšádný, R. Hobzová, and J. Hradil, Morphological and chromatographic characterization of molecularly imprinted monolithic columns. *E-Polymers*, 2007. **117**, 15.
26. He, M., Y. Zeng, X.J. Sun, and D.J. Harrison, Confinement effects on the morphology of photopatterned porous polymer monoliths for capillary and microchip electrophoresis of proteins. *Electrophoresis*, 2008. **29**(14), 2980-2986.
27. Chen, J.R., M.T. Dulay, R.N. Zare, F. Svec, and E. Peters, Macroporous photopolymer frits for capillary electrochromatography. *Analytical Chemistry*, 2000. **72**(6), 1224-1227.
28. Yu, C., F. Svec, and J.M.J. Fréchet, Towards stationary phases for chromatography on a microchip: Molded porous polymer monoliths prepared in capillaries by photoinitiated in situ polymerization as separation media for electrochromatography. *Electrophoresis*, 2000. **21**(1), 120-127.

29. Daley, A.B. and R.D. Oleschuk, Development of fluorinated, monolithic columns for improved chromatographic separations of fluorinated-tagged analytes. *Journal of Chromatography A*, 2009. **1216**(5), 772-780.
30. Hirano, T., S. Kitagawa, and H. Ohtani, Methacrylate-ester-based Reversed Phase Monolithic Columns for High Speed Separation Prepared by Low Temperature UV Photo-polymerization. *Analytical Sciences*, 2009. **25**(9), 1107-1113.
31. Armenta, J.M., B.H. Gu, P.H. Humble, C.D. Thulin, and M.L. Lee, Design and evaluation of a coupled monolithic preconcentrator-capillary zone electrophoresis system for the extraction of immunoglobulin G from human serum. *Journal of Chromatography A*, 2005. **1097**(1-2), 171-178.
32. Courtois, J., E. Byström, and K. Irgum, Novel monolithic materials using poly(ethylene glycol) as porogen for protein separation. *Polymer*, 2006. **47**(8), 2603-2611.
33. Walsh, Z., S. Abele, B. Lawless, D. Heger, P. Klan, M.C. Breadmore, B. Paull, and M. Macka, Photoinitiated polymerisation of monolithic stationary phases in polyimide coated capillaries using visible region LEDs. *Chemical Communications*, 2008(48), 6504-6506.
34. Li, C., W.-C. Lee, and K.H. Lee, Affinity separations using microfabricated microfluidic devices: In situ photopolymerization and use in protein separations. *Biotechnology and Bioengineering*, 2003. **8**(4), 240-245.
35. Fintschenko, Y., W.Y. Choi, S.M. Ngola, and T.J. Shepodd, Chip electrochromatography of polycyclic aromatic hydrocarbons on an acrylate-based UV-initiated porous polymer monolith. *Fresenius Journal of Analytical Chemistry*, 2001. **371**(2), 174-181.
36. Rohr, T., C. Yu, M.H. Davey, F. Svec, and J.M.J. Fréchet, Porous polymer monoliths: Simple and efficient mixers prepared by direct polymerization in the channels of microfluidic chips. *Electrophoresis*, 2001. **22**(18), 3959-3967.
37. Throckmorton, D.J., T.J. Shepodd, and A.K. Singh, Electrochromatography in microchips: Reversed-phase separation of peptides and amino acids using photopatterned rigid polymer monoliths. *Analytical Chemistry*, 2002. **74**(4), 784-789.
38. Proczek, G., V. Augustin, S. Descroix, and M.C. Hennion, Integrated microdevice for preconcentration and separation of a wide variety of compounds by electrochromatography. *Electrophoresis*, 2009. **30**(3), 515-524.
39. Stachowiak, T.B., T. Rohr, E.F. Hilder, D.S. Peterson, M.Q. Yi, F. Svec, and J.M.J. Fréchet, Fabrication of porous polymer monoliths covalently attached to the walls of channels in plastic microdevices. *Electrophoresis*, 2003. **24**(21), 3689-3693.
40. Yang, Y.N., C. Li, K.H. Lee, and H.G. Craighead, Coupling on-chip solid-phase extraction to electrospray mass spectrometry through an integrated electrospray tip. *Electrophoresis*, 2005. **26**(19), 3622-3630.
41. Bedair, M.F. and R.D. Oleschuk, Fabrication of porous polymer monoliths in polymeric microfluidic chips as an electrospray emitter for direct coupling to mass spectrometry. *Analytical Chemistry*, 2006. **78**(4), 1130-1138.
42. Bhattacharyya, A. and C.M. Klapperich, Thermoplastic microfluidic device for on-chip purification of nucleic acids for disposable diagnostics. *Analytical Chemistry*, 2006. **78**(3), 788-792.
43. Mair, D.A., E. Geiger, A.P. Pisano, J.M.J. Fréchet, and F. Svec, Injection molded microfluidic chips featuring integrated interconnects. *Lab on a Chip*, 2006. **6**(10), 1346-1354.

44. Ro, K.W., H. Liu, and D.R. Knapp, Plastic microchip liquid chromatography-matrix-assisted laser desorption/ionization mass spectrometry using monolithic columns. *Journal of Chromatography A*, 2006. **1111**(1), 40-47.
45. Abele, S., F.Q. Nie, F. Foret, B. Paull, and M. Macka, UV-LED photopolymerised monoliths. *Analyst*, 2008. **133**(7), 864-866.
46. Faure, K., M. Albert, V. Dugas, G. Crétier, R. Ferrigno, P. Morin, and J.L. Rocca, Development of an acrylate monolith in a cyclo-olefin copolymer microfluidic device for chip electrochromatography separation. *Electrophoresis*, 2008. **29**(24), 4948-4955.
47. Mair, D.A., T.R. Schwei, T.S. Dinio, F. Svec, and J.M.J. Fréchet, Use of photopatterned porous polymer monoliths as passive micromixers to enhance mixing efficiency for on-chip labeling reactions. *Lab on a Chip*, 2009. **9**(7), 877-883.
48. Faure, K., M. Blas, O. Yassine, N. Delaunay, G. Cretier, M. Albert, and J.-L. Rocca, Electrochromatography in poly(dimethyl)siloxane microchips using organic monolithic stationary phases. *Electrophoresis*, 2007. **28**(11), 1668-1673.
49. Yang, W.C., X.H. Sun, T. Pan, and A.T. Woolley, Affinity monolith preconcentrators for polymer microchip capillary electrophoresis. *Electrophoresis*, 2008. **29**(16), 3429-3435.
50. Bedair, M. and R.D. Oleschuk, Lectin affinity chromatography using porous polymer monolith assisted nanoelectrospray MS/MS. *Analyst*, 2006. **131**(12), 1316-1321.
51. Fisher, J.P., D. Dean, P.S. Engel, and A.G. Mikos, Photoinitiated polymerization of biomaterials. *Annual Review of Materials Research*, 2001. **31**, 171-181.
52. Bandari, R., W. Knolle, A. Prager-Duschke, H.-J. Gläsel, and M.R. Buchmeiser, Monolithic media prepared via electron beam curing for proteins separation and flow-through catalysis. *Macromolecular Chemistry and Physics*, 2007. **208**(13), 1428-1436.
53. Liu, J.K., C.F. Chen, C.W. Tsao, C.C. Chang, C.C. Chu, and D.L. Devoe, Polymer Microchips Integrating Solid-Phase Extraction and High-Performance Liquid Chromatography Using Reversed-Phase Polymethacrylate Monoliths. *Analytical Chemistry*, 2009. **81**(7), 2545-2554.
54. Viklund, C., E. Pontén, B. Glad, K. Irgum, P. Hörstedt, and F. Svec, "Molded" Macroporous Poly(glycidyl methacrylate-co-trimethylolpropane trimethacrylate) Materials with Fine Controlled Porous Properties: Preparation of Monoliths Using Photoinitiated Polymerization. *Chemistry of Materials*, 1997. **9**(2), 463-471.
55. Szumski, M. and B. Buszewski, Effect of temperature during photopolymerization of capillary monolithic columns. *Journal of Separation Science*, 2009. **32**(15-16), 2574-2581.
56. Bernabe-Zafon, V., A. Canto-Mirapeix, E.F. Simo-Alfonso, G. Ramis-Ramos, and J.M. Herrero-Martinez, Comparison of thermal- and photopolymerization of lauryl methacrylate monolithic columns for CEC. *Electrophoresis*, 2009. **30**(11), 1929-1936.
57. Altun, Z., A. Hjelmstrom, M. Abdel-Rehim, and L.G. Blomberg, Surface modified polypropylene pipette tips packed with a monolithic plug of adsorbent for high-throughput sample preparation. *Journal of Separation Science*, 2007. **30**(12), 1964-1972.

58. Breadmore, M.C. and R.M. Guijt, High intensity light emitting diode array as an alternative exposure source for the fabrication of electrophoretic microfluidic devices. *Journal of Chromatography A*, 2008. **1213**(1), 3-7.
59. Kenning, N.S., B.A. Ficek, C.C. Hoppe, and A.B. Scranton, Spatial and temporal evolution of the photoinitiation rate for thick polymer systems illuminated by polychromatic light: selection of efficient photoinitiators for LED or mercury lamps. *Polymer International*, 2008. **57**(10), 1134-1140.
60. Allen, N.S., J. Segurola, M. Edge, E. Santamari, A. McMahon, and S. Wilson, A comparative kinetic study of commercial photoinitiators for UV/visible curable acrylate clear coatings. *Jocca-Surface Coatings International*, 1999. **82**(2), 67-+.
61. Vaz, F.A.S., P.M. de Castro, C. Molina, S.J.L. Ribeiro, F.C. Polachini, Y. Messaddeq, A.P. Nunes, and M.A.L. de Oliveira, External polyacrylate-coating as alternative material for preparation of photopolymerized sol-gel monolithic column. *Talanta*, 2008. **76**(1), 226-229.
62. Becker, H. and L.E. Locascio, Polymer microfluidic devices. *Talanta*, 2002. **56**(2), 267-287.
63. Rohr, T., D.F. Ogletree, F. Svec, and J.M.J. Fréchet, Surface functionalization of thermoplastic polymers for the fabrication of microfluidic devices by photoinitiated grafting. *Advanced Functional Materials*, 2003. **13**(4), 264-270.
64. Rånby, B., W.T. Yang, and O. Tretinnikov, Surface photografting of polymer fibers, films and sheets. *Nuclear Instruments and Methods in Physics Research B*, 1999, 301-305.
65. Yang, W.T. and B. Rånby, Photoinitiation performance of some ketones in the LDPE-acrylic acid surface photografting system. *European Polymer Journal*, 1999. **35**(8), 1557-1568.
66. Yang, W.-T., M.-Z. Yin, and Y.-F. Sun, Performance and initiation mechanism of isopropylthioxanthone in surface photografting. *Chinese Journal of Polymer Science*, 2000. **18**(5), 431-435.
67. Stachowiak, T.B., D.A. Mair, T.G. Holden, L.J. Lee, F. Svec, and J.M.J. Fréchet, Hydrophilic surface modification of cyclic olefin copolymer microfluidic chips using sequential photografting. *Journal of Separation Science*, 2007. **30**(7), 1088-1093.
68. Gibson, G.T.T., S.M. Mugo, and R.D. Oleschuk, Surface-mediated effects on porous polymer monolith formation within capillaries. *Polymer*, 2008. **49**(13-14), 3084-3090.
69. Nischang, I., F. Svec, and J.M.J. Fréchet, Downscaling Limits and Confinement Effects in the Miniaturization of Porous Polymer Monoliths in Narrow Bore Capillaries. *Analytical Chemistry*, 2009. **81**(17), 7390-7396.
70. Byström, E., C. Viklund, and K. Irgum, Differences in porous characteristics of styrenic monoliths prepared by controlled thermal polymerization in molds of varying dimensions. *Journal of Separation Science*, 2010. **33**(2), 191-199.
71. Cabral, J.L., D. Bandilla, and C.D. Skinner, Pore size characterization of monolith for electrochromatography via atomic force microscopy studies in air and liquid phase. *Journal of Chromatography A*, 2006. **1108**(1), 83-89.
72. Courtois, J., M. Szumski, F. Georgsson, and K. Irgum, Assessing the macroporous structure of monolithic columns by transmission electron microscopy. *Analytical Chemistry*, 2007. **79**(1), 335-344.
73. Svec, F. and J.M.J. Fréchet, Kinetic Control Of Pore Formation In Macroporous Polymers - Formation Of Molded Porous Materials With High-

- Flow Characteristics For Separations Or Catalysis. *Chemistry of Materials*, 1995. **7**(4), 707-715.
74. Huang, X.A., S. Zhang, G.A. Schultz, and J. Henion, Surface-alkylated polystyrene monolithic columns for peptide analysis in capillary liquid chromatography-electrospray ionization mass spectrometry. *Analytical Chemistry*, 2002. **74**(10), 2336-2344.
75. Rohr, T., E.F. Hilder, J.J. Donovan, F. Svec, and J.M.J. Fréchet, Photografting and the Control of Surface Chemistry in Three-Dimensional Porous Polymer Monoliths. *Macromolecules*, 2003. **36**(5), 1677-1684.

Chapter 3 Catalyst immobilisation on porous polymer monolith

3.1 Introduction

As PPM's were originally developed for use in separation science applications, their use for the immobilisation of reactive species has focused on enzymatic bioreactors and reactive scavengers [1, 2]. To date there has been relatively little interest in immobilisation of homogeneous transition metal catalysts on PPM's. Izaak *et al.* commented on this in a recent review:

“... the number of papers devoted to ... heterogeneous metal catalysts based on particulate carriers is about several thousands. It should be expected that the results obtained will be used for the synthesis and investigation of properties of heterogeneous metal catalysts based on monolithic systems” [3].

This work represents the first reported use of PPM prepared by radical polymerisation for supported palladium catalysis, utilising Suzuki-Miyaura coupling reactions as a model system [4]. Karbass *et al.* [5] and Nikbin *et al.* [6] have since demonstrated the use of PPM for supported Heck catalysis and Karbass *et al.* immobilised Pd²⁺ on poly(CMS-*co*-DVB) monolith functionalised with 1-methylimidazole within 6.35 mm ID stainless steel columns. The Pd²⁺ was subsequently converted to Pd(0) by reduction with supercritical ethanol. Nikbin *et al.* also utilised poly(CMS-*co*-DVB) monolith, but instead of a ligand, palladium nanoparticles were formed on the PPM and a scavenger column was placed after the 6.6 mm ID glass reactor column to remove the leached palladium from solution.

In the approach taken by our group and Karbass *et al.* catalyst immobilisation is achieved by covalent binding a ligand to a PPM containing reactive functional

groups followed by subsequent coordination to palladium. The choice of ligand is crucial in this approach to producing a successful reactor. In the work reported here, choice of ligand was dictated by the following parameters: commercial availability, suitability as an immobilised ligand, stability, steric factors of the metal centre, and anticipated palladium binding strength. Commercially available ligands were preferred, as the focus of this research was the development of flow-through microreactor technology and not catalytic performance. Coincidentally there is a strong desire in industry for inexpensive ligands and immobilisation techniques, as custom ligand synthesis drastically increases the cost of the catalytic system [7]. For a ligand to be suitable for supported catalysis it must be capable of binding to the support while still being capable of coordinating to palladium. The use of stable ligands, which are neither air nor moisture sensitive, reduces hazards during reactor fabrication and simplifies the manufacturing process. A ligand should also have sufficiently high palladium binding strength while not impeding catalysis to minimise leaching. Based on these requirements, 5-amino-1,10-phenanthroline (5-NH₂phen) (refer to **Scheme 3.1** on page 160) and 1-methylimidazole (Me-im) (refer to **Scheme 3.3** on page 176) were chosen as ligands in this work. The investigation of the catalyst immobilisation was performed to determine attachment conditions which afforded PPM with sufficient palladium loading for catalysis, within a reasonable reactor fabrication time frame. In order to reduce the number of variables under investigation, the effect of reaction time on ligand loading was not investigated and 24 h was used for both the ligand attachment and palladium loading steps. Ligand attachment was performed in batch using bulk monolith to investigate the effect of solvent, temperature, and concentration on ligand loading, as these parameters would have been significantly more difficult and time consuming to investigate in flow-through mode.

3.2 Immobilisation of 5-NH₂phen

1,10-Phenanthroline (1,10-phen) is a bidentate nitrogen donor ligand which is widely used as a metal complexing agent [8-13] and is well established in supported catalysis [14, 15]. A reactive functional group at position 5 or 6 of 1,10-phen allows it to be immobilised onto a solid support while allowing access to the co-ordination site. In our first report of PPM supported catalysis, 5-hydroxy-1,10-phenanthroline (5-OHphen) was reacted with poly(GMA-co-EDMA) monolith under basic conditions [4]. As this ligand required in-house synthesis, the commercially available 5-NH₂phen was a more attractive alternative and has been demonstrated to be suitable as an immobilised ligand on Merrifield resin [16]. Nitrogen-donor ligands, such as 1,10-phen, are well known for supported palladium catalysis although there are relatively few examples of immobilised 1,10-phen for Suzuki-Miyaura catalysis [17].

Ligand immobilisation on PPM imposes restrictions on the solvents and reaction conditions suitable for the attachment reaction. Solvents and temperatures for ligand attachment must be compatible with the PPM's, the polymer tubing and fittings (PEEK and Tefzel®) used for interfacing the various flow-through devices, as well as COC capillary and microchips. PEEK is the least chemically and thermally resistant material present in the system, as it is only compatible with non-aromatic organic solvents up to 90 °C [18].

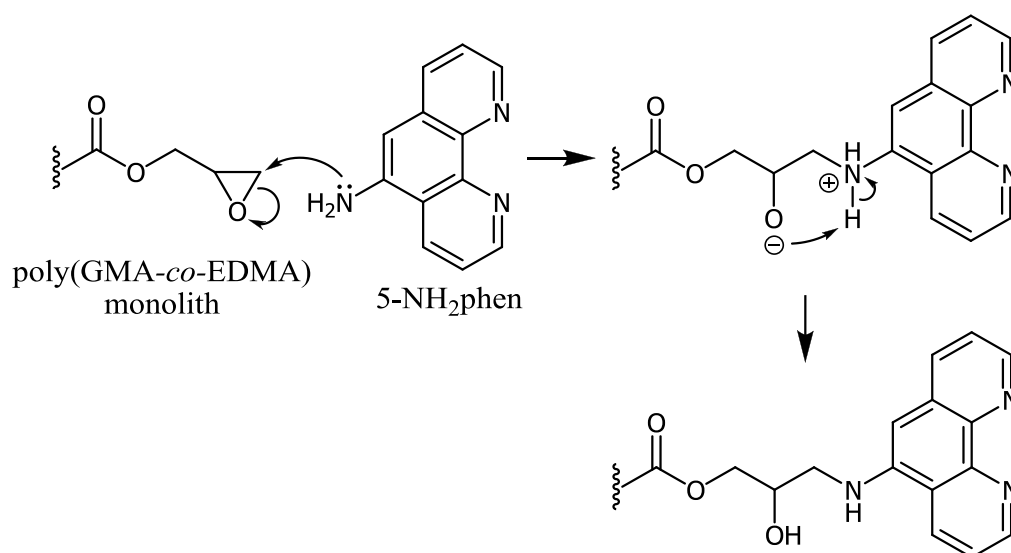
For flow-through ligand attachment it is vital that the ligand solution is completely homogeneous and that no precipitate forms during the reaction with the PPM. Any precipitate formed will eventually fill the pores of the PPM, blocking flow through the device. The solubility of 5-NH₂phen was assessed in a range of polar non-aromatic and non-halogenated solvents including acetone, acetonitrile,

dimethylformamide (DMF), dimethylsulfoxide (DMSO), ethanol, isopropanol, and methanol. The ligand was found to be suitably soluble in methanol, DMF and DMSO, leading to trialling these solvents.

3.2.1 5-NH₂phen attachment to poly(GMA-*co*-EDMA) bulk PPM

The investigation of reaction conditions suitable for the attachment of 5-NH₂phen was performed using bulk PPM under batch conditions as it is quicker and less demanding on infrastructure compared to flow-through. Additionally, bulk PPM can be analysed by destructive techniques such as elemental analysis (EA) and inductively coupled plasma mass spectrometry (ICP-MS), which is difficult to achieve for microfluidic flow-through systems. It was assumed that, even though the ligand loadings obtained from attachment in batch using bulk PPM will not accurately equate to those obtained in flow-through, the optimum conditions obtained under batch conditions would also be optimal for flow-through.

5-NH₂phen is covalently attached to poly(GMA-*co*-EDMA) monolith via ring-opening of the epoxide by a nucleophilic attack of the amine group (**Scheme 3.1**). For the purpose of reaction schematics the PPM is simplified to just the reactive functional group. Attachment of this ligand to a PPM had not been previously reported. EA for nitrogen was performed for the ligand attached bulk monolith in order to determine ligand content. As the untreated PPM contains <0.01 wt% nitrogen, originating from the initiator, any nitrogen content measured can be assumed to be from the monolith-attached 5-NH₂phen. EA gives the mass percentage nitrogen from which the moles of 5-NH₂phen per gram of PPM was calculated, giving a relative measure of the ligand loading for comparison between samples prepared from the same PPM. A measure of the ligand loading, independent of the PPM used, is 'attachment efficiency' - the percentage of functional groups present in the PPM with which the ligand reacts.



Scheme 3.1 5-NH₂phen attachment to poly(GMA-co-EDMA) monolith.

The number of moles of epoxide groups per gram of poly(GMA-co-EDMA) monolith was estimated by assuming the ratio of GMA to EDMA present in the polymerisation mixture was retained in the PPM, and that the PPM mass results solely from these monomers. Based on this assumption, approximately 4.2×10^{-3} mol g⁻¹ of epoxide groups are expected for PPM synthesised from the TGMA1 formulation. All the poly(GMA-co-EDMA) monolith formulations reported in this work feature the same ratio of GMA to EDMA and therefore have the same functional group content by mass.

Batch ligand attachment experiments were performed using 5 mL reaction vials which are designed for small scale synthetic applications. These vials offer excellent mixing and heat transfer and are small enough to allow the use of several vials within the same oil bath. For the attachment experiments, 250 mg of bulk PPM was used which affords more than sufficient material for subsequent analysis and batch catalytic reactions. The initial conditions trialled for 5-NH₂phen attachment were adapted from our work conducted with 5-OHphen using DMSO [4]. Under these conditions a loading of 4.8×10^{-6} mol g⁻¹ of 5-NH₂phen, or attachment efficiency of 0.11% was obtained (**Table 3.1**). This implies that under these

conditions only 0.11% of the epoxide groups present in the polymer monolith reacted with the ligand.

To improve the ligand loading, the influence of temperature, solvent, ligand excess, and the presence of base were investigated. These results are summarised in **Table 3.1**. Increasing the temperature to 90 °C, the maximum allowed for PEEK fittings, only marginally improved the ligand loading. The effect of the solvent was investigated by performing the attachment in both DMF and methanol. The attachment in DMF was performed at 90 °C and in methanol at 70 °C, due to its lower boiling point. The solvent was found to have a significant effect on the ligand loading, improving the loading by a factor of 2.6 in DMF and by a factor of 10.9 in methanol.

In the conditions reported for 5-OHphen, the amount of ligand used was limited owing to difficulty in its preparation [4]. Under these conditions, only 0.24 mol equivalents of ligand were used for the attachment which may have reduced the potential loading by not performing the reaction with large excess. The effect of ligand availability on loading was investigated by performing the attachment using 1.5 mol equivalents of ligand in the same volume of solvent. While using a large excess of ligand improved the attachment efficiency by a factor of 5.3 to 9.87% (**Table 3.1**), 90.13% of the epoxide groups within the PPM still remained unutilised. It would seem feasible that the majority of the epoxide groups of the poly(GMA-co-EDMA) monolith are not accessible to the ligand.

Solvent	Temperature (°C)	Mol. eq. ligand	Nitrogen (wt%)	Ligand loading (mol g ⁻¹)	Attachment efficiency (%)
DMSO	60	0.24	0.02	4.8×10^{-6}	0.11
DMSO	90	0.24	0.03	7.1×10^{-6}	0.17
DMF	90	0.24	0.08	1.9×10^{-5}	0.45
Methanol	70	0.24	0.33	7.9×10^{-5}	1.86
Methanol	70	1.5	1.75	3.4×10^{-4}	9.87
Methanol + NEt ₃	70	0.24	0.26	6.2×10^{-5}	1.49
DMSO + NEt ₃	70	0.24	0.23	5.5×10^{-5}	1.3
DMF + NEt ₃	70	0.24	0.24	5.7×10^{-5}	1.34
DMSO + NEt ₃	70	1.5	0.58	1.4×10^{-4}	3.29
DMSO + NEt ₃	70	0.49	0.26	6.2×10^{-5}	1.47

Table 3.1 Effect of solvent, temperature and triethylamine on attachment of 5-NH₂phen to bulk poly(GMA-co-EDMA).

Preinerstorfer *et al.* investigated modification of poly(GMA-*co*-EDMA) monolith with Na(SH) and also found poor attachment efficiency [19]. To determine the maximum accessibility of the epoxide groups they treated the PPM with excess diethylamine and were able to ring-open 75% of the total epoxide groups. Compared to diethylamine, 5-NH₂phen is a poor nucleophile due to delocalisation of the lone pair on the nitrogen into the aromatic system. Tertiary amines are known to be efficient catalysts for the ring-opening of epoxides with amines [20], so the effect of adding 5% triethylamine to the ligand solution was investigated using 0.24 mol equivalents of ligand in methanol, DMSO, and DMF. The addition of triethylamine was found to significantly increase the ligand loading for both DMF and DMSO, but decreased the ligand loading in methanol. The ligand loadings obtained in DMF and DMSO in the presence of triethylamine were, however, still significantly lower than those obtained in methanol. For comparison, the ligand loading obtained for the attachment reaction when performed in DMSO with 5% triethylamine using 1.5 mol equivalents of 5-NH₂phen was three times lower than in methanol.

While the use of a large excess of 5-NH₂phen improved the ligand loading, the use of a suspension is not suitable for flow-through ligand attachment. To solubilise 1.5 mol equivalents of 5-NH₂phen more than 12 mL of solvent is required, which exceeds the maximum volume of the reaction vials. To determine if using a larger amount of soluble ligand would significantly improve the ligand loading, the ligand attachment was performed using 4 mL of DMSO with 5 % triethylamine and 0.49 mol equivalents of 5-NH₂phen, which was the maximum amount of ligand soluble in this volume. Compared to the ligand attachment performed using 0.24 mol equivalents of ligand in 2 mL of solvent, the ligand loading was only marginally improved by 8% despite doubling the amount of ligand present. Even though the

ligand loading was not improved significantly, the use of 0.49 mol equivalents of 5-NH₂phen was adopted as the optimised attachment procedure.

5-NH₂phen immobilised using the optimised procedure was also performed on ground photo-initiated bulk PPM prepared from the UVGMA4 and UVGMA4-70 formulations (see **Chapter 2**). As the bulk PPM was ground to a fine powder for ligand attachment, only differences in the globule sizes should affect the ligand loading, which were estimated from SEM images. The estimated globule diameters and ligand loadings obtained for each formulation are shown in **Table 3.2**.

Formulation	Estimated globule diameter (μm)	Ligand loading (mol g⁻¹)
TGMA1	1.6	6.2×10 ⁻⁵
UVGMA4	1.3	5.0×10 ⁻⁵
UVGMA4-70	1.0	6.1×10 ⁻⁵

Table 3.2 5-NH₂phen loadings obtained for bulk PPM formulations investigated.

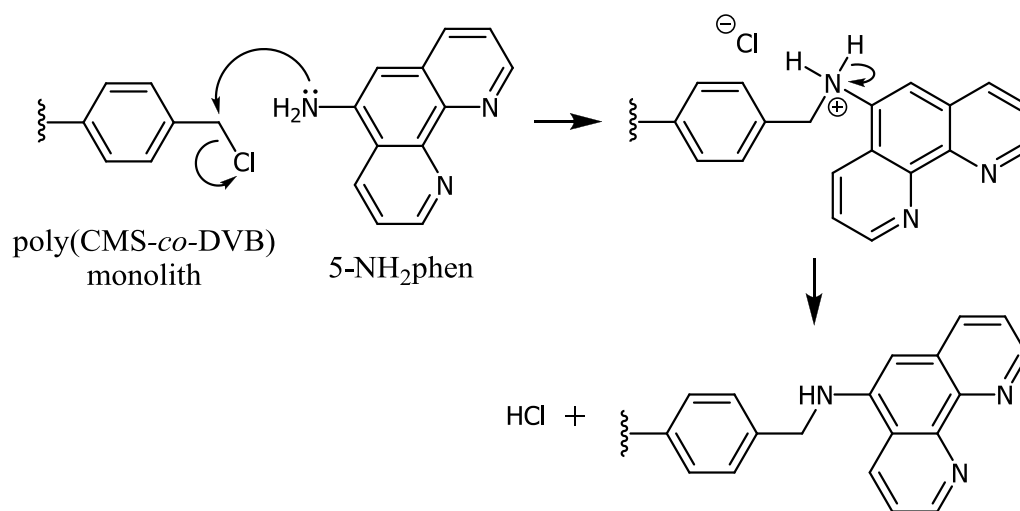
Without a quantitative measure of each PPM's surface area, by BET for instance, it is difficult to speculate on the accuracy of this comparison. However, despite the differences in the PPM formulations and their preparation methods, there was no significant variation in the ligand loading.

3.2.2 5-NH₂phen attachment to poly(CMS-*co*-DVB) bulk monolith

As discussed in **Chapter 2**, poly(CMS-*co*-DVB) monolith cannot be prepared via UV-initiated polymerisation and hence is not suitable for use in microchips. Despite this, poly(CMS-*co*-DVB) monolith is useful as it allows for easy comparison with existing supported catalysis systems based on Merrifield resin as they contain the same reactive functional group [17, 21, 22]. Additionally, poly(CMS-*co*-DVB) monolith is of interest as it is highly hydrophobic and is less

susceptible to swelling and possible side reactions compared to poly(GMA-*co*-EDMA) monolith, which contains ester functionality and forms hydroxyl groups as a by-product of the epoxide ring opening.

5-NH₂phen is covalently attached to poly(CMS-*co*-DVB) monolith via S_N2 substitution between the amine group of the ligand and the benzyl chloride groups of the monolith (**Scheme 3.2**). This reaction generates HCl as a by-product, which is neutralised by the excess of 5-NH₂phen acting as a base.



Scheme 3.2 5-NH₂phen attachment to poly(CMS-*co*-DVB) monolith.

Poly(CMS-*co*-DVB) monolith prepared from the TCMS1 formulation (see **Chapter 2**) contains $2.62 \times 10^{-3} \text{ mol g}^{-1}$ of benzyl chloride groups. The functional group density of this monolith is 38% lower than poly(GMA-*co*-EDMA) due to its higher ratio of crosslinking monomer. The lower availability of reactive functional groups within the poly(CMS-*co*-DVB) monolith was anticipated to result in a lower ligand loading but higher attachment efficiency. The higher attachment efficiency is due to the reactive functional groups being relatively more accessible as the majority of the PPM's structure is composed of the crosslinking monomer and not the non-linking monomer.

Initial attachment experiments were conducted using the same conditions first investigated for 5-NH₂phen attachment to poly(GMA-*co*-EDMA) monolith, with 2.6×10^{-4} mol of ligand in methanol at 70 °C. For the poly(CMS-*co*-DVB) monolith this equates to 0.39 mol equivalents of ligand compared to 0.24 mol equivalents for poly(GMA-*co*-EDMA) monolith. A ligand loading of 1.19×10^{-4} mol g⁻¹ with an attachment efficiency of 4.54% (**Table 3.3**) was obtained using these conditions.

Despite a comparatively lower availability of reactive functional group, the ligand loading obtained for 5-NH₂phen on poly(CMS-*co*-DVB) monolith was 50% higher than that for the poly(GMA-*co*-EDMA) monolith under equivalent conditions. This suggests that the benzyl chloride groups of poly(CMS-*co*-DVB) monolith are significantly more reactive, or available, towards 5-NH₂phen than the epoxide groups of poly(GMA-*co*-EDMA) monolith under the conditions investigated.

The maximum ligand loading for 5-NH₂phen on poly(CMS-*co*-DVB) was investigated using a suspension containing 1.5 mol equivalents of ligand in 4 mL of methanol. Under these conditions the ligand loading was increased by 61% to 3.1×10^{-4} mol g⁻¹, which is similar to the loading obtained by Lenaerts *et al.* who attached 5-NH₂phen to Merrifield resin in dioxane with triethylamine to catalyse the reaction and to neutralise the hydrochloric acid [16]. As with the investigation using poly(GMA-*co*-EDMA) monolith, performing the attachment using a suspension is not representative of flow-through conditions. Therefore the effect of increasing the amount of ligand available was also investigated by using 0.78 mol equivalents of ligand, representing the maximum amount soluble in 4 mL of solvent. Under these conditions the ligand loading is 2.0×10^{-4} mol g⁻¹ (**Table 3.3**).

Solvent	Mol. eq. ligand	Nitrogen (wt%)	Ligand loading (mol g ⁻¹)	Attachment efficiency (%)
Methanol	0.39	0.5	1.2×10^{-4}	4.5
Methanol	0.78	0.84	2.0×10^{-4}	7.7
Methanol	1.5	1.29	3.1×10^{-4}	11.7

Table 3.3 Attachment 5-NH₂phen to bulk poly(CMS-co-DVB).

Overall, attachment of 5-NH₂phen to bulk poly(CMS-co-DVB) monolith was found to be superior to poly(GMA-co-EDMA) monolith in terms of ligand loading and attachment efficiency.

3.2.3 5-NH₂phen attachment to poly(GMA-co-EDMA) in fused-silica capillary

Adaption of ligand attachment developed in batch to flow-through devices was performed using capillary columns as they are relatively inexpensive, compared to microchips, easier to prepare and to interface. As previously discussed in **Chapter 2**, UV-initiated PPM was prepared in 100 µm ID capillary and thermally initiated PPM in 250 µm ID capillary. Ligand attachment under continuous flow conditions is considerably more complex than batch as it introduces the potential for spatial variation of the ligand loading; other factors such as linear velocity and flow rate may affect the attachment reaction. Investigation of these parameters was prevented by the inability to measure ligand loading within the capillary columns. EA of PPM within the capillary columns would either require removal of the PPM from the capillary or the analysis of both the capillary and PPM together. Byström *et al.* showed that PPM covalently anchored within capillary columns could be removed by dissolving the fused-silica in hydrofluoric acid (HF) [23]. Due to the dangers of handling HF this approach was not explored. Analysis of both the PPM and capillary column, by grinding it into a powder, was also not feasible. In 100 µm ID capillary the PPM constitutes approximately 1% of the total mass of the column, hence the PPM would have to contain greater than 10 wt% nitrogen to be detectable which is considerably higher than measured using bulk monolith. In the 250 µm ID monolithic capillary columns the PPM constitutes approximately 18% of the total mass, however the external polyimide coating contains significantly more nitrogen than would be expected from the ligand attached PPM. The success of ligand

attachment was inferred indirectly by ICP-MS analysis for palladium after completion of reactor fabrication. This techniques also did not allow for the determination of spatial variation in the loading due to the low levels present (see **Section 3.4.3**). Since analysis of the ligand loading within the capillary columns was not feasible, the investigation of flow-through ligand attachment focused on flow-through in terms of back-pressure and leakage, and the effect of the attachment conditions on catalysis.

As our reported conditions for 5-OHphen attachment to poly(GMA-*co*-EDMA) monolith in capillary columns gave sufficient loading for catalysis [4], the same conditions were initially investigated for attachment of 5-NH₂phen. Under these conditions the ligand attachment was performed in three stages. The column was rinsed with the same solvent as the ligand solution to prevent precipitation during introduction of the solution, and then the ligand solution was pumped through at low flow rate, followed by a rinse with solvent to remove the free ligand. The flow rates reported for the solvent flushing steps using 250 μm ID capillary columns were not suitable of 100 μm ID capillary columns due to higher back-pressure resulting from the smaller column cross-section. As 250 μL syringes were used for pumping, all flushing steps were performed in multiples of 240 μL . Ligand attachment was performed using a two pass procedure with flow rates chosen to pass 480 μL of the ligand solution through the capillary column within one working day. In the first pass, the capillary column is flushed with 240 μL of ligand solution over 8 h at 30 $\mu\text{L h}^{-1}$, and during the second pass the capillary column is flushed again with the same volume of solution at 15 $\mu\text{L h}^{-1}$ over 16 h in the opposite direction. The flow direction through the capillary was reversed after the first flush, anticipating that this would improve homogeneity of the ligand attachment along the length of the capillary.

At a concentration of 0.13 M, the 480 μL of 5- NH_2 phen solution passed through a 100 μm ID capillary column equates to 6.15×10^{-5} mol of ligand. In order to determine if this volume of solution is sufficient for complete functionalisation of the PPM, the number of reactive functional groups within the column needs to be estimated. Since the mass of PPM within the 100 μm ID capillary is too small to be accurately weighed, the mass of PPM was calculated by using the density measured for bulk PPM (see **Chapter 2**). The volume of the PPM within the column was calculated from the length measured and the internal diameter quoted by the capillary manufacturer. Using this approach, the number of moles of epoxide groups present in a 30 cm long monolithic capillary column of 100 μm ID prepared using the UVGMA4-70 formulation was estimated at 3.90×10^{-6} mol. Therefore, 30 μL of 0.13 M 5- NH_2 phen solution would be sufficient to supply the PPM with an equivalent amount of ligand for all the epoxide groups present, and flushing with 480 μL of ligand solution provided a 16-fold excess of ligand to the capillary column.

The initial evaluation of 5- NH_2 phen attachment in flow-through mode was performed using a 100 μm ID monolithic capillary column prepared using the UVGMA1 formulation (see **Chapter 2**). Methanol was used as the solvent for the ligand solution as it gave the highest loading for bulk poly(GMA-*co*-EDMA) monolith. During the ligand solution flush severe leakage was observed at the syringe and connectors, attributed to excessive back-pressure generated in the capillary column. It was speculated that this could be caused by swelling of the monolith due to hydrogen-bonding, as shown in **Figure 3.1**, as severe leakage did not occur when the ligand attachment was performed in DMSO. The hydroxyl group is formed as a by-product of the ring-opening reaction and is only present after ligand attachment. To prevent leakage during ligand attachment, a solvent not prone

to swelling should be used. Of the other two solvents investigated for ligand attachment in batch, DMF and DMSO, DMF was found to be incompatible with COC, making DMSO the solvent of choice.

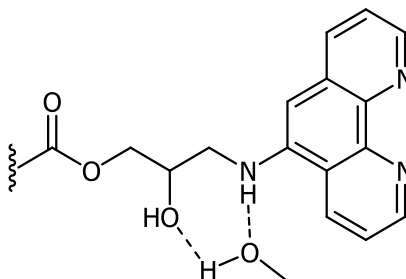


Figure 3.1 Possible hydrogen-bonding interaction that may have contributed to swelling of the poly(GMA-*co*-EDMA) monolith during 5-NH₂phen attachment in methanol.

The use of DMSO for ligand attachment reduced the leakage, although minor leakage was still observed during each stage of the fabrication process. As previously discussed in **Chapter 2**, the permeability of PPM can be manipulated by controlling its pore size and porosity. The UVGMA4-70 formulation was developed specifically to produce a more highly permeable PPM suitable for use in 100 µm ID capillary columns. Leakage was not observed using DMSO as the ligand attachment solvent with monolithic capillary columns prepared from the UVGMA4-70 formulation.

During the solvent flushing steps before and after ligand attachment the temperature in the laboratory would frequently fall below 18 °C causing the DMSO to solidify within the syringes, resulting in breakages. To avoid solidification 10% methanol was added to the DMSO for the flushing steps. This small addition of methanol did not noticeably affect the back-pressure during the post ligand attachment solvent flush.

During the investigation of 5-NH₂phen attachment to poly(GMA-*co*-EDMA) monolith in borosilicate microchips, as discussed in **Section 3.2.4**, it was found that

pumping could only be performed in one direction due to the channel design (see **Chapter 5**). Therefore, the reversal of the pumping direction during ligand attachment was not feasible. Since capillary columns serve as a model for reactor fabrication conditions for borosilicate microchips, ligand attachment in a single direction was examined. As the flow direction was no longer reversed during ligand attachment, the volume of solution used was reduced to 240 μL , delivering an 8-fold excess of 5-NH₂phen. No difference in palladium loading or catalytic performance was measured between capillary reactors prepared using the single pass or two pass ligand attachment methods.

The investigation of 5-NH₂phen attachment to bulk poly(GMA-*co*-EDMA) monolith revealed that adding 5% triethylamine to the ligand solution dramatically improved the ligand loading. The optimised 5-NH₂phen attachment method for 100 μm ID monolithic capillary column used a single pass of 5-NH₂phen in DMSO with 5% triethylamine.

To allow for direct comparison with the reported results obtained using capillary column reactors prepared with 5-OHphen, attachment of 5-NH₂phen was also performed using 25 cm lengths of 250 μm ID monolithic capillary column prepared using thermally initiated poly(GMA-*co*-EDMA) monolith. The two-pass procedure was used for these capillaries to remain consistent with reported methods using the same column dimensions [4].

3.2.4 Optimised 5-NH₂phen attachment to polymer monolith in flow-through devices

Ligand attachment was performed in the other poly(GMA-*co*-EDMA) monolith flow-through formats using the conditions developed in 100 μm ID scaled to suit the dimensions of the particular device, except for 250 μm ID capillary

column. Flow-through attachment of 5-NH₂phen to 25 cm long 250 µm ID poly(CMS-*co*-DVB) capillary columns was performed using the same two-pass procedure used for 250 µm ID poly(GMA-*co*-EDMA) capillary column, with the exception that methanol was used as the attachment solvent.

The mass of PPM contained within each device investigated was calculated from the PPM's volume and the density of the equivalent bulk monolith, as discussed in the previous section. The parameters used to calculate the PPM mass within each device investigated, as well as the estimated PPM masses are shown in **Table 3.4**. From the PPM mass the moles of reactive functional groups were estimated. Using this value, the volume of ligand solution required to deliver excess ligand to the PPM was calculated in multiples of 240 µL. The exception to this were the 2 mm ID columns, as 20 mL plastic syringes were used for fluid delivery instead of the volume limiting 250 µL syringes. For each flow-through device, more than 1.5 mol equivalent of ligand was used for attachment.

While changes to the PPM during ligand attachment were difficult to observe in the sub-millimetre scale devices, obvious colour changes to the PPM were observed in 2 mm ID monolithic columns. The white, untreated poly(GMA-*co*-EDMA) monolith, became pale-yellow after treatment with 5-NH₂phen and the colour remained after the rinsing flush.

Format	Cross-sectional area (μm^2)	Monolith	Monolith length (cm)	Monolith volume (μL)	Monolith density ($\text{mg } \mu\text{L}^{-1}$)	Monolith mass (mg)
100 μm ID capillary	7854	UVGMA4-70	30	2.4	0.306	0.72
250 μm ID capillary	49087	TGMA1	25	12.3	0.439	5.39
250 μm ID capillary	49087	TCMS1	25	12.3	0.356	4.37
340 μm ID capillary	90792	UVGMA7-50	10	9.1	0.337	3.06
Borosilicate microchip	17380	UVGMA4-70	33	5.7	0.306	1.77
COC microchip	54000	UVGMA7-50	4.9	2.6	0.337	0.91
2 mm ID column	3141593	UVGMA7-50	9	283	0.397	112.25

Table 3.4 Physical properties of monolith filled flow-through devices.

The colour was homogeneous along the length of the column as shown in **Figure 3.2**, which suggests a homogeneous distribution of the ligand loading.



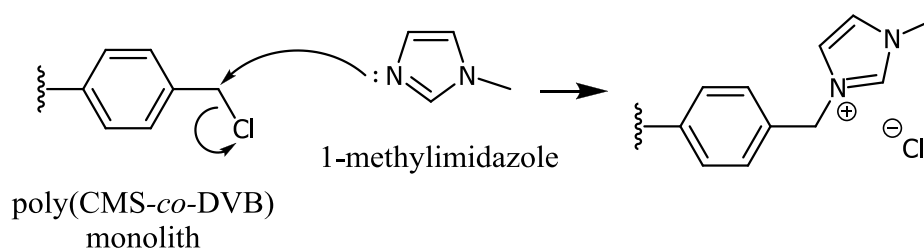
Figure 3.2 Poly(GMA-*co*-EDMA) in 2 mm ID column functionalised with 5-NH₂phen.

3.3 Immobilisation of Me-im

Me-im is an *N*-heterocyclic ligand, a class of ligands that have recently become important in palladium catalysis as they have been found to be remarkably stable towards heat, oxygen and moisture, bind to both Pd(II) and Pd(0) centres substantially more strongly than phosphine ligands, and are highly suitable for attachment to solid supports owing to low leaching [7]. There have been several reported examples of *N*-heterocyclic ligand based catalysts for Suzuki-Miyaura reactions in batch mode [24-28]. Immobilisation of *N*-heterocyclic ligands on poly(CMS-*co*-DVB) monolith has been previously been demonstrated using Me-im by Karbass *et al.* [5] and 1-butylimidazole by Lozano *et al.* [29]. Me-im is attractive as a ligand for this work as it is a liquid under standard laboratory conditions that is miscible with a wide range of organic solvents, it is commercially available and relatively inexpensive, and it can act as a base. The liquid state of this ligand makes it especially attractive for flow-through systems where blockages are a major concern.

3.3.1 Me-im attachment to bulk poly(CMS-*co*-DVB) monolith

Me-im is covalently attached to poly(CMS-*co*-DVB) monolith via S_N2 substitution by the unsubstituted nitrogen on the ligand. The imidazolium salt is formed with chloride as the counter ion, as shown in **Scheme 3.3**.



Scheme 3.3 Me-im attachment to poly(CMS-*co*-DVB) monolith.

The initial conditions investigated for Me-im attachment to bulk poly(CMS-*co*-DVB) monolith were adapted from those reported by Kim *et al.* for attachment of Me-im to Merrifield resin [25]. Bulk poly(CMS-*co*-DVB) monolith was treated using a solution containing 1.4 mol equivalents of Me-im in chloroform at 50 °C for 24 h. Performing the Me-im attachment using these conditions afforded a ligand loading of 1.9×10^{-4} mol g⁻¹ with an attachment efficiency of 7.1%, which is similar to the loading obtained for 5-NH₂phen.

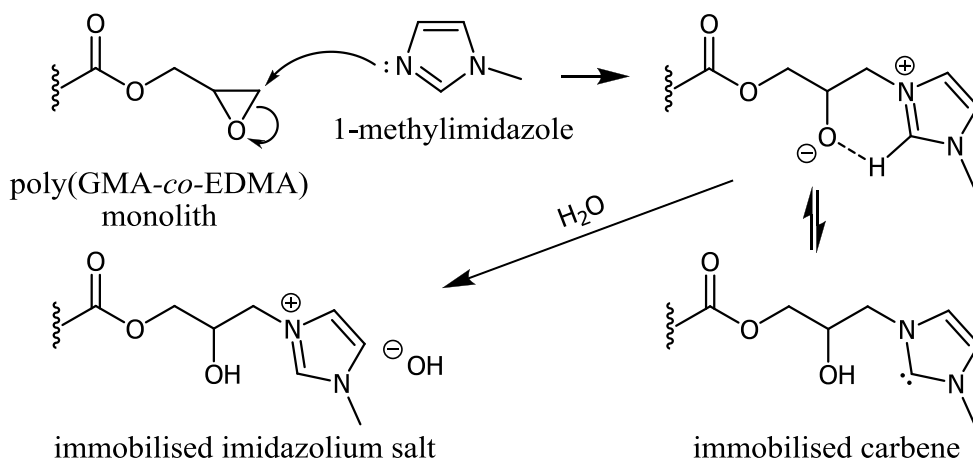
Karbass *et al.* functionalised a poly(CMS-*co*-DVB) monolith column in flow-though using neat ligand [5], an approach that was followed here. The ligand loading and attachment efficiency were increased six-fold by using neat ligand over performing the attachment in chloroform (**Table 3.6**). The attachment efficiency for neat Me-im attachment to poly(CMS-*co*-DVB) monolith, 43.8%, is considerably higher than obtained for 5-NH₂phen. This is, however, significantly less than the 95% attachment efficiency reported by Karbass *et al.*, who used vibrational spectroscopy to monitor the loss of the benzylic chloride functional group [5].

3.3.2 Me-im attachment to poly(GMA-*co*-EDMA) bulk monolith

Me-im is covalently attached to poly(GMA-*co*-EDMA) monolith via ring-opening of the epoxide by nucleophilic attack of the unsubstituted nitrogen. Attachment of this ligand to poly(GMA-*co*-EDMA) monolith had not been previously reported. The attachment is anticipated to proceed to form a carbene or, in

the presence of a proton source, such as water, form the imidazolium group as shown in **Scheme 3.4**. The formation of the imidazolium group is more likely, as the attachment reaction is not performed under inert conditions and only a trace amount of water would be required.

The conditions for Me-im attachment to bulk poly(GMA-*co*-EDMA) monolith were adapted from those used for bulk poly(CMS-*co*-DVB) monolith with neat ligand. The ligand loading obtained for Me-im attachment to bulk poly(GMA-*co*-EDMA) was $1.10 \times 10^{-3} \text{ mol g}^{-1}$ with an attachment efficiency of 26.0% (**Table 3.5**). This attachment efficiency is over 2.5-fold higher than the maximum loading achieved for 5-NH₂phen on poly(GMA-*co*-EDMA), which can be attributed to the absence of a solvent and the stronger nucleophilicity of the ligand. The largest excess of 5-NH₂phen used for attachment to bulk monolith was 1.5 mol equivalents, although for neat Me-im over 23 mol equivalents were present.



Scheme 3.4 Me-im attachment to poly(GMA-*co*-EDMA) monolith.

During the investigation of Me-im attachment, the bulk poly(GMA-*co*-EDMA) monolith was observed to form a translucent gel upon addition of the ligand, as shown in the photograph in **Figure 3.3 (a)**, and form a bright red solution after the attachment reaction, as shown in **Figure 3.3 (b)**.

Solvent	Mol. eq. ligand	Nitrogen (wt%)	Ligand loading (mol g ⁻¹)	Attachment efficiency (%)
Neat	24.3	3.07	1.1×10^{-3}	26
Chloroform	3	1.55	5.5×10^{-4}	13.1
Ethanol	3	1.46	5.2×10^{-4}	12.4
Ethyl acetate	3	1.18	4.2×10^{-4}	10

Table 3.5 Attachment of Me-im to bulk poly(GMA-co-EDMA) monolith.

Solvent	Mol. eq. ligand	Nitrogen (wt%)	Ligand loading (mol g ⁻¹)	Attachment efficiency (%)
Neat	39.3	3.21	1.2×10^{-3}	43.8
Chloroform	1.4	0.52	1.9×10^{-4}	7.1

Table 3.6 Attachment of Me-im to bulk poly(CMS-co-DVB) monolith.

For comparison, the powdered bulk poly(GMA-*co*-EDMA) monolith in ethanol is shown in **Figure 3.3 (c)**, for which a gel does not form. The gelling of the poly(GMA-*co*-EDMA) monolith is likely to be indicative of severe swelling. After filtering off the excess ligand as a clear liquid, the Me-im attached PPM is a bright orange powder. The strong red colour observed when the Me-im attached PPM is immersed in Me-im is consistent with the presence of a strong interaction between ligand attached PPM and excess Me-im, perhaps as a primary interaction resulting in swelling.

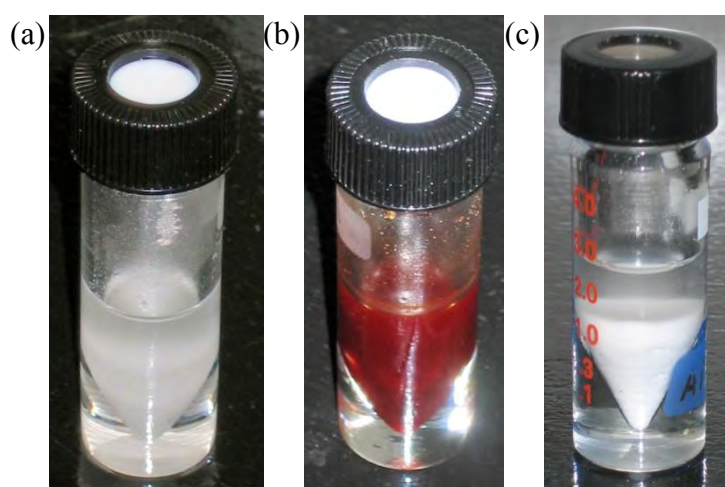


Figure 3.3 (a) Bulk poly(GMA-*co*-EDMA) monolith in Me-im, (b) after the Me-im attachment reaction, (c) bulk poly(GMA-*co*-EDMA) monolith in ethanol.

Formation of a gel would result in excessive back-pressure during ligand attachment in capillaries. As expected, based on observations during attachment in batch, neat Me-im was found to be unsuitable for attachment to poly(GMA-*co*-EDMA) monolith in capillary columns due to excessive back-pressure caused by swelling of the monolith, further discussed in **Section 3.3.3**.

It was proposed that the swelling is due to strong hydrogen-bonding between the ligand treated PPM and the free Me-im, and thus it was anticipated that this could be reduced by diluting the ligand with a non-protic solvent such as chloroform or ethyl acetate. For comparison, the attachment was also studied in ethanol which is a

protic solvent. The ligand concentration used for each solvent was 0.8 M, or 3.0 mol equivalents of Me-im. The non-protic solvents were found to be incompatible with poly(GMA-*co*-EDMA) monolith backbone as they caused swelling. Swelling was not observed with the Me-im attachment in ethanol, which was further tested in flow-through using poly(GMA-*co*-EDMA) filled fused-silica capillary, see **Section 3.3.3**. Moving from neat attachment to attachment in a solvent reduced the ligand loading by over 50%, however the loading was still significantly higher than obtained with 5-NH₂phen. Similar loadings were obtained for each solvent, despite the swelling caused by the non-protic solvents.

3.3.3 Flow-through attachment of Me-im to PPM

The investigation of flow-through Me-im attachment to poly(GMA-*co*-EDMA) monolith was performed in parallel to batch experiments using 100 µm monolithic capillary column. Capillary columns were prepared using the UVGMA4-70 formulation and ligand attachment was performed using the same pumping conditions used for 5-NH₂phen attachment. Neat ligand was initially trialled which lead to leakage due to severe back-pressure. As discussed in the previous section, performing the attachment to bulk PPM in ethanol seemed to reduce swelling but lead to severe back-pressure when used in capillary columns. Thus, Me-im was deemed unsuitable for attachment to the poly(GMA-*co*-EDMA) monolith in capillary columns.

The investigation of flow-through Me-im attachment to poly(CMS-*co*-DVB) monolith was also performed in parallel to batch studies using 250 µm ID monolithic capillary columns. The initial conditions trialled were adapted from our earlier work for 5-OHphen attachment to poly(GMA-*co*-EDMA) monolith in 250 µm ID capillary columns using the two-pass procedure with a 0.9M solution of Me-im in chloroform

[4]. Chloroform was also used for the solvent flushing steps before and after ligand attachment [30].

From the batch investigation, the ligand attachment in neat ligand was found to give a superior ligand loading. Attachment using neat ligand in poly(CMS-*co*-DVB) monolith capillary columns did not result in leakage, so this method was adopted as the preferred method. Also, chloroform was replaced with methanol as the pre-flush solvent and acetonitrile as the post-flush solvent due to poor compatibility of chloroform with the PEEK fittings.

While Me-im attachment to poly(GMA-*co*-EDMA) monolith in 100 μ m ID capillary columns was not feasible due to excessive back-pressure, attachment in 2 mm ID and 4 mm ID monolithic columns was successful due to exceptionally low back-pressure (see **Chapter 2**). The conditions for attachment of Me-im to poly(GMA-*co*-EDMA) in 2 mm ID and 4 mm ID columns were scaled up from those using 100 μ m ID capillary columns, and using neat ligand. Both the 2 mm ID and 4 mm ID monolithic columns were flushed with 10 mL of neat Me-im over 24 h, which delivered 136 and 68 mol equivalents for the present epoxide groups within the PPM respectively. Pumping was performed using 20 mL plastic syringes with no signs of excessive back-pressure during ligand attachment. As observed in batch mode, the poly(GMA-*co*-EDMA) monolith turned deep red during the ligand attachment (**Figure 3.4 (a)**) and became bright orange after the post-flush (**Figure 3.4 (b)**). The colour of the functionalised monolith was homogeneous along the length of the column suggesting that one one-pass of ligand was sufficient for homogeneous loading.



Figure 3.4 (a) During attachment of Me-im to poly(GMA-co-EDMA) monolith in a 4mm ID columns, (b) after the post-flush.

3.4 Palladium attachment to PPM with immobilised ligand

The bis(acetonitrile)dichloropalladium(II) complex is a well established palladium precursor for supported catalysis [31-33]. For PPM immobilised 5-NH₂phen, the palladium is expected to coordinate to the ligand as shown in **Figure 3.5 (a)**.

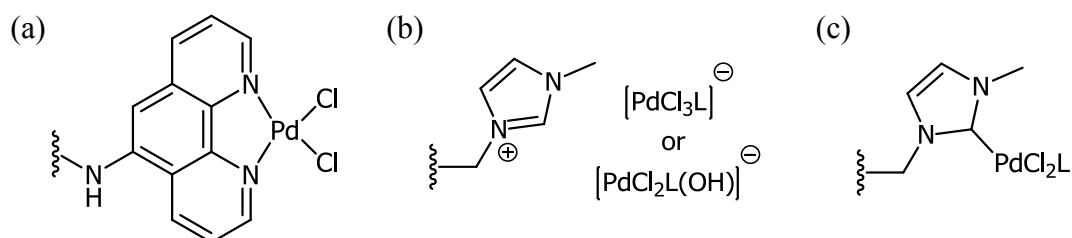


Figure 3.5 (a) Palladium binding to 5-NH₂phen, (b) examples of possible imidazolium salts, (c) an imidazole-based NHC binding to palladium.

Attachment of palladium to Me-im depends upon which form the immobilised ligand occurs in the polymer. For example, if the ligand forms an imidazolium group (**Scheme 3.3** and **Scheme 3.4**) with chloride or hydroxide as counterions, then bis(acetonitrile)dichloropalladium(II) may form $[\text{PdCl}_3(\text{NCMe})]^-$ or $[\text{PdCl}_2(\text{OH})(\text{NCMe})]^-$ as the counterion(s) (**Figure 3.5 (b)**). Alternatively, if an *N*-heterocyclic carbene is formed as shown in **Scheme 3.4**, then the palladium can coordinate to the carbene as shown in **Figure 3.5 (c)**. The ionic form is more likely

in the absence of a strong base, which has been shown to be required to generate the carbene [34]. However it is likely that the carbene is generated during Heck and Suzuki catalysis as a base is present in the catalysis solution.

3.4.1 Palladium attachment to 5-NH₂phen immobilised bulk monolith

Bulk PPM with immobilised 5-NH₂phen was prepared using the optimised conditions described in **Sections 3.2.1** and **3.2.2**. A small sample of the ligand attached PPM was analysed by EA while the remaining PPM was treated with bis(acetonitrile)dichloropalladium(II) and subsequently analysed for palladium content by ICP-MS. The palladium content was measured as weight percent of palladium present in the PPM. Comparing the moles of immobilised palladium and ligand gives a measure of the binding of the immobilised ligand sites to the palladium. The percentage of moles of palladium to moles of ligand immobilised will be referred to as the palladium loading efficiency. **Table 3.7** shows the palladium and 5-NH₂phen loadings, as well as the palladium loading efficiencies, obtained for the different bulk poly(GMA-*co*-EDMA) and poly(CMS-*co*-DVB) monoliths investigated. The mol equivalents of palladium quoted in **Table 3.7** are relative to the numbers of reactive functional groups present in the PPM to remain consistent with the discussion of flow-through attachment in **Section 3.2.3**, where the ligand loading is not known.

The initial investigation of palladium attachment to bulk PPM with immobilised 5-NH₂phen was performed as reported for our work with 5-OHphen [4], where the ligand immobilised bulk PPM was treated with 2 mL of a 0.02 M solution of bis(acetonitrile)dichloropalladium(II). This was the maximum concentration that could be obtained for the palladium complex in acetonitrile. The amount of palladium reagent used for attachment to 5-OHphen was originally chosen arbitrarily, and was later calculated to be sufficient if the 5-NH₂phen loading is

below 1.5×10^{-4} mol g⁻¹. To ensure the maximum palladium loading was obtained, 10 mL of 0.02 M bis(acetonitrile)dichloropalladium(II) solution used.

Interestingly, bulk poly(GMA-*co*-EDMA) monolith with relatively low 5-NH₂phen loading was found to have above 100% palladium loading efficiency. For some of the samples prepared there was as much as 80% more palladium than ligand present. This may be due to weak binding of palladium to the hydroxyl and secondary amine groups of the immobilised ligand as shown in **Figure 3.6**. Treating unmodified PPM showed that palladium does not bind to the PPM backbone, discussed further in **Chapter 4**.

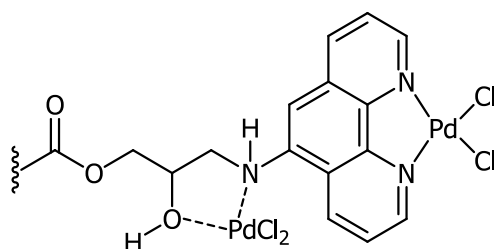


Figure 3.6 Palladium bound to hydroxyl and secondary amine groups of poly(GMA-*co*-EDMA) monolith with immobilised 5-NH₂phen.

The weakly retained palladium is expected to leach off the monolith during catalysis. To test how strongly bound the extra palladium was, bulk PPM prepared using the UVGMA4 with 181% palladium loading efficiency was treated with excess 2,2'-bipyridine (bipy). Bipy is a bidentate chelating ligand with a similar affinity for palladium as 1,10-phen. There should be little-to-no exchange of palladium between bipy and 1,10-phen, however bipy is anticipated to remove the weakly bound palladium as it should have a higher affinity than the hydroxyl-secondary amine system. After treatment with bipy the palladium loading efficiency for the PPM was reduced to 65%. Assuming no exchange between the immobilised 5-NH₂phen and the bipy in solution, this suggests that a majority of the original palladium loading was only weakly retained.

The palladium loadings and loading efficiencies obtained for poly(CMS-*co*-DVB) monolith with immobilised 5-NH₂phen, shown in **Table 3.7**, were significantly lower than obtained with poly(GMA-*co*-EDMA) monolith, despite the poly(CMS-*co*-DVB) monolith having significantly higher ligand loading and attachment efficiencies. As discussed previously, a majority of the reactive functional groups present in the PPM do not bind to ligand reagents [2], and it is assumed that mainly only the highly accessible functional groups at the surface of the microglobules become functionalised with ligand. It is feasible that, at high ligand loading the additional ligand is buried deeper within the PPM structure and less accessible to the palladium reagent.

3.4.2 Palladium attachment to bulk Me-im immobilised monolith

As discussed in **Sections 3.3.1** and **3.3.2**, the ligand loading values obtained for poly(GMA-*co*-EDMA) and poly(CMS-*co*-DVB) monolith functionalised with Me-im were considerably higher than for 5-NH₂phen. The highest ligand loading obtained was $1.2 \times 10^{-3} \text{ mol g}^{-1}$ for poly(CMS-*co*-DVB) monolith. Assuming the palladium binding is as depicted in **Figure 3.5(c)**, then 15 mL of the 0.02 M bis(acetonitrile)dichloropalladium(II) solution is required to form the palladium complex with all the available ligand. However, 10 mL of solution, as used for bulk monolith with immobilised 5-NH₂phen, proved to be sufficient as the highest palladium loading obtained was $2.7 \times 10^{-4} \text{ mol g}^{-1}$ with an attachment efficiency of 25%. The palladium loading and attachment efficiency for Me-im immobilised poly(GMA-*co*-EDMA) and poly(CMS-*co*-DVB) monoliths are shown in **Table 3.8**.

The palladium loading efficiency for both polymer monoliths functionalised with Me-im was significantly lower than that obtained with 5-NH₂phen.

Monolith formulation	Ligand loading (mol g ⁻¹)	Ligand attachment efficiency (%)	Mol eq. palladium	Palladium loading (mol g ⁻¹)	Palladium loading efficiency (%)
TGMA1	6.2×10 ⁻⁵	1.5	0.37	8.0×10 ⁻⁵	129
TGMA1	1.4×10 ⁻⁴	3.3	0.37	1.1×10 ⁻⁴	76
UVGMA4	5.0×10 ⁻⁵	1.2	0.37	9.0×10 ⁻⁵	181
UVGMA4-70	6.1×10 ⁻⁵	1.4	0.37	1.1×10 ⁻⁴	176
TCMS1	1.2×10 ⁻⁴	4.5	0.06	2.0×10 ⁻⁵	17
TCMS1	2.0×10 ⁻⁴	7.7	0.59	2.9×10 ⁻⁵	14
TCMS1	3.1×10 ⁻⁴	11.7	0.59	4.1×10 ⁻⁵	13

Table 3.7 Palladium loading on 5-NH₂phen immobilised bulk PPM.

To investigate the effect of Me-im loading on palladium loading efficiency, two batches of bulk poly(CMS-*co*-DVB) monolith were prepared, one functionalised using neat ligand and the other with 0.9 M ligand in chloroform. Both were subsequently treated with excess palladium. The palladium loading obtained for the poly(CMS-*co*-DVB) monolith treated with neat ligand was over 4-fold higher than the PPM treated with ligand in chloroform, however the palladium loading efficiency was 8% lower at 18%. Despite its lower palladium attachment efficiency, bulk poly(CMS-*co*-DVB) monolith treated with neat ligand had the highest palladium content obtained, $2.0 \times 10^{-4} \text{ mol g}^{-1}$ or 2.2 wt% which is typical for supported palladium catalysts [35].

3.4.3 Flow-through palladium attachment to ligand immobilised monolith

Flow-through palladium attachment to ligand immobilised onto 250 μm ID monolithic capillary columns was achieved using the two-pass procedure described in **Section 3.2.3** [4]. For 100 μm ID capillaries, conditions were developed using the single pass procedure to remain compatible with the borosilicate microchips. In terms of reactor performance, no difference was observed between the 250 μm ID and 100 μm ID capillary columns prepared using the two different procedures. The conditions developed for 100 μm ID capillary were also used for the other flow-through devices investigated and scaled appropriately.

As discussed in **Section 3.2.3**, determination of the ligand loading in fused-silica capillary was not feasible, which also means that the amount of palladium reagent required for flow-through reactor fabrication cannot be directly determined.

Monolith formulation	Ligand loading (mol g ⁻¹)	Mol eq. palladium	Palladium loading (mol g ⁻¹)	Palladium loading efficiency (%)
TGMA1	1.1×10 ⁻³	0.37	2.7×10 ⁻⁴	25
TCMS1	1.9×10 ⁻⁴	0.59	4.8×10 ⁻⁵	26
TCMS1	1.2×10 ⁻³	0.59	2.0×10 ⁻⁴	18

Table 3.8 Palladium loading on Me-im immobilised bulk monolith.

The PPM masses calculated in **Table 3.4** were used to determine the amount of palladium required for each device, at least 2.0×10^{-4} mol g⁻¹ of PPM, and in most cases a large excess was used by pumping in multiples of 240 µL. The only exception was for the 4 mm ID columns where exactly 2.0×10^{-4} mol g⁻¹ was used.

ICP-MS analysis for palladium was performed on 100 µm and 250 µm ID monolithic capillary columns. This required the capillaries to be ground to a fine powder. The polyimide coating of the 250 µm ID fused-silica capillary made grinding very difficult. Removal of the coating before grinding was attempted by burning it off with a torch however this significantly reduced the amount of palladium measured. As an alternative, flow-through leaching of palladium with aqua regia was trialled, however the capillaries blocked due to precipitation.

The mass of palladium in the sample was analysed by ICP-MS and the value was converted to mass of palladium in the original capillary column by using the mass of the capillary column before grinding. The absolute mass of palladium present within the capillary column is not a useful measure of palladium loading as it is dependent on the dimensions of the column. The two metrics used to compare palladium content between columns are *palladium density* giving the moles of palladium per µL, and *palladium loading* giving the moles of palladium per gram of monolith. Calculation of these values is dependent on the volume of PPM, which is estimated from the dimensions of the capillary column. As discussed in **Section 3.2.3**, the monolith volume is used to estimate the PPM mass using the monolith density of the equivalent bulk PPM, as summarised in **Table 3.9**. Palladium density is a more accurate measure of palladium content as the uncertainty in the values generated mostly originates from variation in column dimensions. Deviation between the bulk and column PPM density inevitably leads to significant variation in the calculated palladium loading, which is derived from the column volume and PPM

density. Despite its limited accuracy, the palladium loading is useful for direct comparison with the loading values obtained in batch. The loadings obtained for 5-NH₂phen immobilised on poly(GMA-*co*-EDMA) monolithic columns prepared from the UVGMA4-70 formulation using the various light source/initiator combinations and the TGMA1 formulation, **Table 3.9**, agree well with the value obtained for bulk monolith prepared using the TGMA1 formulation, **Table 3.7**. However, the palladium loading obtained for Me-im immobilised on poly(CMA-*co*-DVB) monolithic columns was 4.3-fold lower than the equivalent bulk monolith. This suggests that the catalyst immobilisation using Me-im in flow-through mode is considerably less efficient than in batch, which may be due to reduced access to functional groups within the complete, non-ground, monolith.

ICP-MS analysis for palladium was attempted on the COC capillary reactors using the same sample preparation as for fused-silica capillary, but the COC was found to be too soft to successfully grind into a powder. As COC is soluble in toluene, the capillary was simply dissolved, leaving behind the catalyst immobilised PPM. Analysis of the PPM gave only background palladium levels suggesting that the dissolved COC was not completely removed and encapsulated the palladium.

ICP-MS analysis for palladium was performed on a 2 mm ID Me-im, UVGMA7-50 PPM reactor using the same sample preparation method as for fused-silica capillary. The data obtained was used to determine the palladium density and loading, shown in **Table 3.9**, which were found to be similar to those for TCMS1 Me-im capillary reactors. Again the column ligand loading was significantly lower, by nine-fold, than the equivalent bulk monolith. For the other reactors palladium loadings were estimated from either the equivalent bulk monolith or the data in **Table 3.9** and is further discussed in **Chapter 4**.

3.5 Conclusions

Conditions were successfully developed for immobilisation of 1,10-phen and imidazolium palladium complexes onto poly(GMA-*co*-EDMA) and poly(CMS-*co*-DVB) monolith under batch and flow-through conditions. Flow-through reactors were prepared in several formats (capillary, microchip, and column) in both glass and COC.

This investigation verified the previously reported poor capacity of poly(GMA-*co*-EDMA) monolith and its dependence on the nature of the nucleophile, highlighted by the large difference in loading obtained for 5-NH₂phen and Me-im. Also of interest was the discovery that very high ligand loading can potentially limit the palladium loading, possibly to inaccessibility of the ligand coordination site.

The palladium loadings obtained for 5-NH₂phen on poly(GMA-*co*-EDMA) monolith in both bulk and capillary columns were found to be similar, however the palladium loading for Me-im on poly(CMS-*co*-DVB) monolith for bulk were over four fold higher than for capillary columns. This may suggest that the reduced accessibility of the PPMs reactive functional groups in a capillary column, compared to ground bulk monolith, has little effect on the loading for bulky ligands, such as 5-NH₂phen, but impacts significantly on the loading smaller ligands, such as Me-im.

While ligand loadings obtained for Me-im were superior to 5-NH₂phen for both monoliths, the severe swelling incurred during attachment to poly(GMA-*co*-EDMA) monolith prevented its use in capillary, making 5-NH₂phen the preferred ligand for microreactors utilising this monolith. Me-im attachment to poly(CMS-*co*-DVB) monolith in capillary or poly(GMA-*co*-EDMA) monolith in columns did not

result in observable swelling, hence this ligand was preferred in these formats due to its high loading and simpler utilisation.

Monolith formulation	Light source / initiator	Ligand	Capillary ID	Palladium density (mol μL^{-1})	Palladium loading (mol g^{-1})
UVGAM4-70	DUV / DMPAP	5-NH ₂ phen	100 μm	3.4×10^{-8}	1.1×10^{-4}
UVGAM4-70	XL-1500-UVC / DMPAP	5-NH ₂ phen	100 μm	5.3×10^{-8}	1.7×10^{-4}
UVGAM4-70	UV-LED / BAPO	5-NH ₂ phen	100 μm	4.5×10^{-8}	9.9×10^{-5}
TGMA1	N/A	5-NH ₂ phen	250 μm	6.5×10^{-8}	1.1×10^{-4}
TCMS1	N/A	Me-im	250 μm	1.7×10^{-8}	4.6×10^{-5}
UVGMA7-50	DUV / DMPAP	Me-im	2 mm	1.2×10^{-8}	3.0×10^{-5}

Table 3.9 Palladium loadings obtained for reactors.

3.6 Experimental

3.6.1 5-Amino-1,10-phenanthroline attachment to bulk monolith

Poly(GMA-*co*-EDMA) and poly(CMS-*co*-DVB) bulk PPM were prepared as described in **Chapter 2** using the TGMA1, TCMS1, UVGMA4, and UVGMA4-70 formulations. The bulk PPM was ground to a fine powder using a mortar and pestle. The ground bulk PPM (250 mg) was added to a 5 mL reaction vial with 5-NH₂phen (100 mg), DMSO (4 mL), and triethylamine (0.2 mL) and stirred for 24 h at 70 °C (oil bath). The treated PPM was recovered by vacuum filtration, stirred vigorously for 60 min in methanol (10 mL), and recovered again by filtration. The treated PPM was dried under vacuum overnight.

3.6.2 1-Methylimidazole attachment to bulk monolith

Poly(GMA-*co*-EDMA) and poly(CMS-*co*-DVB) bulk PPM were prepared as described in **Chapter 2** using the TGMA1 and TCMS1 formulations. The bulk PPM was ground to a fine powder using a mortar and pestle. The ground bulk PPM (250 mg) was added to a 5 mL reaction vial with Me-im (4 mL) and stirred for 24 h at 50 °C (oil bath). The treated PPM was recovered by vacuum filtration, stirred vigorously for 60 min in methanol (10 mL), and recovered again by filtration. The treated PPM was dried under vacuum overnight.

3.6.3 Palladium attachment to bulk monolith

The ligand attached bulk PPM was added to a solution of bis(acetonitrile)dichloropalladium(II) (100 mg) in acetonitrile (10 mL) in a screw-top 20 mL vial and stirred for 24 h at room temperature. The treated PPM was recovered by vacuum filtration, resuspended in acetonitrile (10 mL), stirred vigorously for 60 min and recovered again by filtration. The treated PPM was dried under vacuum overnight.

3.6.4 5-Amino-1,10-phenanthroline attachment in 100 μm ID

monolithic capillary column

A stock ligand solution was prepared by dissolving 5-NH₂phen (250 mg) in DMSO (10 mL) with triethylamine (0.5 mL) and then filtering through a 0.2 μm syringe filter. A 30 cm long 100 μm ID poly(GMA-*co*-EDMA) monolithic capillary column was prepared as described in **Chapter 2** using the UVGMA1, UVGMA4, and UVGMA4-70 formulations, and interfaced within a Waters Millipore 112/WTC-120 temperature controlled column heater, as described in **Chapter 5**. The capillary column was flushed with DMSO + 10% v/v methanol for 16 h at 15 $\mu\text{L h}^{-1}$ within a column heater at 70 °C, followed by ligand solution at 10 $\mu\text{L h}^{-1}$ for 24 h in a column heater at 70 °C, and DMSO + 10% v/v methanol for 16 h at 15 $\mu\text{L h}^{-1}$ at the same temperature.

3.6.5 5-Amino-1,10-phenanthroline attachment in 250 μm ID

poly(GMA-*co*-EMDA) monolithic capillary column

A 25 cm long 250 μm ID poly(GMA-*co*-EDMA) monolithic capillary column was prepared as described in **Chapter 2** using the TGMA1 formulation, and interfaced within a column heater as described in **Chapter 5**. The capillary column was flushed with DMSO + 10% v/v methanol for 4 h at 60 $\mu\text{L h}^{-1}$ within a column heater at 70 °C. Ligand solution was then flushed through the capillary column at 30 $\mu\text{L h}^{-1}$ for 8 h, and the capillary reversed and a second flush of ligand solution was passed through the capillary at 15 $\mu\text{L h}^{-1}$ for 16 h within a column heater at 70 °C. The capillary column was finally flushed with DMSO + 10% v/v methanol for 4 h at 60 $\mu\text{L h}^{-1}$ at the same temperature.

3.6.6 5-Amino-1,10-phenanthroline attachment in 250 μm ID poly(CMS-*co*-DVB) monolithic capillary column

A stock ligand solution was prepared by dissolving 5-NH₂phen (250 mg) in methanol (10 mL) and then filtered through a 0.2 μm syringe filter. A 25 cm long 250 μm ID poly(CMS-*co*-DVB) monolithic capillary column was prepared as described in **Chapter 2** using the TCMS1 formulation, and interfaced within a column heater as described in **Chapter 5**. The capillary column was flushed with methanol for 4 h at 60 $\mu\text{L h}^{-1}$ within a column heater at 70 °C, then ligand solution at 30 $\mu\text{L h}^{-1}$ for 8 h, the capillary was reversed and a second flush of ligand solution was passed at 15 $\mu\text{L h}^{-1}$ for 16 h within a column heater at 70 °C. Finally, the capillary column was flushed with methanol for 4 h at 60 $\mu\text{L h}^{-1}$ at the same temperature.

3.6.7 5-Amino-1,10-phenanthroline attachment to PPM in glass microchip

Poly(GMA-*co*-EDMA) monolith was prepared within borosilicate microchips as described in **Chapter 2**, following the same procedure as for the 100 μm ID capillary columns except the solvent flushes were scaled up to 8 h at 30 $\mu\text{L h}^{-1}$ for the larger cross-section.

3.6.8 5-Amino-1,10-phenanthroline attachment to PPM in COC capillary and microchip

Poly(GMA-*co*-EDMA) monolith was prepared within 276 μm ID COC capillary and microchip as described in **Chapter 2**, with the solvent flushes scaled as described above to 4 h at 60 $\mu\text{L h}^{-1}$.

3.6.9 5-Amino-1,10-phenanthroline attachment in 2 mm ID monolithic columns

2 mm ID poly(GMA-*co*-EDMA) monolithic column was prepared as described in **Chapter 2**, using the UVGMA7-50 formulation, and interfaced within a column heater as described in **Chapter 5**. The procedure was as described for 100 μm ID capillary column except scaled up for the larger column diameter and PPM mass. The column was flushed with DMSO + 10% v/v methanol for 40 min at 0.25 mL min⁻¹ within a column heater at 70 °C, then flushed with ligand solution at 416.7 $\mu\text{L h}^{-1}$ for 24 h, followed by DMSO + 10% v/v methanol for 40 min at 0.25 mL min⁻¹ at the same temperature.

3.6.10 1-Methylimidazole attachment in 100 μm ID monolithic capillary column

30 cm long 100 μm ID poly(GMA-*co*-EDMA) monolithic capillary column was prepared as described in **Chapter 2**, using the UVGMA4-70 formulation, and interfaced within a column heater as described in **Chapter 5**. The capillary column was flushed with methanol for 8 h at 30 $\mu\text{L h}^{-1}$ within a column heater at 50 °C, neat Me-im at 10 $\mu\text{L h}^{-1}$ for 24 h in a column heater at 50 °C, followed by acetonitrile for 8 h at 30 $\mu\text{L h}^{-1}$ at the same temperature.

3.6.11 1-Methylimidazole attachment in 250 μm ID poly(CMS-*co*-DVB) monolithic capillary column

A 25 cm long 250 μm ID poly(CMS-*co*-DVB) monolithic capillary column was prepared as described in **Chapter 2**, using the TCMS1 formulation, and interfaced within a column heater as described in **Chapter 5**. The capillary column was flushed with methanol for 4 h at 60 $\mu\text{L h}^{-1}$ within a column heater at 50 °C. The capillary column was then flushed with neat Me-im at 30 $\mu\text{L h}^{-1}$ for 8 h, the capillary

was reversed and a second flush of Me-im was passed at $15 \mu\text{L h}^{-1}$ for 16 h within a column heater at 70°C . Finally, the capillary column was flushed with acetonitrile for 4 h at $60 \mu\text{L h}^{-1}$ at the same temperature.

3.6.12 1-Methylimidazole attachment in large ID monolithic column

2 mm and 4 mm ID poly(GMA-*co*-EDMA) monolithic columns were prepared as described in **Chapter 2**, using the UVGMA7-50 formulation, and interfaced within a column heater as described in **Chapter 5**. The procedure was as described for 100 μm ID capillary column except scaled up for the larger column diameter and PPM mass. The 2 mm column was flushed with methanol for 40 min at 0.25 mL min^{-1} within a column heater at 50°C , then with neat Me-im at $416.7 \mu\text{L h}^{-1}$ for 24 h in a column heater at 70°C , followed by acetonitrile for 40 min at 0.25 mL min^{-1} at the same temperature. The sample procedure was followed for 4 mm ID column except the rinse with acetone was performed for 120 min at 0.5 mL min^{-1} .

3.6.13 Palladium attachment in 100 μm ID ligand attached monolithic capillary column

A stock palladium solution was prepared by dissolving bis(acetonitrile)dichloropalladium(II) (100 mg) in acetonitrile (10 mL) and then filtering through a $0.2 \mu\text{m}$ syringe filter. Ligand treated monolithic capillary column was flushed with acetonitrile for 16 h at $15 \mu\text{L h}^{-1}$ at room temperature (this step was not performed for Me-im treated capillary columns) The capillary column was then flushed with palladium solution at $10 \mu\text{L h}^{-1}$ for 24 h, followed by acetonitrile for 8 h at $30 \mu\text{L h}^{-1}$.

3.6.14 Palladium attachment in 250 μm ID ligand attached monolithic capillary column

Ligand treated monolithic capillary column was flushed with acetonitrile for 2 h at $120\ \mu\text{L h}^{-1}$ at room temperature (this step was not performed for Me-im treated capillary columns). The capillary column was then flushed with palladium solution at $30\ \mu\text{L h}^{-1}$ for 8 h, the capillary was reversed and a second flush of palladium solution was passed through the capillary at $15\ \mu\text{L h}^{-1}$ for 16 h. Finally, the capillary column was flushed with acetonitrile for 2 h at $120\ \mu\text{L h}^{-1}$.

3.6.15 Palladium attachment to ligand attached PPM in borosilicate microchip

The procedure was as described for 100 μm ID capillary column except scaled up for the larger column diameter. Solvent flushes were performed for 8 h at $30\ \mu\text{L h}^{-1}$.

3.6.16 Palladium attachment to ligand attached PPM in COC capillary and microchip

The procedure was as described for 100 μm ID capillary column except scaled up for the larger column diameter. Solvent flushes were performed for 4 h at $60\ \mu\text{L h}^{-1}$.

3.6.17 Palladium attachment in 2 mm ID ligand attached monolithic capillary column

The procedure was as described for 100 μm ID capillary column except scaled up for the larger column diameter and PPM mass. The ligand treated monolithic column was flushed with acetonitrile for 40 min at $0.25\ \text{mL min}^{-1}$ at room temperature (not performed for Me-im treated columns). The column was then

flushed with palladium solution at $416.7 \mu\text{L h}^{-1}$ for 24 h, followed by acetonitrile for 120 min at 0.25 mL min^{-1} .

3.6.18 Palladium attachment in 4 mm ID ligand attached monolithic capillary column

The procedure was as described for $100 \mu\text{m}$ ID capillary column except scaled up for the larger column diameter and PPM mass. The column was flushed palladium solution at $416.7 \mu\text{L h}^{-1}$ for 24 h, followed by acetonitrile for 120 min at 0.5 mL min^{-1} .

3.6.19 Capillary column ICP-MS sample preparation

Monolithic capillary columns were externally cleaned with methanol and tissue then dried under vacuum overnight. The capillary column length was measured to 0.05 cm accuracy and its mass measured to 0.05 mg accuracy. The capillary column was cut into ~ 4 cm lengths and ground to a fine powder with a mortar and pestle. The ground capillary was transferred into a pre-weighed vial and the mass of the ground capillary recorded. The ground capillary was submitted for ICP-MS analysis.

3.6.20 Palladium content analysis by ICP-MS

Analysis for palladium content was determined by Dr Ashley Townsend at the Central Science Laboratory, University of Tasmania, using a EL-ELEMENT high resolution inductively coupled plasma mass spectrometer.

Samples were placed in a larger plastic sealed container with 1 ml fresh aqua regia and sonicated for 24 h. Water was added to give a final volume of 10 ml and 100 ppb indium was added as an internal standard.

3.6.21 Nitrogen content analysis by EA

The analysis for total nitrogen was determined by Dr Thomas Rodemann at the Central Science Laboratory, University of Tasmania, using a Thermo Finnigan EA 1112 Series Flash Elemental Analyser.

Between 0.7 and 1.7 mg of sample were weighed into tin capsules using a Sartorius SE2 ultra-microbalance with an accuracy of 0.2 µg. Combustion of the pressed tin cups was achieved in ultra high purity oxygen at 1000 °C using tungstic oxide on alumina as an oxidising agent followed by reduced copper wires as a reducing agent. The results were calibrated using a certified sulphanilamide standard.

3.7 References

1. Svec, F., Less common applications of monoliths: I. Microscale protein mapping with proteolytic enzymes immobilized on monolithic supports. *Electrophoresis*, 2006. **27**(5-6), 947-961.
2. Buchmeiser, M.R., Polymeric monolithic materials: Syntheses, properties, functionalization and applications. *Polymer*, 2007. **48**(8), 2187-2198.
3. Izaak, T.I. and O.V. Vodyankina, Macroporous monolithic materials: synthesis, properties and application. *Russian Chemical Reviews*, 2009. **78**(1), 77-88.
4. Bolton, K.F., A.J. Canty, J.A. Deverell, R.M. Guijt, E.F. Hilder, T. Rodemann, and J.A. Smith, Macroporous monolith supports for continuous flow capillary microreactors. *Tetrahedron Letters*, 2006. **47**(52), 9321-9324.
5. Karbass, N., V. Sans, E. Garcia-Verdugo, M.I. Burguete, and S.V. Luis, Pd(0) supported onto monolithic polymers containing IL-like moieties. Continuous flow catalysis for the Heck reaction in near-critical EtOH. *Chemical Communications*, 2006(29), 3095-3097.
6. Nikbin, N., M. Ladlow, and S.V. Ley, Continuous flow ligand-free Heck reactions using monolithic Pd 0 nanoparticles. *Organic Process Research & Development*, 2007. **11**(3), 458-462.
7. Alonso, F., I.P. Beletskaya, and M. Yus, Non-conventional methodologies for transition-metal catalysed carbon-carbon coupling: a critical overview. Part 2: The Suzuki reaction. *Tetrahedron*, 2008. **64**(14), 3047-3101.
8. Ali, A., X.F. Yin, H. Shen, Y.X. Ye, and X. Gu, 1,10-phenanthroline as a complexing agent for on-line sorbent extraction preconcentration for flow injection-flame atomic absorption spectrometry. *Analytica Chimica Acta*, 1999. **392**(2-3), 283-289.
9. Bhattacharya, S., S.K. Roy, and A.K. Chakraborty, Spectrophotometric Determination Of Traces Of Iron After Extraction Of Fe(II)-Phenanthroline Complex On Polyurethane Foam. *Talanta*, 1990. **37**(11), 1101-1104.
10. Faizullah, A.T. and A. Townshend, Application Of A Reducing Column For Metal Speciation By Flow-Injection Analysis - Spectrophotometric Determination Of Iron(III) And Simultaneous Determination Of Iron(II) And Total Iron. *Analytica Chimica Acta*, 1985. **167**, 225-231.
11. Girousi, S.T., I. Gherghi, A.N. Voulgaropoulos, and J.A. Stratis, Voltammetric determination of vanadium, by using 1,10-phenanthroline as a complexing agent. *International Journal of Environmental Analytical Chemistry*, 1999. **75**(1-2), 83-91.
12. Lynch, T.P., N.J. Kernoghan, and J.N. Wilson, Speciation Of Metals In Solution By Flow-Injection Analysis .2. Determination Of Iron(III) And Iron(II) In Mineral Process Liquors By Simultaneous Injection Into Parallel Streams. *Analyst*, 1984. **109**(7), 843-846.
13. Tawali, A.B. and G. Schwedt, Combination of solid phase extraction and flame atomic absorption spectrometry for differentiated analysis of labile iron(II) and iron(III) species. *Fresenius Journal of Analytical Chemistry*, 1997. **357**(1), 50-55.
14. Slough, G.A., V. Krchňák, P. Helquist, and S.M. Canham, Synthesis of readily cleavable immobilized 1,10-phenanthroline resins. *Organic Letters*, 2004. **6**(17), 2909-2912.
15. Zhang, Z.Y., H.W. Hu, and T.Y. Kao, Poly(styryl)phenanthroline Palladium As Heterogeneous Catalyst For Heck Arylation Using Iodobenzene. *Reactive Polymers*, 1990. **12**(3), 229-235.

16. Lenaerts, P., K. Driesen, R. Van Deun, and K. Binnemans, Covalent Coupling of Luminescent Tris(2-thenoyltrifluoroacetato)lanthanide(III) Complexes on a Merrifield Resin. *Chemistry of Materials*, 2005. **17**(8), 2148-2154.
17. Fan, G.Z., H.J. Zhang, S.Q. Cheng, Z.D. Ren, Z.J. Hu, and Z.L. Wang, Lewis acid-promoted Suzuki reaction using palladium chloride anchored on a polymer as a catalyst. *Australian Journal of Chemistry*, 2008. **61**(8), 610-614.
18. Troy Turner, B.O.-B., Genessa Ottomann, IDEX® Health & Science 2009-2010 Catalog, I.H.S. LLC., Editor. 2009, Visual Ventures.
19. Preinerstorfer, B., W. Bicker, W. Lindner, and M. Lämmerhofer, Development of reactive thiol-modified monolithic capillaries and in-column surface functionalization by radical addition of a chromatographic ligand for capillary electrochromatography. *Journal of Chromatography, A*, 2004. **1044**(1-2), 187-199.
20. Wu, J. and H.-G. Xia, Tertiary amines as highly efficient catalysts in the ring-opening reactions of epoxides with amines or thiols in H₂O: expeditious approach to β -amino alcohols and β -aminothioethers. *Green Chemistry*, 2005. **7**(10), 708-710.
21. Altava, B., M.I. Burguete, E. Garcia-Verdugo, N. Karbass, S.V. Luis, A. Puzary, and V. Sans, Palladium N-methylimidazolium supported complexes as efficient catalysts for the Heck reaction. *Tetrahedron Letters*, 2006. **47**(14), 2311-2314.
22. Jones, R.C., A.J. Canty, J.A. Deverell, M.G. Gardiner, R.M. Guijt, T. Rodemann, J.A. Smith, and V.A. Tolhurst, Supported palladium catalysis using a heteroleptic 2-methylthiomethylpyridine-N,S-donor motif for Mizoroki-Heck and Suzuki-Miyaura coupling, including continuous organic monolith in capillary microscale flow-through mode. *Tetrahedron*, 2009. **65**(36), 7474-7481.
23. Byström, E., C. Viklund, and K. Irgum, Differences in porous characteristics of styrenic monoliths prepared by controlled thermal polymerization in molds of varying dimensions. *Journal of Separation Science*, 2010. **33**(2), 191-199.
24. Byun, J.W. and Y.S. Lee, Preparation of polymer-supported palladium/N-heterocyclic carbene complex for Suzuki cross-coupling reactions. *Tetrahedron Letters*, 2004. **45**(9), 1837-1840.
25. Kim, J.H., B.H. Jun, J.W. Byun, and Y.S. Lee, N-heterocyclic carbene-palladium complex on polystyrene resin surface as polymer-supported catalyst and its application in Suzuki cross-coupling reaction. *Tetrahedron Letters*, 2004. **45**(30), 5827-5831.
26. Kim, J.H., J.W. Kim, M. Shokouhimehr, and Y.S. Lee, Polymer-Supported N-Heterocyclic Carbene-Palladium Complex for Heterogeneous Suzuki Cross-Coupling Reaction. *Journal of Organic Chemistry*, 2005. **70**(17), 6714-6720.
27. Gürbüz, N., I. Özdemir, T. Seçkin, and B. Çetinkaya, Surface modification of inorganic oxide particles with a carbene complex of palladium: A recyclable catalyst for the Suzuki reaction. *Journal of Inorganic and Organometallic Polymers*, 2004. **14**(2), 149-159.
28. Kim, J.W., J.H. Kim, D.H. Lee, and Y.S. Lee, Amphiphilic polymer supported N-heterocyclic carbene palladium complex for Suzuki cross-coupling reaction in water. *Tetrahedron Letters*, 2006. **47**(27), 4745-4748.
29. Lozano, P., E. Garcia-Verdugo, R. Piamtongkam, N. Karbass, T. De Diego, M.I. Burguete, S.V. Luis, and J.L. Iborra, Bioreactors based on monolith-

- supported ionic liquid phase for enzyme catalysis in supercritical carbon dioxide. *Advanced Synthesis & Catalysis*, 2007. **349**(7), 1077-1084.
30. Gömann, A., J.A. Deverell, K.F. Munting, R.C. Jones, T. Rodemann, A.J. Canty, J.A. Smith, and R.M. Guijt, Palladium-mediated organic synthesis using porous polymer monolith formed in situ as a continuous catalyst support structure for application in microfluidic devices. *Tetrahedron*, 2009. **65**(7), 1450-1454.
31. Zeng, F. and Z. Yu, Pyridyl-Supported Pyrazolyl-N-Heterocyclic Carbene Ligands and the Catalytic Activity of Their Palladium Complexes in Suzuki-Miyaura Reactions. *Journal of Organic Chemistry*, 2006. **71**(14), 5274-5281.
32. Colacot, T.J., E.S. Gore, and A. Kuber, High-throughput screening studies of fiber-supported catalysts leading to room-temperature Suzuki coupling. *Organometallics*, 2002. **21**(16), 3301-3304.
33. Lv, G.H., W.P. Mai, R. Jin, and L.X. Gao, Immobilization of dipyridyl complex to magnetic nanoparticle via click chemistry as a recyclable catalyst for Suzuki cross-coupling reactions. *Synlett*, 2008(9), 1418-1422.
34. Storey, J.M.D. and C. Williamson, Imidazole based solid-supported catalysts for the benzoin condensation. *Tetrahedron Letters*, 2005. **46**(43), 7337-7339.
35. Leadbeater, N.E. and M. Marco, Preparation of polymer-supported ligands and metal complexes for use in catalysis. *Chemical Reviews*, 2002. **102**(10), 3217-3273.

Chapter 4 Suzuki-Miyaura reactions

4.1 Introduction

The Suzuki-Miyaura reaction, involving the cross-coupling of aryl halides with organoboron compounds, was chosen as a model reaction for microreactor testing as it is one of the most important and convenient methods for the preparation of biaryls [1]. Most forms of palladium can be used as pre-catalysts, and in some cases only extremely small amount of palladium (ppm or ppb levels) are sufficient to give very high turnover numbers [2]. The reaction is tolerant towards a large range of functional groups, involves low toxicity reagents and by-products, a wide range of compatible compounds (especially boronic acids) are readily available, and can be performed under mild aerobic conditions. The generally accepted Suzuki-Miyaura catalytic cycle for the coupling of aryl halides and aryl boronic acids to form biaryls is shown in **Figure 4.1**. Often a palladium(II) pre-catalyst is used for the reaction which is believed to be reduced to palladium(0) *in situ* under reaction conditions, allowing it to oxidatively add the aryl halide forming a Pd(II) intermediate [2]. This intermediate undergoes a transmetallation with the boronate, from which the product is expelled by reductive elimination, regenerating Pd(0). The role of the base is believed to be in the activation of the boronic acid in order to form the more reactive boronate, which facilitates the transmetallation step.

The Suzuki-Miyaura reaction has been relatively popular for demonstrating transition metal mediated catalysis under continuous-flow conditions, in both minireactors for laboratory scale synthesis [3-8], and also in microreactors [9-12]. As previously discussed in **Chapter 1**, Suzuki-Miyaura reactions in microreactors have been demonstrated using both homogeneous [5, 10], and immobilised catalysts [9, 11-13].

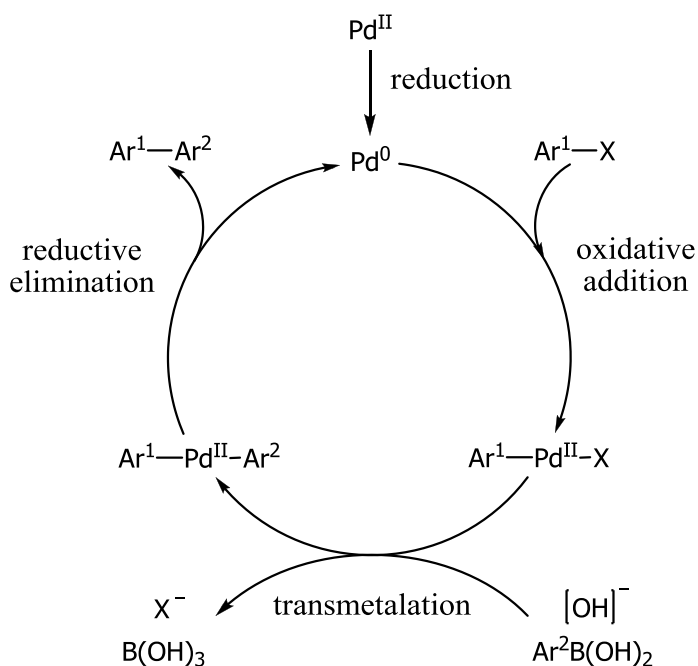


Figure 4.1 Suzuki-Miyaura catalytic cycle

In general, reactions performed using these devices were found to proceed faster than the equivalent batch process with similar or improved reaction yields. Unfortunately none of these palladium immobilisation techniques are suitable for use as microreactors integrated with other microfluidic components to form a lab-on-a-chip, as the catalyst immobilisation cannot be easily confined to a particular region within the device. PPM's were specifically utilised in this work to allow spatial control over the region of catalyst immobilisation, providing a way of integrating microreactors in lab-on-a-chip devices.

4.2 Considerations

Typically Suzuki-Miyaura coupling reactions are performed using an aryl halide, a boronic acid and a base, in a solvent which is brought into contact with the palladium catalyst. In this work, the coupling of iodobenzene and *p*-tolylboronic acid is used to demonstrate the proof of concept of the microreactors. The solvent and base are known to have a significant influence on the efficiency of Suzuki-Miyaura coupling reactions [14], and as such a large variety of different solvents and bases

have been tested for its application. Generally simple organic solvents are employed [1, 14-16], often with water as a co-solvent to solubilise an inorganic base [1, 3-7, 10-12, 14, 17-19]. From the wide variety of bases used for Suzuki-Miyaura catalysis [1, 3-7, 9-12, 14-20] inorganic bases are by far the most commonly utilised, however alkylammonium salts [8] and organic bases [1, 4, 14] have also been shown to successfully promote catalysis.

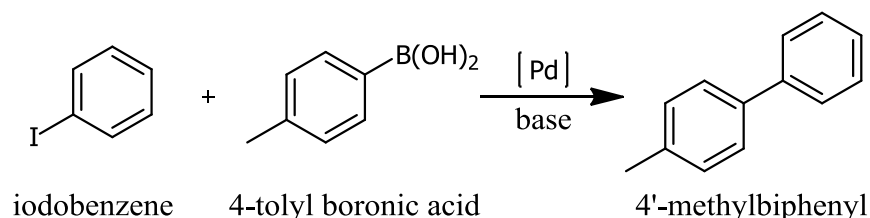
For our flow-through system, additional requirements are imposed on the reaction mixture. To prevent blocking of the PPM, no particulates should be present in the reaction mixture, i.e. the iodobenzene, *p*-tolylboronic acid, base and diphenyl ether (internal standard) should be completely soluble in the solvent. The same requirement is valid for the reaction products and intermediates [21]. The reaction mixture should also be homogeneous, so care should be taken to avoid phase separation. Additionally, the solvent and reagents should all be compatible with the PPM as well as the substrate of the microreactor.

It is important to note that Suzuki-Miyaura reactions were performed to demonstrate the reactor technology and to evaluate the reactor fabrication process. The aim was not to optimise reaction conditions in order to get the best possible reactor performance, hence the effects of system parameters such as reactor dimensions, residence time, linear velocity, reaction temperature, reagent concentration, and palladium loading on reaction yield were not systematically explored. Due to the extra requirements imposed by the flow-through system, different solvent/base systems were explored as discussed below.

The initial solvent/base system investigated was developed by Lee *et al.* for continuous-flow Suzuki-Miyaura reactions performed using a 5 cm long, 450 μm ID column reactor packed with palladium(II) acetate microencapsulated in polyurea

(PdEnCat) [8]. Using toluene/methanol (9:1) as the solvent system, Lee *et al.* investigated a range of soluble tetra-*n*-butylammonium salts of which tetrabutylammonium methoxide (TBAM) was found to be the best performing base, giving quantitative yields [8]. *p*-Tolylboronic acid was used for these reactions, which is an excellent choice for performing test reactions with phenyl halides as the reaction product, 4'-methylbiphenyl, can be easily distinguished from the homocoupled boronic acid, 4-4'-dimethylbiphenyl. The specific coupling reaction investigated is shown in **Scheme 4.1**. When phenylboronic acid is used instead, the product formed is the same as the homocoupling of the boronic acid, which is biphenyl for phenyl halides [10, 22].

The conditions developed by Lee *et al.* were slightly modified for use with catalyst immobilised polymer monolith, and 1 mol eq of diphenyl ether was included as an internal standard to allow the reaction yield to be determined by GC analysis.



Scheme 4.1 Suzuki-Miyaura coupling of iodobenzene and *p*-tolylboronic acid.

While TBAM is a highly soluble and relatively strong base, and is available as a methanol solution, it is also moisture sensitive requiring the use of anhydrous solvents for the reaction mixtures and refrigerated storage under argon. The reaction mixtures were completely soluble and homogeneous, but would become biphasic at <4 °C.

The toluene/methanol system was initially investigated using bulk poly(GMA-*co*-EDMA) monolith with 5-OHphen as the ligand (palladium loading of

1.79×10^{-5} mol g⁻¹ of monolith). After a reaction time of 90 min at 80 °C, a yield of 75% was obtained (under these conditions there is 1.8 mol% of palladium present). A typical chromatogram for this reaction is shown in **Figure 4.2**, in which the peaks for tetrabutylammonium salt and boronic acid homocoupled product, 4,4'-dimethylbiphenyl, are identified by MS. When performing the reaction using 5-OHphen based 250 μ m ID monolithic capillary reactors, prepared using the TGMA1 formulation, no signs of leakage were observed over four days, suggesting that no precipitate formed during the reaction. Precipitation would have resulted in a pressure build-up and consequent leakage.

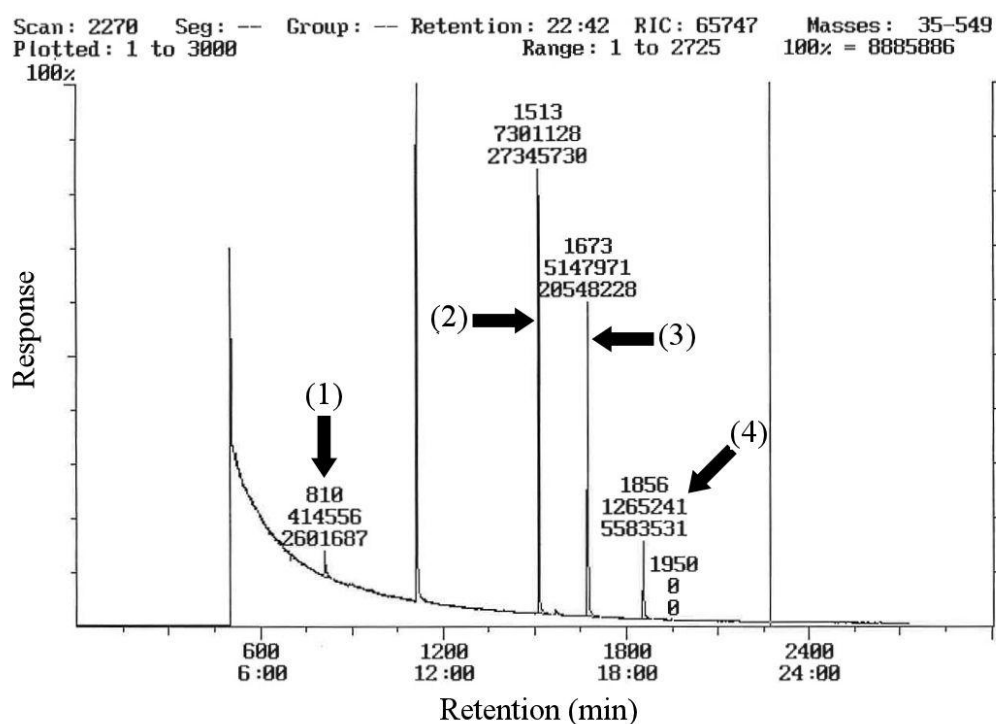


Figure 4.2 Chromatogram of batch reaction using toluene/methanol system (analysis by GC-MS). Identification of peaks: (1) iodobenzene, (2) diphenyl ether, (3) 4'-methylbiphenyl, (4) 4,4'-dimethylbiphenyl.

While this solvent/base system proved to be compatible with monolith-based continuous-flow reactors, toluene is not compatible with most polymers and hence this system is not suitable for reactors fabricated from COC. The use of toluene was

therefore abandoned, and methanol was used as the sole solvent while the amount of base was increased to 1.5 eq to improve the reaction yield. Reaction mixtures prepared in methanol were found to be completely soluble. At this stage of catalyst immobilisation development, bulk monolith catalyst was prepared using 5-NH₂phen in DMSO. As discussed in **Chapter 3**, the palladium loading for this system was 0.04%, or 3.8×10^{-7} mol g⁻¹ of monolith. After a reaction time of 60 min at 80 °C (with 0.09 mol% palladium present), a yield of 80% was obtained, which was a minor improvement over the toluene/methanol system. When performing the reaction using 5-NH₂phen based monolithic capillary reactors no signs of leakage were observed over two days, suggesting that no precipitate formed during the reaction.

While the methanol system was an improvement over the toluene/methanol system, it still required anhydrous conditions due to the presence of the hygroscopic base. In order to allow reactions to be performed under aerobic conditions, tetrabutylammonium hydroxide (TBAH) was investigated as an alternative base. Lee *et al.* found that reactions performed using TBAH gave only slightly lower yields than with TBAM for Suzuki-Miyaura reactions [8]. TBAH is commercially available as either aqueous or methanol solutions, both of which were investigated.

Using aqueous TBAH, water was added as a co-solvent, which is known to significantly improve the reaction efficiency for Suzuki-Miyaura reactions [17, 23]. To make the solvents identical to those using either TBAH source 5% v/v water was also added to the reaction mixture of the methanol TBAH system. The addition of this small amount of water was found to drastically reduce the solubility of diphenyl ether, making it partially immiscible. The main solvent was then changed to ethanol to improve the reaction mixture homogeneity.

Reaction mixtures were prepared using both aqueous and methanol solutions of TBAH, both of which were found to be completely soluble. Reactions were performed utilising bulk monolith catalyst prepared using 5-NH₂phen in DMSO with triethylamine, which at that stage was the catalyst immobilisation method under development. As discussed in **Chapter 3**, the palladium loading for this system was 0.85%, or 8.0×10^{-5} mol g⁻¹ of monolith. Reactions were performed for 60 min at 80 °C (2.00 mol% palladium present), which resulted in quantitative yields when using TBAH in methanol, but poor yields were obtained with the aqueous TBAH. Therefore TBAH in methanol was used for subsequent testing. A typical chromatogram for this reaction is shown in **Figure 4.3**, in which the tetrabutylammonium salt and boronic acid homocoupled product, 4,4'-dimethylbiphenyl, are identified. Iodobenzene was not detected as it is completely consumed in the reaction. The ethanol/methanol/water with TBAH system is ideal for reactions with simple phenyl halides using polymer-based reactors, but may not be suitable for substituted aryl halides or aryl boronic acids with low solubility in ethanol. One of the most commonly used solvent systems for batch and continuous-flow Suzuki-Miyaura catalysis is DMF/water, which has been shown to be compatible with a variety of aryl halides and aryl boronic acids [3-5, 7, 12, 14, 17-19]. As discussed in **Chapter 3**, DMF was found to be incompatible with poly(GMA-*co*-EDMA) monolith due to swelling. It is however compatible with poly(CMS-*co*-DVB) monolith, and thus this solvent system was specifically investigated for use with poly(CMS-*co*-DVB) monolith reactors.

The reported DMF/water systems generally have a high water content in order to solubilise an inorganic base, but to ensure solubility of the reaction mixture triethylamine was chosen as the base [14].

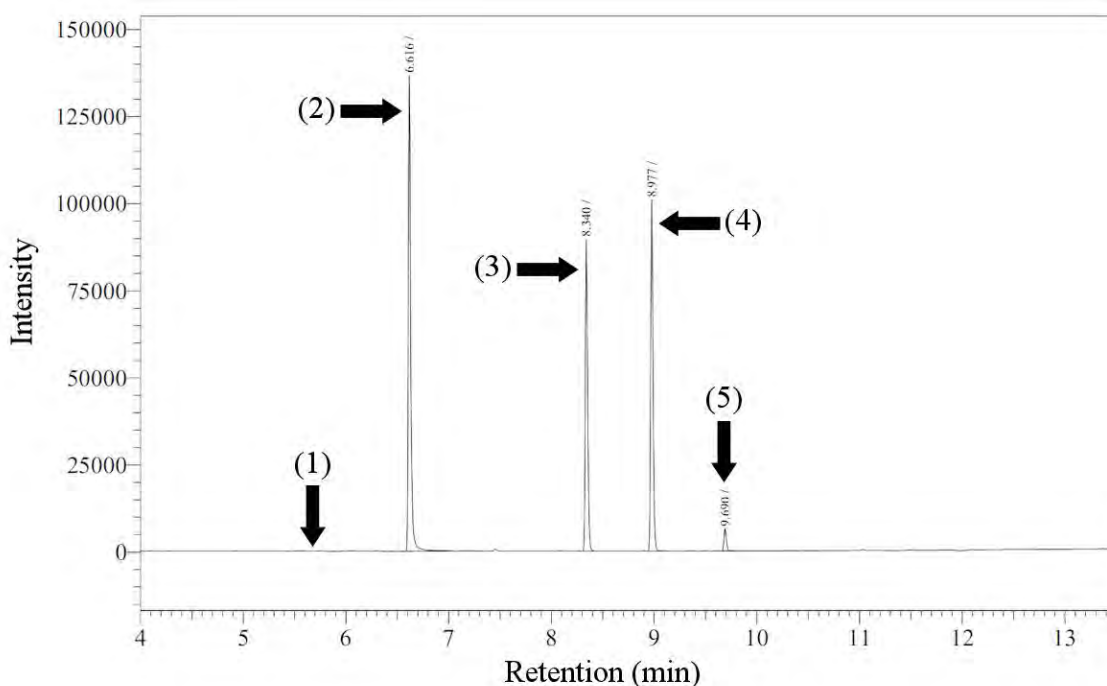


Figure 4.3 Chromatogram of batch reaction using ethanol/methanol/water system (analysis by GC-FID). Identification of peaks: (1) iodobenzene (not present), (2) tetrabutylammonium salt, (3) diphenyl ether, (4) 4'-methylbiphenyl, (5) 4,4'-dimethylbiphenyl.

Reaction mixtures (0.1M) containing 1.5 mol eq base and 1.5 mol eq boronic acid, were prepared using different ratios of DMF to water in order to determine the maximum amount of water that could be used maintaining complete solubility of the reagents. The maximum water content was found to be 25%. This solvent/base system was tested under batch conditions using bulk poly(CMS-*co*-DVB) monolith catalyst prepared using 5-NH₂phen or Me-im ligand. As discussed in **Chapter 3**, the palladium loading for the monolith with immobilised Me-im was 2.15 wt%, or 2.0×10^{-4} mol g⁻¹ of monolith and 0.30 wt% or 2.9×10^{-5} mol g⁻¹ of monolith for immobilised 5-NH₂phen. Reactions were performed for 60 min at 80 °C (4.04 mol% palladium present for the bulk monolith with immobilised Me-im and 0.56 mol% palladium for the 5-NH₂phen immobilised bulk monolith) giving a yield of 96% and 86% respectively. The difference in the yields obtained using the two different

ligands is likely due to the difference in their respective palladium loadings. For continuous-flow testing, the reaction was performed in Me-im based monolithic capillary reactors and no signs of leakage were observed over two days suggesting that no precipitate formed during the reaction.

4.3 Continuous flow reaction results

As stated in the previous section, the development of conditions for catalyst immobilisation PPM's was investigated in parallel with Suzuki-Miyaura reaction development. The previous section discussed the development of reaction conditions suitable for continuous-flow. This section will discuss the application of those conditions using the various reactors investigated in terms of the reactor performance and reaction yield.

The majority of the continuous-flow reactions investigated were performed using monolithic capillary reactors. As noted in **Chapters 2 and 3**, capillary columns were used to simulate microchips to assist in the development of microchip compatible reactor fabrication conditions, with the exception of reactors prepared from thermally initiated PPM. These 250 μm ID capillary reactors form a separate line of enquiry into the use of capillary reactors for laboratory-scale synthesis and as such are not the main focus of this work. The reaction conditions and results for each different type of capillary reactor investigated are summarised in **Table 4.1**. Similarly, the results obtained for microchip reactors and column reactors are summarised in **Tables 4.2 and 4.3**. The reactions and reactor performance for each of the different types of reactors will be discussed.

The capillary reactor system initially investigated, known here as CR1, was based on 5-OHphen immobilised on poly(GMA-*co*-EDMA) monolith, prepared from the TGMA1 formulation as described in **Chapter 3**, in 15 cm long lengths of

250 μm ID fused-silica capillary. This was the first PPM-based continuous-flow reactor system investigated and was studied merely for proof-of-principle. CR1 reactors were tested using the toluene/methanol reaction system at a flow rate chosen to give a 90 min residence time in order to match the reaction time used for the equivalent batch reaction. The flow rate was calculated assuming that the void volume of the monolithic column was the same volume of the porogenic solvents, as MIP data was not available at the time. Fortunately subsequent MIP showed that this assumption was valid for this particular PPM. The mol% palladium content of CR1 reactors was estimated to be 17%, using data for ICP-MS analysis of the equivalent bulk monolith, which is over 9-fold higher than the equivalent batch reaction palladium content. In batch-mode the catalyst, supported on a particle or bead substrate for instance, is dispersed through the reaction mixture by vigorous mixing. In continuous-flow reactors, the catalyst is stationary and the reaction mixture flows through the solid support, which allows for a greater opportunity for the reactants to interact with the catalyst due to its higher availability.

The coupling of iodobenzene with *p*-tolylboronic acid was performed using the CR1 reactors over four days and resulted in a stable yield of 68% over that time, samples taken every 12 h. Catalytic performance is generally measured using the turn-over number (TON), which is the molar ratio of product produced to catalyst present. This value is particularly relevant to closed batch systems where the reaction is performed until completion. TON cannot be applied to continuous-flow systems where the product produced is time dependent.

Capillary reactor system	PPM formulation	Initiator/source	Flow rate ($\mu\text{L h}^{-1}$)	Estimated contact time (min)	Stable yield	Turn-over frequency (h^{-1})
CR1 ¹	TGMA1	N/A	3	90	68	2.6
CR2 ²	UVGMA1	DUV/DMPAP	1.4	60	87	No data
CR3 ³	UVGMA4-70	DUV/DMPAP	5	21	>99	6.2
CR4 ³	UVGMA 4-70	UV-LED/BAPO	5	20	>99	4.0
CR5 ³	UVGMA 4-70	XL-1500 UVC/DMPAP	5	21	>99	4.7
CR6 ⁴	UVGMA7-50	DUV/DMPAP	4.3	56	88	2.0
CR7 ⁴	UVGMA7-50	UV-LED/BAPO	4.3	64	94	No data
CR8 ⁵	TCMS1	N/A	6	45	86	5.2
CR9 ⁶	TCMS1	N/A	6	45	97	0.8

Table 4.1 Suzuki-Miyaura reactions using capillary reactors.

(1) toluene/methanol, 250 μm ID fused-silica, 5-OHphen, (2) methanol, 100 μm ID fused-silica, 5-NH₂phen, (3) ethanol/methanol/water, 100 μm ID fused-silica, 5-NH₂phen, (4) ethanol/methanol/water, 276 μm ID COC, 5-NH₂phen, (5) DMF/water, 250 μm ID fused-silica, 5-NH₂phen, (6) DMF/water, 250 μm ID fused-silica, Me-im.

Microchip reactor system	PPM formulation	Initiator/source	Flow rate ($\mu\text{L h}^{-1}$)	Estimated contact time (min)	Stable yield	Turn-over frequency (h^{-1})
MR1 ¹	UVGMA1	DUV/DMPAP	3.7	60	87	No data
MR2 ²	UVGMA4-70	DUV/DMPAP	5	48	>99	2.7
MC3 ²	UVGMA4-70	UV-LED/BAPO	5	47	>99	2.1
MC4 ³	UVGMA7-50	DUV/DMPAP	1.6	73	93	2.0
MC5 ³	UVGMA7-50	UV-LED/BAPO	2.2	48	95	No data

Table 4.2 5-NH₂phen microchip reactor data.

(1) methanol, 150 $\mu\text{m} \times 150 \mu\text{m}$ borosilicate, 5-NH₂phen, (2) ethanol/methanol/water, 150 $\mu\text{m} \times 150 \mu\text{m}$ borosilicate, 5-NH₂phen, (3) ethanol/methanol/water, 610 $\mu\text{m} \times 100 \mu\text{m}$ COC, 5-NH₂phen.

Column Reactor System	Initiator/source	Column ID (mm)	Flow rate ($\mu\text{L h}^{-1}$)	Estimated contact time (min)	Stable yield	Turn-over frequency (h^{-1})
LR1 ¹	DUV/DMPAP	2	469.4	26	97	7.3
LR1 ¹	DUV/DMPAP	2	938.7	13	91	13.8
LR1 ¹	DUV/DMPAP	2	1877.4	7	83	25.1
LR2 ¹	UV-LED/BAPO	2	537.2	22	97	No data
LR2 ¹	UV-LED/BAPO	2	1074.4	11	93	No data
LR2 ¹	UV-LED/BAPO	2	2148.4	6	87	No data
LR3 ¹	DUV/DMPAP	4	2262.0	20	>99	9.1

Table 4.3 Large ID Column reactor data.
(1) UVGMA7-50.

A measure of continuous-flow catalytic performance is turn-over frequency (TOF), which is the moles of product produced per hour for every mole of catalyst present. The TOF obtained for reactions performed in the CR1 reactors was 2.6 h^{-1} , which is relatively low compared to reported continuous-flow reactors [9]. While TOF is a useful measure catalytic performance, this value alone does not determine the success of a reactor as it also depends on the amount of product produced per hour and does not take into account product yield. For example, consider a reactor that gives quantitative reaction yields at a particular flow rate. Running the reactor at a higher flow rate increases the production rate and consequently improves the TOF while possibly reducing the reaction yield. The TOF may very well be higher despite less than optimal reaction performance. As the most likely application of this reactor technology is integration with other microfluidic functionalities, complete conversion is preferred over high reactor performance. Additionally, the high catalyst content and relatively low reaction volume within the reactor significantly reduces the TOF, while potentially making a better reactor. High TOFs are therefore not a goal for this particular approach to microreactor technology.

The next reactor system investigated for continuous-flow reactions, CR2, was based on 5-NH₂phen immobilised on poly(GMA-*co*-EDMA) monolith prepared from the UVGMA1 formulation in 30 cm long 100 μm ID fused-silica capillary, using the DUV lamp with DMPAP and a 1 min exposure time. As discussed in **Chapter 2**, this PPM was intentionally under-polymerised to improve its permeability and to improve the photomasking in glass microchips. As a result, its density and porous properties could not be readily determined, and therefore the TOF cannot be calculated. Reactions were performed using the methanol reaction system at a flow rate chosen to give a 60 min residence time. In order to calculate the residence time, the void volume of the monolithic column was assumed to be the same as the

porogen volume of the formulation. However, since complete polymerisation was not achieved, this is unlikely to be the case. Additionally, as discussed in **Chapter 3**, the palladium loading for CR2 reactors was very low as the ligand attachment was performed in DMSO without the addition of triethylamine. Despite the low palladium loading, the CR2 reactors performed well, giving a higher yield for the coupling of iodobenzene with *p*-tolylboronic acid than the equivalent bulk PPM at 87%. The equivalent microchip reactor system, known here as MR1, was operated under similar conditions and gave the same reaction yield (**Table 4.2**). The borosilicate microchips required a considerably higher flow rate to maintain the 60 min contact time as their cross-sectional area is 2.2-fold larger than the 100 μm ID capillary.

Capillary reactors CR3-5 are equivalent in all aspects, except that different light source/initiator combinations were used to prepare the monolithic column. The monolithic columns were prepared using the UVGMA4-70 formulation to give higher permeability, as discussed in **Chapter 2**. These reactors, like CR2, are based on immobilised 5-NH₂phen, however the palladium loadings of these reactors are significantly higher due to addition of triethylamine during ligand attachment (**Chapter 3**). Additionally, the ethanol/methanol/water reaction system was first employed on these devices.

For reactors CR3-5, a reaction flow rate of 5 $\mu\text{L h}^{-1}$ was used so that the entire syringe volume (240 μL) of reaction mixture was pumped through in 48 h. This higher flow rate increased the sample volume, taken every 12 h, which made sample preparation for GC analysis simpler. The contact times shown in **Table 4.1** were calculated in retrospect as porosimetry data was not available during the reactor testing. MIP data was only available for the PPM used in reactors CR3-4 as bulk PPM could not be prepared for the PPM used in reactor CR5, as discussed in

Chapter 2. The porosity of the CR5 PPM was assumed to be the same as the PPM in CR3 for calculation of the reactor properties. The contact time for CR3-5 were calculated to be approximately 20 min for each light source/initiator combination. The catalyst availability for reactors CR3-5 was 47, 72, and 63 mol% palladium respectively, which are considerably higher than the CR1 reactor due to the higher catalyst loading. Reactions performed using reactors CR3-5 gave quantitative yields with TOFs between 4.0 and 6.2 h⁻¹. The improved yields, over those obtained using CR1 and CR2, can be attributed to the reaction system and does reflect improved reactor performance as indicated by only moderately increased TOFs. Unlike the previous reactors, the palladium content of the CR3-5 reactors were measured by direct analysis of duplicate capillary reactors by ICP-MS, as described in **Chapter 3**.

As discussed in **Chapter 2**, the CR5 reactor could not be prepared in borosilicate microchips due to incomplete polymerisation. The equivalent microchip reactors for CR3 and CR4 were MR2 and MR3 respectively. The microchip reactors were operated under exactly the same conditions to their capillary reactor counterparts, even using the same flow rate. Operating the microchip reactors at the same flow rate resulted in contact times that are more than twice as long due to their larger dimensions.

As discussed in **Chapter 3**, analysis of the microchip reactors for palladium content was not feasible. Therefore the palladium content of the microchips was estimated from the loading data obtained for the equivalent capillary reactors. Using the estimated volume of the monolithic column in the borosilicate microchips and the palladium density measured in the equivalent capillary reactors, the palladium content for the microchips was estimated. This was subsequently used to estimate the TOFs and mol% palladium for MR2-3. Under the reaction conditions used, the mol% palladium was 43 and 58 for MR2 and MR3 respectively, which are similar to the

values for CR3-5. Quantitative yields were also obtained for reactions performed using MR2-3, and the TOFs were approximately half of those obtained for CR3-4 due to the longer contact time. The borosilicate microchip reactors showed reasonable catalytic performance, demonstrating their potential for supported catalysis.

The polymer capillary reactors, CR6-7, were prepared in order to test the suitability of COC for continuous-flow catalysis before investigation of polymer microchips. The reactors were prepared as described in Chapters 2 and 3, using the UVGMA7-50 formulation in 276 μm ID COC capillary. Reactions were performed using the ethanol/methanol/water reaction system at a flow rate to give a residence time of 60 min, based on the porosity data available at the time. The residence times quoted for CR6-7 are calculated using subsequently collected MIP data for the equivalent bulk monolith. Palladium loading data was not obtained directly for any of the polymer-based reactors, as discussed in Chapter 3, neither was loading data obtained using the equivalent bulk PPM. The palladium loading for CR6 was estimated using the palladium density obtained for the equivalent reactor system prepared in a 2 mm ID column. Unfortunately no loading data was obtained to allow the palladium content of CR7 to be estimated. The catalyst availability for CR6 was estimated to be 45 mol% palladium, which is similar to that for the CR3-5 reactors.

Both CR6-7 reactors had lower performance than the CR3-5 reactors using the same reaction and ligand system, especially CR6 which only gave a reaction yield of 88%. Due to shortage of COC capillary, replicates of these reactors could not be prepared in order to confirm the reaction performance. Therefore it is unclear if the lower yield obtained using the CR6 reaction reflects that particular reactor's configuration or that something erroneous occurred during fabrication that resulted in an under-performing reactor. The TOF calculated for CR6 was considerably lower

than those obtained for the similar CR3-5 reactors due to the considerably longer contact time.

The equivalent COC microchip reactors, MC4-5, had very similar reaction performance, although MC4 had a higher reaction yield than its capillary equivalent, CR6. The flow rates used for MC4-5 were chosen to give a 60 min contact time based on MIP data available at the time, which was later re-measured using more reliable methods. Hence the contact times for MC4 and MC5 differ by 25 min. The flow rates in **Table 4.2** were calculated using the MIP data reported in **Chapter 2**. The performance obtained is acceptable and demonstrates catalysis at elevated temperatures using polymer devices.

The final capillary reactor systems investigated were CR8-9, which were poly(CMS-*co*-DVB) monolithic columns with reactor CR8 based on immobilised 5-NH₂phen and CR9 in immobilised Me-im. As with the CR1 reactors, the palladium loadings for these reactors were estimated using data obtained from the equivalent bulk PPM. Using these loadings, the mol% palladium for reactors CR8-9 was calculated to be 14 and 102 respectively. Reactor CR8 has a mol% palladium similar to CR1, as the loading values were similar. The mol% palladium for reactor CR9 was the highest of all the reactors investigated as the equivalent bulk PPM had the highest loading.

Both CR8-9 reactors were tested using the DMF/water reaction system at a flow rate chosen to give a 45 min contact time. Reactions were performed on these reactors over eight days, with sampling every 12 h. The reaction yield using reactors CR8-9 were 86% and 97% respectively, both of which were stable over the reaction period. These yields are almost identical to those obtained under batch conditions using bulk monolith. The higher TOF for CR8 reflects its relatively lower palladium

loading, while the TOF obtained for CR9 was the lowest for all the continuous-flow reactors investigated, again since the palladium loading was the highest.

Originally the 2 mm and 4 mm ID monolithic columns were prepared in order to test the limits of the light source/initiator systems, as discussed in **Chapter 2**. They were investigated to demonstrate that the microreactor technology described here could potentially be applied to laboratory or industrial scale synthesis. These column reactors were prepared using the UVGMA7-50 formulation with Me-im as the immobilised ligand, as described in **Chapters 2 and 3**. The column reactors were tested for continuous-flow reactions using the ethanol/methanol/water reaction system with initial flow rates chosen to give a 20 min residence time, the same as for reactors CR3-5. As with the CR3-5 reactors, the palladium loading of the LR1 reactor was obtained by direct analysis of a replicate column reactor. However loading data was not obtained for the LR2 reactor and hence the mol% palladium or TOF this system cannot be estimated. It is anticipated that the performance of LR2 should be similar to LR1 as the only difference between the reactors is the preparation of the PPM, as observed with the CR3 and CR4 capillary reactors. Since the monolithic column used in LR1 is prepared in a similar fashion to the one in LR3, the palladium density obtained for LR1 was used to estimate the palladium loading for LR3. From this data, the mol% palladium for LR1 and LR3 were estimated to be 36 and 20 respectively.

Due to the size of the columns, using a 20 min residence time produces sufficient material for analysis every 5 min, therefore investigating the effect of flow rate on reaction yield is considerably easier at this scale. Additionally, at this scale, reactor performance is very important. Hence the reaction performance of the 2 mm ID reactors, LR1-2, were evaluated at several different flow rates to determine the effect on yield and TOF. Initially the reactions performed on the 2 mm ID column

reactors, LR1-2, used a 20 min residence time. Once a stable reaction yield was obtained at this flow rate, it was increased to give 10 min residence time and later to 5 min. When altering the flow rate, the reaction was sampled until the yield stabilised and then the flow rate increased. As can be seen in **Table 4.3**, the reaction yield decreased with increasing flow rate while the TOF proportionally increased. Complete conversion of iodobenzene was not achieved in these reactors and the decreasing trend of the yield with increasing flow rate may suggest that a slower flow rate is required for quantitative yields.

In order to demonstrate the use of a column reactor for laboratory scale synthesis, the 4 mm ID reactor, LR3, was tested under a practical scenario for the gram-scale preparation of 4'-methylbiphenyl, including off-line workup. As with the LR1-2 reactors, the flow rate for the reaction on LR3 was chosen to give an approximate 20 min contact time. The reaction mixture (50 mL) was pumped through the reactor, with 50 μ L samples taken at 5 h and 22 h. As the reaction was performed with the aim of working up the product an internal standard was not included. GC analysis of the reaction samples showed only trace amounts of iodobenzene. After workup and isolation of the product, it was analysed by GC-MS to verify its purity. It was found to be >99% pure, containing only a trace amount of the homocoupled boronic acid. The reaction yield of >99% was calculated from the mass of the isolated product, 4'-methylbiphenyl, and the starting material, iodobenzene. The TOF for this reaction was similar to the TOF obtained for the LR1 reactor with the same contact time.

During the reactions, the monolithic columns were observed to change colour from the yellow-orange of the immobilised pre-catalyst, as shown in **Figure 4.4(a)**, to a dark yellow, shown in **Figure 4.4(b)**.



Figure 4.4 (a) LR3 reactor before reaction, (b) during the reaction.

Colour changes were observed for the other continuous-flow reactors, but most of these devices have sub-millimetre dimensions and require special photography conditions in order to obtain images. Unfortunately this meant that only pictures of used microreactors could be obtained. Typical images of borosilicate microchip reactors, MR1-3, before and after use for catalysis are shown in **Figure 4.5** and similar images of a COC microchip reactor, MR4-5, are shown in **Figure 4.6**. Acquiring photographs of these devices was quite challenging as they are fabricated from optically transparent materials. The monolithic columns within the used microchip reactors, shown in **Figures 4.5** and **4.6**, appear to be considerably darker than the 4 mm column reactor in **Figure 4.4(b)**. This difference in colour may be due to the different ligand system employed in the reactors. The reactors in **Figures 4.5** and **4.6** used 5-NH₂phen while the reactor in **Figure 4.4(b)** used Me-im. The observed colour change may indicate the reduction of the pre-catalyst to form the active catalyst, however this is merely speculative.



Figure 4.5 (a) Borosilicate microchip reactor before reaction, (b) and after.

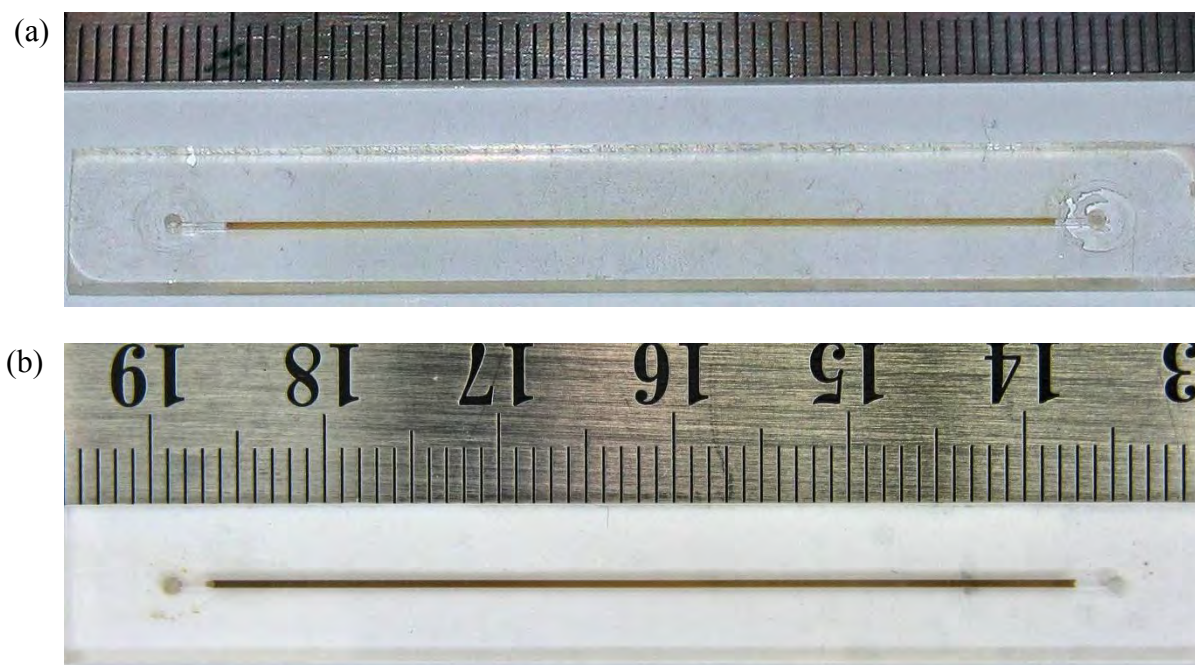


Figure 4.6 (a) COC microchip reactor before reaction, (b) and after.

4.4 Reactor catalysis validation, palladium leaching, and homogeneous catalysis

In order to validate that catalysis occurs due to the immobilised catalyst within the CR1 reactors, a solution of 1,10-phen was passed through an unmodified monolithic capillary column, prepared using the TGMA1 formulation, followed by a solution of palladium. A reaction was performed on the capillary column using the toluene/methanol system and a yield of 4% was obtained. Using this approach, it was unclear if the observed catalysis was due to the catalyst being weakly retained on the PPM or by trace amounts of palladium in solution.

For validation of the CR2-5 reactors, two reactors identical to CR4 were prepared. One was not treated with ligand and only palladium during fabrication, and the other was treated with ligand but not palladium. Reactions were performed on these reactors using the same conditions as used for CR4 and no product was detected for either reactor. This suggests that catalysis only occurs when the complete catalyst is assembled and that palladium is not retained on the PPM itself. Similar validations were deemed not necessary on the other reactors due to these conclusive results.

Leaching of the metal from the solid support is a major concern for all metal-catalyst immobilised continuous-flow reactor systems as it continually reduces the catalyst loading and the life-time of the reactor, and also leads to metal contamination in the product [2, 7, 24]. Palladium leaching was determined by performing a reaction on a reactor, collecting the effluent into a single vial, and then analysing both the used reactor and reaction effluent for palladium content via ICP-MS. As this method requires destructive analysis of the reactor, only capillary reactors were used to investigate leaching. The leached palladium is expressed as the

percentage of the palladium in the reaction effluent versus the total palladium (based on reactor plus effluent palladium content). The leaching experiment was performed using a CR4 reactor with new syringes and fittings in order to prevent cross-contamination. The palladium content of the reaction effluent was found to be similar to background levels and was less than 0.01%, which is considerably lower than other reported reactors [7].

For comparison with its supported catalytic performance, the palladium 5-NH₂phen complex was prepared and used as a homogeneous catalysis under batch conditions using the ethanol/methanol/water reaction system. The complex (1.9 mg) was used with 2.0 mL of reaction mixture, which equates to 2.6 mol% palladium. This mol% palladium is only slightly higher than the equivalent bulk monolith supported catalytic system. A relatively poor yield of 63% was obtained for this reaction. Therefore the PPM supported catalyst performs significantly better than the homogeneous catalyst under the conditions investigated.

4.5 Alternative reactor system

Commercially available ligands were investigated for fabrication of microreactors during this project as they were intended to be proof-of-concept devices used to demonstrate the potential of the technology. These ligands are relatively simple and were not expected to yield high performance palladium catalysis. In realistic applications of this technology to microscale synthesis, specifically designed catalysts are desirable in order to achieve high catalyst performance and to facilitate activation of difficult substrates, such as electron withdrawing aryl bromides and chlorides [23]. Another project within our research group, undertaken by Dr Roderick Jones, explored applications of the technology using a heteroleptic *N,S*-bidendate ligand, based on a 2-organothiomethylpyridine-

N,S donor for palladium catalysis [25]. As part of the investigation of this ligand system, a phenol derivative, shown in **Figure 4.7**, was immobilised on Merrifield and Wang resin as well as on poly(CMS-*co*-DVB) monolith in bulk and in monolithic capillary column.

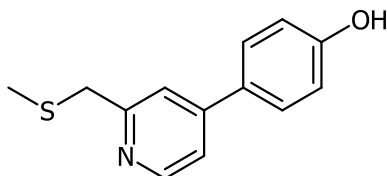
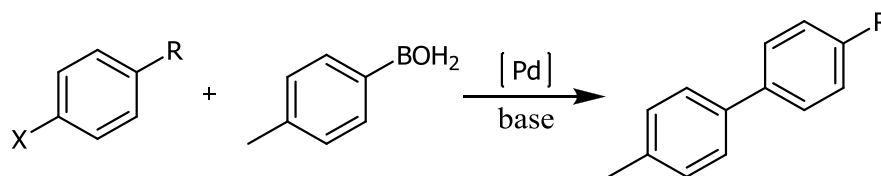


Figure 4.7 4-(4-hydroxyphenyl)-2-methylthiomethylpyridine

The palladium loadings obtained for each of the supports were 1.19 wt% for bulk PPM, 0.75 wt% for Merrifield resin, and 0.32 wt% for Wang resin. The palladium content of the capillary reactors was estimated using the bulk PPM palladium loading, as previously discussed. Suzuki-Miyaura reactions were performed in batch mode using all three polymer supports and flow-through mode using monolithic capillary reactors with several different aryl halides as shown in **Scheme 4.1**, including iodobenzene, bromobenzene, and *p*-chloroacetophenone with the latter in batch only. Reactions were performed using the DMF/water system described in **Section 4.3**. The reaction yields obtained with their respective TONs for the Suzuki-Miyaura reactions investigated are shown in **Table 4.4**. For comparison, a homogeneous reaction was also performed with bromobenzene using the same mol% palladium as present in the batch reactions with bulk PPM, which gave a yield of 64% with a TON of 3434.

Support material	Palladium loading (wt%)	Iodobenzene reaction yield (%) / TON	Bromobenzene reaction yield (%) / TON	<i>p</i> -Chloroacetophenone reaction yield (%) / TON
Bulk PMM	1.19	>99/5365	>99/5365	12/644
Wang resin	0.32	>99/19,950	85/16,958	<1/<199
Merrifield resin	0.75	>99/8512	>99/8512	8/681

Table 4.4 Palladium loadings, reaction yields and performance for the polymer supports investigated.



Scheme 4.2 Suzuki-Miyaura reactions performed with 2-methylthiomethylpyridine ligand. X = I, Br, Cl and R = H, COMe.

In terms of yield, the bulk PPM was found to outperform both of the resins, however in terms of catalytic performance the Wang resin was superior to the other two supports. This greater performance, indicated by the significantly higher TON, results from the lower palladium loading of the Wang resin as reducing the catalyst while maintaining the same yield increases the TON.

The Suzuki-Miyaura flow-through reactions were performed using similar conditions previously discussed for CR8-9 reactors, with the only differences being that the base content was increased to 2 mol eq and the reactor length was decreased to 10 cm. This shorter reactor length also results in a shorter residence time, which was estimated to be 35 min. Under these conditions, the estimated mol% palladium was 61, which is similar to the CR3-5 reactors. The reactions were performed for 24 h and a stable yield of 96% was obtained using iodobenzene with a TOF of 2.7 h^{-1} , which is similar to the capillary reactors CR1 and CR3-5. Using bromobenzene a yield of 65% was obtained with a TOF of 1.9 h^{-1} . Palladium leaching experiments for these reactors were performed using the same method as used for the CR4 reactor described previously. Using this method, the palladium leaching was found to be 0.05%. Reactor validation was performed using the same method as previously discussed for the CR2-5 reactors, and no product was detected on either incomplete reactor. Clearly these results show that is reactor technology is also applicable to novel, synthesised ligand systems.

4.6 Conclusions

Conditions were developed to allow the Suzuki-Miyaura coupling of iodobenzene and *p*-tolylboronic acid to be performed in high yield under continuous flow within reactors featuring PPM immobilised palladium complexes in several different formats, using both glass and polymer substrates. A variety of different solvent and base combinations were investigated, where ethanol/methanol/water with TBAH was found to be the most suitable combination for poly(GMA-*co*-EDMA) PPM reactors and DMF/water with triethylamine was best suited to poly(CMS-*co*-DVB) reactors. This was also the first example of a supported palladium polymer microreactor for non-room temperature Suzuki-Miyaura catalysis.

These reactors showed negligible leaching of the immobilised palladium. While direct evidence of the formation of PPM immobilised palladium complexes was not obtained, catalysis did not occur in the absence of palladium within a capillary containing just PPM or PPM with immobilised ligand. Suggesting the formation of a complex between the introduced palladium and the immobilised ligand during reactor fabrication.

Despite being outside the scope of this project, up-scaling of the flow reactors to millimetre dimensions was shown to be viable, allowing laboratory scale production.

Additionally the immobilised 5-NH₂phen palladium complex was found to outperform its homogenous analogue.

4.7 Experimental

4.7.1 Reaction mixture preparation

Stock reaction mixtures were prepared using iodobenzene (1 mmol, 110 μL), *p*-tolylboronic acid (1.5 mmol, 201.3 mg), tetrabutylammonium hydroxide (1.5 mmol, 1.5 mL 1M in methanol), ethanol (8.5 mL), water (0.5 mL), and diphenyl ether as an internal standard (1 mmol, 160 μL). The mixture was placed in an ultrasonic bath for approximately 5 min, filtered through a 0.2 μm syringe filter, and then used immediately.

4.7.2 Batch reactions using bulk monolith catalyst

Catalyst immobilised bulk monolith (50 mg) was added to a reaction vial with stock reaction mixture (2 mL) and heated in an 80 $^{\circ}\text{C}$ oil bath with constant stirring. After 60 min the vial was quickly transferred into an ice bath to quench the reaction. Once cool, the reaction mixture was filtered through a 0.2 μm syringe filter and analysed by GC-FID.

4.7.3 Flow-through reactions in 100 μm ID capillary reactors

The capillary reactor was flushed with a mixture of ethanol/methanol/water (17:2:1) for 8 h at 30 $\mu\text{L h}^{-1}$ in an 80 $^{\circ}\text{C}$ column heater. The capillary reactor was then flushed with stock reaction mixture at 5 $\mu\text{L h}^{-1}$ at the same temperature. The effluent was collected into a vial, which was replaced every 12 h. The reaction effluent was analysed by GC-FID.

4.7.4 Flow-through reactions in 250 μm ID 5-OHphen based capillary reactors

The capillary reactor was flushed with a mixture of toluene/methanol (9:1) for 1 h at 120 $\mu\text{L h}^{-1}$ in an 80 $^{\circ}\text{C}$ column heater. The capillary reactor was then

flushed with stock reaction mixture at $3 \mu\text{L h}^{-1}$ at the same temperature. The effluent was collected into a vial over 18 h. The reaction effluent was analysed by GC-FID.

4.7.5 Flow-through reactions in 250 μm ID poly(CMS-co-DVB) capillary reactors

The capillary reactor was flushed with a mixture of DMF/water (3:1) with triethylamine (2 mmol) for 1 h at $120 \mu\text{L h}^{-1}$ in an 80°C column heater. The capillary reactor was then flushed with stock reaction mixture at $6 \mu\text{L h}^{-1}$ at the same temperature. The effluent was collected into a vial, which was replaced every 12 h. The reaction effluent was analysed by GC-FID.

4.7.6 Flow-through reactions in borosilicate microchip reactors

The conditions used are identical to those in **Section 4.7.3**, except scaled up for the larger reactor dimensions. The solvent flush was performed at $60 \mu\text{L h}^{-1}$ and the reaction performed at $5 \mu\text{L h}^{-1}$.

4.7.7 Flow-through reactions in COC capillary reactors

The conditions used are identical to those in **Section 4.7.3**, except scaled to the reactor dimensions. The solvent flush was performed at $60 \mu\text{L h}^{-1}$ and the reaction performed at $4.3 \mu\text{L h}^{-1}$.

4.7.8 Flow-through reactions in COC microchip reactors

The conditions used are identical to those in **Section 4.7.3**, except scaled to the reactor dimensions. The solvent flush was performed at $60 \mu\text{L h}^{-1}$ and the reaction performed at $2.2 \mu\text{L h}^{-1}$.

4.7.9 Flow-through reactions in 2 mm ID column reactors

The conditions used are identical to those in **Section 4.7.3**, except scaled to the reactor dimensions. Also the stock reaction mixture was scaled 5-fold larger to

accommodate the larger volume. The solvent flush was performed at 0.25 mL min^{-1} . The reaction was started using a flow rate of $537.2 \text{ } \mu\text{L h}^{-1}$, with the collection vial replaced at 1 h, 2 h, and 4 h. After 4 h, the flow rate was increased to $1074.4 \text{ } \mu\text{L h}^{-1}$, with the collection vial replaced at 1 h and 1.5 h. After 1.5 h, the flow rate was further increased to $2148.8 \text{ } \mu\text{L h}^{-1}$, with the collection vial replaced after 30 min. All the samples collected were analysed by GC-FID.

4.7.10 Flow-through reactions in 4 mm ID column reactors

The conditions used are identical to those in **Section 4.7.3**, except scaled to the reactor dimensions. Also the stock reaction mixture was scaled 5-fold. The solvent flush was performed at 0.5 mL min^{-1} . The reaction mixture (50 mL) was flushed through the reactor at 2.262 mL h^{-1} , with the effluent collected in a conical flask. A $50 \text{ } \mu\text{L}$ sample was taken from the reaction at 5 h and 22 h. The reaction effluent was worked up extracting it into DCM ($3 \times 20 \text{ mL}$) and then drying with MgSO_4 . The DCM was evaporated off, added water (90 mL) and extracted using diethyl ether ($3 \times 30 \text{ mL}$) and then dried with MgSO_4 . This was filtered and then the diethyl ether was evaporated off. The product was dried and weighed, then analysed by GC-MS.

4.7.11 GC-FID reaction effluent analysis

The collected reaction effluent was diluted with DCM (1 mL) and analysed using a Shimadzu GC-2014. The GC was operated using helium carrier gas column, with the injector at $275 \text{ }^\circ\text{C}$ with a 1 to 20 split ratio, and the detector at $300 \text{ }^\circ\text{C}$. The temperature program started with at $50 \text{ }^\circ\text{C}$ with a hold time of 2 min, then the temperature was ramped up to $110 \text{ }^\circ\text{C}$ at $30 \text{ }^\circ\text{C min}^{-1}$, then ramped up to $280 \text{ }^\circ\text{C}$ at $20 \text{ }^\circ\text{C min}^{-1}$ where it was held for 1 min.

4.7.12 GC-MS reaction effluent analysis

GC-MS analysis was performed using a Varian Star 3400 CX gas chromatograph coupled with a Varian Saturn 4D mass spectrometer. The GC was operated using helium carrier gas column, with the injector at 280 °C with a 1 to 40 split ratio. The temperature program started with at 50 °C with a hold time of 2 min, then the temperature was ramped up to 280 °C at 10 °C min⁻¹.

4.7.13 GC-FID/MS calibration

The amount of iodobenzene and 4'-methylbiphenyl relative to diphenyl ether was calibrated by preparing five mixtures the same as described in **Section 4.7.1**, without *p*-tolylboronic acid or iodobenzene. To the first mixture, iodobenzene (110 µL) and 4'-methylbiphenyl (168.2 mg) were added. To each successive mixture, the amounts of iodobenzene and 4'-methylbiphenyl were reduced by 20 mol%, giving the calibration series. 50 µL samples were taken from each of the mixtures and analysed according to the procedure in **Sections 4.7.11** and **4.7.12**.

4.7.14 Determination of reactor palladium leaching

A 100 µm ID 5-NH₂phen based capillary reactor was preparing using the UVGMA4-70 formulation with the UV-LED/BAPO combination. A reaction was performed on this reactor according to the method described in **Section 4.7.3**, with all the reaction effluent collected into a single vial. After passing through 240 µL of reaction mixture a 50 µL sample was taken from collected effluent and analysed. The solvent was evaporated off the remaining reaction effluent by passing nitrogen over the surface and then drying under vacuum in a desiccator. Air was blown through the capillary reactor using a compressed 60 mL syringe overnight at room temperature. The exterior of the capillary was cleaned with acetone, and then it was cut into ~4 cm lengths and weighed. The capillary was ground to a fine powder with a mortar and

pestle, then transferred into a pre-weighed vial and the ground mass recorded. The palladium content of the ground capillary and dried reaction effluent were determined by ICP-MS.

4.8 References

1. Maegawa, T., Y. Kitamura, S. Sako, T. Udzu, A. Sakurai, A. Tanaka, Y. Kobayashi, K. Endo, U. Bora, T. Kurita, A. Kozaki, Y. Monguchi, and H. Sajiki, Heterogeneous Pd/C-catalyzed ligand-free, room-temperature Suzuki-Miyaura coupling reactions in aqueous media. *Chemistry-a European Journal*, 2007. **13**(20), 5937-5943.
2. Phan, N.T.S., M. Van Der Sluys, and C.W. Jones, On the nature of the active species in palladium catalyzed Mizoroki-Heck and Suzuki-Miyaura couplings - homogeneous or heterogeneous catalysis, a critical review. *Advanced Synthesis & Catalysis*, 2006. **348**(6), 609-679.
3. Shore, G., S. Morin, and M.G. Organ, Catalysis in capillaries by Pd thin films using microwave-assisted continuous-flow organic synthesis (MACOS). *Angewandte Chemie, International Edition*, 2006. **45**(17), 2761-2766.
4. Phan, N.T.S., J. Khan, and P. Styring, Polymer-supported palladium catalysed Suzuki-Miyaura reactions in batch and a mini-continuous flow reactor system. *Tetrahedron*, 2005. **61**(51), 12065-12073.
5. Comer, E. and M.G. Organ, A microcapillary system for simultaneous, parallel microwave-assisted synthesis. *Chemistry - A European Journal*, 2005. **11**(24), 7223-7227.
6. Solodenko, W., H. Wen, S. Leue, F. Stuhlmann, G. Sourkouni-Argirusi, G. Jas, H. Schönfeld, U. Kunz, and A. Kirschning, Development of a continuous-flow system for catalysis with palladium(0) particles. *European Journal of Organic Chemistry*, 2004(17), 3601-3610.
7. Mennecke, K. and A. Kirschning, Polyionic polymers - heterogeneous media for metal nanoparticles as catalyst in Suzuki-Miyaura and Heck-Mizoroki reactions under flow conditions. *Beilstein Journal of Organic Chemistry*, 2009. **5**(21), 6.
8. Lee, C.K.Y., A.B. Holmes, S.V. Ley, I.F. McConvey, B. Al-Duri, G.A. Leeke, R.C.D. Santos, and J.P.K. Seville, Efficient batch and continuous flow Suzuki cross-coupling reactions under mild conditions, catalysed by polyurea-encapsulated palladium (II) acetate and tetra-n-butylammonium salts. *Chemical Communications*, 2005(16), 2175-2177.
9. Uozumi, Y., Y.M.A. Yamada, T. Beppu, N. Fukuyama, M. Ueno, and T. Kitamori, Instantaneous carbon-carbon bond formation using a microchannel reactor with a catalytic membrane. *Journal of the American Chemical Society*, 2006. **128**(50), 15994-15995.
10. Basheer, C., F.S. Jahir Hussain, H.K. Lee, and S. Valiyaveetil, Design of a capillary-microreactor for efficient Suzuki coupling reactions. *Tetrahedron Letters*, 2004. **45**(39), 7297-7300.
11. Greenway, G.M., S.J. Haswell, D.O. Morgan, V. Skelton, and P. Styring, The use of a novel microreactor for high throughput continuous flow organic synthesis. *Sensors and Actuators B-Chemical*, 2000. **63**(3), 153-158.
12. He, P., S.J. Haswell, and P.D.I. Fletcher, Microwave heating of heterogeneously catalysed Suzuki reactions in a micro reactor. *Lab on a Chip*, 2004. **4**(1), 38-41.
13. He, P., S.J. Haswell, and P.D.I. Fletcher, Microwave-assisted Suzuki reactions in a continuous flow capillary reactor. *Applied Catalysis a-General*, 2004. **274**(1-2), 111-114.
14. Papp, A., D. Toth, and A. Molnar, Suzuki-Miyaura coupling on heterogeneous palladium catalysts. *Reaction Kinetics and Catalysis Letters*, 2006. **87**(2), 335-342.

15. Steel, P.G. and C.W.T. Teasdale, Polymer supported palladium N-heterocyclic carbene complexes: long lived recyclable catalysts for cross coupling reactions. *Tetrahedron Letters*, 2004. **45**(49), 8977-8980.
16. Sommer, W.J. and M. Weck, Poly(norbornene)-supported N-heterocyclic carbenes as ligands in catalysis. *Advanced Synthesis & Catalysis*, 2006. **348**(15), 2101-2113.
17. Kim, J.H., B.H. Jun, J.W. Byun, and Y.S. Lee, N-heterocyclic carbene-palladium complex on polystyrene resin surface as polymer-supported catalyst and its application in Suzuki cross-coupling reaction. *Tetrahedron Letters*, 2004. **45**(30), 5827-5831.
18. Byun, J.W. and Y.S. Lee, Preparation of polymer-supported palladium/N-heterocyclic carbene complex for Suzuki cross-coupling reactions. *Tetrahedron Letters*, 2004. **45**(9), 1837-1840.
19. Lee, D.H., J.H. Kim, B.H. Jun, H. Kang, J. Park, and Y.S. Lee, Macroporous polystyrene-supported palladium catalyst containing a bulky N-heterocyclic carbene ligand for Suzuki reaction of aryl chlorides. *Organic Letters*, 2008. **10**(8), 1609-1612.
20. Schönfelder, D., O. Nuyken, and R. Weberskirch, Heck and Suzuki coupling reactions in water using poly(2-oxazoline)s functionalized with palladium carbene complexes as soluble, amphiphilic polymer supports. *Journal of Organometallic Chemistry*, 2005. **690**(21-22), 4648-4655.
21. Mennecke, K. and A. Kirschning, Immobilization of NHC-Bearing Palladium Catalysts on Polyvinylpyridine; Applications in Suzuki-Miyaura and Hartwig-Buchwald Reactions under Batch and Continuous-Flow Conditions. *Synthesis-Stuttgart*, 2008(20), 3267-3272.
22. Kim, J.W., J.H. Kim, D.H. Lee, and Y.S. Lee, Amphiphilic polymer supported N-heterocyclic carbene palladium complex for Suzuki cross-coupling reaction in water. *Tetrahedron Letters*, 2006. **47**(27), 4745-4748.
23. Alonso, F., I.P. Beletskaya, and M. Yus, Non-conventional methodologies for transition-metal catalysed carbon-carbon coupling: a critical overview. Part 2: The Suzuki reaction. *Tetrahedron*, 2008. **64**(14), 3047-3101.
24. Leadbeater, N.E. and M. Marco, Preparation of polymer-supported ligands and metal complexes for use in catalysis. *Chemical Reviews*, 2002. **102**(10), 3217-3273.
25. Jones, R.C., A.J. Canty, J.A. Deverell, M.G. Gardiner, R.M. Guijt, T. Rodemann, J.A. Smith, and V.A. Tolhurst, Supported palladium catalysis using a heteroleptic 2-methylthiomethylpyridine-N,S-donor motif for Mizoroki-Heck and Suzuki-Miyaura coupling, including continuous organic monolith in capillary microscale flow-through mode. *Tetrahedron*, 2009. **65**(36), 7474-7481.

Chapter 5 Engineering

5.1 Flow-through devices and interfaces

When working with miniaturised devices, interfacing between the microscopic and macroscopic dimensions is of vital importance. In this section the interfacing of these devices will be discussed. Throughout this work a similar setup was used, which consisted of a syringe pump and syringe for fluid delivery, a column heater housing the reactor, and a vial for collecting the reaction effluent. Depending on the dimensions of the microreactor, fused silica capillary or Teflon® tubing was used for fluid transport. The reactor setup is schematically represented in **Figure 5.1**.

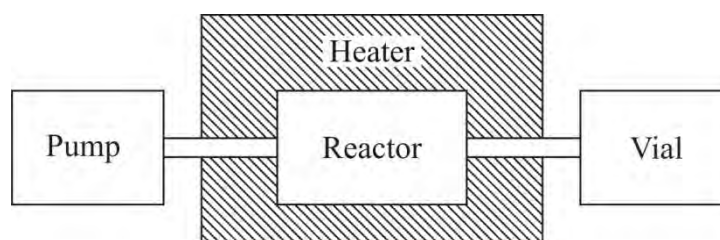


Figure 5.1 Schematic overview of the experimental setup used for microreactors.

As illustrated, the pump and collection vial are outside the heater to restrict the reaction to within the microreactor.

For interfacing the microreactors, commercially available capillary/tubing and fittings were used. All fittings and the ID and length of the tubing/capillary used for fluid transport contribute to the ‘dead volume’ of the system. The dead volume contributes additional time to that spent within the reactor system, and should therefore be minimised as discussed below.

5.1.1 Capillary microreactors

Fused-silica capillary was obtained from Polymicro Technologies LLC and featured ID's of 100 μm ($\pm 4 \mu\text{m}$) and 250 μm ($\pm 6 \mu\text{m}$), both with OD's of 360 μm ($\pm 10 \mu\text{m}$). This capillary has a polymer coating (polyimide or Teflon® AF) on the

outer wall in order to improve its structural integrity. Polyimide coated capillary is utilised in most applications as it is highly flexible and heat resistant up to 350 °C. For fluid transport and preparation of thermally initiated monolithic columns, capillary with a 20 µm thick polyimide coating was used. Teflon® AF coated capillary is only utilised in applications where UV-VIS transparency is required as this capillary is more brittle compared to the polyimide coated capillary and frequently breaks when put under strain. The Teflon® AF coated capillary is heat resistant up to 160 °C. For preparation of UV initiated monolithic column, capillary with a 15 µm thick Teflon® AF coating was used. The polyimide coated capillary was used in 100 µm and 250 µm ID, while the Teflon® AF coated capillary was only used in 100 µm (the largest ID available). The Teflon® AF coated capillary was significantly more brittle compared to the polyimide coated capillary, and at times broke when put under strain.

Cyclic olefin co-polymer (COC) capillary was custom fabricated by Paradigm Optics Inc. using the 6013 S04 grade which, as discussed in **Chapter 2**, was specifically chosen for its optical and thermal properties. Capillary was produced in several different ID and OD's, each with an ID to OD ratio of 0.4 which is an artefact of the fabrication process. The capillary used for reactor fabrication was 314 µm ID 785 µm OD which was chosen in order to reduce the back-pressure observed in the 100 µm ID fused-silica capillary. Since the COC capillary was not coated it was found to be very fragile and extreme care had to be taken not to break it during interfacing.

As capillary columns are a well established technology in gas and liquid chromatography, there is a large variety of commercially available fittings for interfacing sub-millimetre OD capillary under a broad range of conditions, including high temperatures and pressures. Fittings are also available for interfacing sub-

millimetre OD tubing/capillary with the Luer-lok™ connection of the Hamilton Gastight® syringes used for fluid delivery. Interfacing of the fused-silica and COC capillary employed Upchurch® PEEK unions, fittings and sleeves. A diagram of this interface is shown in **Figure 5.2**.

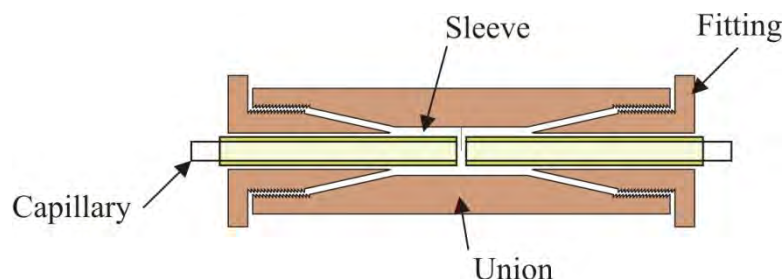


Figure 5.2 Capillary union interface.

Fittings specifically designed for 360 µm OD capillary were found to be considerably more expensive and less robust than the use of a combination of Upchurch® PEEK unions, fittings and sleeves, and therefore these sleeve-based interfaces were used in this work. As illustrated in **Figure 5.2**, a narrow sleeve is placed around the capillary enabling the formation of a liquid-tight seal when the tip is compressed by tightening the union.

In order to keep the materials and the internal diameters of the fluid transport tubing consistent with the capillary reactor properties, 0.25 mm ID 1.6 mm OD Teflon® FEP tubing was used for fluid transport for the COC capillary reactors and 100 µm ID 360 µm OD fused-silica capillary was used for the fused-silica capillary reactors. As such, different sleeving, fittings, unions, and fluid transport tubing were required for the fused-silica and COC capillary due to the difference in their ODs.

The choice of fittings and fluid transport tubing diameter contributes significantly to the ‘dead volume’ of the reactor systems. In this case this includes the syringe adapter fittings, the fluid transport tubing, and the capillary reactor interface fittings. In order to minimise the dead volume for the fused-silica reactors,

100 μm ID capillary was used for fluid transport and zero dead volume unions were used for the reactor interface. The smallest ID available for the Teflon® FEP tubing was 254 μm ID, and the unions used for the COC capillary interface have internal dead volume, resulting in a greater lag time for the COC capillary reactors.

5.1.2 Microchip reactors

Glass microchips were purchased from Micronit Microfluidics BV and were fabricated from two plates of an undisclosed grade of borosilicate, the top plate containing the microchannel and reservoirs being 1.1 mm thick and the sealing bottom plate 0.7 mm. These chips were designed to be simple mixing reactors, where two reagent streams enter at the top of the Y and mix along the channel length. The layout of the microchip is shown in **Figure 5.3** and features an approximately 33 cm long microchannel which is 150 μm wide and deep giving it an internal volume of 6 μL . The microchannel was etched by powder-blasting which gives it a larger depth to width ratio than is achievable by wet etching [1].

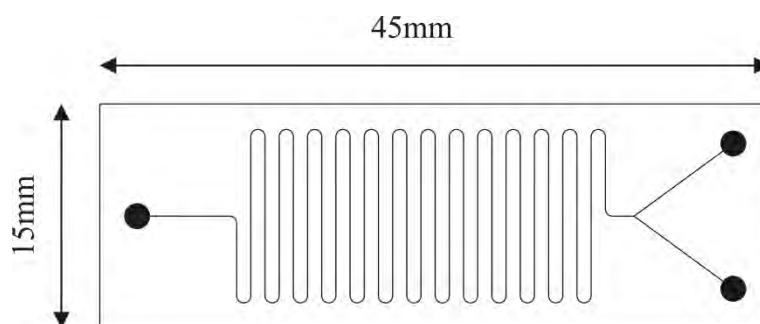


Figure 5.3 Schematic of a borosilicate microchip showing the reservoirs and microchannel.

Cross-sectional images of the microchip are shown in **Chapter 2** on pages 91 and 92. As discussed in **Chapters 1** and **2**, direct fabrication techniques, such as powder blasting, have poor reproducibility and hence the exact dimensions of the microchannel cross-section varies between individual devices.

The COC microchips were custom fabricated by the Microfluidic Chip Shop GmbH in the 6013 S04 grade. Details of the device fabrication were not disclosed by the manufacturer, but hot embossing was probably used. These microchips feature a trapezoidal microchannel cross section with a top width of 610 μm , a bottom width of 470 μm and a depth of 100 μm . The channel length is 54 mm, giving the microchips an internal volume of 3 μL . These dimensions were specifically chosen to improve flow-through by reducing back-pressure. A diagram of the microchip layout is shown in **Figure 5.4**. A cross-sectional image of a COC microchip is shown in **Chapter 2** on page 120. As discussed in **Chapter 2**, these microchips were machined thinner in order to allow photografting.

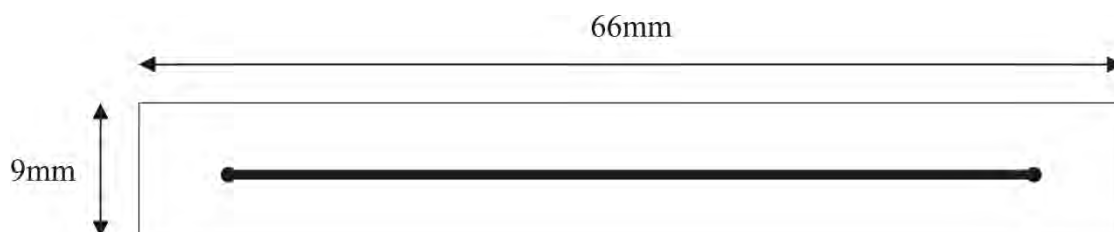


Figure 5.4 Schematic of a COC microchip showing the reservoirs and microchannel.

While a wide range of commercial products are available for interfacing capillary columns, only limited products are available for microfluidic chips as they are still a relatively recent technology and no industry-wide standards have been set. The dimensions and port configurations of commercially available microchips vary significantly between manufacturers. Generally microchips are interfaced by means of a chip holder, which is in essence just an device containing ports that hold the microchip in position allowing fittings to interface with the microchips wells. These devices usually completely enclose the microchip. Alternatively, polymer microchips may contain directly integrating ports which eliminate the need for a chip holder [2]. Other methods for directly interfacing microchips include glueing on pipette tips or by mounting on Upchurch® Nanoports™. These later approaches have limited

solvent and temperature compatibility, and also require a significant amount of space around the reservoirs for the adhesive.

Micronit produces a chip holder specifically designed for their range of microchips, consisting of two stainless steel plates held together with bolts. There is a hole through the centre of both plates which allows viewing of the microchannel and a cavity between the two plates which houses the microchip. Access to the microchip wells is via ports connecting the cavity to the top plate of the chip holder, as shown in **Figure 5.5**.



Figure 5.5 Micronit chip holder. Also visible is a glass microchip (bottom right) and fittings (bottom left). Image supplied by Micronit Microfluidics BV.

This chip holder was found to be unsuitable for the microreactors investigated here as the fittings supplied were only suitable for low-pressure applications and not compatible with the chemicals and solvents of interest. When using alternative fittings, the force placed on the microchip required to create a seal often caused the chips to break. As the Micronit chip holder was designed specifically for their microchips, it was not compatible with the Microfluidic ChipShop COC chips.

Hence a custom chip holder was designed to meet the following requirements:

- Compatible with a range of different fittings.
- Small enough to fit within a column heater.
- Adjustable port locations allowing different microchips to be interfaced.
- Compatible with temperatures up to 100 °C.
- Able to hold several chips at once for parallel processing.

The initial chip holder design consisted of a base plate and two port holders which could be moved along the length of the plate, 10 cm long and 8.9 cm wide. Two different and interchangeable port holders were designed, the first featured six fixed ports and was intended for use with multiple straight-channel microchips, like the COC microchips. The second port holder featured adjustable port locations that were designed for use with multi-reservoir microchips, such as the glass microchips. A diagram of this chip holder is shown in **Figure 5.7**. This chip holder was fabricated by Peter Dove of the Central Science Laboratory (CSL) from high tensile strength aluminium. The interface between the microchip reservoirs and the tubing used Upchurch® Super Flangeless™ ferrules, illustrated in **Figure 5.6**. The ferrule sits over the microchip reservoir and compresses around the tubing by a stainless steel o-ring when pressure is applied by tightening the fitting. This pressure also forces the ferrule to seal over the top of the well.

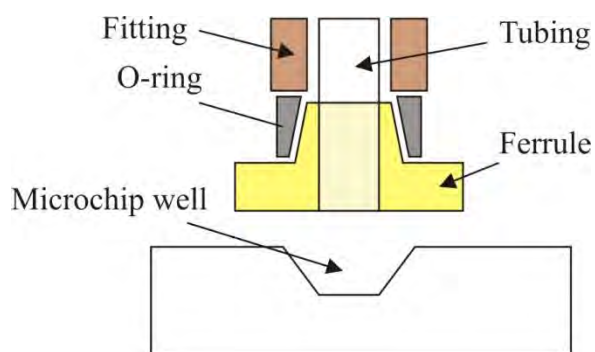


Figure 5.6 Ferrule interface with microchip wells.

This chip holder functioned well but alignment of the ports over the microchip reservoirs was difficult as they were not visible. To overcome this problem, the aluminium base plate was replaced with a transparent PMMA version, but as PMMA was found to deform when heated to reaction temperatures in a column heater. A glass plate held within a aluminium frame was used instead, as shown in **Figure 5.8**.

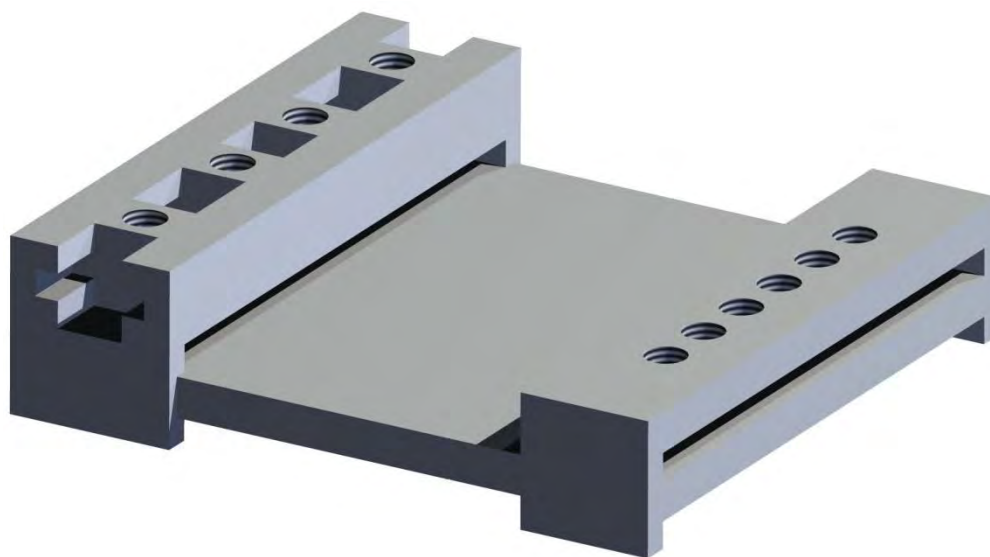


Figure 5.7 Initial adjustable microchip interface with aluminium base plate.

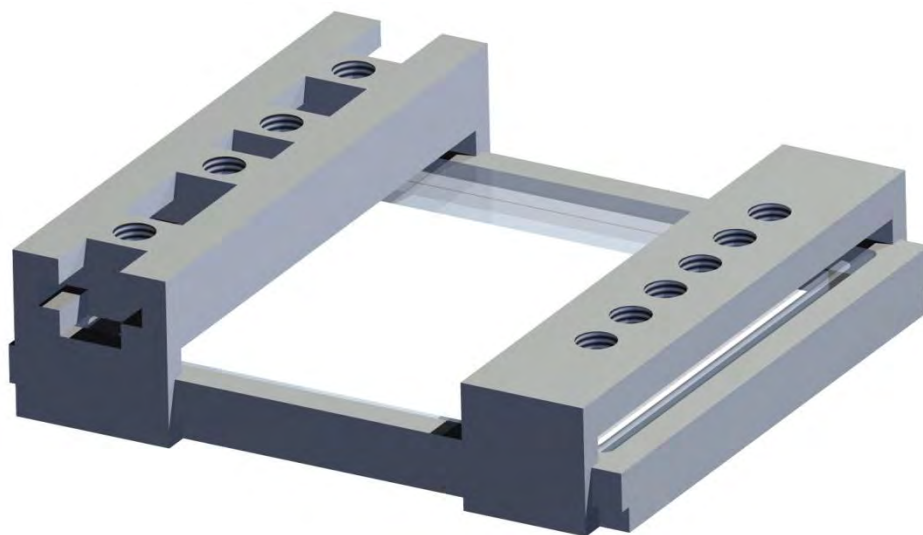


Figure 5.8 Adjustable microchip interface with glass/aluminium base plate.

The complete microchip interface, featuring fittings, tubing, heat source, and pumping system, is shown in **Figure 5.9**, which also shows an interfaced COC microchip reactor. Initially the interface for the glass microchips had the Y section as the output with two tubes connected to the same vial which prevented the flow from being reversed, as discussed in **Chapter 3**. Later, this problem was overcome by adding a T-piece to combine the tubing from both outlets into a single stream for collection, although the single flow-direction approach was retained.



Figure 5.9 Complete microchip interface featuring a COC microreactor.

Visible in **Figure 5.9** is the temperature probe of the column heater resting on the chip holder. In its original configuration, it was observed that the temperature at the microreactor was several degrees lower than measured by the column heater. The column heater for this work was modified by moving the temperature probe from the

base of the heater into the heating chamber and into direct contact with the microreactor.

5.1.3 Glass column

Several different interfaces were utilised for the glass columns, discussed in **Chapter 2**. During the surface modification of the columns before monolith formation, several of the columns were connected in series using PVC tubing and connected to a syringe via Teflon® FEP tubing and Upchurch® fittings. After PPM formation, the columns were connected to a syringe with PVC tubing and a vacuum applied to draw solvent through the column. For reactor fabrication and use, glass columns were interface in the same manner as COC capillary, except Swagelok® stainless steel reducing unions were used to connect to the tubing as shown in **Figure 5.10**. The reducing unions featured Teflon® ferrules which sealed around the glass column when the fitting was tightened.

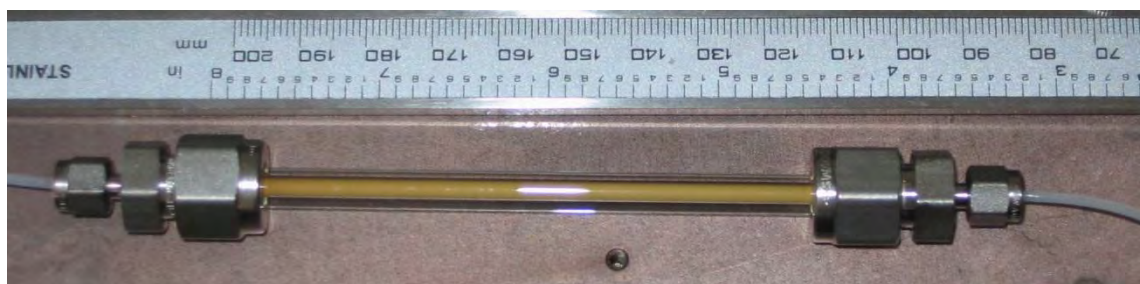


Figure 5.10 Glass column reactor and interface showing Swagelok® unions and tubing.

5.2 Development of a UV initiated bulk monolith polymerisation container

As discussed in **Chapter 2**, a container for UV initiated polymerisation of bulk monolith was designed based on a design by Rohr *et al.*[3]. This container consisted of a polytetrafluoroethylene (PTFE) base plate with a 4 in glass wafer separated by a 700 μm thick polysiloxane gasket, which was wedged between two

aluminium rings to hold the device together and seal the chamber. This design was modified by replacing the gasket with 500 μm disc recess in the PTFE base plate to form the depth of the polymerisation chamber. The initial container design, shown in **Figure 5.11**, consisted of an aluminium base plate with threaded screw holes housing a PTFE plate. The PTFE plate had an inset ring for a 1.8 mm thick o-ring, and a 34.8 mm diameter 0.5 mm deep inset disc that comprised the base of the polymerisation chamber with two 1 mm troughs on opposite sides, allowing syringe needles to penetrate through the o-ring. On top of the PTFE plate was a 1 mm thick quartz disc which was held in position by an aluminium ring with holes corresponding to the screw holes in the base plate. The purpose of the ring was to press down on the quartz disc to compress the o-ring sealing the polymerisation chamber. Quartz was chosen as the window material in order to maximise UV transmission into the polymerisation chamber.

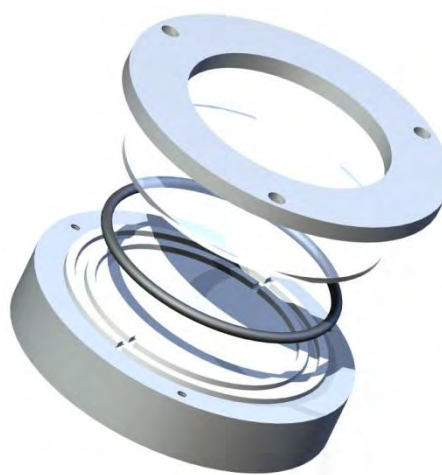


Figure 5.11 First UV initiated bulk polymerisation container.

Introduction of the polymerisation mixture into the polymerisation chamber was achieved by injection of the mixture through the o-ring by means of a syringe needle, with a needle on the opposite side to allow gas to escape at ambient pressure. It was found that not all of the trapped gas could be removed using this syringe needle and some small air bubbles remained in the chamber after filling.

All polymerisation containers were fabricated by Peter Dove of the Central Science Laboratory (CSL). This initial design allowed easy and reliable production of between 300-500 mg of bulk monolith with minimal waste. However this container design was found to be unsuitable when using BAPO as the photoinitiator due to its relatively large exposure depth, as discussed in **Chapter 2**. Thus a second container was designed to minimise the exposure depth in order to prepare bulk monolith with porous properties as close as possible to that formed in the sub-millimetre ID devices, while still being large enough area to produce sufficient material for analysis. The exposure depth that could be achieved using in-house milling was 200 μm using a metal substrate. To provide sufficient material for analysis, the diameter of the container had to be increased, but not beyond the 100 mm diameter of the exposure areas of both the UV-LED and Model 30. The main difficulty in designing a shallower container was how to fill such a narrow chamber with the polymerisation mixture without forming air bubbles and without the mixture to come into contact with air. The chamber height of 200 μm is too shallow to use a syringe needle as employed in the previous design. The problem was addressed by designing the chamber to resemble a bowl which is filled with solution to a certain depth. A thick transparent window is positioned on top of the solution and pressed down, hereby expelling the trapped air and excess solution and sealing the chamber. The shallow polymerisation container is shown in **Figure 5.12**.

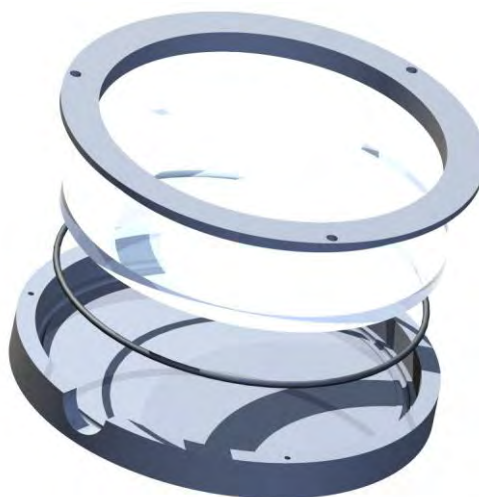


Figure 5.12 Shallow-depth UV initiated polymerisation container.

This container consisted of an aluminium dish with a recessed ring on the inside to house an o-ring. This ring was machined such that when the o-ring was compressed it became flush with the base of the dish so that the o-ring did not contribute to the chamber depth. The dish featured a semi-circular hole on one side to allow the air and excess polymerisation mixture to escape. A 91 mm diameter, 0.2 mm deep disc was recessed into the base of the dish to form the polymerisation chamber. A 100 mm diameter, 5 mm thick quartz disc formed the window of the container and an aluminium ring with screw holes held the disc in place. This container was not practical as the quartz disc could not be removed from the base after PPM formation, which was likely due to the rough machined surface of the aluminium dish and the inability to lift the quartz disc from the base of the dish to break the seal. The design of the container was revised to enable the base of the dish to be removed. Also the surface of the base was coated with PTFE to ensure it was smooth and chemically inert. This revised design of the shallow container is shown in **Figure 5.13**.



Figure 5.13 Revised shallow-depth polymerisation container.

The base plate screws into a ring, sealed with an o-ring, to form a dish into which the polymerisation is poured. Otherwise the design is the same as the previous container, except for the addition of another semi-circular hole for the excess polymerisation mixture to escape from, which also renders the quartz disc easier to position. Practically, this container design required the use of a two-fold excess of polymerisation mixture in order to expel all of the air. This container was utilised to produce 2-3 g of bulk monolith for analysis using low intensity light sources, such as the UV-LED.

It was found that after repeated use the bulk monolith would adhere to the quartz disc. This may be due to glycidylisation of the surface silanol groups by GMA as suggested by Sirc *et al.* [4]. To prevent this from occurring the quartz discs were treated with trichloro(1*H*,1*H*,2*H*,2*H*-perfluorooctyl)silane, which enabled easy removal of the bulk monolith.

5.3 Conclusions

Due the inherent novelty of this research, a chip holder was developed capable of interfacing multiple microchips with different designs and port layouts while withstanding temperatures up to 80 °C. The design of this chip holder was optimised over several versions to allow easy port alignment. Conversely the capillary and column reactors interfaces utilised readily available commercial components.

A chamber for producing bulk photopolymerised PPM in sufficient quantity for analysis was successfully developed based on a reported design, but was tailored for use with low intensity light sources by reducing the chamber depth.

5.4 References

1. Schlautmann, S., H. Wensink, R. Schasfoort, M. Elwenspoek, and A. van den Berg, Powder-blasting technology as an alternative tool for microfabrication of capillary electrophoresis chips with integrated conductivity sensors. *Journal of Micromechanics and Microengineering*, 2001. **11**(4), 386-389.
2. Mair, D.A., E. Geiger, A.P. Pisano, J.M.J. Fréchet, and F. Svec, Injection molded microfluidic chips featuring integrated interconnects. *Lab on a Chip*, 2006. **6**(10), 1346-1354.
3. Rohr, T., E.F. Hilder, J.J. Donovan, F. Svec, and J.M.J. Fréchet, Photografting and the Control of Surface Chemistry in Three-Dimensional Porous Polymer Monoliths. *Macromolecules*, 2003. **36**(5), 1677-1684.
4. Širc, J., Z. Bosáková, P. Coufal, J. Michálek, M. Pøádný, R. Hobzová, and J. Hradil, Morphological and chromatographic characterization of molecularly imprinted monolithic columns. *E-Polymers*, 2007. **117**, 15.

Chapter 6 Conclusion and outlook

Supported Suzuki-Miyaura catalysis was successfully demonstrated in microreactors utilising palladium complexes of 5-OHphen, 5-NH₂phen and Me-im on poly(GMA-*co*-EDMA) and poly(CMS-*co*-DVB) monoliths, satisfying the main goal of this work. This proof-of-concept investigation had an intentionally limited scope as development of the reactor technology was the main focus and not the immobilised catalyst and reactions. Using the developed techniques as a framework, future work should demonstrate a greater variety of precursors for Suzuki-Miyaura catalysis, other palladium-mediated reactions and investigate other catalysts for immobilisation.

One of the most significant benefits of immobilisation on PPM is accurate control over the location of catalyst within the microreactor, which was demonstrated using photopolymerised poly(GMA-*co*-EDMA) in COC microchips. This technique enables localisation of the supported catalyst within microdevices featuring multiple integrated microfluidic components, which will have significant application in drug discovery. Further development of this technology should integrate on-chip separation and analysis components with the microreactor. Localisation of the immobilised catalyst could also be employed to create reactors featuring multiple catalysts in a specific sequence through use of photografting.

For the first time, Suzuki-Miyaura catalysis was demonstrated within a polymer microreactor using a supported catalyst well above room temperature. Prior to this work, chemical transformations polymer microreactors have been mostly limited mild reaction conditions, aqueous solutions are room temperature. The ability to heat the reactor up to 80 °C will enable the use of a greater variety and improved

efficiencies for reactions performed in polymer microreactors, making polymer substrates more attractive for microreactor fabrication.

Although there has been a great deal of interest in photopolymerisation of PPM, as discussed in **Chapter 2**, few groups justify their combination of photoinitiator and light source. This work has shown that matching the photoinitiator to the light source can significantly improve the PPM homogeneity. The combination of BAPO with inexpensive UV-LED light sources should improve the adoption of this technology by reducing infrastructure costs, while still affording PPM with excellent morphology in columns up to 2 mm ID.

The results obtained during the investigation of PPM preparation at >1 mm ID suggest that there are secondary effects of porogens choice that have not previously been reported, such as shrinkage due to highly solvating porogens and sheath layer formation caused by interaction of the vinylised surface with the porogens. A more rigorous investigation than presented here is needed to further probe these effects in order to better understand PPM formation. This could significantly affect several applications of PPMs.

While commercial microfluidic chips fabrication become more common in recent years, there are currently no industry standard architectures. In this work, rather than have a single chip holder for each microchip design, a highly configurable, 'universal', chip holder was developed. While the device designed is relatively crude, a further refined design could prove highly useful where microchips from different manufacturers with different port layouts need to be utilised.

The polymerisation container for photopolymerisation of bulk PPM with low intensity light sources designed during this work was successfully applied to the preparation of poly(GMA-*co*-EDMA) using the UV-LED with BAPO. This

container could be further improved by changing the method for introducing the polymerisation mixture, as the current method is highly wasteful, and also adding the ability to control the chamber depth and set it to specific values.

Macroporous monolith supports for continuous flow capillary microreactors

Katrina F. Bolton,^{a,b} Allan J. Canty,^a Jeremy A. Deverell,^{a,b} Rosanne M. Guijt,^{b,*}
Emily F. Hilder,^b Thomas Rodemann^a and Jason A. Smith^{a,*}

^a*School of Chemistry, University of Tasmania, Private Bag 75, Hobart, Tasmania 7001, Australia*

^b*Australian Centre for Research on Separation Science, University of Tasmania, Private Bag 75, Hobart, Tasmania 7001, Australia*

Received 4 September 2006; revised 9 October 2006; accepted 19 October 2006

Available online 9 November 2006

Abstract—A solid macroporous monolith is shown to be a suitable substrate for anchoring a palladium complex to obtain a continuous porous material suitable for conducting flow-through catalysis in capillary microreactors.

© 2006 Elsevier Ltd. All rights reserved.

Chip- and capillary-based microreactor research for organic synthesis is a rapidly growing field following the realisation of the benefits of microfluidic technology over conventional chemical synthesis; including improved temperature control, selectivity, and both environmental and safety issues resulting from the use of small quantities of reagents and solvents.¹ Application of this emerging technology to reactions catalysed by transition metal complexes have included homogeneous and heterogeneous catalysis, and supported catalysis involving ligands covalently bonded to inorganic and organic supports such as silica and Merrifield polystyrene beads.¹ The development of flow-through microreactors is potentially one of the most significant advances to the way organic synthesis is performed. The most recent advances in this area involve the packing of nickel or palladium catalysts supported on polystyrene or silica beads² and polyurea³ into chromatography columns.

A major challenge for flow-through supported catalysis is to utilise more highly intensive surface properties.⁴ We have commenced investigations on a new strategy which involves the attachment of transition metal catalysts onto macroporous organic monolith supports. These monolithic materials have been utilised as stationary phases for chromatographic separations⁵ and often perform better than the corresponding packed chromato-

graphic materials. They have many potential benefits over traditional catalyst supports as they are essentially an incompressible solid material that fully occupies a channel or capillary space.^{6a,b} The material's excellent flow-through properties^{6c} make them of interest for catalysis reactions. Initial work⁷ has involved capillaries (Fig. 1) in view of their recently demonstrated application in parallel synthesis,⁸ although the ultimate aim is incorporation into a chip device. The monolith chosen for this study was GMA-*co*-EDMA^{6a} [poly(glycidyl methacrylate-*co*-ethylene dimethacrylate)] due to its extensive use in capillaries for chromatographic separations. The Suzuki–Miyaura reaction was chosen as a model process in view of its wide application in synthesis and microreactor development,^{2,3,9} and the classic 1,10-phenanthroline moiety as a donor in polymer supported

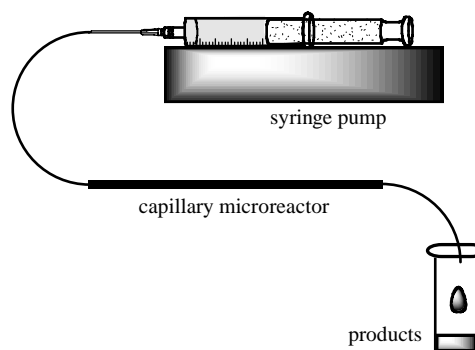


Figure 1. Schematic of the flow-through microreactor comprising a 15 cm length of 250 μ m capillary driven by a syringe pump.

* Corresponding authors. Tel.: +61 3 6226 2182; fax: +61 3 6226 2858 (J.A.S.); e-mail addresses: Jason.Smith@utas.edu.au; Rosanne.Guijt@utas.edu.au

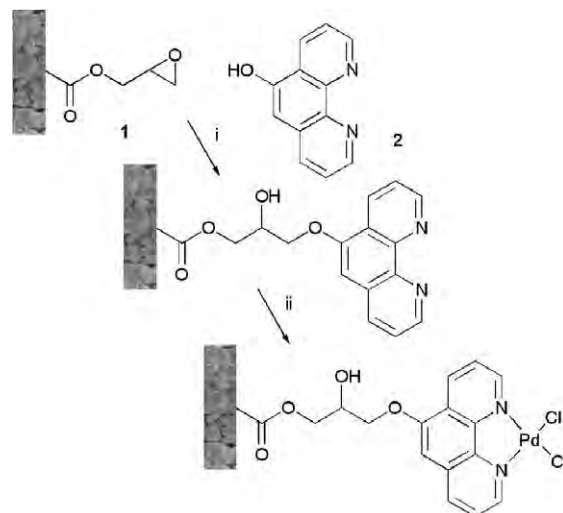
catalysis¹⁰ including palladium catalysis.^{10a} There is also the potential for facile detection of attached phenanthroline by complexation with iron(II).¹¹

The internal surface of fused silica capillaries (250 μm internal diameter, outer surface coated with polyimide; Polymicro Technologies, Phoenix, Arizona) were modified as described^{12a} to covalently anchor the GMA-co-EDMA monolith to the capillary wall. This avoids the need for frits or other devices to hold the support in place which simplifies the design of the microreactor and hence limits the potential for blockages. The monolith was then synthesised in situ, following the reported method of Preinerstorfer et al.^{12b} and characterised by scanning electron microscopy to confirm a complete filling of the capillary (Fig. 2). The median pore diameter of the monolith of the capillary is assumed to be similar to that of the bulk samples of monolith prepared in sample vials which exhibited expected¹³ pore sizes of $\sim 1.07 \pm 0.06 \mu\text{m}$ as determined by mercury intrusion porosimetry.

Capillaries with a length of 20 cm were flushed with dimethylsulfoxide at 60 $^{\circ}\text{C}$ ($2 \mu\text{L min}^{-1}$ for 30 min) using a syringe pump. The phenanthroline ligand was then covalently attached to the monolith by the ring-opening of the electrophilic epoxide groups as has been reported.^{12b,13} Thus, immobilisation of ligand was achieved by passing a solution of 5-hydroxy-1,10-phenanthroline (50 mg)¹⁴ in DMSO (2.5 mL) containing NaOH (10 mg) at $0.5 \mu\text{L min}^{-1}$ for 8 h at 60 $^{\circ}\text{C}$, followed by pumping the solution in the reverse direction and washing with DMSO (Scheme 1). DMSO was required as the solvent due to the low solubility of **2** in other solvents, which could lead to blockage of the microreactor. As a test for ligand attachment, the passage of iron(II) sulfate through the capillary gave the capillary the pink appearance expected for Fe(II) coordinated by phenanthroline,¹¹ being absent for capillaries in which phenanthroline had simply been passed through the capillary and therefore had not been immobilised.¹⁵ To prepare the catalytic microreactor the ligand modified monolith was flushed with acetonitrile followed by a solution of $\text{PdCl}_2(\text{NMe}_2)_2$ (10 mg) in MeCN (2 mL)



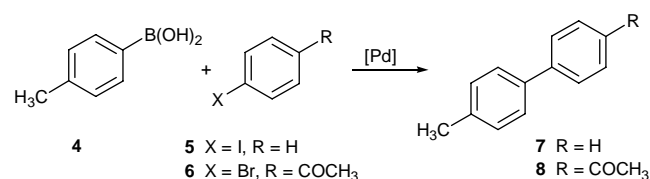
Figure 2. SEM of the monolith completely filling a 250 μm capillary.



Scheme 1. Reagents and conditions: (i) NaOH, DMSO, 60 $^{\circ}\text{C}$; (ii) $\text{PdCl}_2(\text{NMe}_2)_2$, MeCN 25 $^{\circ}\text{C}$.

at a rate of $0.5 \mu\text{L min}^{-1}$ for 8 h at 25 $^{\circ}\text{C}$. The capillary was then reversed and the process repeated before flushing with MeCN. ICP-MS showed a metal loading of 0.02 mmol g^{-1} , close to typical values for metal loadings on organic polymer supports, $\sim 0.04\text{--}0.5 \text{ mmol g}^{-1}$.¹⁶

The Suzuki–Miyaura reaction was examined using a solution of iodobenzene (50 mM) and *p*-tolylboronic acid (75 mM), and was carried out in 9:1 toluene/methanol (Scheme 2). Due to the potential for blockage of the microreactor and to ensure that there was a homogeneous single liquid phase,³ Bu_4NOMe (50 mM) was utilised as a base; diphenyl ether (50 mM) was present as an internal standard for GC–MS analysis. The capillaries of length 15 cm were flushed with the solvent ($2 \mu\text{L min}^{-1}$) for 1 h at 80 $^{\circ}\text{C}$, and the reaction solution then passed through at $0.05 \mu\text{L min}^{-1}$ over 18 h at 80 $^{\circ}\text{C}$, equivalent to a contact time of ca. 90 min, and the product collected in vials. GC–MS analysis showed a yield of 68% for 4-methylbiphenyl (Table 1). The samples taken at different intervals showed that the yield of product remained consistent over time. The stability of the catalyst was exceptional, thus, when the process was continued uninterrupted for four days, the yield for the eluent collected in the final 4 h remained at 68%, demonstrating the application of this approach for sustainable continuous flow processes. Similar results (59% yield) were obtained for the reaction of the less reactive *p*-bromoacetophenone with *p*-tolylboronic acid. Again, to be sure that the catalyst was covalently attached to the monolith and simply not sequestered in the pores of the structure, 1,10-phenanthroline was



Scheme 2. Suzuki–Miyaura reaction.

Table 1. Yields of product from the Suzuki–Miyaura reaction using a continuous flow microreactor^a

Entry	Product	Reaction time ^b (h)	Yield ^b (%)	TOF ^c
1	7	18	68	2.2
2	7	96	68	2.2
3	8	96	59	1.8

^a A solution of aryl halide (50 mmol), *p*-tolylboronic acid (75 mmol) and tetrabutyl ammonium methoxide (50 mmol) in toluene–methanol (9:1) was passed through the capillary heated at 80 °C with a column heater at a flow rate of 0.05 μL per min.

^b Yields were determined by GC/MS using diphenyl ether as an internal standard.

^c TOF = [mmol of product/mmol of catalyst] · h^{−1}.

passed through the capillary followed by a solution of palladium. Under these conditions there was only 4% conversion for iodobenzene while *p*-bromoacetophenone was <1%. The conversions from these new microreactors are similar to those reported by Styring and co-workers^{2a} although the flow rates are less than both those of Styring and co-workers^{2a} and Ley and co-workers,³ primarily due to the difference in diameter of the devices (≥3 mm vs 250 μm). The turnover frequencies (TOF's) of ~2 are also within the ranges reported previously. ICP-MS of the residual monolith after four days of operation indicated leaching of 15–20% of Pd. However, analysis of the reaction products after 18 h suggests that the leaching occurs at the early stages of reaction.

To compare the difference between flow-through catalysis and a typical batch reaction, a bulk sample of the functionalised monolith was formed in a similar manner to the monolith in capillaries.¹⁷ Due to the residence time of the flow reactor, the catalysis runs were conducted over 90 min in order to compare results with those obtained for capillaries.¹⁸ Similar yields were obtained (75% for 4-methylbiphenyl, 62% for 4-(*p*-tolyl)acetophenone after 90 min), demonstrating the application of an anchored transition metal on a solid macroporous monolith in conventional batch process mode.

These results establish the methodology for a new approach for constructing flow-through microreactors and future work will focus on increasing palladium loading and different catalysts.

The excellent flow-through properties, firm attachment to capillary walls, and robustness of the capillary systems for catalysis demonstrated after continuous reaction for four days indicate that this approach is suitable for further development of capillary-based microreactors that are suitable for continuous flow processes and parallel synthesis.

Note added in proof

After submission of this manuscript the authors became aware of the related work by Garcia-Verdugo and Luis (*Chem. Commun.* **2006**, 3095) who report that palladium

carbene complexes attached to organic monoliths catalyse the Heck reaction in near critical ethanol in a flow-through system.

Acknowledgement

We thank the Australian Research Council and the University of Tasmania for financial support.

References and notes

- (a) Watts, P.; Haswell, S. J. *Chem. Soc. Rev.* **2005**, *34*, 235; (b) Brivio, M.; Verboom, W.; Reinhoudt, D. N. *Lab. Chip* **2006**, *6*, 329.
- (a) Phan, N. T. S.; Khan, J.; Styring, P. *Tetrahedron* **2005**, *61*, 12065; (b) Phan, N. T. S.; Brown, D. H.; Styring, P. *Green Chem.* **2004**, *6*, 526.
- Lee, C. K. Y.; Holmes, A. B.; Ley, S. V.; McConvey, I. F.; Al-Duri, B.; Leeke, G. A.; Santos, R. C. D.; Seville, J. P. K. *Chem. Commun.* **2005**, 2175.
- He, P.; Haswell, S. J.; Fletcher, P. D. I. *Lab. Chip* **2004**, *4*, 38.
- Al Bokari, M.; Cherrak, D.; Guiochon, G. *J. Chromatogr., A* **2002**, *975*, 275.
- (a) Svec, F.; Fréchet, J. M. J. *Anal. Chem.* **1992**, *64*, 820; (b) Svec, F.; Fréchet, J. M. J. *Ind. Eng. Chem. Res.* **1999**, *38*, 34; (c) Svec, F.; Huber, C. G. *Anal. Chem.* **2006**, *78*, 2101; (d) Tallarek, U.; Leinweber, F. C.; Seidel-Morgenstern, A. *Chem. Eng. Technol.* **2002**, *25*, 1177.
- Bolton, K. F.; Canty, A. J.; Deverell, J. A.; Guijt, R. M.; Rodemann, T.; Smith, J. A. Aust. Prov. Pat., 2006901698, 2006.
- (a) Comer, E.; Organ, M. G. *Chem. Eur. J.* **2005**, *11*, 7223; (b) Shore, G.; Morin, S.; Organ, M. G. *Angew. Chem., Int. Ed.* **2006**, *45*, 2761; (c) Shi, G.; Hong, F.; Liang, Q.; Fang, H.; Nelson, S.; Weber, S. G. *Anal. Chem.* **2006**, *78*, 1972.
- (a) Greenway, G. M.; Haswell, S. J.; Morgan, D. O.; Skelton, V.; Styring, P. *Sens. Actuators, B* **2000**, *63*, 153; (b) Basheer, C.; Hussain, F. S. J.; Lee, H. K.; Valiyaveetil, S. *Tetrahedron Lett.* **2004**, *45*, 7297.
- (a) Zhuangyu, Z.; Hongwen, H.; Tsi-yu, K. *React. Polym.* **1988**, *9*, 249; (b) Slough, G. A.; Krchňák, V.; Helquist, P.; Canham, S. M. *Org. Lett.* **2004**, *6*, 2909; (c) Lenaerts, P.; Driesen, K.; Van Deun, R.; Binnemans, K. *Chem. Mater.* **2005**, *17*, 2148.
- Bassett, J.; Denney, R. C.; Jeffery, G. H.; Mendham, J. *Vogel's Textbook of Quantitative Inorganic Analysis*; Longman: London, 1983.
- (a) Rohr, T.; Hilder, E. F.; Donovan, J. J.; Svec, F.; Fréchet, J. M. J. *Macromolecules* **2003**, *36*, 1677; (b) Preinerstorfer, B.; Bicker, W.; Lindner, W.; Lämmerhofer, M. *J. Chromatogr., A* **2004**, *1044*, 187.
- For a recent example, see: Hutchinson, J. P.; Hilder, E. F.; Shellie, R. A.; Smith, J. A.; Haddad, P. R. *Analyst* **2006**, *131*, 215.
- Prepared from 5,6-dihydro-5,6-epoxy-1,10-phenanthroline (Sigma–Aldrich) in one step as reported.^{10b}
- The 'blank' experiment involved the passage of a solution of 1,10-phenanthroline and KOH through the capillary which is unable to react with the epoxide groups of the monolith.
- Leadbeater, N. E.; Marco, M. *Chem. Rev.* **2002**, *102*, 3217.
- Finely ground monolith was added to a solution of 5-hydroxy-1,10-phenanthroline (50 mg) and NaOH (10 mg) in DMSO (2.5 mL), then degassed using nitrogen. The suspension was stirred for 18 h at 60 °C, collected by

filtration (Whatman No. 1), resuspended in MeOH and stirred vigorously for 25 min, recovered by filtration, washed with MeOH and dried in a vacuum. After complexation with $\text{PdCl}_2(\text{NCMe})_2$ and washing with MeCN, ICP-MS shows 0.19 wt % palladium.

18. Monolith (100 mg) was placed in a 5 mL *Reacti-Vial* with 2 mL of a reaction mixture identical to that used for the studies of reactions in capillaries. The suspension was stirred vigorously at 80 °C for 90 min, then cooled using an ice bath and filtered through a plug of cotton wool.

Microfluidic Devices for Flow-Through Supported Palladium Catalysis on Porous Organic Monolith

Allan J. Canty,^A Jeremy A. Deverell,^{A,B} Anissa Gömann,^{A,B}
Rosanne M. Guijt,^{A,B,D} Thomas Rodemann,^C and Jason A. Smith^A

^ASchool of Chemistry, University of Tasmania, Private Bag 75, Hobart, TAS 7001, Australia.

^BAustralian Centre for Research on Separation Science (ACROSS), School of Chemistry,
University of Tasmania, Private Bag 75, Hobart, TAS 7001, Australia.

^CCentral Science Laboratory (CSL), University of Tasmania, Private Bag 75,
Hobart, TAS 7001, Australia.

^DCorresponding author. Email: rosanne.guijt@utas.edu.au

Flow-through microreactors are described, constructed of fused silica capillaries with an internal diameter of 100 μm and glass microchips with a channel dimension of 150 μm and involving the in situ UV-initiated synthesis of a poly(glycidyl methacrylate-*co*-ethylene dimethacrylate) porous polymer monolith. The monolith is a continuous material covalently bonded to the capillary or chip walls, with good flow-through properties. Epoxide ring-opening through amine attack by 5-amino-1,10-phenanthroline and coordination to dichloropalladium(II) allows use of the microreactors for Suzuki–Miyaura catalysis. The long-term stability and reliability of the robust chip microreactor is demonstrated by operation for 96 h, exhibiting undiminished reactivity, and very low leaching of palladium.

Manuscript received: 17 April 2008.

Final version: 2 July 2008.

Introduction

Miniaturization has changed the face of modern analytical chemistry, e.g. complicated and time-consuming analyses may be routinely performed quickly and easily in a highly automated fashion using micro-Total-Analytical-Systems (μTAS) or Laboratory-on-a-Chip devices.^[1] Synthetic chemists are seeking more efficient and environmentally friendly methodologies, and in this respect the use of microreactors, generally defined as capillary or chip-based devices with a diameter smaller than ~ 1 mm, have been shown to offer advantages over conventional synthesis.^[1–7] Advantages include improved yield, greater selectivity and purity, reduced reaction times, and allowing integration of reactors with other functional units such as micropumps for fluid transfer, detectors, and separation systems for on-line reaction monitoring and biotesting.

Catalytic reactions are of particular value in synthesis as they significantly improve efficiency. Solid-supported catalysts are suitable for flow-through applications, simplifying product isolation providing that leaching of the catalyst is minimal. Polymer resin beads are commonly used for catalyst immobilization when miniaturization at the microscale level is not involved. However, these are difficult to pack into and retain in microscale capillaries and channels in chips, and thus open capillaries or open channels in chips have generally been employed to date.

In analytical chemistry, polymer monoliths have been shown to be a good alternative to polymer beads.^[8] Polymer monoliths are covalent network solids with continuous covalent bonding throughout the confinement vessel. They may be formed in situ and have excellent flow-through properties, and we have recently

reported the use of thermally polymerized polymer monoliths for catalyst support in batch reactions and in capillary microreactors of internal diameter (ID) 250 μm .^[9] We describe here catalysis studies using poly(glycidyl methacrylate-*co*-ethylene dimethacrylate) monolith formed by UV-initiated polymerization in much more robust glass microchips (channel dimensions 150 μm) functionalized with palladium(II) centres (Fig. 1b), and compared the performance of capillaries of ID 100 μm (Fig. 1a), of smaller ID than examined previously^[9] for thermal polymerization. Microreactor chips may also be readily integrated with other functionalities on the chip, or with external devices.^[1,2,5] Glass was chosen as a material for chip development in view of its compatibility with a wider range of temperatures and solvents than plastic chips, e.g. cyclic olefin copolymer (COC).^[10] Studies of capillaries under identical conditions were included to allow ease of analysis of monolith, including determination of void volume fraction and catalyst loading, and in view of their significant recently demonstrated application in parallel synthesis.^[11–13]

The Suzuki–Miyaura catalysis (Fig. 2) was used in view of its current role as a standard test reaction in microreactors of typical ID $< \sim 1$ mm, confined so far to open capillaries (homogeneous palladium catalyst (ID 200–1150 μm),^[11] suspended palladium nanoparticle (ID 400 μm),^[14] palladium thin film on walls (ID 1150 μm)^[12]), and, in partly or completely filled systems, heterogeneous catalysis by Pd/SiO₂ and Pd/Al₂O₃ particles in capillaries (ID 800 μm),^[15] and in glass chips containing a microporous Pd/SiO₂ frit (channel dimensions 300 \times 115 μm)^[16] or powdered Pd/Al₂O₃ or Pd-polymer (1500 \times 80 μm).^[17]

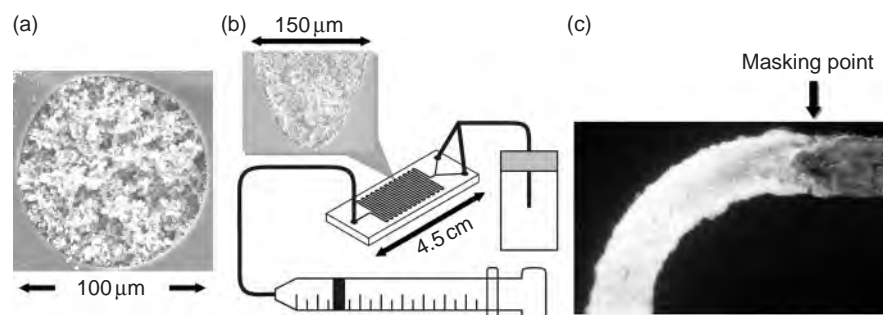


Fig. 1. (a) Scanning electron micrograph of a cross-section of a capillary microreactor ($\times 2133$); (b) flow-through configuration for glass chips showing a cross-section of channel ($\times 1300$); where these were obtained after applications in catalysis; and (c) view of edge of monolith (at left) in chip at a masking point.

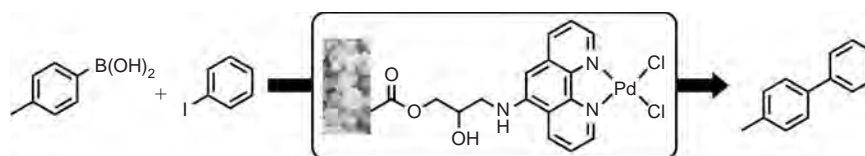


Fig. 2. Suzuki–Miyaura catalysis.

Results and Discussion

Previous studies using capillaries containing organic monolith involved thermal initiation of polymerization^[9] but, for applications in chips, UV-initiation would be preferred as this allows lithographic control of confinement of the monolith to defined sections of channels (Fig. 1c). Procedures modelled on those reported for UV-initiation in COC chips designed for analytical applications^[10] were developed and, for comparison, UV-initiation was used for studies of the same monolith in capillaries.

The internal surface of capillaries and chips were treated with 3-(trimethoxysilyl)propyl methacrylate to enable the polymer monolith to anchor to the surface, ensuring filling of the microreactor by continuous polymer.^[18] The polymerization mixture was chosen modelled on the recommended 2:3 monomer/porogenic solvent ratio for macroporous poly(glycidyl methacrylate-*co*-ethylene dimethacrylate) materials,^[19] using porogens that facilitate formation of pore diameters of $\sim 1.1 \mu\text{m}$ ^[20] and a void volume fraction of $\sim 60\%$ ^[8] to provide low flow resistance with high surface area.^[21] After polymerization using a deep-UV lamp for 60 s, a void volume fraction of 65% was obtained. The capillaries and chips were rinsed with methanol, water and dimethyl sulfoxide (DMSO), followed by reaction with 5-amino-1,10-phenanthroline in DMSO to effect ligand attachment via ring opening of the epoxide groups in a procedure similar to that reported for 5-hydroxy-1,10-phenanthroline.^[9] Hydrolytic and aqueous solutions often cause elevated backpressure, and this was alleviated by treatment with dimethoxydimethylsilane to cap exposed hydroxy and amine groups as this procedure was found to assist flow-through using methanol. Dichloropalladium(II) was attached to the phenanthroline donor by passing a solution of $\text{PdCl}_2(\text{NCMe})_2$ in acetonitrile.

The capillary microreactors were analyzed for palladium, and the loading on the monolith was found to be 0.04 wt-%, lower than normally found for loadings in conventional polymer-supported catalysis (typically $\sim 0.45 \text{ wt-\%}$),^[22]

corresponding to a palladium loading of $0.58 \mu\text{g}$ in the 30 cm capillary used for catalysis, and $\sim 1.41 \mu\text{g}$ for the chip microreactors based on approximate dimensions of the microreactor. Scanning electron micrographs of the cross-section of capillary and chip-based microreactors are shown in Figs 1a and 1b, respectively.

The microreactors were evaluated using the Suzuki–Miyaura reaction of iodobenzene with *p*-tolylboronic acid in methanol. The reaction mixture was pumped through the microreactor at $3.7 \mu\text{L h}^{-1}$ (chips) and $1.4 \mu\text{L h}^{-1}$ at 80°C (capillaries), allowing a contact time of $\sim 1 \text{ h}$ of the reagents with the support, calculated based on a 65% void volume. Samples were taken every 12 h and analyzed by gas chromatography–mass spectrometry (GC-MS). The results in Fig. 3 indicate yields of $\sim 87\%$ for chips and capillaries, undiminished during operation for 96 h, which, based on iodobenzene as reagent, correspond to a product:palladium ratio of ~ 2200 and 2080 for the chip and capillary microreactors, respectively. Monolith without palladium resulted in no catalysis. For the capillary microreactor, the sample collected during the first 24 h represented 0.02% of the total amount of palladium present in the microreactor, and subsequent samples corresponded to a leaching rate of 0.0025% per day. Similar concentrations were found in the eluent from a chip microreactor.

Conclusions

Glass chip flow-through microreactors may be constructed by in situ synthesis of a polymer monolith for catalyst support by UV-initiated polymerization. When functionalized with a (1,10-phenanthroline)dichloropalladium(II) precatalyst centre, an average yield of 87% was obtained over 96 h in Suzuki–Miyaura catalysis, identical to that obtained for a capillary model system. Together with very low palladium leaching, these results indicate that robust glass chip microreactors employing continuous organic monolith phases as catalyst support are suitable for further development in the miniaturization of organic synthesis procedures.

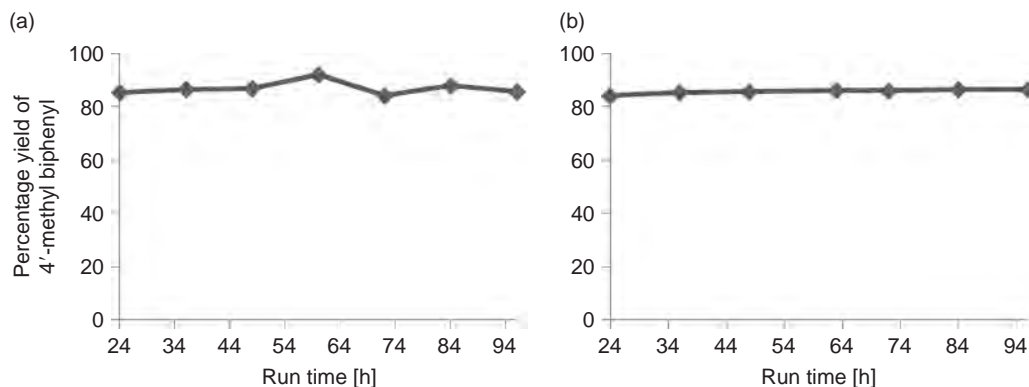


Fig. 3. Yield for Suzuki–Miyaura reaction examined in flow-through mode in: (a) silica capillaries; and (b) glass chips.

Experimental

General Experimental

Capillary microreactors were made of UV-transparent fused silica capillary with an ID of 100 μm (Polymicro, USA). Chip microreactors were made of powder-blasted borosilicate microchips (channel dimensions 33.2 cm long, 150 μm wide and 150 μm deep (Micronit, Enschede, the Netherlands)). A 500 W Hg-Xe lamp was used (20 mW cm^{-2} at 260 nm). Characterization used equipment housed in the Central Science Laboratory, University of Tasmania, including an FEI Quanta 600 MLA ESEM and an ELEMENT high resolution inductively coupled plasma-mass spectroscopy (ICP-MS) allowing detection down to 0.1 ppb; capillary samples were crushed using a mortar and pestle before palladium analysis. GC-MS analyses were carried out on a Varian 1200 triple quadrupole bench-top gas chromatograph-mass spectrometer, calibrated against diphenyl ether as an internal standard. Determination of void volume fraction used a Sartorius SE2 Ultra-Microbalance (0.1 μg readability).

Fused Silica Capillary Surface Modification

The internal capillary surface was treated following the reported procedure, slightly modified.^[18] The 4–5 m length of capillary was rinsed with acetone (250 μL), water (1 mL), and sodium hydroxide (0.2 M) until a basic pH was detected at the capillary terminus and continued at 15 $\mu\text{L h}^{-1}$ for 30 min, followed by water until neutral pH. The capillary was then flushed with hydrochloric acid (0.2 M) until an acidic pH was detected and continued at 15 $\mu\text{L h}^{-1}$ for 30 min, followed by water until neutral pH, then rinsed with ethanol (1 mL). The surface modification mixture (20 wt-% 3-(trimethoxysilyl)propyl methacrylate in ethanol adjusted to pH 5 with acetic acid) was pumped through at 15 $\mu\text{L h}^{-1}$ for 1 h, followed by acetone (250 μL), and then dried by flushing with compressed air. The capillary was then stored for at least 24 h to allow the condensation reaction to become complete.

Formation of Monolith in Fused Silica Capillaries

Cyclohexanol (1.5 g), glycidyl methacrylate (GMA, 0.6 g), ethylene glycol dimethacrylate (EDMA, 0.4 g), and 2,2-dimethyl-2-phenylacetophenone (DMPAP, 10 mg) were mixed thoroughly in a 4-mL vial (glass screw top, Alltech) and then purged with nitrogen for 10 min. A capillary (35 cm) was flushed with the mixture until no bubbles were apparent, sealed at both ends with inert rubber septa and exposed under a deep-UV lamp

(20 mJ cm^{-2}) for 60 s. The monolith-filled capillary was then rinsed with filtered methanol (60 $\mu\text{L h}^{-1}$, 1 h), followed by filtered water (60 $\mu\text{L h}^{-1}$, 1 h), and trimmed to 30 cm by cutting 2.5 cm from each end. The void volume fraction (65%) was determined by comparing the mass of a dried monolith-filled capillary (11.6 cm) capped with a septum with that of the same capillary filled with ethanol. The monolith was dried by passage of air overnight at 80°C.

Ligand and Palladium Attachment to Monolith-Filled Capillary

The capillary was flushed with DMSO (60 $\mu\text{L h}^{-1}$, 1 h) at 70°C. The ligand-attachment solution, prepared by filtering a solution of 5-amino-1,10-phenanthroline (50 mg) in DMSO (2 mL) through a cotton wool plug, was flushed through the capillary (30 $\mu\text{L h}^{-1}$, 8 h) at 70°C and then for 18 h (12 $\mu\text{L h}^{-1}$), followed by DMSO (60 $\mu\text{L h}^{-1}$, 1 h) at 70°C to remove unattached ligand. The capillary was flushed with dimethoxydimethylsilane (6 $\mu\text{L h}^{-1}$, 36 h) at 50°C, followed by filtered acetonitrile (60 $\mu\text{L h}^{-1}$, 1 h) at room temperature. The palladium-attachment solution, prepared by filtering a solution of bis(acetonitrile)dichloropalladium(II) (10 mg) in acetonitrile (2.5 mL) through a cotton wool plug, was flushed through the capillary (30 $\mu\text{L h}^{-1}$, 8 h) and then 18 h (12 $\mu\text{L h}^{-1}$), followed by acetonitrile (60 $\mu\text{L h}^{-1}$, 2 h) to remove any unattached palladium.

Formation of Monolith in Borosilicate Microchips

In-house fabricated microchip holders fitted with Upchurch tubing and fittings were used to interface the microchips. The microchannels were surface-modified using the procedure for capillaries described above. The surface-treated microchannel was filled with prepolymerization mixture by capillary action and by applying a low vacuum to the exit well. The wells of the filled microchip were sealed with inert rubber septa and the wells masked off with black electrical tape, leaving only the main microchannel exposed. The microchip was then exposed under a deep-UV lamp for 1 min (20 mJ cm^{-2}) and then flushed with filtered methanol (60 $\mu\text{L h}^{-1}$, 1 h) followed by filtered water (60 $\mu\text{L h}^{-1}$, 1 h). Ligand and palladium attachment was accomplished as for capillaries.

Reaction Mixtures for Catalysis

Stock reaction mixtures were prepared using methanol (8.0 mL), aryl halide (1 mmol; 110 μL iodobenzene), 4-tolylboronic acid (1.5 mmol; 203.9 mg), tetrabutylammonium methoxide

(1.5 mmol; 2.5 mL 20% v/v in methanol), and diphenyl ether as internal standard (1 mmol; 160 μ L). These mixtures were purged with nitrogen and stored at 4°C.

Acknowledgements

The present research was supported under the Australian Research Council's Discovery Projects funding scheme (DP0663416) and the University of Tasmania Research College Board. Dr R. M. Guijt is the recipient of an ARC APD fellowship (DO0557803); Dr N. Davies, Mr P. Dove, Dr K. Gömann, and Dr A. Townsend (ICP-MS), Central Science Laboratory, are acknowledged for technical support; and Dr E. F. Hilder and Mrs K. F. Munting for useful discussions.

References

- [1] S. Haeberle, R. Zengerle, *Lab Chip* **2007**, *7*, 1094. doi:10.1039/B706364B
- [2] V. Hessel, H. Löwe, *Chem. Eng. Technol.* **2005**, *28*, 267. doi:10.1002/CEAT.200407167
- [3] M. Brivio, W. Verboom, D. N. Reinhoudt, *Lab Chip* **2006**, *6*, 329. doi:10.1039/B510856J
- [4] K. Geyer, J. D. C. Codée, P. H. Seeberger, *Chem. Eur. J.* **2006**, *12*, 8434. doi:10.1002/CHEM.200600596
- [5] (a) P. Watts, S. J. Haswell, *Chem. Soc. Rev.* **2005**, *34*, 235. doi:10.1039/B313866F
(b) P. Watts, C. Wiles, *Chem. Commun.* **2007**, 443. doi:10.1039/B609428G
- [6] B. Ahmed-Omer, J. C. Brandt, T. Wirth, *Org. Biomol. Chem.* **2007**, *5*, 733. doi:10.1039/B615072A
- [7] B. P. Mason, K. E. Price, J. L. Steinbacher, A. R. Bogdan, D. T. McQuade, *Chem. Rev.* **2007**, *107*, 2300. doi:10.1021/CR050944C
- [8] M. R. Buchmeiser, *Polymer* **2007**, *48*, 2187. doi:10.1016/J.POLYMER.2007.02.045
- [9] K. F. Bolton, A. J. Canty, J. A. Deverell, R. M. Guijt, E. F. Hilder, T. Rodemann, J. A. Smith, *Tetrahedron Lett.* **2006**, *47*, 9321. doi:10.1016/J.TETLET.2006.10.113
- [10] T. B. Stachowiak, T. Rohr, E. F. Hilder, D. S. Peterson, M. Yi, F. Svec, J. M. J. Fréchet, *Electrophoresis* **2003**, *24*, 3689. doi:10.1002/ELPS.200305536
- [11] (a) E. Comer, M. G. Organ, *Chem. Eur. J.* **2005**, *11*, 7223. doi:10.1002/CHEM.200500820
(b) E. Comer, M. G. Organ, *J. Am. Chem. Soc.* **2005**, *127*, 8160. doi:10.1021/JA0512069
- [12] G. Shore, S. Morin, M. G. Organ, *Angew. Chem. Int. Ed.* **2006**, *45*, 2761. doi:10.1002/ANIE.200503600
- [13] G. Shi, F. Hong, Q. Liang, H. Fang, S. Nelson, S. G. Weber, *Anal. Chem.* **2006**, *78*, 1972. doi:10.1021/AC051844+
- [14] C. Basheer, F. S. J. Hussain, H. K. Lee, S. Valiyaveetil, *Tetrahedron Lett.* **2004**, *45*, 7297. doi:10.1016/J.TETLET.2004.08.017
- [15] P. He, S. J. Haswell, P. D. I. Fletcher, *Appl. Catal. A-Gen.* **2004**, *274*, 111. doi:10.1016/J.APCATA.2004.05.042
- [16] G. M. Greenway, S. J. Haswell, D. O. Morgan, B. V. Skelton, P. Styring, *Sensors Actuat. B-Chem.* **2000**, *63*, 153. doi:10.1016/S0925-4005(00)00352-X
- [17] P. He, S. J. Haswell, P. D. I. Fletcher, *Lab Chip* **2004**, *4*, 38. doi:10.1039/B313057F
- [18] T. Rohr, E. F. Hilder, J. J. Donovan, F. Svec, J. M. J. Fréchet, *Macromolecules* **2003**, *36*, 1677. doi:10.1021/MA021351W
- [19] F. Svec, J. M. J. Fréchet, *Chem. Mater.* **1995**, *7*, 707. doi:10.1021/CM00052A016
- [20] B. Preinerstorfer, W. Bicker, W. Lindner, M. Lämmerhofer, *J. Chromatogr. A* **2004**, *1044*, 187. doi:10.1016/J.CHROMA.2004.04.078
- [21] C. Viklund, F. Svec, J. M. J. Fréchet, K. Irgum, *Chem. Mater.* **1996**, *8*, 744. doi:10.1021/CM950437J
- [22] N. E. Leadbeater, M. Marco, *Chem. Rev.* **2002**, *102*, 3217. doi:10.1021/CR010361C



Palladium-mediated organic synthesis using porous polymer monolith formed in situ as a continuous catalyst support structure for application in microfluidic devices

Anissa Gömann^a, Jeremy A. Deverell^a, Katrina F. Munting^a, Roderick C. Jones^b, Thomas Rodemann^c, Allan J. Canty^b, Jason A. Smith^{b,*}, Rosanne M. Guijt^{a,*}

^a Australian Centre for Research on Separation Science (ACROSS), School of Chemistry, University of Tasmania, Private Bag 75, Hobart TAS 7001, Australia

^b School of Chemistry, University of Tasmania, Private Bag 75, Hobart TAS 7001, Australia

^c Central Science Laboratory (CSL), University of Tasmania, Private Bag 74, Hobart TAS 7001, Australia

ARTICLE INFO

Article history:

Received 14 July 2008

Received in revised form 12 November 2008

Accepted 4 December 2008

Available online 9 December 2008

Keywords:

Microreactor

Catalysis

Microfluidic

Monolith

Flow-through

ABSTRACT

The development and advantages of in situ synthesis of organic polymer monolith supports for metal pre-catalysts in narrow bore fused silica capillary microreactors are described. Catalyst immobilisation involves the covalent attachment of ligand binding sites to the porous polymer monolith, followed by coordination to metal centres. Flow-through microreactors using poly(chloromethylstyrene-co-divinylbenzene) monolith in capillaries of internal diameter 250 μm were used successfully for Suzuki–Miyaura and Sonogashira reactions, utilising both 1,10-phenanthroline and imidazole/carbene binding to palladium and with very low palladium leaching, illustrating the potential of flow-through technology at the microscale level using organic monolith support for transition metal catalysed reactions.

Crown Copyright © 2008 Published by Elsevier Ltd. All rights reserved.

1. Introduction

Microreactors have the potential to revolutionise the fields of chemistry and biotechnology by replacing conventional glassware with small flow-through devices.^{1–8} Excellent performance can be achieved by taking advantage of microchannel system features such as rapid heat and mass transfer. Reactions can be carried out under isothermal conditions with well-defined residence times, so that undesirable side reactions and fragmentations are limited. The small dimensions of microreactors also allow the use of minimal amounts of reagents and solvents under precisely controlled conditions, which reduces potential hazards and thus reduces environmental impacts.

Major issues encountered in the development of narrow bore flow-through microreactors [typical Internal Diameter (ID) < ca. 1 mm] for heterogeneous or polymer-supported catalysis are the packing and retention of the supported catalyst inside the microreactor, as well as the high back pressure over the capillary caused either by the densely packed small particle bed or swelling.⁹

In chromatography, silica and polymer based monolithic columns have been developed to overcome these difficulties. Monoliths can be synthesised in situ, eliminating the need for packing, and can be designed to have pore sizes in the order of 1 μm ensuring good flow-through properties.¹⁰ A polymer monolith can be formed by polymerisation in the presence of a high proportion of cross-linking monomer and a porogen. The physical properties (pore size and surface area) of the monolith are predominantly determined by the solubility of the forming polymer and the nature of the porogen,¹¹ whereas its chemical properties are determined predominantly by the monomer.^{11,12}

Catalytic reactions in microreactors have been explored,^{1–7} including for palladium catalysis with ID < ca. 1 mm for hydrogenation (ID 200–530 μm),¹³ Suzuki–Miyaura (ID 200–1500 μm),¹⁴ Stille (ID 75 μm),¹⁵ carbonylative cross-coupling (ID 200 μm),¹⁶ and sequential aryl amination/Heck coupling.¹⁷ We have recently reported results for the Suzuki–Miyaura cross-coupling of *p*-tolylboronic acid with iodobenzene using poly(glycidyl-co-ethylene dimethacrylate) monolith (GMA/EDMA),^{18,19} but see considerable advantage in developing this system for poly(chloromethylstyrene-co-divinylbenzene) monolith as it has a structure similar to widely used conventional chloromethylpolystyrene beads and does not have functional groups present in GMA/EDMA that could potentially interfere with catalysis. The Suzuki–Miyaura and Sonogashira

* Corresponding authors. Tel.: +61 3 6226 2171; fax: +61 3 6226 2858.

E-mail address: rosanne.guijt@utas.edu.au (R.M. Guijt).

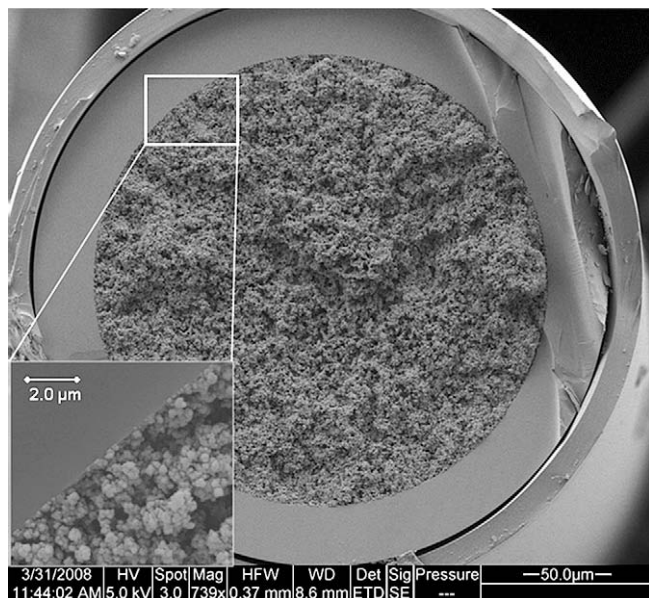
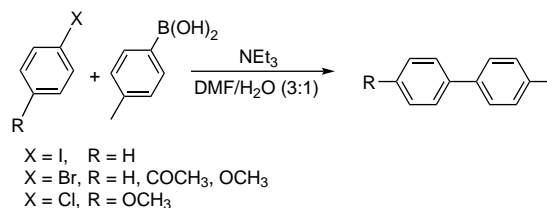


Figure 1. Scanning electron micrographs (magnification of 739× and 15,000×) of a cross-section of a 250 µm capillary completely filled with CMS/DVB monolith.

systems were chosen for the work reported here, as established model reactions for metal complexes anchored onto conventional organic polymers in large scale catalysis.²⁰ Microreactors were constructed using fused silica capillaries with an internal diameter of 250 µm. Polymeric monoliths were synthesised in situ and used as a pre-catalyst support. The performance of capillary microreactors was compared with that of batch reactions using bulk monolith, and bulk monolith was used to estimate catalyst loadings for capillaries.

2. Results and discussion

The polymer monolith was prepared inside the capillaries after modifying the surface of the inner wall of the capillaries²¹ to ensure anchoring of the monolith. A mixture containing 60% porogens (1-dodecanol and toluene), 24% monovinyl monomer and 16% cross-linking monomer was used, in accord with the recommended 6:4 porogen/monomer ratio,^{21,22} in order to achieve a suitable porosity and void volume fraction of ca. 60%²³ consistent with good flow-through and high surface area characteristics.²² The surface modification successfully anchored the formed monolith inside the capillary (Fig. 1), allowing the microreactors to withstand pressures up to at least 500 psi.



Scheme 1. Suzuki–Miyaura cross-coupling of aryl halides and *p*-tolylboronic acid.

The benzyl chloride groups on the monolith were used to covalently attach 5-amino-1,10-phenanthroline or 1-methylimidazole (Fig. 2). In previous work with GMA/EDMA monolith 5-hydroxy-1,10-phenanthroline was used as the reagent,¹⁸ but this compound was successfully replaced by the commercially available amine reagent.¹⁹ Loading with palladium was facilitated by the passage of PdCl₂(NCMe)₂ through the modified monolith. For imidazole, present as the imidazolium group when attached to related polymers²⁴ and a CMS/DVB monolith recently reported,²⁵ formation of the resulting material may involve the palladium present as an anion to balance the imidazolium group, e.g., [PdCl₃(NCMe)][−],²⁵ or bonded to the heterocycle present as an *N*-heterocyclic carbene (NHC).²⁴ If present as NHC an additional donor (L) to complete square-planar coordination is assumed, as illustrated in Figure 2, e.g., MeCN. For the CMS/DVB monolith containing Pd–NHC groups, the void volume fraction was found to be 55%.

With 1-methylimidazole functionalised CMS/DVB, palladium loadings of ca. 0.4 wt% were obtained for bulk material and ca. 0.3 wt% with phenanthroline as the ligand. For comparison, the palladium loadings of polymer-supported catalysts are typically ~0.4–5 wt%.²⁰ Capillaries that were not functionalised with ligands, but which were subjected to passage of PdCl₂(NCMe)₂ as described above, were inactive in catalysis.

2.1. Suzuki–Miyaura reactions

2.1.1. Bulk material

The Suzuki–Miyaura reaction was examined at 80 °C using a range of aryl halides and *p*-tolylboronic acid as indicated in Scheme 1 and Table 1, utilising triethylamine as a homogeneous base. The solvents and bases used were chosen to ensure solubilities of all substrates, and 25% water was a good compromise between reactivity and solubility of the substrates.

In general, the results show lower activity for the less reactive halides, as expected: PhI > PhBr (entries 1, 2 and 6, 7), BrC₆H₄CO-Me > ClC₆H₄CO-Me (3, 4 and 8, 9), and PhBr > *p*-MeOC₆H₄Br (2, 5 and 7, 10). Both ligands gave similar results even though the catalyst

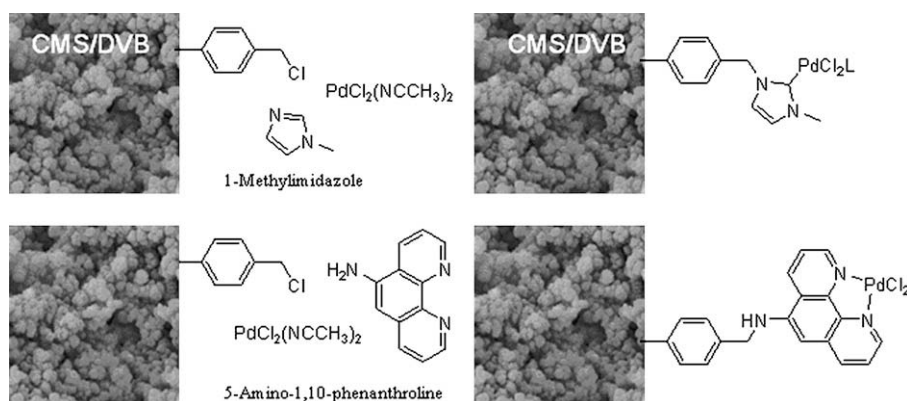


Figure 2. Ligand and PdCl₂ attachment to the monolithic support.

Table 1

Suzuki–Miyaura cross-coupling in batch reactions of aryl halide (0.1 mol) with *p*-tolylboronic acid (0.15 mol), utilising triethylamine (0.15 mol/L) as the base in *N,N*-dimethylformamide/water (3:1), 20 mg modified bulk monolithic material was reacted in 1.0 mL of reaction solution; phen=1,10-phenanthroline, NHC=*N*-heterocyclic carbene; 80 °C for 60 min

Entry	Ligand	Aryl halide	Yield (%)
1	phen	Iodobenzene	86
2	phen	Bromobenzene	51
3	phen	<i>p</i> -Bromoacetophenone	96
4	phen	<i>p</i> -Chloroacetophenone	13
5	phen	Bromoanisole	30
6	NHC	Iodobenzene	96
7	NHC	Bromobenzene	52
8	NHC	<i>p</i> -Bromoacetophenone	97
9	NHC	<i>p</i> -Chloroacetophenone	9
10	NHC	Bromoanisole	44

Table 2

Suzuki–Miyaura cross-coupling in capillaries of aryl halide (0.1 mol) with *p*-tolylboronic acid (0.15 mol), utilising triethylamine (0.15 mol) as the base in *N,N*-dimethylformamide (3:1); phen=1,10-phenanthroline, NHC=*N*-heterocyclic carbene; 80 °C; product collected over a 48-h period, contact time of reagents in capillary ca. 45 min.

Entry	Ligand	Aryl halide	Yield (%)
1	phen	Iodobenzene	97
2	phen	<i>p</i> -Bromoacetophenone	94
3	NHC	Iodobenzene	95
4	NHC	Bromobenzene	53
5	NHC	<i>p</i> -Bromoacetophenone	91
6	NHC	<i>p</i> -Chloroacetophenone	11
7	NHC	Bromoanisole	28

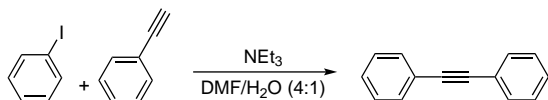
loadings are much lower for phenanthroline. The reaction products were relatively clean with very small amounts of by-products detected only for the coupling of bromobenzene.

2.1.2. Capillaries

Flow-through catalysis in capillaries under similar conditions was studied (Table 2). Flow rates of 0.1 $\mu\text{L min}^{-1}$ in 20 cm capillaries at 80 °C were used throughout. The sampling interval is restricted by the volume required for analysis, and experiments using 12 h sampling intervals over a period of 8 days showed no drop in yield for the conversion of iodobenzene over this period, and with total leaching of palladium at ca. 4%. No other products were detected. Trends in reactivity were identical to bulk samples: $\text{PhI} > \text{PhBr}$ (entries 3, 4), $\text{BrC}_6\text{H}_4\text{COMe} > \text{ClC}_6\text{H}_4\text{COMe}$ (entries 5, 6) and $\text{PhBr} > p\text{-MeOC}_6\text{H}_4\text{Br}$ (entries 4, 7).

2.2. Sonogashira reactions

The coupling of iodoacetophenone with phenylacetylene (Scheme 2) employed NEt_3 as a base in DMF/ H_2O (4:1) and reaction conditions adapted from a copper-free protocol reported recently.²⁶ The performance of bulk material in a common batch process using the phen system gave yields of 99% in 3 h at 80 °C (Table 3), compared with 92% with the NHC system. In capillaries, the high catalytic activity of both systems resulted in nearly complete conversion, and no by-products could be detected by GC. Small amounts of by-product were detected in all samples originating



Scheme 2. Sonogashira coupling of iodobenzene with phenylacetylene.

Table 3

Sonogashira cross-coupling of iodobenzene (0.1 mol) with phenylacetylene (0.15 mol), utilising triethylamine (0.15 mol) as the base in *N,N*-dimethylformamide/water (4:1). For bulk reactions, 20 mg of modified monolith was reacted in 1.0 mL of reaction solution; phen=1,10-phenanthroline, NHC=*N*-heterocyclic carbene; 80 °C.

Entry	Ligand	Solid support	Contact time/run time	Yield (%)
1	phen	Bulk	3 h	99
2	phen	Capillary	45 min/48 h	96
3	NHC	Bulk	3 h	91
4	NHC	Capillary	45 min/48 h	95

from the bulk experiments. Leaching of palladium from capillaries was minimal, ca. 4% of loading after 8 days of continual operation.

3. Conclusion

Polymer monoliths, present as a continuous phase filling capillaries and bonded to the internal surface, are promising new materials for solid supported catalysis in 250 μm internal diameter narrow bore microreactors. The performance of the flow-through microreactors included quantitative yields for the conversion of iodobenzene in the Suzuki–Miyaura reaction, and quantitative yields for Sonogashira coupling of *p*-iodoacetophenone with phenylacetylene. No significant differences were observed in the performance of the two different ligand systems. The methodology reported here represents a new strategy for the fabrication of capillary flow-through microreactors for cross-coupling reactions, and the application of CMS/DVB monolith is notable owing to the robust and unreactive nature of the polymer.

4. Experimental section

4.1. Materials

Commercially available chloromethylstyrene (CMS), divinylbenzene (DVB), 1-methylimidazole, 5-amino-1,10-phenanthroline and solvents were purchased from Sigma–Aldrich Pty. Ltd (Castle Hill, Australia). Divinylbenzene was purchased as a mixture of different isomers and the wanted isomer (1,4-divinylbenzene) was purified by distillation. 2,2-Azobis(2-isobutyronitrile) (AIBN) was purchased from MP Biomedicals Australasia Pty. Limited (Seven Hills, Australia) and recrystallised before usage. All solvents and mixtures used in the capillaries were filtered prior to use. Sonogashira bulk reactions were performed under an argon atmosphere using standard Schlenk techniques. Non-commercially available reaction products required for the calibration of the GC instruments were synthesised using conventional techniques.

4.2. General

Controlled solvent pumping was performed using a Harvard Apparatus model PHD 2000 (Holliston, Massachusetts, USA) twin syringe pump and 250 μL Hamilton (Reno, Nevada, USA) Gastight® glass syringes. All capillaries and syringes were connected using Upchurch Scientific (Oak Harbor, Washington, USA) capillary connections. Fused silica capillaries of internal diameter 250 μm with the outer surface coated with polyimide (Polymicro Technologies, Phoenix, Arizona) were heated using a Waters Millipore (Billerica, Massachusetts, USA) 112/WTC-120 temperature controlled column heater. Leading and trailing capillary sections were used to ensure that the whole microreactor was inside the column heater. Figure 3 shows the general experimental setup for flow-through microreactors. Characterisation utilised equipment housed in the Central Science Laboratory, University of Tasmania, including an FEI Quanta 600 MLA ESEM and an ELEMENT high resolution ICP-MS allowing detection down to 0.1 ppb; determination of void volume

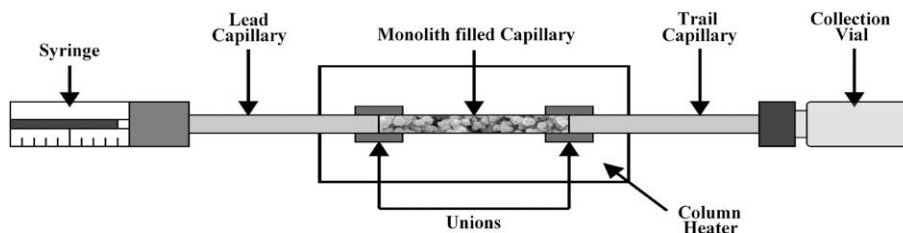


Figure 3. Experimental setup of flow reactions using a porous polymer monolith as a catalyst support structure.

fraction utilised a Sartorius SE2 Ultra-Microbalance ($0.1 \mu\text{g}$ readability).

The palladium content determinations of the bulk monolith were performed by Inductively Coupled Plasma Mass Spectroscopy (ICP-MS). For preparation, samples (50–100 mg) were digested in freshly prepared *aqua regia* (4 mL) for 18 h with sonication, diluted to a final mass of 30 g and indium (100 ppb) was added as an internal standard. The measurements were performed using an ELEMENT high resolution ICP-MS (Finnigan-MAT, Bremen, Germany) on the low resolution setting of $300 m/\Delta m$ at 10% valley definition; palladium was measured as a total of isotopes 105, 106 and 108.

Gas Chromatography–Mass Spectrometry (GC–MS) measurements were performed using a Varian 3800 gas chromatograph coupled with a triple quadrupole mass spectrometer or a Varian Star 3400 CX gas chromatograph coupled with a Varian Saturn 4D mass spectrometer. Gas Chromatography–Flame Ionisation Detection (GC–FID) measurements were performed on a Shimadzu GC-2014AFsc gas chromatograph equipped with a 25 m length (ID 0.32 mm) ID-BPX5 SGE capillary column. Standards were purchased or synthesised using conventional techniques, and mixtures with different concentration ratios were used for calibration.

Polymerisations were performed using a temperature controlled water bath.

4.2.1. Bulk material

The monolith was prepared by thoroughly mixing toluene (0.606 mL) and 1-dodecanol (1.53 mL), to which chloromethylstyrene (0.48 g), divinylbenzene (DVB, 0.72 g) and AIBN (12 mg) were added and the solution purged with nitrogen for 10 min prior to use. The monolith formed after heating at 70°C for 24 h was crushed and washed with tetrahydrofuran (THF) in a Soxhlet apparatus for 14 h and then dried in vacuo.

4.2.2. Ligand attachment in bulk material

4.2.2.1. 1-Methylimidazole. 1-Methylimidazole (0.30 g) was dissolved in chloroform and added to finely ground monolith (1.0 g). The mixture was stirred for 24 h at 50°C and the monolith recovered by vacuum filtration, resuspended in chloroform, stirred vigorously for 30 min and recovered again by filtration. The monolith was washed twice with chloroform, and dried in vacuo.

4.2.2.2. 5-Amino-1,10-phenanthroline. Monolith (1.0 g) was finely ground and added to a solution of 5-amino-1,10-phenanthroline (200 mg) in methanol (10 mL). The mixture was stirred for 18 h at 60°C and the monolith recovered by vacuum filtration, resuspended in methanol, stirred vigorously for 30 min and recovered again by filtration. The monolith was washed twice with methanol, and dried in vacuo.

4.2.3. Palladium attachment in bulk material

Modified monolithic material (100 mg) was added to a solution of $\text{PdCl}_2(\text{NCMe})_2$ (10 mg) in acetonitrile (2 mL) and the mixture was stirred for 18 h at room temperature. The monolith was recovered by vacuum filtration, resuspended in acetonitrile, stirred vigorously

for 30 min and recovered again by filtration. The monolith was washed twice with acetonitrile, and dried in vacuo.

4.3. General procedure for cross-coupling in bulk material

Modified monolith (20 mg) was placed in a 5 mL *Reacti-Vial* (Thermo Scientific, Rockford, USA) under argon along with 2 mL of the reaction mixture and heated at 80°C (unless stated otherwise). The catalyst was removed by filtration through a plug of cotton wool and the products analysed by GC.

4.4. Capillaries

Prior to the monolith attachment, the inner surface of capillaries was modified by briefly rinsing the capillary with acetone followed by 0.2 M NaOH ($2.0 \mu\text{L min}^{-1}$) for 2 h. The capillaries were washed with water, and rinsed with 0.2 M HCl ($2.0 \mu\text{L min}^{-1}$) for 2 h before being rinsed with water, followed by ethanol ($2.0 \mu\text{L min}^{-1}$) for 30 min and finally the surface modifying agent (solution of 20 wt % of 3-(trimethoxysilyl)propyl methacrylate in ethanol adjusted to pH 5, $0.25 \mu\text{L min}^{-1}$) was passed through the capillaries for 1 h.²² The capillaries were then washed with acetone and dried by passing air through the capillaries for 24 h.

Toluene (0.606 mL) and 1-dodecanol (1.53 mL) were thoroughly mixed and, to this, chloromethylstyrene (0.48 g), divinylbenzene (DVB, 0.72 g) and AIBN (12 mg) were added and the solution purged with nitrogen for 10 min prior to use. The capillaries were completely filled with the CMS/DVB pre-polymerisation mixture until no air bubbles were apparent, sealed at both ends and placed in a water bath at 70°C for 20 h. The monolith filled capillary was then flushed with THF ($2.0 \mu\text{L min}^{-1}$, 1 h).

4.4.1. Ligand attachment in capillaries

4.4.1.1. 1-Methylimidazole. The monolith filled capillary was flushed with chloroform for 30 min at 50°C ($2.0 \mu\text{L min}^{-1}$) before the undiluted 1-methylimidazole was pumped through the capillary at 50°C for 8 h ($0.5 \mu\text{L min}^{-1}$). The capillaries were then reversed and the solution was pumped for a further 18 h ($0.2 \mu\text{L min}^{-1}$). The capillary was washed with chloroform for 1 h ($2.0 \mu\text{L min}^{-1}$) to remove unreacted ligand from the monolith.

4.4.1.2. 5-Amino-1,10-phenanthroline. The monolith filled capillary was flushed with methanol for 30 min at 60°C ($2.0 \mu\text{L min}^{-1}$). A solution of 5-amino-1,10-phenanthroline (40 mg) in methanol (2 mL) was pumped through the capillary at 60°C for 8 h ($0.5 \mu\text{L min}^{-1}$), then the capillary was reversed and the solution was pumped for a further 18 h ($0.2 \mu\text{L min}^{-1}$). The capillary was washed with methanol for 1 h ($2.0 \mu\text{L min}^{-1}$) to remove unreacted ligand from the monolith.

4.4.2. Palladium attachment in capillaries

The monolith filled capillary was flushed with acetonitrile for 30 min at room temperature ($2.0 \mu\text{L min}^{-1}$). A solution of $\text{PdCl}_2(\text{CNMe})_2$ (10 mg) in acetonitrile (2 mL) was filtered to remove

any undissolved solids and passed through the capillary at room temperature for 8 h ($0.5 \mu\text{L min}^{-1}$), then the capillary was reversed and the solution was pumped for further 18 h ($0.2 \mu\text{L min}^{-1}$). The capillary was flushed with acetonitrile for 1 h ($2.0 \mu\text{L min}^{-1}$).

4.5. Determination of void volume fraction for CMS/DVB monolith after Pd/NHC functionalisation

A 5 cm piece of monolith filled capillary was flushed with acetone and dried by flushing with air ($2.0 \mu\text{L min}^{-1}$) overnight in a column heater at 80°C , sealed with a septum and weighed prior to filling with ethanol and reweighed. Removal of ethanol (flushing with air overnight at 80°C) confirmed an identical weight to that prior to addition of ethanol.

4.6. General procedure for cross-coupling reactions in capillaries

To equilibrate the microreactor prior to the reaction the capillary (20 cm) was flushed with the solvent for 1 h at room temperature ($2.0 \mu\text{L min}^{-1}$), then with a mixture of the solvent with 2 mmol of the base for 2 h at the required reaction temperature ($2.0 \mu\text{L min}^{-1}$) by placing the microreactor in the pre-heated column heater. The reaction mixtures were passed through the capillary at a flow rate of $0.1 \mu\text{L min}^{-1}$ (contact time of 45 min) and the product was collected from the opposing end in small glass sample vials. GC–MS or GC–FID analysis was performed to monitor the yields.

Acknowledgements

This research was supported under the Australian Research Council's Discovery Projects funding scheme (DP0663416) and the University of Tasmania Research College Board. Dr. R.M.G. is the recipient of ARC APD fellowship (DO0557803). We thank Dr. E.F. Hilder for useful discussions. Dr. N.W. Davies (GC–MS), Mr. P. Dove (mechanical workshop), Dr. K. Gömann (SEM), and Dr. A.T. Townsend (ICP–MS analysis), of the Central Science Laboratory, University of Tasmania, are acknowledged for technical support.

References and notes

- Ehrfeld, W.; Hessel, V.; Löwe, H. *Microreactors: New Technology for Modern Chemistry*; Wiley-VCH: Weinheim, 2000.
- Jähnisch, K.; Hessel, V.; Löwe, H.; Baerns, M. *Angew. Chem., Int. Ed.* **2004**, *43*, 406–446.
- Geyer, K.; Codée, J. D. C.; Seeberger, P. H. *Chem.—Eur. J.* **2006**, *12*, 8434–8442.
- Brivio, M.; Verboom, W.; Reinhoudt, D. N. *Lab Chip* **2006**, *6*, 329–344.
- Kobayashi, J.; Mori, Y.; Kobayashi, S. *Chem. Asian J.* **2006**, *22*–35.
- Watts, P.; Wiles, C. *Chem. Commun.* **2007**, 443–467.
- Mason, B. P.; Price, K. E.; Steinbacher, J. L.; Bogdan, A. R.; McQuade, D. T. *Chem. Rev.* **2007**, *107*, 2300–2318.
- Haerberle, S.; Zengerle, R. *Lab Chip* **2007**, *7*, 1094–1110.
- (a) Nikbin, N.; Watts, P. *Org. Process Res. Dev.* **2004**, *8*, 942–944; (b) Phan, N. T. S.; Brown, D. H.; Styring, P. *Green Chem.* **2004**, *6*, 526–532; (c) Baumann, M.; Baxendale, I. R.; Ley, S. V.; Nikbin, N.; Smith, C. D. *Org. Biomol. Chem.* **2008**, *6*, 1587–1593.
- Svec, F.; Huber, C. G. *Anal. Chem.* **2006**, *78*, 2100–2107.
- Xie, S.; Svec, F.; Fréchet, J. M. J. *J. Polym. Sci., Part A: Polym. Chem.* **1997**, *35*, 1013–1021.
- (a) Viklund, C.; Svec, F.; Fréchet, J. M. J.; Irgum, K. *Chem. Mater.* **1996**, *8*, 744–750; (b) Wang, Q. C.; Svec, F.; Fréchet, J. M. J. *Anal. Chem.* **1995**, *67*, 670–674.
- (a) Kobayashi, J.; Mori, Y.; Kobayashi, S. *Chem. Commun.* **2005**, 2567–2568; (b) Ueno, M.; Suzuki, T.; Naito, T.; Oyama, H.; Kobayashi, S. *Chem. Commun.* **2008**, 1647–1649.
- (a) Greenway, G. M.; Haswell, S. J.; Morgan, D. O.; Skelton, B. V.; Styring, P. *Sensors Actuator B* **2000**, *63*, 153–158; (b) He, P.; Haswell, S. J.; Fletcher, P. D. I. *Appl. Catal., A* **2004**, *274*, 111–114; (c) He, P.; Haswell, S. J.; Fletcher, P. D. I. *Lab Chip* **2004**, *4*, 38–41; (d) Basheer, C.; Hussain, F. S. J.; Lee, H. K.; Valiyaveetil, S. *Tetrahedron Lett.* **2004**, *45*, 7297–7300; (e) Comer, E.; Organ, M. G. *Chem.—Eur. J.* **2005**, *11*, 7223–7227; (f) Comer, E.; Organ, M. G. *J. Am. Chem. Soc.* **2005**, *127*, 8160–8167; (g) Shore, G.; Morin, S.; Organ, M. G. *Angew. Chem., Int. Ed.* **2006**, *45*, 2761–2766.
- Shi, G.; Hong, F.; Liang, Q.; Fang, H.; Nelson, S.; Weber, S. G. *Anal. Chem.* **2006**, *78*, 1972–1979.
- Miller, P. N.; Long, N. J.; de Mello, A. I.; Vilar, R.; Gee, A. *Chem. Commun.* **2006**, 546–548.
- Shore, G.; Morin, S.; Mallik, D.; Organ, M. G. *Chem.—Eur. J.* **2008**, *14*, 1351–1356.
- Bolton, K. F.; Canty, A. J.; Deverell, J. A.; Guijt, R. M.; Hilder, E. F.; Rodemann, T.; Smith, J. A. *Tetrahedron Lett.* **2006**, *47*, 9321–9324.
- Canty, A. J.; Deverell, J. A.; Gömann, A.; Guijt, R. M.; Rodemann, T.; Smith, J. A. *Aust. J. Chem.* **2008**, *61*, 630–633.
- Leadbeater, N. E.; Marco, M. *Chem. Rev.* **2002**, *102*, 3217–3273.
- Rohr, T.; Hilder, E. F.; Donovan, J. J.; Svec, F.; Fréchet, J. M. J. *Macromolecules* **2003**, *36*, 1677–1684.
- (a) Svec, F.; Fréchet, J. M. J. *Chem. Mater.* **1995**, *7*, 707–715; (b) Preinerstorfer, B.; Bicker, W.; Lindner, W.; Lämmerhofer, M. *J. Chromatogr., A* **2004**, *1044*, 187–199.
- Buchmeiser, M. R. *Polymer* **2007**, *48*, 2187–2198.
- (a) Schwarz, J.; Böhm, V. P. W.; Gardiner, M. G.; Grosche, M.; Herrmann, W. A.; Heringer, W.; Raudaschl-Sieber, G. *Chem.—Eur. J.* **2000**, *6*, 1773–1780; (b) Steel, P. G.; Teasdale, C. W. T. *Tetrahedron Lett.* **2004**, *45*, 8977–8980; (c) Byun, J. W.; Lee, Y. S. *Tetrahedron Lett.* **2004**, *45*, 1837–1840; (d) Kim, J.-H.; Jun, B.-H.; Byun, J.-W.; Lee, Y.-S. *Tetrahedron Lett.* **2004**, *45*, 5827–5831; (e) Kim, J.-H.; Kim, J.-W.; Shokouhimehr, M.; Lee, Y.-S. *J. Org. Chem.* **2005**, *70*, 6714–6720; (f) Schönfelder, D.; Nuyken, O.; Weberskirch, R. *J. Organomet. Chem.* **2005**, *690*, 4648–4655; (g) Altava, B.; Burguete, M. I.; García-Verdugo, E.; Karbass, N.; Luis, S. V.; Puzary, A.; Sans, V. *Tetrahedron Lett.* **2006**, *47*, 2311–2314; (h) Sommer, W. J.; Weck, M. *Adv. Synth. Catal.* **2006**, *348*, 2101–2113; (i) Lee, D.-H.; Kim, J.-H.; Jun, B.-H.; Kang, H.; Park, J.; Lee, Y.-S. *Org. Lett.* **2008**, *10*, 1609–1612.
- Karbass, N.; Sans, V.; Garcia-Verdugo, E.; Burguete, M. I.; Luis, S. V. *Chem. Commun.* **2006**, 3095–3097.
- Djakovitch, L.; Rollet, P. *Adv. Synth. Catal.* **2004**, *346*, 1782–1792.



Supported palladium catalysis using a heteroleptic 2-methylthiomethylpyridine–*N,S*–donor motif for Mizoroki–Heck and Suzuki–Miyaura coupling, including continuous organic monolith in capillary microscale flow-through mode

Roderick C. Jones^{a,*}, Allan J. Canty^{a,*}, Jeremy A. Deverell^{a,b}, Michael G. Gardiner^a, Rosanne M. Guijt^b, Thomas Rodemann^c, Jason A. Smith^a, Vicki-Anne Tolhurst^a

^a School of Chemistry, University of Tasmania, Private Bag 75, Hobart TAS 7001, Australia

^b Australian Centre for Research on Separation Science (ACROSS), Private Bag 75, Hobart TAS 7001, Australia

^c Central Science Laboratory (CSL), University of Tasmania, Private Bag 74, Hobart TAS 7001, Australia

ARTICLE INFO

Article history:

Received 16 April 2009

Received in revised form 24 June 2009

Accepted 2 July 2009

Available online 8 July 2009

Keywords:

Catalysis

Supported catalysis

Monolith

Flow-through microreactor

Pyridine

Methylthiomethylpyridine

ABSTRACT

Flow-through catalysis utilising (2-methylthiomethylpyridine)palladium(II) chloride species covalently attached to a macroporous continuous organic polymer monolith synthesised within fused silica capillaries of internal diameter 250 μm is described, together with related studies of ground bulk monolith compared with supported catalysis on Merrifield and Wang beads and homogeneous catalysis under identical conditions to bulk supported catalysis. The monolith substrate, poly(chloromethylstyrene-co-divinylbenzene), has a backbone directly related to Merrifield and Wang resins. The homogeneous precatalyst $\text{PdCl}_2(\text{L}^2)$ ($\text{L}^2=4-(4\text{-benzyloxyphenyl})-2\text{-methylthiomethylpyridine}$) contains the benzyloxyphenyl group on its periphery as a model for the spacer between the ' $\text{PdCl}_2(\text{N}\sim\text{S})$ ' centre and the polymer substituent of the resins and monolith. Suzuki–Miyaura and Mizoroki–Heck catalysis exhibit anticipated trends in reactivity with variation of aryl halide reagents for each system, and show that supported catalysis on beads and monolith gives higher yields than for homogeneous catalysis. The synthesis of 2-methylthiomethylpyridines is presented, together with crystal structures of 4-bromo-2-bromomethylpyridine hydrobromide, 4-(4-hydroxyphenyl)-2-methylthiomethylpyridine (L^1), $\text{PdCl}_2(\text{L}^1)$ and $\text{PdCl}_2(\text{L}^2)$. Hydrogen bonding occurs in 4-bromo-2-bromomethylpyridine hydrobromide as $\text{N-H}\cdots\text{Br}$ interactions, in 4-(4-hydroxyphenyl)-2-methylthiomethylpyridine as $\text{O-H}\cdots\text{N}$ to form chains, and in $\text{PdCl}_2(\text{L}^1)$ as $\text{O-H}\cdots\text{Cl}$ interactions leading to adjacent π -stacked chains oriented in an antiparallel fashion.

© 2009 Elsevier Ltd. All rights reserved.

1. Introduction

We have recently examined the ability of palladium(II) complexes of neutral 2-organothiomethylpyridine–*N,S* donor ligands to facilitate Mizoroki–Heck catalysis, in order to explore potential roles for heteroleptic ligands that may exhibit hemilabile activity during the catalytic cycle (Fig. 1).¹ The role of this ligand motif in palladium catalysis has also been explored by Chelucci for addition of diethylzinc to benzaldehyde^{2a,b} and for allylic substitution,^{2a} and by Canovese for trimerisation of dimethylacetylene dicarboxylate,^{2c} and the stoichiometric synthesis of fluoranthenes^{2d–f} and 2,4-diene-6-yne.^{2f} We have recently commenced the development of flow-through capillary³ and chip^{3b} based microreactors (100–

250 μm internal diameter) employing continuous macroporous organic monolith as support for palladium-catalysed Suzuki–Miyaura³ and Sonogashira^{3c} reactions. This flow-through

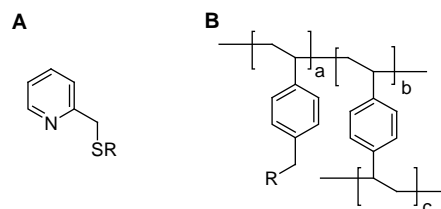


Figure 1. (A) 2-Organothiomethylpyridine ligands ($\text{R}=\text{Me}, \text{Ph}$). (B) Polymeric supports (i) Merrifield resin [$\text{R}=\text{Cl}$, typically 2–3% divinylbenzene (DVB) crosslinker]; (ii) Wang resin [$\text{R}=\text{p-BrCH}_2\text{C}_6\text{H}_4\text{O}$, typically 1% DVB]; and (iii) poly(chloromethylstyrene-co-divinylbenzene) monolith (CMS/DVB, $\text{R}=\text{Cl}$, typically CMS/DVB ratio $\sim 3:2$ and (CMS/DVB)/(porogen) ratio $\sim 2:3$ in preparations to give highly porous continuous polymeric monolith).

* Corresponding authors. Tel.: +61 3 6226 2162; fax: +61 3 6226 2858.

E-mail addresses: rcj@utas.edu.au (R.C. Jones), allan.canty@utas.edu.au (A.J. Canty).

technology to date has mainly utilised 1,10-phenanthroline and *N*-methylimidazole moieties,³ e.g., attack by 5-amino-1,10-phenanthroline at the benzylic chloride group of poly-(chloromethylstyrene-co-divinylbenzene) monolith [CMS/DVB, Fig. 1B(iii)], and with *N*-methylimidazole to most likely form palladium(II) carbene species on addition of PdCl₂(NCMe)₂.^{3c}

The principles of flow-through organic synthesis at the microscale level in capillaries and chips of internal dimensions <~1 mm have been elucidated recently.⁴ Advantages over conventional reaction systems include high surface/volume ratio leading to excellent heat transfer allowing higher concentrations and better selectivity in reactions, environmental and safety advantages from use of less solvent and reagents, synthesis of quantities of product sufficient for biological assay and integration with analysis instrumentation, significant advantages in simplicity of scale-out via multiple microreactors in parallel, together with applications in combinatorial chemistry. For metal catalysis in capillary⁵ and chip⁶ microreactors (internal diameter <~1 mm), innovative systems developed to date have included homogeneous catalysis in open tubes/channels,^{5c,e,6c} homogeneous with gas/liquid interface,^{6e} palladium as nanoparticles,^{5b} palladium^{5d} or gold^{5h} thin film on internal walls, palladium thin film together with complex,^{5g} palladium on metal oxide particles^{5a,6a,b} and on polysilane/metal oxide particles^{5f} and, in our recent reports, palladium complexes supported on continuous organic polymer monolith³ (e.g., Fig. 1B(iii)).^{3b,c} For supported catalysis, the latter approach avoids difficulties in filling capillaries with particles and in confining particles within capillaries, difficulties associated with swelling of polymer beads and compaction of particles if high pressure is required for flow-through operation. The monolith is fully anchored to walls during synthesis, the solid phase is uniform with absence of particles, and the void volume fraction for the monolith used in the present study is 79%. Organic polymer monoliths have high surface area and excellent flow-through properties.⁷

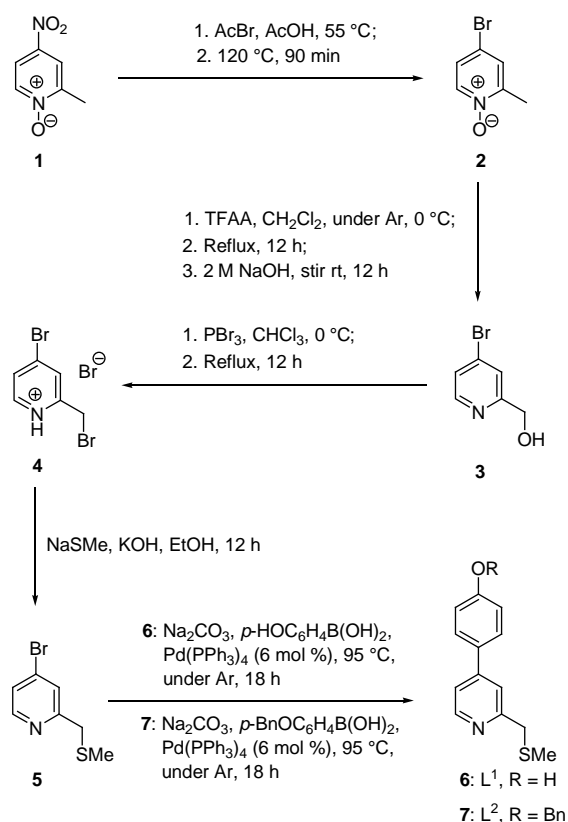
These promising developments are explored further here via the synthesis and characterisation of an *N,S*-heteroleptic motif known to be active in several palladium-catalysed processes and organic syntheses functionalised by *p*-HOC₆H₄ at the 4-position allowing covalent attachment to organic polymer supports (Fig. 1A; R=Me). Mizoroki–Heck and Suzuki–Miyaura cross-coupling activity is examined for [PdCl₂(*N,S*)] complexes, and compared with supported catalysis where the ligand is attached to Merrifield and Wang beads (Fig. 1B(i) and B(ii)), ground bulk monolith, and the dichloropalladium(II) complex of a closely related ligand as a homogeneous catalyst. To date, *N,S*-bidentate catalysts do not appear to have been explored in Suzuki–Miyaura catalysis.

2. Results and discussion

2.1. Ligand synthesis

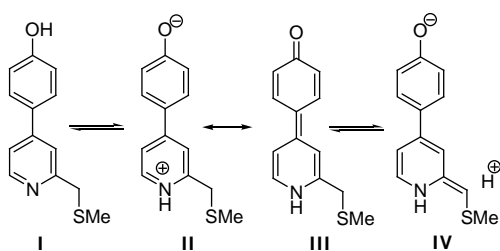
For the ligand motif A (R=Me) (Fig. 1) the pyridine and thiomethyl groups are anticipated to be unreactive towards the benzylic halide group of the organic polymers B. A suitable reagent containing this motif, and facilitating covalent attachment to the polymers, could include a hydroxyl group. To achieve this, functionalisation of the 4-position of the pyridine ring with a phenolic group was considered desirable in order to minimise any steric interaction between the phenolic group and the metal centre. The synthesis in Scheme 1 was developed based on the reaction of commercially available **1** with acetyl bromide to give **2** with slight modification of a reported method⁸ (glacial acetic acid as solvent rather than neat reagents) to increase the yield from 31 to 91%; employing the protocol of van den Heuvel et al. (trifluoroacetic

anhydride to generate 4-bromo-2-trifluoroacetoxyethylpyridine, followed by hydrolysis with NaOH)^{9a} for synthesis of the 5-bromo analogue to obtain known compound **3** (62%); bromination of **3** to give **4** (87%), a modification of the protocol of Canovese et al. (reaction with thiomethoxide)¹⁰ for the synthesis of related compounds to give **5** (72%); and Suzuki–Miyaura chemistry to give **6** (90%; overall yield 32%). Compound **7** was synthesised as a model for the benzyl ether connectivity between ligand and the polymer backbone (overall yield 30%), and palladium(II) complexes of **6** and **7**, PdCl₂(L¹) (**8**) and PdCl₂(L²) (**9**), respectively, were obtained on reaction with PdCl₂(NCMe)₂ under reaction conditions identical to those used to add palladium(II) to polymers functionalised with compound **6**.



Scheme 1. Synthesis of 2-methylthiomethylpyridines **6** and **7**.

NMR spectra were readily interpreted, noting that **6** alone, containing the phenol group, undergoes deuterium exchange of the methylene group in (CD₃)₂CO providing that D₂O is present, attributed to tautomeric and mesomeric effects encouraging exchange via **IV**, which is illustrated in Scheme 2; X-ray structural data (see below) indicate little if any contribution from the 'pyridone' form **III** in the solid state.



Scheme 2.

2.2. X-ray crystal structures of reagents and palladium(II) complexes as models for the supported catalyst

Aspects of the structure of reagents **4**, **6** and complexes **8**, **9** are illustrated in Figures 2 and 3. The compounds containing a phenolic hydroxy group (as well as the hydrobromide salt **4**) exhibit hydrogen bonding, for which refinement of the hydrogen atom positions indicate N–H⋯Br[−] interaction in **4**, O–H⋯N in **6** and O–H⋯Cl in **8**. The N⋯Br distance in **4**, 3.139(7) Å, is similar to that reported for 2,6-bis(bromomethyl)pyridinium bromide, 3.242(2) Å.¹¹ Other close bromide contacts are a π -face of a pyridyl ring, a methylene proton, a 6H-pyridyl and Br of a 2-CH₂Br substituent. Molecules of **6** form linear polymeric chains through O–H⋯N hydrogen bonding involving the pyridyl nitrogen and phenolic substituent. These arrange themselves into parallel running stacks displaying limited π -stacking between adjacent pyridyl and aryl rings owing to disruptions brought about by the positioning of the methylene protons and the torsion angle of aromatic rings in the molecule. The O⋯N distance (2.700(3) Å) is similar to that reported for 4-(3,5-dimethylphenyl)-3,5-dimethylphenol, 2.721(2) Å.¹² Consistent with the presence of C–O–H⋯N in **6**, rather than C=O⋯H–N that could be anticipated for tautomer **III**, the C–O and inter-ring C–C distances, 1.353(3) and 1.476(3) Å, respectively, are both much longer than quinoidal structures [\sim 1.222 and \sim 1.349 Å].¹³ The ring–ring dihedral angle, 29.9(2)°, is also supportive of the absence of inter-ring multiple bonding.

Complexes **8** and **9** exhibit distorted square planar coordination geometries (Fig. 3). As for the free ligand **6**, molecules of **8** form hydrogen-bonded linear polymeric chains in the solid state, though these involve OH⋯Cl interactions involving a chloride ligand (trans to S) and the phenolic substituent. In contrast to **6**, these polymeric strands stack antiparallel into dimeric units involving offset face–face π -stacking that is aided by the near planar aryl–pyridyl moieties allowing an intermolecular distance of 3.43(2) Å. Palladium coordination planes between paired sets of chains are close to being directly aligned, but the Pd⋯Pd contact of 3.711(3) Å indicates the absence of a metal–metal interaction (van der Waals radius 1.63 Å).¹⁵ The polymeric chain structure is similar to those reported

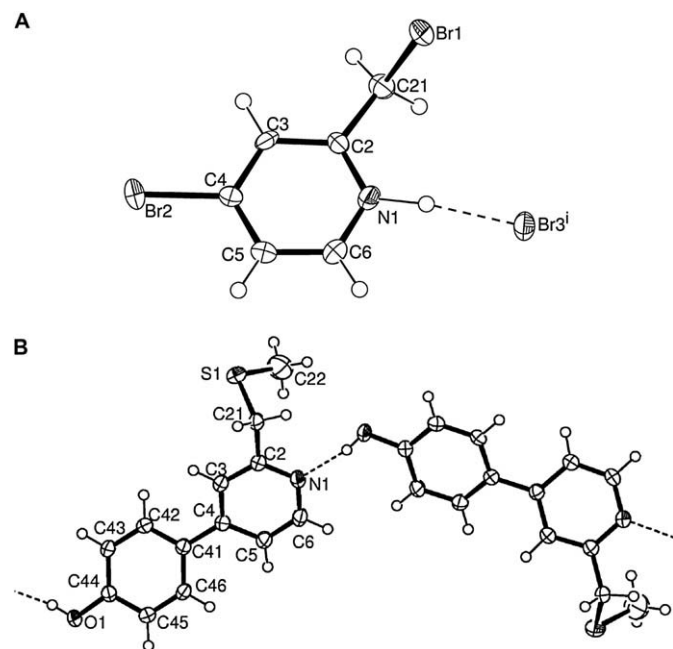


Figure 2. Molecular structures of **4** (A) [symmetry code: (i) $-x-1/2, y+1/2, -z+1/2$] and **6** (B). For **6**, the partial packing diagram shows a portion of the linear polymeric strands resulting from hydrogen bonding.

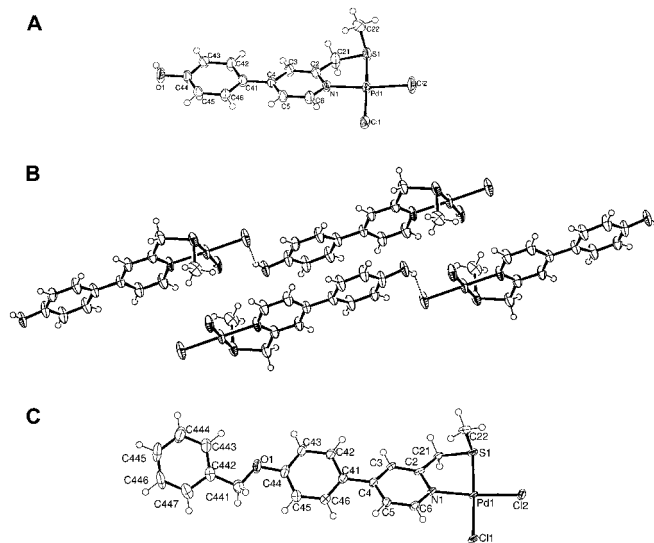


Figure 3. Molecular structures of PdCl₂(L¹) (**8**) (A) and PdCl₂(L²) (**9**) (C). For **8**, the partial packing diagram (B) shows the antiparallel arrangement of the linear polymeric strands resulting from hydrogen bonding. Palladium–donor atom distances [N1 2.039(8), 2.037(3); S1 2.247(3), 2.2617(9); Cl1 (trans to S1) 2.321(3), 2.3305(9); Cl2 (trans to N1) 2.299(3), 2.2967(10) Å, for **8** and **9**, respectively] and chelate angles [84.5(2)°, 84.58(6)°] are similar to values reported for related Pd(II) complexes.¹⁴ The pyridyl mean plane forms a dihedral angle of 16.2(4)° (**8**) and 18.9(1)° (**9**) with the mean metal coordination plane, the aryl/pyridyl inter-ring dihedral angles are 8.1(7)° (**8**) and 19.8(2)° (**9**), and the C–O and inter-ring C–C distances of both **8** and **9** are within 1 esd of those for ligand **6**.

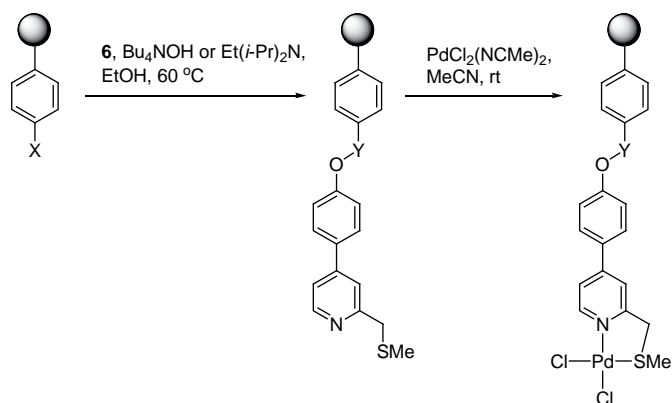
for ‘[ECE]’ (E=N, S) pincer complexes having a hydroxyl group hydrogen-bonded to a chloro-ligand in MCl{C₆H₂(CH₂NMe₂)₂-2,6-OH-4} (M=Pt,^{16a,b} Pd^{16c}) and PdCl{C₆H₂(CH₂SPh)₂-2,6-OH-4}^{16c}, which have O–H⋯Cl with O⋯Cl 3.1040(18)–3.127(8) Å compared with 3.002(8) Å in **8**.

For complex **9**, the linear polymeric chains noted for **6** and **8** are absent as hydrogen bonding is absent. Some packing features are retained in that there is rough alignment of the, now, quite extended polyaromatic ligand framework in the overall structure. π -Stacking between molecules is limited to the central aryl rings (3.632 Å) that extends indefinitely. The limited π -stacking, in relation to complex **8**, is presumably due to the influences of the greater torsion angle between the pyridyl and aryl rings (19.8(2)°) and the incorporation of the saturated benzylic carbon centre of the ether substituent. Coplanarity of metal coordination planes (3.633(2) Å) within these stacks is noted, however, the metal centres are offset somewhat, giving a metal–metal separation of 5.133(1) Å.

2.3. Formation of polymer with supported precatalyst sites

As illustrated in Scheme 3, commercially obtained polymer beads were treated with reagent **6** in ethanol at 60 °C in the presence of excess base (*i*-Pr₂NEt or Bu₄NOH). Similar results were obtained for both bases. Scanning electron micrographs of Merrifield beads indicated considerable bead fragmentation after this treatment, as reported for a recent study of catalyst immobilisation,¹⁷ but Wang beads were unaffected. Ground bulk monolith and capillaries filled with continuous monolith, obtained as documented,^{3c} were treated with ligand **6** in a similar manner, following the documented protocol,^{3c} and for capillaries involved flow-through of the solution in each direction. The base Bu₄NOH was used for ligand attachment to monolith as it promotes higher solubility of **6** than does *i*-Pr₂NEt, and thus minimises the possibility of precipitation. Subsequently, the systems were treated with

$\text{PdCl}_2(\text{NCMe})_2$ under identical conditions, matching that for the synthesis of $\text{PdCl}_2(\text{L}^1)$ (**8**) and $\text{PdCl}_2(\text{L}^2)$ (**9**). A scanning electron micrograph of bulk monolith after attachment of ligand and palladium (Fig. 4) is unchanged in appearance from that prior to attachment, and appears similar to monolith obtained on attachment of other ligands.^{3c} Palladium analysis showed levels of 0.75 wt % (Merrifield resin), 0.32 wt % (Wang) and 1.19 wt % (bulk monolith). Analysis for capillaries was not attempted as essentially identical conditions were used for functionalisation of the monolith in bulk and in capillaries. The capillaries (internal diameter 250 μm , length 30 cm) were cut to 10 cm lengths for catalytic studies.



Scheme 3. Functionalisation of Merrifield resin and monolith ($\text{X}=\text{CH}_2\text{Cl}$, $\text{Y}=\text{CH}_2$) or Wang resin ($\text{X}=\text{CH}_2\text{OC}_6\text{H}_4\text{CH}_2\text{Br}$, $\text{Y}=\text{CH}_2\text{OC}_6\text{H}_4\text{CH}_2$).

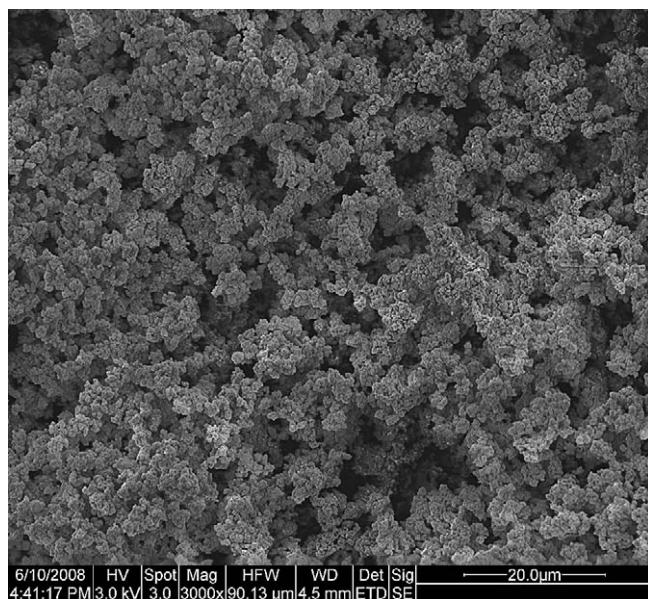


Figure 4. Scanning electron micrograph of ground bulk monolith after attachment of ligand and palladium ($\times 3000$, accelerating voltage 3.0 kV).

2.4. Studies of Suzuki–Miyaura and Mizoroki–Heck catalysis

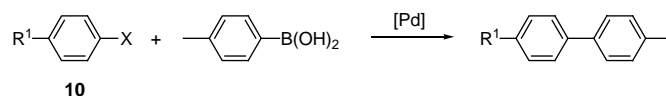
In addition to the supported systems, catalysis using the model complex $\text{PdCl}_2(\text{L}^2)$ (**9**) was undertaken as the ligand L_2 contains the same benzyl ether linker on its periphery as that present in the ligand motif attached to solid supports. Direct comparison between catalysis for this complex, the resins, bulk monolith and capillary systems is problematic, mainly due to the different experimental protocol required for flow-through studies. Microreactors have a much higher effective mol % precatalyst in the flow-through architecture, as noted previously.¹⁷ Thus, for the 10 cm length

capillary of internal diameter 250 μm filled with monolith of mass 1.76 mg and 1.19 wt % Pd, a void volume fraction of 79% results in an effective mol % Pd of $\sim 51\%$ for an aryl halide concentration of 0.1 M.

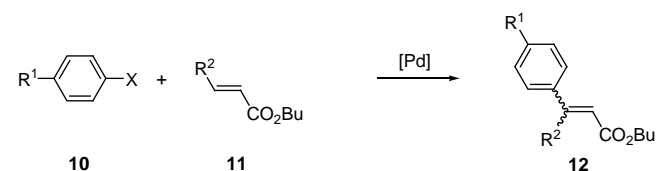
However, an approximate comparison between beads, bulk monolith and homogeneous catalysis is feasible as the homogeneous catalysis can be conducted using the same mol % precatalyst. To ascertain whether palladium was not simply adhered to the solid phase, support materials that had not been treated in any way, or treated with ligand only, or treated with $\text{PdCl}_2(\text{NCMe})_2$ only followed by flushing, did not act as catalysts in Mizoroki–Heck reactions, and for these trials palladium could not be detected in the supports by ICP-MS analysis.

Reactions studied are illustrated in Scheme 4 and results are presented in Tables 1 and 2. For beads, bulk monolith and homogeneous systems the preferred base Na_2CO_3 was used, but for capillaries Et_3N was used as Na_2CO_3 has low solubility that may lead to blockages.

Suzuki–Miyaura catalysis



Mizoroki–Heck catalysis



Scheme 4.

For both Suzuki–Miyaura and Mizoroki–Heck reactions using beads and bulk monolith (Table 1), similar results are obtained for each support, with trends on variation of reagent as expected, in particular aryl iodides > bromides > chlorides, e.g., for Suzuki–Miyaura ($\text{PhI} > \text{PhBr} > p\text{-AcC}_6\text{H}_4\text{Cl}$, entries 1–3); and for Mizoroki–Heck ($\text{PhI} > \text{PhBr} > p\text{-TolBr} > p\text{-AcC}_6\text{H}_4\text{Cl}$ and PhCl , entries 5–9, and $\text{PhI} > \text{PhBr}$, entries 10 and 11). High yields of the trisubstituted Mizoroki–Heck product were obtained (entries 10 and 11). Moderate activation of 4-chloroacetophenone in the Mizoroki–Heck reaction (entry 3) indicates that further development of catalyst design may lead to improved aryl chloride activation. For both catalysis systems, the solid supports provide higher yield than comparable homogeneous catalysis (entries 2, 4 and 6, 12), and the homogeneous systems provide lower yields than widely used phosphine systems.¹⁸

Detailed comparison of values obtained from different bulk supports is difficult in view of the differing mol % of precatalyst and differences in anticipated access of reagents to precatalyst sites, e.g., observed fracture of the Merrifield beads compared with unaltered appearance of Wang beads, and anticipated better access to interior sites for monolith than for beads. However, for bulk reactions the trend in loadings (monolith > Merrifield > Wang) is reflected in the same trend in yield (entries 3, 5–7, 10). If it is assumed that precatalyst sites have identical activities for the three supported systems, trends in turnover number (TON) may reflect the accessibility of sites. Thus, it is of interest to note that, except where yields are >99% or very low (entry 9, Wang entries 3 and 8), turnover numbers (TON, moles of product/moles of palladium) for Merrifield and Wang beads are greater than those for monolith (entries 3, 6–8, 11), even when the yield is lower for beads (entries 3 and 8). Leaching of palladium could not be detected by ICP-MS analysis above background levels that were obtained in blank runs using reagents and the three supports without precatalyst.

Table 1
Comparison of Suzuki–Miyaura and Mizoroki–Heck catalysis for Merrifield and Wang beads and ground monolith with anchored palladium(II) precatalyst, and homogeneous catalysis using PdCl₂(L²) (**9**) as precatalyst^a

Entry	X	10 (R ¹)	11 (R ²)	Yield (%)			TON
				Merrifield	Wang	Monolith	
Suzuki–Miyaura, beads and monolith							
1	I	H		>99	>99	>99	8512, 19,950, 5365
2	Br	H		>99	85	>99	8512, 16,958, 5365
3	Cl	Ac		8	<1	12	681, <199, 644
Suzuki–Miyaura, homogeneous, identical mol % loading as analogous supported catalysis							
4	Br	H		57	6.4	64	4852, 1227, 3434
Mizoroki–Heck, beads and monolith							
5	I	H	H	>99	>99	>99	8512, 19,950, 5365
6	Br	H	H	95	86	93	8086, 17,157, 4989
7	Br	Me	H	85	70	78	7235, 13,965, 4185
8	Cl	Ac	H	12	<1	15	1021, <199, 804
9	Cl	H	H	<1	<1	1	<85, <199, 54
10	I	H	Ph	>99	>99	>99	8512, 19,950, 5365
11	Br	H	Ph	85	72	87	7235, 14,364, 4668
Mizoroki–Heck, homogeneous, identical mol % loading as analogous supported catalysis							
12	Br	H	H	6	<1	11	511, <199, 590

^a Reagents shown in Scheme 3. Suzuki–Miyaura conditions: ArX (**10**, 0.3 M), *p*-TolB(OH)₂ (0.45 M), polymer (5 mg), Na₂CO₃ (0.6 M) in DMF/H₂O (3:1, 10 mL), 80 °C, 24 h. Mizoroki–Heck conditions: ArX (**10**, 0.3 M), alkene (**11**, 0.45 M), polymer (5 mg), Na₂CO₃ (0.6 M), Bu₄NCl (0.45 M) in DMA (10 mL), 120 °C, 48 h. Merrifield beads and homogeneous catalysis: 0.012 mol % Pd. Wang beads and homogeneous catalysis: 0.005 mol % Pd, monolith and homogeneous catalysis: 0.019 mol % Pd.

Table 2
Suzuki–Miyaura and Mizoroki–Heck catalysis in capillary microreactors^a

Entry	X	10 (R ¹)	11 (R ²)	Yield (%)
Suzuki–Miyaura				
1	I	H		96
2	Br	H		65
Mizoroki–Heck				
3	I	H	H	98
4	Br	H	H	45

^a ~39 min contact time of reagent solution within capillaries of internal diameter 250 μm, length 10 cm, flow rate 0.1 μL min⁻¹; ~51 mol % Pd. Suzuki–Miyaura conditions: ArX (**10**, 0.10 M), *p*-TolB(OH)₂ (0.15 M), Et₃N (0.2 M) in DMF/H₂O (3:1), 80 °C, 24 h. Mizoroki–Heck conditions: ArX (**10**, 0.10 M), alkene (**11**, 0.15 M), Et₃N (0.2 M) in DMA, 120 °C, 24 h.

Results for the bulk studies demonstrate that the *N,S*-bidentate system facilitates catalysis. The capillary microreactor was examined for reaction of iodo- and bromobenzene, and the same trend in reactivity was observed for both catalyses (entries 1, 2 and 3, 4) (Table 2), illustrating the feasibility of this microreactor technology. Assuming that the palladium loading is identical to that of the bulk monolith, leaching of Pd over a 24 h period corresponded to ~0.05% for the Suzuki–Miyaura and Mizoroki–Heck reactions.

3. Experimental section

3.1. General techniques

All solvents were dried and distilled by conventional methods prior to use. 4-Nitro-2-picoline *N*-oxide (Oakwood), 4-hydroxyphenylboronic acid (Boron Molecular), (chloromethyl)polystyrene (Merrifield Resin, 200–400 mesh, 37–74 μm) (Fluka), (4-bromomethyl)phenoxyethylpolystyrene (Wang Resin, 100–200 mesh, 74–149 μm) (Novabiochem), ultra high purity argon (BOC Gases) and

other reagents (Aldrich) were used as received. Bulk monolith and fused silica capillaries (internal diameter 250 μm, outer surface coated with polyimide (Polymicro Technologies, Phoenix, Arizona)) filled with monolith bonded to the walls were prepared as reported.^{3c} Bulk monolith was ground, resulting in a range of particle sizes up to ~200 μm. NMR spectra were recorded at 20 °C on a Varian Mercury Plus 300 spectrometer and chemical shifts are reported in parts per million relative to TMS; assignments were facilitated by gHMBC, gHMQC and gCOSY techniques. For **6** and **8** the C₆H₄ group atoms are denoted H4b and H4c; for **7** and **9** the phenyl group atoms are denoted H4b–d2. Microanalyses, LSIMS mass spectra, scanning electron micrographs (FEI Quanta 600 MLA ESEM) and ICP-MS (ELEMENT high resolution) allowing detection down to 0.1 ppb were performed by the Central Science Laboratory. GC–MS measurements were performed using a Varian 3800 gas chromatograph coupled with a triple quadrupole mass spectrometer; GC–FID measurements were performed on a Shimadzu GC-2014 AFsc gas chromatograph equipped with a 25 m length (ID 0.32 mm) ID-BPX5 SGE capillary column. Standards were purchased or synthesised using conventional techniques, and mixtures with different concentration ratios were used for calibration. The mass of monolith in a capillary was determined using a Sartorius SE2 Ultra-Microbalance (0.1 μg readability), and the void volume fraction was determined as described previously.^{3c} For palladium analyses, samples (50–100 mg) were digested in freshly prepared *aqua regia* (4 mL) for 18 h with sonication, diluted to a final mass of 30 g, indium (100 ppb) was added as an internal standard, and measurements performed on the low resolution setting of 300m (Δm)⁻¹ at 10% valley definition, and palladium was measured as a total of isotopes 105, 106 and 108.

For microreactor catalysis, as reported,^{3c} controlled solvent pumping was performed using a Harvard Apparatus model PHD 2000 (Holliston, Massachusetts, USA) twin syringe pump and 250 μL Hamilton (Reno, Nevada, USA) Gastight® glass syringes. All capillaries and syringes were connected using Upchurch Scientific

(Oak Harbor, Washington, USA) capillary connections. Capillaries were heated using a Waters Millipore (Billerica, Massachusetts, USA) 112/WTC-120 temperature controlled column heater. Leading and trailing capillary sections were used to ensure that the whole microreactor was inside the column heater.

3.2. Synthetic procedures

3.2.1. 4-Bromo-2-methylpyridine *N*-oxide (**2**)

Acetyl bromide (34.6 mL, 0.46 mol) was added in small portions to a solution of 4-nitro-2-picoline *N*-oxide (2.47 g, 0.02 mol) in glacial AcOH (35 mL) at 55 °C. The resulting solution was heated to 120 °C with stirring for 2.5 h in air. After cooling to rt the solution was poured into crushed ice and made basic with K₂CO₃ and the product extracted with CH₂Cl₂ (4×30 mL). The combined organic phases were washed with brine, and dried over Na₂SO₄. The solvent was removed in vacuum resulting in a pale orange oil, which was used without further purification (2.75 g, 91%). ¹H NMR (300 MHz, CDCl₃): δ 8.11 (d, *J*=6.9 Hz, 1H, H₆), 7.41 (d, *J*=2.4 Hz, 1H, H₃), 7.27 (dd, *J*=6.9, 2.4 Hz, 1H, H₅), 2.48 (s, 3H, CH₃); ¹³C{¹H} NMR (75.4 MHz, CDCl₃): δ 150.6 (C₂), 140.2 (C₆), 129.6 (C₃), 127.0 (C₅), 119.4 (C₄), 17.9 (CH₃). MS (EI) *m/z* 187 [M⁺], [¹²C₆H₆⁷⁹Br¹⁴N¹⁶O 187]. HRMS (EI) *m/z* [M–H]⁺ 186.96339, [C₆H₆BrNO]⁺ requires 186.96328.

3.2.2. 4-Bromo-2-hydroxymethylpyridine (**3**)

Under argon, TFAA (9.24 mL, 66.48 mmol) was added dropwise (with extreme caution) to a solution of **2** (2.50 g, 13.30 mmol) in dry CH₂Cl₂ (40 mL) at 0 °C, and the resulting solution refluxed for 12 h with stirring. After cooling to rt the TFAA and CH₂Cl₂ were removed in vacuum to give a dark yellow oil; CH₂Cl₂ (40 mL) was added followed by 2 M NaOH with vigorous stirring until the resulting biphasic mixture was basic (pH 12–14). Vigorous stirring was continued for 12 h under Ar, and the mixture extracted with CH₂Cl₂ (3×30 mL). The organic phase was washed with brine and dried over Na₂SO₄. The solvent was removed in vacuum resulting in a dark brown oil, which was used without further purification. (1.55 g, 62%). ¹H NMR (300 MHz, CDCl₃): δ 8.36 (d, *J*=5.4 Hz, 1H, H₆), 7.52 (dd, *J*=1.8 Hz, 1H, H₃), 7.39 (dd, *J*=5.4, 1.8 Hz, 1H, H₅), 4.75 (s, 2H, CH₂), 4.16 (s, 1H, OH); ¹³C{¹H} NMR (75.4 MHz, CDCl₃): δ 161.1 (C₂), 149.2 (C₆), 134.1 (C₄), 126.0 (C₅), 124.3 (C₃), 63.9 (CH₂). MS (EI) *m/z* 187 [M–H]⁺, [¹²C₆H₅⁷⁹Br¹⁴N¹⁶O 186]. HRMS (EI) *m/z* [M–H]⁺ 185.95554, [C₆H₅BrNO]⁺ requires 185.95545.

3.2.3. 4-Bromo-2-bromomethylpyridine hydrobromide (**4**)

PBr₃ (5.55 mL, 59.03 mmol) was added dropwise (with extreme caution) to a solution of **3** (1.85 g, 9.84 mmol) in dry CHCl₃ (50 mL) at 0 °C, and the resulting solution was heated to reflux for 12 h with vigorous stirring. After cooling to rt the suspension was poured into crushed ice and made basic (pH ~ 14) with K₂CO₃, and the product was extracted with CH₂Cl₂ (4×50 mL). The organic phase was washed with brine and dried over Na₂SO₄. The solvent was removed in vacuum, and the resulting pale brown oil was then dissolved in Et₂O and with vigorous stirring; HBr/AcOH solution was added dropwise to precipitate an off white solid, which was collected by filtration and washed thoroughly with Et₂O (2.84 g, 87%). Single crystals for X-ray and elemental analysis were grown from vapour diffusion of Et₂O into MeNO₂. ¹H NMR (300 MHz, CD₃OD): δ 8.70 (d, *J*=6.3 Hz, 1H, H₆), 8.42 (d, *J*=2.1 Hz, 1H, H₃), 8.21 (dd, *J*=6.3, 2.1 Hz, 1H, H₅), 4.81 (s, 2H, CH₂); ¹³C{¹H} NMR (75.4 MHz, CD₃OD): δ 153.4 (C₂), 144.1 (C₄), 143.7 (C₆), 130.9 (C₅), 130.1 (C₃), 24.8 (CH₂). MS (EI) *m/z* 251 [M–HBr]⁺, [¹²C₆H₅⁷⁹Br₂¹⁴N 251]. HRMS (EI) *m/z* [M–HBr]⁺ 248.87875, [C₆H₅Br₂N]⁺ requires 248.87887. Anal. Calcd for C₆H₅Br₂N: C, 21.72; H, 1.82; N, 4.22. Found: C, 22.12; H, 1.78; N, 4.20.

3.2.4. 4-Bromo-2-methylthiomethylpyridine (**5**)

A stirred solution of NaOMe (0.35 g, 4.97 mmol) in dry EtOH (50 mL) was added dropwise over 10 min to a stirred solution of **4** (1.50 g, 4.52 mmol) and powdered KOH (0.76 g, 13.56 mmol) in dry EtOH (100 mL). Stirring was continued for 12 h after which the EtOH was removed in vacuum resulting in a pale brown oil. Water (25 mL) was added and the product extracted with CH₂Cl₂ (3×25 mL). The organic phase was washed with brine and dried over Na₂SO₄. The solvent was removed in vacuum to give a pale brown oil, which was purified by column chromatography [40% EtOAc in hexanes], to give a pale yellow oil (0.75 g, 72%). ¹H NMR (300 MHz, CDCl₃): δ 8.34 (d, *J*=5.4 Hz, 1H, H₆), 7.56 (d, *J*=1.8 Hz, 1H, H₃), 7.34 (dd, *J*=5.4, 1.8 Hz, 1H, H₅), 3.76 (s, 2H, CH₂), 2.06 (s, 3H, SCH₃); ¹³C{¹H} NMR (75.4 MHz, CD₃OD): δ 159.1 (C₂), 148.6 (C₆), 132.7 (C₄), 125.4 (C₃), 124.4 (C₅), 38.5 (CH₂), 14.2 (SCH₃). MS (EI) *m/z* 218 [M]⁺, [¹²C₇H₈⁷⁹Br¹⁴N³²S 218]. HRMS (EI) *m/z* [M]⁺ 216.95611, [C₇H₈BrNS]⁺ requires 216.95608.

3.2.5. 4-(4-Hydroxyphenyl)-2-methylthiomethylpyridine (**6**)

Pd(PPh₃)₄ (0.397 g, 5 mol %) and **5** (1.50 g, 6.88 mmol) in toluene (28.0 mL) were treated with a degassed solution of Na₂CO₃ (1.60 g, 13.11 mmol, 2.2 equiv) in H₂O (14.0 mL), followed by a solution of *p*-HOC₆H₄B(OH)₂ (1.42 g, 10.32 mmol) in MeOH (10.0 mL). The resulting mixture was stirred at 95 °C under Ar; after 6 h another 0.5 equiv of *p*-HOC₆H₄B(OH)₂ and a further 1 mol % of catalyst was added to the solution, and after 12 h the solution was cooled to rt and treated with a saturated solution of Na₂CO₃. The product was extracted with CH₂Cl₂ (3×25 mL), the organic phase was washed with saturated NaCl solution, dried over Na₂SO₄ and the solvent removed in vacuum to give a dark oil. The oil was dissolved in CH₂Cl₂ (5 mL) and hexane added to precipitate a tan solid (1.56 g, 98%). The product was recrystallised from hot EtOH to give a dark brown solid (1.43 g, 90%). ¹H NMR (300 MHz, (CD₃)₂CO): δ 9.01 (s, 1H, OH), 8.47 (dd, *J*=5.1, 1.5 Hz, 1H, H₆), 7.66 (m, 3H, H₃, H_{4b}), 7.47 (dd, *J*=5.1, 1.5 Hz, 1H, H₅), 6.83 (d, *J*=8.7 Hz, 2H, H_{4c}), 3.82 (s, 2H, CH₂), 2.08 (s, 3H, SCH₃); ¹³C{¹H} NMR (75.4 MHz, (CD₃)₂CO): δ 159.7 (C₂), 158.1 (COH), 149.8 (C₆), 149.7 (C₄), 128.7 (C_{4a}), 128.4 (C_{4b}), 119.8 (C₃), 119.0 (C₅), 116.3 (C_{4c}), 39.8 (CH₂), 14.5 (SCH₃). MS (APCI) *m/z* 232 [M+H]⁺, [¹²C₁₃H₁₄¹⁴N¹⁶O³²S 232]. HRMS (EI) *m/z* [M+H]⁺ 232.07941, [C₁₃H₁₄NOS]⁺ requires 232.07961. Anal. Calcd for C₁₃H₁₃NSO: C, 67.50; H, 5.66; N, 6.06. Found: C, 67.54; H, 5.62; N, 6.11.

3.2.6. 4-(4-Benzoyloxy)-2-methylthiomethylpyridine (**7**)

This compound was prepared from **5** (1.50 g, 6.88 mmol) and 4-BnOC₆H₄B(OH)₂ (2.35 g, 10.32 mmol) using a similar procedure to that described for **6**. The product was purified by column chromatography (40% EtOAc in hexanes) to remove contamination by BnOPh to give a pale yellow oil (1.88 g, 85%). ¹H NMR (300 MHz, (CD₃)₂SO): δ 8.53 (d, *J*=5.4 Hz, 1H, H₆), 7.76 (dd, *J*=5.4, 1.8 Hz, 1H, H₅), 7.60 (d, *J*=8.7 Hz, 2H, H_{4b}), 7.56 (d, *J*=1.8 Hz, 1H, H₃), 7.46–7.34 (m, 5H, H_{4b2}, H_{4c2}, H_{4d2}), 7.07 (d, *J*=8.7 Hz, 1H, H_{4c}), 5.12 (s, 2H, OCH₂), 3.86 (s, 2H, SCH₂), 2.10 (s, 3H, SCH₃); ¹³C{¹H} NMR (75.4 MHz, (CD₃)₂SO): δ 160.1 (C₂), 158.9 (C_{4d}), 149.4 (C₆), 149.1 (C₄), 136.8 (C_{4a2}), 128.9 (C_{4b}), 128.6 (C_{4c2}), 128.4 (C_{4d2}), 127.7 (C_{4b2}), 120.7 (C₅), 119.8 (C₃), 115.7 (C_{4c}), 70.0 (OCH₂), 40.0 (SCH₂), 22.9 (SCH₃). MS (EI) *m/z* 321 [M]⁺, [¹²C₂₀H₁₉¹⁴N¹⁶O³²S 321]. HRMS (EI) *m/z* [M]⁺ 321.11868, [C₂₀H₁₉NOS]⁺ requires 321.11873. Anal. Calcd for C₁₃H₁₃NSO: C, 67.50; H, 5.66; N, 6.06. Found: C, 67.54; H, 5.62; N, 6.11.

3.2.7. Dichloro[4-(4-hydroxyphenyl)-2-methylthiomethylpyridine]palladium(II) (**8**)

PdCl₂(NCMe)₂ (0.15 g, 0.64 mmol) was added to a stirred suspension of **6** (0.18 g, 0.77 mmol) in dry MeCN (30 mL) and the brown suspension was stirred for 12 h at 50 °C. The solvent was

then reduced in vacuum to ~5 mL and Et₂O was added to precipitate the title complex as a yellow solid, which was collected by filtration and washed with Et₂O (0.23 g, 87%). Single crystals suitable for X-ray structure determination and elemental analysis were grown from a vapour diffusion of Et₂O into MeNO₂. ¹H NMR (300 MHz, (CD₃)₂SO): δ 10.18 (s, 1H, OH), 8.99 (dd, *J*=6.6, 1.8 Hz, 1H, H₆), 8.04 (d, *J*=1.8 Hz, 1H, H₃), 7.83 (dd, *J*=6.6, 1.8 Hz, 2H, H₅), 7.78 (d, *J*=9.0 Hz, 2H, H_{4b}), 6.91 (d, *J*=8.7 Hz, 2H, H_{4c}), 4.76, 4.47 (AB spin system, *J*=16.5 Hz, 2H, CH₂), 2.55 (s, 3H, SCH₃); ¹³C{¹H} NMR (75.4 MHz, (CD₃)₂SO): δ 163.8 (C₂), 160.9 (HOC), 151.7 (C₆), 150.5 (C₄), 129.7 (C_{4b}), 125.7 (C_{4a}), 120.7 (C₅), 120.4 (C₃), 117.0 (C_{4c}), 45.3 (CH₂), 22.9 (SCH₃). MS (LSIMS) *m/z* 373 [M–Cl]⁺, [¹²C₁₃H₁₃³⁵Cl¹⁴N³²S¹⁶O 373]. HRMS (EI) *m/z* [M–Cl]⁺ 371.94412, [C₁₃H₁₃ClNSO]⁺ requires 371.94521. Anal. Calcd for PdC₁₃H₁₃NSOCl₂: C, 38.21; H, 3.21; N, 3.43; S, 7.85. Found: C, 38.30; H, 3.07; N, 3.67; S, 7.45.

3.2.8. Dichloro[4-(4-Benzyloxy)-2-methylthiomethylpyridine]palladium(II) (9)

PdCl₂(NCMe)₂ (0.15 g, 0.64 mmol) was added to a stirred suspension of **7** (0.25 g, 0.77 mmol, 1.2 equiv) in dry MeCN (30 mL), instantly affording a bright yellow suspension, which was stirred for 12 h at rt. The solvent was reduced in vacuum to ~5 mL and Et₂O was added. The title complex was collected by filtration as a bright yellow solid and washed with Et₂O (0.27 g, 85%). Single crystals suitable for elemental analysis were grown from hot MeNO₂. ¹H NMR (300 MHz, (CD₃)₂SO): δ 9.02 (dd, *J*=6.3, 1.8 Hz, 1H, H₆), 8.10 (d, *J*=1.8 Hz, 1H, H₃), 7.89 (m, 3H, H₅, H_{4b}), 7.39 (m, 5H, H_{4b2}, H_{4c2}, H_{4d2}), 7.19 (d, *J*=8.7 Hz, 1H, H_{4c}), 5.19 (s, 2H, OCH₂), 4.77, 4.48 (AB spin system, *J*=16.8 Hz, 2H, SCH₂), 2.55 (s, 3H, SCH₃); ¹³C{¹H} NMR (75.4 MHz, (CD₃)₂SO): δ 163.9 (C₂), 161.3 (C_{4d}), 151.7 (C₆), 150.2 (C₄), 137.3 (C_{4a2}), 129.6 (C_{4b}), 129.2 (C_{4c2}), 128.7 (C_{4d2}), 128.5 (C_{4b2}), 127.6 (C_{4a}), 121.1 (C₅), 120.9 (C₃), 116.4 (C_{4c}), 70.1 (OCH₂), 45.3 (SCH₂), 22.9 (SCH₃). MS (LSIMS) *m/z* 463 [M–Cl]⁺, [¹²C₂₀H₁₉³⁵Cl¹⁴N³²S¹⁶O 463]. HRMS *m/z* [M–Cl]⁺ 461.99107, [C₂₀H₁₉ClNSO]⁺ requires 461.99215. Anal. Calcd for PdC₂₀H₁₉NSOCl₂: C, 48.16; H, 3.84; N, 2.81. Found: C, 47.89; H, 3.74; N, 2.72.

3.3. Structural determinations

Data for **4**, **6** and **8** were collected at –80 °C with an Enraf Nonius TurboCAD4 with Mo K α radiation (0.71073 Å) on crystals of **4**, **6** and **8** mounted on glass fibres. Data for **9** were collected at –173 °C for crystals mounted on a Hampton Scientific cryoloop at the PX1 beamline of the Australian Synchrotron. Views of the structures are shown in Figures 2 and 3. The structures were solved by direct methods with SHELXS-97, refined using full-matrix least-squares routines against *F*² with SHELXL-97,¹⁹ and visualised using X-SEED.²⁰ All non-hydrogen atoms were refined anisotropically. Nitrogen-bound and O-bound hydrogen atoms were positionally refined and other hydrogen atoms were placed in calculated positions and refined using a riding model with fixed C–H distances of 0.95 Å (sp²C–H), 0.99 Å (CH₂), 0.98 Å (CH₃). The thermal parameters of all hydrogen atoms were estimated as *U*_{iso}(H)=1.2 *U*_{eq}(C) except for CH₃ where *U*_{iso}(H)=1.5 *U*_{eq}(C).

3.4. Attachment of ligand and palladium to resins and bulk monolith

A suspension of polymer (0.05 g), **6** (0.08 g) and Bu₄NOH (1.75 mmol) in EtOH (5 mL) was stirred at 60 °C for 24 h, after which the resin was filtered under vacuum, resuspended in EtOH and stirred for 30 min, and recovered again by filtration. The polymer was washed twice more with EtOH and dried in vacuum. The modified polymer and PdCl₂(NCMe)₂ (0.70 g) in MeCN

(5 mL) were stirred for 24 h at rt, filtered under vacuum, resuspended in MeCN, stirred for 30 min and recovered again by filtration. The polymer was washed twice more with EtOH and dried in vacuum.

3.5. Suzuki–Miyaura catalysis for resins and bulk monolith

Aryl halide (3.0 mmol) was added to a solution of *p*-Tol-B(OH)₂ (0.612 g, 4.5 mmol), Na₂CO₃ (0.5 g, 6.0 mmol), catalyst (5.0 mg) in a 3:1 DMF/H₂O mixture (10 mL) under Ar. The resulting mixture was stirred at 80 °C for 24 h under Ar. Once cooled to rt, Ph₂O (0.17 g, 1.0 mmol) was added and an aliquot (1.50 mL) was taken and diluted with CH₂Cl₂, washed three times with a saturated NaCl solution. The organic layer was extracted, dried over MgSO₄ and filtered, and analysed by GC-FID and GC-MS.

3.6. Mizoroki–Heck catalysis for resins and bulk monolith

Aryl halide (3.0 mmol) was added to a solution of *n*-butylacrylate (0.75 mL, 4.5 mmol) (or *n*-butylcinnamate for entries 10 and 11 in Table 1), Na₂CO₃ (0.5 g, 6.0 mmol), catalyst (5.0 mg) and *n*-Bu₄NCl (1.25 g, 4.5 mmol) in DMA (10 mL) under Ar. The resulting mixture was stirred at 120 °C for 48 h under Ar. The cooled mixture was treated and analysed as for Suzuki–Miyaura catalysis by GC-FID and GC-MS.

3.7. Ligand and palladium attachment to monolith in capillaries

The monolith filled capillary was flushed with EtOH for 30 min at 60 °C (2.0 μL min^{–1}). A filtered solution of **6** (85 mg) and Bu₄NOH (1.5 mL) in EtOH (3.5 mL) was pumped through the capillary at 60 °C for 18 h (0.2 μL min^{–1}), then the capillary was reversed and the solution was pumped through for a further 8 h (0.5 μL min^{–1}). The capillary was washed with EtOH for 1 h at rt (2.0 μL min^{–1}) to remove unreacted ligand and base. The monolith filled capillary was flushed with MeCN for 30 min at rt (2.0 μL min^{–1}), prior to a filtered solution of PdCl₂(NCMe)₂ (10 mg) in MeCN (2 mL) being pumped through the capillary at rt for 8 h (0.5 μL min^{–1}), then the capillary was reversed and the solution was pumped through for a further 18 h (0.2 μL min^{–1}). The capillary was flushed with MeCN for 1 h (2.0 μL min^{–1}).

3.8. Suzuki–Miyaura catalysis for capillaries

To equilibrate the microreactor prior to the reaction, the capillary (10 cm) was flushed with DMF/H₂O (3:1) for 1 h at rt (2.0 μL min^{–1}), then with solvent mixture containing 2 M of Et₃N for 2 h at 80 °C (2.0 μL min^{–1}) with the microreactor placed in the pre-heated column heater. The reaction mixtures were passed through the capillary at a flow rate of 0.1 μL min^{–1} for 24 h. The product was collected from the opposing end and analysed by GC-FID.

3.9. Mizoroki–Heck Catalysis for capillaries

A similar procedure was followed, using DMA initially, then DMA with Et₃N, and reactions were carried out at 120 °C for 248 h.

4. Supplementary data

Crystallographic data for **4**, **6**, **8** and **9** have been deposited with the Cambridge Crystallographic Data Centre with deposition

numbers CCDC 726966–726969; data can be obtained free of charge via www.ccdc.cam.ac.uk/data_request/cif.

Acknowledgements

The present research was supported by the Australian Research Council, Dr. R.M.G. is the recipient of an ARC APD fellowship; Dr. A. Townsend (CSL) and Julian Adams (Australian Synchrotron) are acknowledged for technical support. Data for the structure of **9** were obtained on the PX1 beamline at the Australian Synchrotron, Victoria, Australia. The views expressed herein are those of the authors and are not necessarily those of the owner or operator of the Australian Synchrotron.

References and notes

- Jones, R. C.; Madden, R. L.; Skelton, B. W.; Tolhurst, V.-A.; White, A. H.; Williams, A. M.; Wilson, A. J.; Yates, B. F. *Eur. J. Inorg. Chem.* **2005**, 1048.
- (a) Chelucci, G.; Berta, D.; Saba, A. *Tetrahedron* **1997**, 53, 3843; (b) Chelucci, G.; Berta, D.; Fabbri, D.; Pinna, G. A.; Saba, A.; Ulgheri, F. *Tetrahedron: Asymmetry* **1998**, 9, 1933; (c) Canovese, L.; Visentin, F.; Chessa, G.; Santo, C.; Levi, C.; Uguagliati, P. *Inorg. Chem. Commun.* **2006**, 9, 388; (d) Canovese, L.; Visentin, F.; Chessa, G.; Uguagliati, P.; Santo, C.; Maini, L. *J. Organomet. Chem.* **2007**, 692, 2342; (e) Canovese, L.; Visentin, F.; Santo, C. *J. Organomet. Chem.* **2007**, 692, 4187; (f) Canovese, L.; Visentin, F.; Levi, C.; Santo, C. *J. Organomet. Chem.* **2008**, 693, 3324.
- (a) Bolton, K. F.; Canty, A. J.; Deverell, J. A.; Guijt, R. M.; Hilder, E. F.; Rodemann, T.; Smith, J. A. *Tetrahedron Lett.* **2006**, 47, 9321; (b) Canty, A. J.; Deverell, J. A.; Gömann, A.; Guijt, R. M.; Rodemann, T.; Smith, J. A. *Aust. J. Chem.* **2008**, 61, 630; (c) Gömann, A.; Deverell, J. A.; Munting, K. F.; Jones, R. G.; Rodemann, T.; Canty, A. J.; Smith, J. A.; Guijt, R. G. *Tetrahedron* **2009**, 65, 1450.
- (a) Fletcher, P. D. I.; Haswell, S. J.; Pombo-Vilar, E.; Warrington, B. H.; Watts, P.; Wong, Y. F.; Zhang, X. *Tetrahedron* **2002**, 58, 4735; (b) Haswell, S. J.; Watts, P. *Green Chem.* **2003**, 5, 5240; (c) Watts, P.; Haswell, S. J. *Curr. Opin. Chem. Biol.* **2003**, 7, 380; (d) Watts, P.; Haswell, S. J. *Chem. Soc. Rev.* **2005**, 34, 235; (e) Hessel, V.; Löwe, H. *Chem. Eng. Technol.* **2005**, 28, 267; (f) Brivio, M.; Verboom, W.; Reinhoudt, D. N. *Lab Chip* **2006**, 6, 329; (g) Kobayashi, J.; Mori, Y.; Kobayashi, S. *Chem. Asian J.* **2006**, 22; (h) Watts, P.; Wiles, C. *Chem. Commun.* **2007**, 443; (i) Haerberle, S.; Zengerle, R. *Lab Chip* **2007**, 7, 1094; (j) Ahmed-Omer, B.; Brandt, J. C.; Wirth, T. *Org. Biomol. Chem.* **2007**, 5, 733; (k) Mason, B. P.; Price, K. E.; Steinbacher, J. L.; Bogdan, A. R.; McQuade, D. T. *Chem. Rev.* **2007**, 107, 2300; (l) Kockmann, N.; Gottsponer, M.; Zimmermann, B.; Roberge, D. M. *Chem.—Eur. J.* **2008**, 14, 7470.
- (a) He, P.; Haswell, S. J.; Fletcher, P. D. I. *Appl. Catal., A: Gen.* **2004**, 274, 111; (b) Basheer, C.; Hussain, F. S. J.; Lee, H. K.; Valiyaveetil, S. *Tetrahedron Lett.* **2004**, 45, 7297; (c) Comer, E.; Organ, M. G. *Chem.—Eur. J.* **2005**, 11, 7223; (d) Shore, G.; Morin, S.; Organ, M. G. *Angew. Chem., Int. Ed.* **2006**, 45, 2761; (e) Shi, G.; Hong, F.; Liang, Q.; Fang, H.; Nelson, S.; Weber, S. G. *Anal. Chem.* **2006**, 78, 1972; (f) Ueno, M.; Suzuki, T.; Naito, T.; Oyamada, H.; Kobayashi, S. *Chem. Commun.* **2008**, 1647; (g) Shore, G.; Morin, S.; Mallik, D.; Organ, M. G. *Chem.—Eur. J.* **2008**, 14, 1351; (h) Shore, G.; Organ, M. G. *Chem.—Eur. J.* **2008**, 14, 9641.
- (a) Greenway, G. M.; Haswell, S. J.; Morgan, D. O.; Skelton, B. V.; Styring, P. *Sens. Actuators, B: Chem.* **2000**, 63, 153; (b) He, P.; Haswell, S. J.; Fletcher, P. D. I. *Lab Chip* **2004**, 4, 38; (c) Jönsson, C.; Lundgren, S.; Haswell, S. J.; Moberg, C. *Tetrahedron* **2004**, 60, 10515; (d) Kobayashi, J.; Mori, Y.; Kobayashi, S. *Chem. Commun.* **2005**, 2567; (e) Miller, P. W.; Long, N. J.; de Mello, A. J.; Vilar, R.; Passchier, J.; Gee, A. *Chem. Commun.* **2006**, 546.
- Svec, F.; Huber, C. G. *Anal. Chem.* **2006**, 78, 2101.
- Klunder, J. M.; Hoermann, M.; Cywin, C. L.; David, E.; Brickwood, J. R.; Schwartz, R.; Barringer, K. J.; Pauletti, D.; Shih, C.-K.; Erickson, D. A.; Sorge, C. L.; Joseph, D. P.; Hattox, S. E.; Adams, J.; Grob, P. M. *J. Med. Chem.* **1998**, 41, 2960.
- (a) van den Heuvel, M.; van den Berg, T. A.; Kellogg, R. M.; Choma, C. T.; Feringa, B. L. *J. Org. Chem.* **2004**, 69, 250; (b) Ashimori, A.; Ono, T.; Uchida, T.; Ohtaki, Y.; Fukaya, C.; Watanabe, M.; Yokoyama, K. *Chem. Pharm. Bull.* **1990**, 38, 2446.
- Canovese, L.; Visentin, F.; Uguagliati, P.; Chessa, G.; Pesce, A. *J. Organomet. Chem.* **1998**, 566, 61.
- Lozano, V.; Jones, P. G. *Acta Crystallogr.* **2004**, C60, o653.
- Kang, H.; Facchetti, A.; Jiang, H.; Cariat, E.; Righetto, S.; Ugo, R.; Zuccaccia, C.; Macchioni, A.; Stern, C. L.; Liu, Z.; Ho, S.-T.; Brown, E. C.; Ratner, M. A.; Marks, T. J. *J. Am. Chem. Soc.* **2007**, 129, 3267.
- Database of average bond-lengths in organic compounds: Allen, F. H.; Kennard, O.; Watson, D. G.; Brammer, L.; Orpen, A. G.; Taylor, R. *J. Chem. Soc., Perkin Trans. 2* **1987**, S1.
- (a) Canovese, L.; Visentin, F.; Chessa, G.; Uguagliati, P.; Bandoli, G. *Organometallics* **2000**, 19, 1461; (b) Canovese, L.; Visentin, F.; Chessa, G.; Uguagliati, P.; Santo, C.; Dolmella, A. *Organometallics* **2005**, 24, 3297; (c) Canovese, L.; Visentin, F.; Santo, C.; Levi, C.; Dolmella, A. *Organometallics* **2006**, 26, 5590.
- Bondi, A. *J. Phys. Chem.* **1964**, 68, 441.
- (a) Davies, P. J.; Veldman, N.; Grove, D. M.; Spek, A. L.; Lutz, B. T. G.; van Koten, G. *Angew. Chem., Int. Ed.* **1996**, 35, 1959; (b) Albrecht, M.; Lutz, M.; Schreurs, A. M. M.; Lutz, E. T. H.; Spek, A. L.; van Koten, G. *J. Chem. Soc., Dalton Trans.* **2000**, 3797; (c) Mehendale, N. C.; Lutz, M.; Spek, A. L.; Klein Gebbink, R. J. M.; van Koten, G. *J. Organomet. Chem.* **2008**, 693, 2791.
- Phan, N. T. S.; Brown, D. H.; Styring, P. *Green Chem.* **2004**, 6, 526.
- (a) Kotha, S.; Lahiri, K.; Kashinath, D. *Tetrahedron* **2002**, 58, 9633; (b) Whitcombe, N. J.; Hii, K. K.; Gibson, S. E. *Tetrahedron* **2001**, 57, 7449.
- Sheldrick, G. M. *SHELX97, Programs for Crystal Structure Analysis*; Universität Göttingen: Germany, 1998.
- Barbour, L. J. *J. Supramol. Chem.* **2001**, 1, 189.



Contents lists available at ScienceDirect

Sensors and Actuators B: Chemical

journal homepage: www.elsevier.com/locate/snb



UV initiated formation of polymer monoliths in glass and polymer microreactors

Jeremy A. Deverell^{a,b}, Thomas Rodemann^c, Jason A. Smith^b, Allan J. Canty^b, Rosanne M. Guijt^{a,*}

^a Australian Centre for Research on Separation Science, School of Chemistry, University of Tasmania, Hobart, Australia

^b School of Chemistry, University of Tasmania, Hobart, Australia

^c Central Science Laboratory, University of Tasmania, Hobart, Australia

ARTICLE INFO

Article history:

Received 6 July 2010

Received in revised form 14 October 2010

Accepted 14 November 2010

Available online xxx

Keywords:

Polymer monolith

Photoinitiated polymerisation

UV LED

Heterogeneous catalysis

Microreactor

Lab on a Chip

ABSTRACT

Polymer monoliths with good flow-through properties were prepared by UV initiated polymerisation to form a support for heterogeneous palladium catalysis in glass and polymer microchips. Preparation of homogeneous polymer monoliths required investigation of different light source/photoinitiator combinations and manipulation of the polymerisation mixture to accommodate different channel dimensions. A deep UV (DUV) flood exposure lamp, UV tubes with respective outputs at 255 and 365 nm and a UV LED array with output at 365 nm were used to initiate the polymerisation. The spectra of light source and initiator were matched; 2,2-dimethoxy-2-phenylacetophenone (DMPAP) was selected for polymerisation in the DUV and bis(2,4,6-trimethylbenzoyl)phenylphosphine oxide (BAPO) was used for polymerisation in the near UV (NUV). This is the first report of the use of a BAPO-type photoinitiator for the formation of organic polymer monoliths. Only the DUV lamp and 365 nm UV LED array resulted in the formation of homogenous and continuous monoliths which were subsequently used to create continuous-flow microreactors in fused silica capillaries, borosilicate chips and in cyclic olefin copolymer (COC) capillaries and chips. All microreactors gave high to quantitative yields for the Suzuki–Miyaura's coupling of iodobenzene with 4-tolyl boronic acid. In addition to demonstrating the first polymer chip for heterogeneous Suzuki–Miyaura's catalysis, the UV LED array in combination with BAPO was found to be a suitable budget alternative to a DUV exposure source for monolith formation in devices with internal diameter of up to 2 mm.

© 2010 Elsevier B.V. All rights reserved.

1. Introduction

Lab on a Chip devices may contain a large variety of chemical, biological and analytical functionalities integrated on a single microchip. A large variety of materials has been explored for microchip fabrication, with polymer microdevices considered to be most attractive because of their accurate replication and suitability towards mass production [1]. Our research focuses on the development of a continuous-flow microreactor for heterogeneous palladium catalysis in glass and in polymer devices. Microreactors have the potential to revolutionise the fields of chemistry and biotechnology by providing an attractive alternative to conventional glassware [2–8]. Excellent performance can be achieved by taking advantage of microchannel system features such as rapid heat transfer and faster diffusion-based processes. Reactions can be carried out under isothermal conditions with well-defined

residence times, so that undesirable side reactions and product degradation are limited. The small dimensions of microreactors also allow the use of minimal amounts of reagents and solvents under precisely controlled conditions, which reduces potential hazards and makes chemical processes more environmentally friendly.

While many reported microreactors are essentially efficient micromixers, the aim of our work is to develop continuous-flow microreactors for heterogeneous catalysis. The use of a heterogeneous reagent or catalyst in flow-through microreactors is complicated by the risk of catalyst particles clogging up the channel. For catalytic reactions, this issue has been resolved by immobilizing catalytic particles in packed beds [9–11] or by coating microstructured features with a catalyst [12]. We have recently reported the use of organic polymer monoliths as a solid support in capillaries and microchips for continuous-flow Suzuki–Miyaura's, Sonogashira and Heck reactions with low leaching of palladium [13–16]. A monolith is a single macroporous polymer structure. The favourable mass transfer characteristics and high porosity have made monoliths a popular solid support in separation science [17]. A polymer monolith is typically formed by polymerisation of a functional monomer in the presence of a cross-linking monomer and a

* Corresponding author at: ACROSS, School of Chemistry, University of Tasmania, Private Bag 75, Hobart TAS 7001, Australia. Tel.: +61 3 6226 2171; fax: +61 3 6226 2858.

E-mail address: Rosanne.Guijt@utas.edu.au (R.M. Guijt).

porogen. The physical properties (pore size and surface area) of the monolith are predominantly determined by the solubility of the forming polymer in the porogen, whereas its chemical properties are determined predominantly by the monomers [18–20]. A commonly used approach for polymer monolith formation is via free radical polymerisation, initiated thermally or photochemically [21–22]. UV initiated polymerisation is most suitable for the formation of polymer monoliths in microfluidic devices as it offers the capability of controlling the region of formation of the monolith by masking [23]. Recently, a micromixer consisting of regularly repeating 100 μm monolith segments was presented using this technique [24].

The rate of radical formation is crucial for the morphology of the formed monolith, making a good spectral match between the spectra of the photoinitiator and exposure source essential for efficient radical formation. The optical characteristics of the photodegradation products of the photoinitiator are often overlooked, but absorption at the initiation wavelength will increasingly reduce the transparency of the mixture at the excitation wavelength and therefore reduce rate of radical formation, a process which is also referred to as photodarkening [25].

Light sources for the formation of photoinitiated monoliths vary from expensive dedicated flood exposure systems [26] to more common UV tubes [27] or UV LEDs [28–29]. Despite the importance of the light source for the quality of the monolith, poor spectral matches between the light source, the photoinitiator and the photodegradation products can result in non-homogenous and irreproducible monolith formation, little attention is paid to justification of the light source and photoinitiator in the literature. In this work, a comprehensive study is presented where monoliths were formed in borosilicate and COC substrates using various light sources (a DUV flood exposure system, 254 nm and 365 nm UV tubes and a 365 nm UV LED array) to initiate the polymerisation. DMPAP and BAPO were selected for initiation in the DUV and NUV, respectively. Only the DUV lamp and UV LED array were found to yield homogenous and continuous monoliths. The monoliths prepared using these light sources were functionalised and applied as microreactors for the Suzuki–Miyaura's reaction, as illustrated in Fig. 1. The importance of palladium-catalyzed cross-coupling reactions is also illustrated by the award of the 2010 Nobel prize, and the Suzuki–Miyaura reaction was chosen as established model reactions for metal complexes anchored onto conventional organic polymers in large scale catalysis [30]. To the authors' best knowledge, the COC microreactors are the first polymeric microreactors for heterogeneous catalysis.

2. Materials and methods

2.1. Reagents

All chemical reagents were purchased from Sigma–Aldrich and were used without purification, except for glycidyl methacrylate (GMA), ethylene dimethacrylate (EDMA), and methyl methacrylate (MMA) which were purified by vacuum distillation. All solvents and mixtures used were filtered through 0.2 μm syringe filters before use.

Polymerisation mixture A was prepared by mixing together cyclohexanol (0.93 g), 1-dodecanol (1.40 g), GMA (0.6 g), EDMA (0.4 g), and photo-initiator (2,2-dimethoxy-2-phenylacetophenone (DMPAP) or bis(2,4,6-trimethylbenzoyl)phenylphosphine oxide (BAPO), 10 mg) in a 4 mL vial (glass screw top, Alltech) and then purging with nitrogen for 10 min.

Polymerisation mixture B was based on that reported by Yu et al. [31] by reducing the porogen content to 50 wt% to reduce shrinkage. It was prepared by mixing together methanol (0.5 g), ethanol (0.5 g), GMA (0.6 g), EDMA (0.4 g), and photo-initiator DMPAP or BAPO (10 mg) in a 4 mL vial (glass screw top, Alltech) and then purging with nitrogen for 10 min.

2.2. Instrumentation

UV-transparent fused-silica capillary (100 μm ID) was purchased from Polymicro (USA) and Tycona Topaz[®] grade 6013 capillary (276 μm ID) was purchased from Paradigm Optics (USA). Borosilicate microchips (channel dimensions 33.2 cm long, 150 μm wide and 150 μm deep) were purchased from Micronit (The Netherlands). Tycona Topaz[®] grade 6013 microchips (channel dimensions 54.5 mm long, 610 μm wide and 100 μm deep) were purchased from Microfluidic ChipShop GmbH (Germany). Low expansion borosilicate tubing with 4 mm ID (6 mm OD) and 2 mm ID (5.8 mm OD) was obtained locally from the scientific glass blower (Central Science Laboratory, University of Tasmania, Hobart, Australia).

The COC microchips were machined from both sides using a fly-cutter in a vertical mill to reduce the thickness from 2.8 mm down to 1.8 mm. The machined microchips were polished to remove the cuts and abrasions from the milling via a two-stage process. The surface was smoothed using wet and dry silicon carbide paper with water, followed by polishing with an alumina/water mixture on a Pan-W cloth disc. The polished microchips were cleaned by ultra sonication in a Teepol/water mixture followed by rinsing with water and methanol.

The light sources used were: a Model 30 LS 500W Hg–Xe arc lamp (20.0 mW cm^{-2} at 260 nm) from OAI (USA), a Spectrolinker XL1500 UV Crosslinker (5.5–6.5 mW cm^{-2} at 254 nm or 4.5–5.5 mW cm^{-2} at 365 nm) from Spectronics Corporation (USA), and a Shark Series[™] high flux UV LED array (0.80 mW cm^{-2} at 365 nm) from Opto Technology (USA).

Characterisation utilised equipment housed in the Central Science Laboratory, University of Tasmania, including an FEI Quanta 600 MLA ESEM (FEI, USA) and an ELEMENT high resolution ICP-MS (Finnigan-MAT, Germany) allowing detection down to 0.1 ppb. Prior to analysis by ICP-MS, fused-silica capillary samples were crushed using a mortar and pestle. GC analysis was carried out on a Shimadzu GC-2014AF gas chromatograph (Shimadzu, Japan), equipped with a 25 m (0.32 mm ID) ID-BPX5 SGE column, calibrated against diphenyl ether as an internal standard. Pore size analysis was performed on a Micromeritics AutoPore IV 9500 mercury intrusion porosimeter (Micromeritics, USA).

A Harvard Apparatus model PHD 22/2000 dual syringe pump (Harvard Apparatus, USA) was used in combination with 250 μL Gastight[®] glass syringes (Hamilton, USA) to pump liquids through

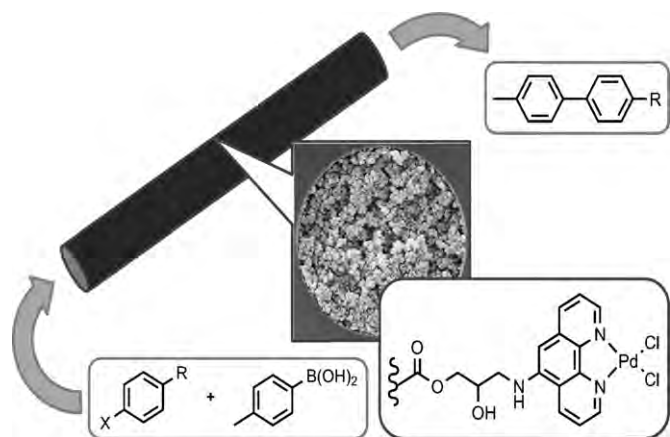


Fig. 1. Schematic illustration of a flow-through microreactor for the Suzuki–Miyaura reaction.

the capillaries and microchips. For the fused silica capillaries, two 20 cm long polyimide coated fused silica capillaries (100 μm ID, Polymicro, USA) were used for interfacing the microreactor with the syringe pump and collection vial, respectively. For the borosilicate microchips, COC capillaries and chips, two 20 cm long pieces of Tefzel tubing (254 μm ID, Upchurch, USA) were used. Standard Upchurch fittings were used to connect the capillaries and chips. In-house fabricated microchip holders fitted with Upchurch tubing and fittings was used to interface both borosilicate and COC microchips. A 1122/WTC-120 column heater (Waters Millipore, USA) was used for heating.

2.3. Surface modification

The internal surface of the fused silica capillary and glass tubes was treated following a procedure based on that of Rohr et al. [26]. A length of fused-silica capillary was rinsed with acetone (250 μL), water (1 mL), and sodium hydroxide (0.2 M) until a basic pH was detected at the capillary terminus and continued at 15 $\mu\text{L h}^{-1}$ for 30 min, followed by water until neutral pH was detected. The capillary was then flushed with hydrochloric acid (0.2 M) until an acidic pH was detected and continued at 15 $\mu\text{L h}^{-1}$ for 30 min, followed by water until neutral pH, then rinsed with ethanol (1 mL). The surface modification mixture (20 wt% 3-(trimethoxysilyl)propyl methacrylate in ethanol adjusted to pH 5 with acetic acid) was pumped through 15 $\mu\text{L h}^{-1}$ for 1 h, followed acetone (250 μL) and then dried by flushing with compressed air. The capillary was then stored for at least 24 h to allow the condensation reaction to complete.

The borosilicate microchannels were surface modified using the procedure for fused-silica capillaries described above.

The internal COC capillary surface was treated using a method tailored to the capillary dimensions and particular grade of COC. A 30–40 cm length of capillary was filled with benzophenone solution (3 wt% in methanol), ends sealed with inert rubber septa and exposed in the Spectroline XL1500 with 254 nm tubes for 20 min, rotated 180° along the capillary axis and exposed again for another 20 min. The capillary was flushed with methanol (3 mL) and dried with compressed nitrogen. The capillary was then filled with monomer mixture (methyl methacrylate/ethylene diacrylate, 1:1), ends sealed with inert rubber septa and exposed in the Spectroline XL1500 with 254 nm tubes for 10 min, rotated 180° along the capillary axis and exposed again for another 10 min. The capillary was flushed with methanol (3 mL) and dried with compressed nitrogen. The COC microchip channels were surface modified using a similar procedure for COC capillaries described above. For chip the benzophenone graft time was 2 \times 40 min and the monomer graft time was 2 \times 15 min.

The surface modification method described for the fused silica capillary and borosilicate chips was adapted to suit the larger scale of the borosilicate tubing. Glass columns were prepared by cutting borosilicate tubing (2 mm and 4 mm ID) into 10–11 cm lengths and smoothing the edges with a blowtorch. To speed up the surface modification, four columns were joined together using 5 mm ID polyethylene tubing and connected to a syringe pump. The columns were rinsed with acetone (10 mL for 2 mm ID, 25 mL for 4 mm ID), water (10 mL), and sodium hydroxide (0.2 M) until a basic pH was detected at the column terminus and continued at 0.1 mL min⁻¹ for 30 min, followed by water until neutral pH was detected. The column was then flushed with hydrochloric acid (0.2 M) until an acidic pH was detected and continued at 0.1 mL min⁻¹ for 30 min, followed by water until neutral pH, then rinsed with ethanol (10 mL for 2 mm ID, 25 mL for 4 mm ID). The individual columns were disconnected from the PE tubing and one end of each column was sealed with parafilm. Each column was filled with 3-(trimethoxysilyl)propyl methacrylate and left at room

temperature for 1 h. The parafilm seal was removed and each column was rinsed with acetone and dried with compressed air. The columns were then stored for at least 24 h to allow the condensation reaction to complete.

2.4. Monolith formation

A length of surface treated fused silica capillary (35 cm) was flushed with polymerisation mixture A until no bubbles were apparent, sealed at both ends with inert rubber septa and exposed. Exposure times of 10, 20 and 40 min were used for the DUV lamp, the Crosslinker XL1500 at 254 and 365 nm and the UV LED array, respectively. The monolith filled capillary was then rinsed with filtered methanol (30 $\mu\text{L h}^{-1}$, 8 h) and trimmed to a length of 30 cm.

For the borosilicate chip, a similar procedure was followed. The surface treated microchannel was partially filled with polymerisation mixture A and a low vacuum was applied to the exit well, leaving only the main microchannel filled. The wells of the chip were sealed with rubber septa. The microchip was then exposed (exposure times of 10, 20 and 40 min were used for the DUV lamp, the Crosslinker XL1500 at 254 and 365 nm and the UV LED array, respectively) and then flushed with filtered methanol (30 $\mu\text{L h}^{-1}$, 8 h).

A length of surface treated COC capillary (12 cm) was flushed with polymerisation mixture B until no bubbles were apparent, sealed at both ends with inert rubber septa and exposed. The monolith filled capillary was then rinsed with filtered methanol (60 $\mu\text{L h}^{-1}$, 4 h), and trimmed to 10 cm. The capillary was then exposed and then flushed with filtered methanol (60 $\mu\text{L h}^{-1}$, 4 h). Exposure times of 10 and 40 min were used for the DUV lamp and the UV LED array, respectively.

The surface treated microchannel was filled with polymerisation mixture B by applying a low vacuum to the exit well. The wells of the filled microchip were sealed with inert rubber septa and masked off with electrical tape leaving only the main microchannel exposed. The microchip was then exposed and then flushed with filtered methanol (60 $\mu\text{L h}^{-1}$, 4 h). Exposure times of 10 and 40 min were used for the DUV lamp and the UV LED array, respectively.

One end of a surface modified borosilicate tubing (2 mm or 4 mm ID) was sealed using PTFE tape and parafilm. The column was slowly filled with polymerisation mixture to avoid the formation of air bubbles. Once filled, the open end of the column was sealed with PTFE tape and parafilm and exposed using the DUV lamp and UV LED for 1 h and 2 h, respectively. The monolithic column was interfaced using Swagelok fittings and rinsed with filtered methanol (30 mL at 0.25 mL min⁻¹ for 2 mm ID, 60 mL at 1 mL min⁻¹ for 4 mm ID).

Bulk monolith was made using an in-house fabricated circular polymerisation container (internal dimensions of 0.3 \times 90 mm). The container was filled with polymerisation mixture and exposed under the DUV lamp for 30 min or the UV LED for 40 min. The monolith formed was washed with methanol in a Soxhlet apparatus for 18 h and then dried *in vacuo*. The monoliths were analysed by mercury intrusion porosimetry by Particle & Surface Sciences Pty. Limited (Gosford, Australia).

2.5. Microreactor fabrication

The monolith in the capillaries and chips was flushed with dimethyl sulfoxide (DMSO)/methanol (9:1) at 30 $\mu\text{L h}^{-1}$, 8 h for fused silica capillaries and borosilicate chips; 60 $\mu\text{L h}^{-1}$, 4 h for COC capillaries and chips at 70 °C. A solution of 5-amino-1,10-phenanthroline (100 mg) in DMSO (4 mL) with triethylamine (0.2 mL), was pumped through the monolith (10 $\mu\text{L h}^{-1}$, 24 h) at 70 °C, followed by DMSO/methanol (9:1) (30 $\mu\text{L h}^{-1}$, 8 h for fused

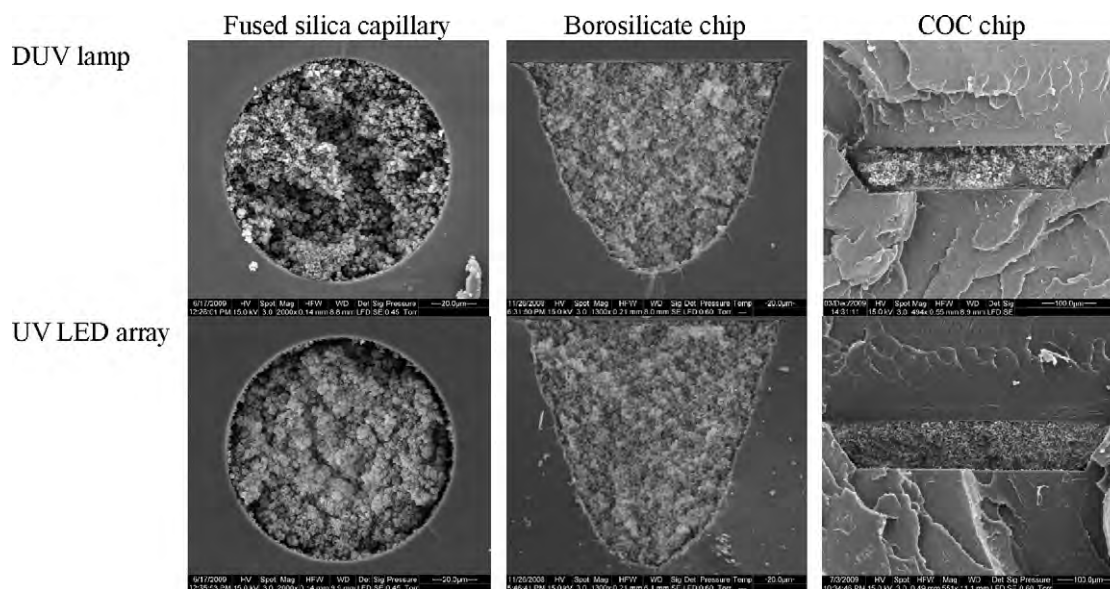


Fig. 2. SEM images of poly(GMA-co-EDMA) monoliths in fused silica capillaries and borosilicate and COC microchannels by UV initiated polymerisation using the DUV flood exposure source and the UV LED array.

silica capillaries and borosilicate chips; $60\ \mu\text{L h}^{-1}$, 4 h for COC capillaries and chips) at 70°C to remove unattached ligand. The capillary was flushed with acetonitrile ($30\ \mu\text{L h}^{-1}$, 8 h for fused silica capillaries and borosilicate chips; $60\ \mu\text{L h}^{-1}$, 4 h for COC capillaries and chips) at room temperature. A solution containing bis(acetonitrile)dichloropalladium(II) (20 mg) in acetonitrile (4 mL) was flushed through the monolith ($10\ \mu\text{L h}^{-1}$, 24 h), followed by acetonitrile ($30\ \mu\text{L h}^{-1}$, 8 h) to remove the excess palladium complex.

The monolith in the borosilicate tubing was flushed with methanol ($0.25\ \text{mL min}^{-1}$, 40 min for 2 mm ID; $1\ \text{mL min}^{-1}$, 10 min for 4 mm ID) at 50°C . Neat 1-methylimidazole was flushed through the column ($208.3\ \mu\text{L h}^{-1}$, 24 h for 2 mm ID; $417.6\ \mu\text{L h}^{-1}$, 24 h for 4 mm ID) at 50°C , followed by acetonitrile ($0.25\ \text{mL min}^{-1}$, 40 min for 2 mm ID; $1\ \text{mL min}^{-1}$, 80 min for 4 mm ID) at 50°C to remove unreacted ligand. A solution of bis(acetonitrile)dichloropalladium(II) (100 mg) in acetonitrile (20 mL) was filtered through a $0.2\ \mu\text{m}$ syringe filter and flushed through the column ($416.7\ \mu\text{L h}^{-1}$, 24 h), followed by acetonitrile ($0.25\ \text{mL min}^{-1}$, 40 min for 2 mm ID; $1\ \text{mL min}^{-1}$, 60 min for 4 mm ID) to remove any unattached palladium complex.

2.6. Flow-through reactions

Stock reaction mixtures were prepared using ethanol (8.5 mL), water (0.5 mL) aryl halide (1 mmol; $110\ \mu\text{L}$ iodobenzene), 4-tolylboronic acid (1.5 mmol; 203.9 mg), tetrabutylammonium hydroxide (1.5 mmol; 1.5 mL 1.0 M in methanol), and diphenyl ether as internal standard (1 mmol; $160\ \mu\text{L}$). All amounts were multiplied by five for reactions performed using the 2 mm and 4 mm ID reactors.

Suzuki–Miyaura's cross-coupling reactions were performed at 80°C with flow-rates of $5.0\ \mu\text{L h}^{-1}$ in fused-silica capillary, $4.3\ \mu\text{L h}^{-1}$ for COC capillary, $5\ \mu\text{L h}^{-1}$ for borosilicate microchips, and $1.6\text{--}2.2\ \mu\text{L h}^{-1}$ for COC microchips, $0.47\text{--}0.54\ \text{mL h}^{-1}$ for 2 mm ID borosilicate tubing and $2.26\ \text{mL h}^{-1}$ for 4 mm ID borosilicate tubing. Samples were taken every 12 h over 24 h for the capillary and chip systems, every 2 h over 4 h for the tubing reactors and analysed by GC-FID. For the 4 mm ID reactor, 50 mL of reaction mixture was pumped through the reactor and the product isolated by workup of the collected effluent.

3. Results and discussion

3.1. Monolith formation

3.1.1. Fused silica capillaries

For the formation of polymer monoliths in DUV light, 2,2-dimethoxy-2-phenylacetophenone (DMPAP) has been proven to be a fast and efficient commercially available photoinitiator [26]. Poly(GMA-co-EDMA) monolith was formed in surface-treated fused silica capillary using polymerisation formulation A and with 10 min exposure under the DUV lamp to function as a reference in the remainder of this work. An SEM of a cross section of this capillary is given in Fig. 2a, and shows a homogeneous monolith that is attached to the capillary walls. A similar monolith was formed when exposing for 20 min using the Spectroline XL1500 with 254 nm tubes, as illustrated in Fig. 3. Both monoliths had a low flow resistance and could be easily rinsed with solvent using a syringe pump.

Initiation of the polymerisation in DUV introduces significant restrictions on the optical properties of the material, the monomers and porogens as well as on the photoinitiator and its degradation products. Some of these limitations were removed by using a 660 nm LED or 480 nm LED arrays for the formation of styrene-based monoliths [29,32]. Photoinitiators in the NUV region, however, are more common and in this study two 365 nm sources were included: 365 nm fluorescent tubes and a UV LED array with output at 365 nm. BAPO is a highly active type I photoinitiator developed for UV curing of coatings [25] that to our knowledge has not previously been used for the formation of organic polymer monoliths. It is a specially attractive photoinitiator for this work because its photoproducts have limited absorption at the exposure wavelength.

BAPO was successfully used for the formation of poly(GMA-co-EDMA) monolith in fused silica capillary following a 40 min exposure using the UV LED array, as illustrated in Fig. 2b. The monolith formed homogeneously, attached to the capillary wall and generated a low back pressure enabling pumping through solvents using a syringe pump. The homogeneous monolith formation along the length of the capillary illustrates the intensity homogeneity of the UV LED array [33].

Poly(GMA-co-EDMA) monolith formed in fused silica capillary using the Spectroline XL1500 (20 min exposure time) was patchy

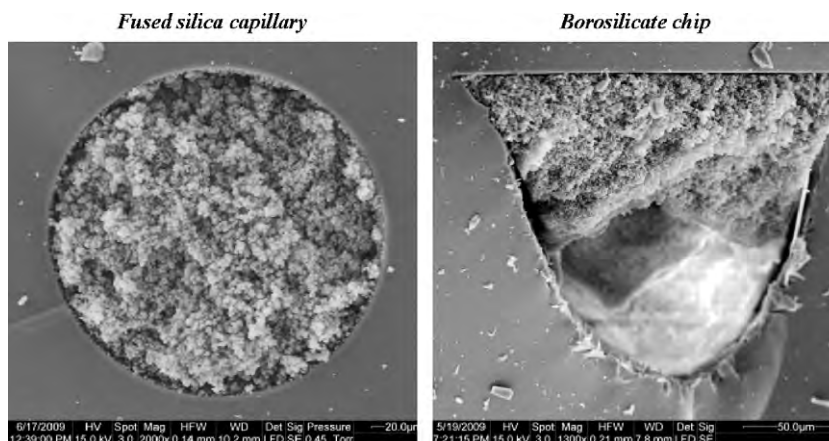


Fig. 3. SEM of poly(GMA-co-EDMA) formed using the Crosslinker XL1500 with 254 nm tubes. The monolith formed completely in the fused silica capillary but only partially in the borosilicate chip.

and incomplete. The reason for the patchy monolith formation using the 365 nm fluorescent tube remains unclear, but UV LEDs are known to outperform other light sources for UV initiation based on the superior spectral match with the initiators [34].

3.1.2. Borosilicate chips

The surface chemistry of borosilicate is similar to that of the fused silica, allowing the use of the surface modification method described for fused silica capillaries for the borosilicate chips. Following this treatment, the microchannels were filled with polymerisation mixture A, using DMPAP as photoinitiator for polymerisation under the DUV lamp and BAPO for the formation of the monolith using the UV LED array. Both poly(GMA-co-EDMA) monoliths were formed homogeneously and attached to the channel wall, as illustrated in Fig. 2c and d. Again, solvents could be easily pumped through the monolith using a syringe pump, illustrating good flow-through properties. When using the Spectroline XL1500 with 254 nm tubes, partial monolith only formation was observed in the borosilicate microchannels, as illustrated in Fig. 3. This may have been due to the limited transmission of borosilicate at 254 nm, but doubling the exposure time to 40 min did not result in complete filling of the microchannel. Other factors that may have compromised the monolith formation are the inhomogeneous light intensity and photodarkening of DMPAP.

3.1.3. COC capillaries

The DUV lamp and UV LED array in combination with DMPAP and BAPO, respectively, were selected for the formation of polymer monolith in COC. Photoinitiated monoliths have been presented in the COC grade Topaz®8007x10 because of excellent transparency in DUV [35]. The softening point of Topaz®8007 is 78 °C and while this is sufficient for most applications in separation science, this grade of COC cannot be used here since the Suzuki–Miyaura's coupling reaction will be conducted at 80 °C. For this study, Topaz®5013, 6013, 6015, 6017, all with glass temperatures above 130 °C, were selected because these grades have some transparency in DUV. Upon exposure through a 1 mm thick plate using the DUV source, a polymer monolith was only formed when using Topaz®6013, which was therefore selected for further work. COC capillaries of this grade with an ID of 276 µm were used to optimise the surface attachment and monolith formation in COC.

The surface of COC consists of aliphatic carbon atoms, requiring surface modification to enable covalent attachment of the monolith to the channel or capillary wall. Abele et al. proposed the use of 3-(trimethoxysilyl)propyl methacrylate to promote surface attachment of the monolith to the COC surface [28]. The mechanism of

this method is unclear due to the lack of surface hydroxyl groups typically required for the silanising reaction. In our hands, treatment of the Topaz®6013 surface with 3-(trimethoxysilyl)propyl methacrylate did not result in anchoring of the poly(GMA-co-EDMA) monolith to the capillary wall.

Grafting of the monolith to the capillary wall without further surface modification was observed when using DMPAP as initiator in the DUV lamp. SEM analysis of the same devices after their use as microreactor, however, showed detachment of the monolith from the wall, indicating that only a weak bond was formed when using DMPAP for grafting and monolith formation. This method was considered not suitable for the development of flow-through microreactors.

Photografting using benzophenone is based on the abstraction of hydrogen from the COC surface. The main activation for hydrogen abstraction for benzophenone is at 250 nm [36]. At higher wavelengths radicals will still be formed but not the high energy singlet state required for hydrogen abstraction from aliphatic carbons, restricting surface attachment by photografting using benzophenone in capillaries and microchannels to materials with DUV transparency. Stachowiak et al. introduced a single step photografting method using benzophenone to graft methacrylate functionalities onto COC [37]. This method was found not suitable for Topaz®6013, possibly due to poor transmission in the DUV region.

Based on two different methods reported by the Svec group [35,38] a new sequential grafting method was developed. The photoinitiator is photografted to the surface in the first step and reacted with a monomer using a second exposure. As a result, the grafting starts from the wall and the graft layer grows inward, avoiding homopolymer formation during longer grafting times.

Despite the sequential grafting method, monoliths formed using formulation A were not wall attached using either the DUV or UV LED array to initiate the polymerisation process. A detailed SEM study found that the monolith did form homogeneously and attached to the graft layer at the surface, but radial shrinkage of the monolith after removal of the porogens resulted in breaking of the monolith at the weakest point. SEM images of the poly(GMA-co-EDMA) monolith breaking through the centre supported the shrinkage theory and illustrated the effectiveness of the two-step grafting method.

When using formulation B in capillaries and channels with ID >200 µm, the monolith was found to contract after removal of the porogens, which may have been due to collapse of globules stabilised by the porogens. To reduce this effect, a monolith formulation was developed based on a formulation described by

Yu et al. [31] using ethanol and methanol as porogens. Ethanol and methanol are smaller and more polar solvents than cyclohexanol and dodecanol and therefore expected to play a minor role in stabilizing the monolith and thus to reducing the collapse upon removal of the porogens. Changing the porogens to ethanol/methanol indeed resulted in decreased contraction of the monolith upon porogen removal. Decreasing the total porogen content to 50 wt% was found to further reduce the contraction of the monolith. When reducing the total porogen content beyond 50%, monolith shrinkage increased due to the increased monomer content, cancelling out the effect of the porogen on monolith collapse. Formulation B was therefore based on 50% ethanol/methanol as porogenic solvent.

Using formulation B, poly(GMA-co-EDMA) monoliths with good flow-through properties were successfully formed in the COC capillaries both using the UV LED array and using the DUV exposure source. SEM images, however, showed a homogeneous monolith detached from the walls with monolith residues on the COC surface. Different sample preparation techniques were trialled including snapping the capillaries following scoring, snapping of the capillaries in liquid nitrogen as well as breaking the capillaries encased in resin. The SEM of a COC capillary split lengthwise after sample preparation given in Fig. 4 illustrates that stretching of the COC during sample preparation causes the monolith to break away from the capillary wall. Based on the complete filling of the remainder of the capillary in Fig. 4 and the monolith residues present on the COC wall, it was concluded that the two-step grafting method was successful but could not be visualized by SEM in COC capillaries. This hypothesis was confirmed when using the COC chips, as discussed below.

3.1.4. COC chips

The thickness of the commercially available Topaz®6013 chips was about 2.8 mm. At this thickness, the absorption at 254 nm is too great to allow the two-step grafting method to be successful. The COC chips were milled down and the improved transmission at 254 nm resulted in successful grafting of acrylate functionality to the surface, as illustrated by binding of the poly(GMA-co-EDMA) monolith to the channel walls following exposure under the DUV lamp (10 min) and UV LED array (40 min). SEMs of cross-sections of these monolith-filled microchannels are given in Fig. 2e and f. Both exposure sources resulted in the formation of homogeneous

monoliths with good flow properties and the effectiveness of the two-step grafting method is illustrated by the attachment of the monoliths to the channel wall. The larger amount of COC bulk in the chips probably prevented the stretching of the COC during sample preparation for SEM.

3.1.5. Quartz tubes

To further explore the effectiveness of BAPO as a photoinitiator for the formation of polymer monoliths, borosilicate tubing with internal diameter of 2 mm and 4 mm were surface modified using a surface treatment process similar to that described for the fused silica capillaries and borosilicate chips. The tubes were sealed on one side using parafilm and PTFE tape, filled with formulation B and BAPO as photoinitiator and irradiated for 120 min using the UV LED array. A homogeneous monolith formed in the 2 mm ID tubing, as illustrated in Fig 5a, but when using 4 mm ID tubes no monolith was formed in the centre of the tube, as illustrated in Fig. 5b. In comparison, poly(GMA-co-EDMA) monoliths were successfully formed in 2 mm ID and 4 mm ID tubing using the DUV exposure source and DMPAP as photoinitiator. At ID > 4 mm, the formed monolith pulled away from the tubing wall after removal of the porogens, probably as a result of shrinkage due to drying as no gaps at the wall were observed for the solvated monolith[39].

3.2. Characterisation of monolith

Bulk poly(GMA-co-EDMA) monolith was made using polymerisation mixture A and B. To mimic the physical conditions during polymerisation in the capillaries and microchannels, a bulk polymerisation container was designed with a depth of 200–300 μm . Following exposure, the monolith was removed from the container and porogens were removed by washing with solvent using a Soxhlet apparatus. After drying of the monolith, samples were analysed by mercury intrusion porosimetry. The average pore size and porosity of the poly(GMA-co-EDMA) monolith prepared using polymerisation mixture A and B using the DUV lamp and UV LED array are given in Table 1. The differences between the values obtained for the monoliths made using the high flux UV LED and DUV lamp are possibly due to the different polymerisation kinetics because of the different initiators and light intensities.

Bulk poly(GMA-co-EDMA) monolith of formulation A polymerised with the DUV lamp was functionalised with 5-amino-1,10-phenanthroline and analysed for N by elemental analysis. The ligand loading was 6.1×10^{-5} moles/g monolith, which represents a conversion of 1.4% of the theoretically available epoxide groups. This low attachment efficiency indicates that most of the epoxide groups are not accessible, either because they are buried in the monolith or due to the size of the ligand. Based on ICP-MS analysis of the 5-amino-1,10-phenanthroline functionalised poly(GMA-co-EDMA) monolith after loading with palladium, the palladium loading was calculated to be 1.1×10^{-4} mol/g monolith. ICP-MS analysis of the unmodified poly(GMA-co-EDMA), confirmed that palladium does not bind to the non-functionalised poly(GMA-co-EDMA). The excess of Pd relative to the ligand loading may be due to weak binding of palladium to the hydroxyl and secondary amine groups of the immobilised ligand. The Pd leaching from the

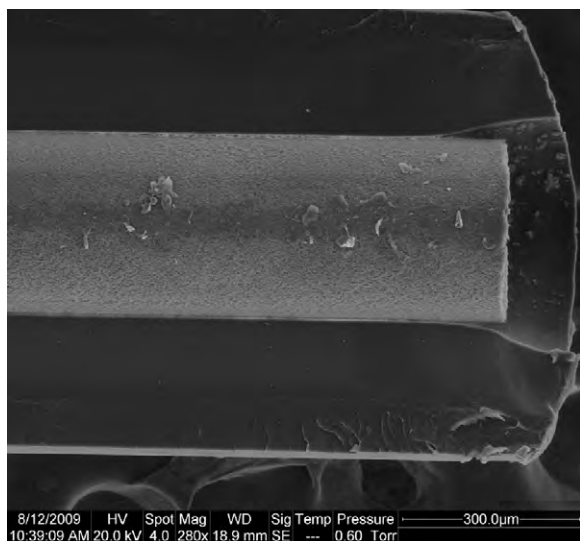


Fig. 4. SEM of COC capillary filled with poly(GMA-co-EDMA) monolith. The left shows the stretching of the COC during sample preparation.

Table 1

Porosity and average pore size for the poly(GMA-co-EDMA) monoliths.

Monolith formulation	Light source	Porosity (%) ^a	Median pore size (μm) ^a
A	UV LED array	72	0.45
A	DUV	74	0.47
B	UV LED array	63	2.22
B	DUV	70	2.01

^a Analysis conducted using bulk monolith.

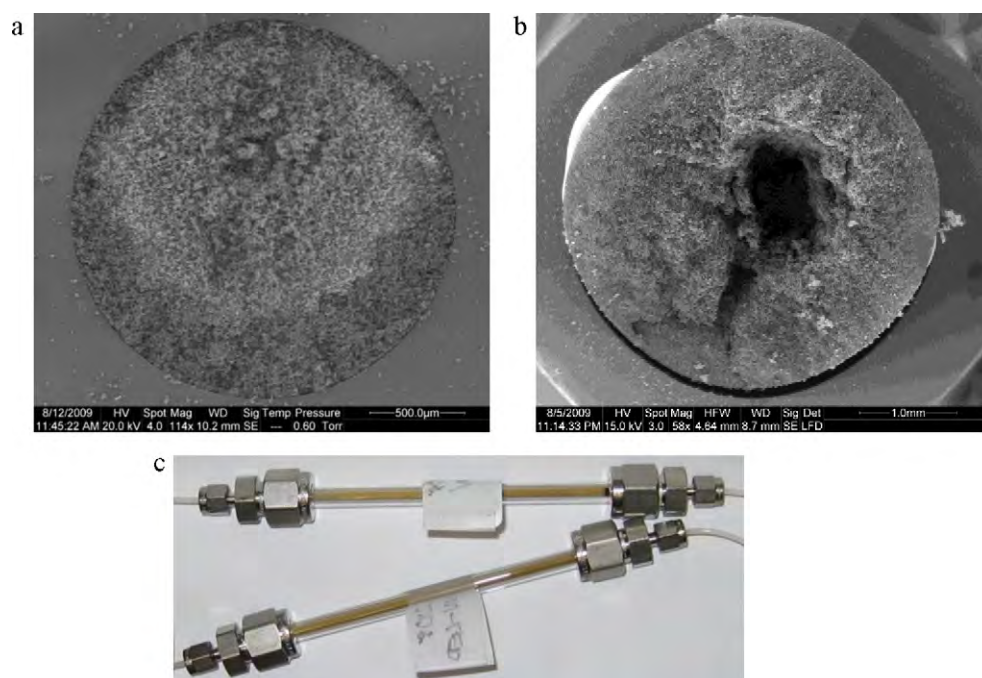


Fig. 5. (a and b) SEM of a poly(GMA-co-EDMA) monolith in a 2 mm ID (a) and 4 mm ID (b) glass tube. (c) Photograph of the 2 mm ID microreactor. Brown colour indicates binding of Pd to the ligand.

microreactor, however, was $<0.01\%$ over 24 h, indicating that this weakly bound Pd does not affect the performance of the microreactor.

New fused silica microreactors (ID 100 μm) containing poly(GMA-co-EDMA) monolith of formulation A formed using the DUV lamp and the UV LED array were analysed for palladium following a method previously developed in our group [14], resulting in a palladium loading of 1.1×10^{-4} mol/g for the DUV/DMPAP monolith and 9.9×10^{-5} mol/g for the UV LED array/BAPO monolith. The small difference is within the error margin of the laborious sample preparation method, confirming the similarities between the monoliths formed using the DUV lamp/DMPAP and UV LED array/BAPO systems. As the use of formulation B in 100 μm ID fused silica capillaries resulted in very high back pressures, this analysis was not repeated for formulation B.

3.3. Flow-through Suzuki–Miyaura's reaction

The poly(GMA-co-EDMA) monoliths made in the capillaries, chips were functionalised with a phenanthroline ligand and palladium to be applied as flow-through microreactors for the

Suzuki–Miyaura reaction. Because of difficulties in accessing of large amounts of the phenanthroline ligand, the 2 mm and 4 mm ID borosilicate devices were functionalised with methyl imidazole, which is likely to form an ion pair upon reaction with palladium [40]. These devices were also used for the Suzuki–Miyaura coupling of iodobenzene with 4-tolyl boronic acid. A photograph of the 2 mm glass tube reactor is given in Fig. 5c; the formation of the biaryl product is schematically illustrated in Fig. 1.

High yields were obtained for the reaction performed using the fused silica capillaries and borosilicate chips and tubing while similarly high yields (>88 – 95%) were obtained using the COC chips and capillaries. No significant differences can be observed for microreactors based on a monolith made using the UV LED array and BAPO initiator and those made using the DUV lamp and a conventional photoinitiator. The yields for the different microreactors are summarized in Table 2. The contact time is reported with flow rate as the contact time changes with the void volume and therefore with the porosity of the monolith in the different reactors.

Fused silica capillary microreactors were crushed using mortar and pestle, digested in *aqua regia* and analysed by ICP-MS for palladium. The Pd loading of the monolith in the microreactors was

Table 2

Yields for the Suzuki–Miyaura conversion of iodobenzene and 4-tolylboronic acid in the microreactors.

Reactor	Exposure source	Flow rate ($\mu\text{l/h}$)	Contact time (min) ^a	Yield (%)
Fused silica capillary	UV LED array	5.0	20 ^a	>99
	DUV	5.0	21 ^a	>99
Borosilicate chip	UV LED array	5.0	47 ^a	>99
	DUV	5.0	48 ^a	>99
COC capillary	UV LED array	4.3	53 ^a	94
	DUV	4.3	58 ^a	88
COC chip	UV LED array	1.6	73 ^a	95
	DUV	2.2	48 ^a	93
2 mm ID borosilicate tube	UV LED array	537	22 ^b	97
	DUV	469	26 ^b	97
4 mm ID borosilicate tube	DUV	2262	19 ^c	>99

^a Samples collected after 24 h.

^b Samples collected after 4 h.

^c Product recovered and isolated.

calculated based on the density of the monolith, resulting in a Pd loading of 1.20 wt% and 1.05 wt% for the monoliths formed using the UV LED array and DUV flood exposure source initiation sources, respectively. These values correspond well with values between 0.4% and 5% for solid supported catalysis reported in the literature [30], and results in a total amount of 7.2 μg and 10.1 μg palladium in the microreactors made using the UV LED array and DUV flood exposure source, respectively. Compared with our previous work, the Pd loading has been increased 30-fold from 0.04% by optimising ligand and Pd attachment conditions [16]. Similar loadings are expected for the COC and chip-based microreactors. The leaching of palladium was analysed for the 100 μm ID fused silica capillary microreactor by ICP-MS and considered very low at <0.01% over 24 h.

4. Conclusions

In this work, microreactors for heterogeneous catalysis were successfully made based on the formation of poly(GMA-co-EDMA) monoliths inside glass and COC capillaries and microchips, demonstrating the first polymeric microreactor for heterogeneous palladium catalysis. Monolith formation was both demonstrated by photoinitiated polymerisation using a DUV flood exposure system in combination with 2,2-dimethoxy-2-phenylacetophenone (DMPAP) and using a 365 nm UV LED array in combination with bis(2,4,6-trimethylbenzoyl)phenylphosphineoxide (BAPO). For only a fraction of the price, the UV LED array in combination with BAPO was found to be a suitable alternative for the formation of polymer monoliths in devices with ID up to 2 mm.

Acknowledgements

This research was supported under the Australian Research Council's Discovery Projects funding scheme (DP0663416) and the University of Tasmania Research College Board. Dr R.M. Guijt is the recipient of ARC APD fellowship (DO0557803). We thank Dr M.C. Breadmore for useful discussions. Mr P. Dove (mechanical workshop), Dr K. Gömann (SEM), and Dr A.T. Townsend (ICP-MS analysis), of the Central Science Laboratory and Mr S. Stevens (lapidary) of the ARC Centre of Excellence in Ore Deposits University of Tasmania, are acknowledged for technical support.

References

- [1] H. Becker, C. Gartner, Polymer microfabrication technologies for microfluidic systems, *Analytical and Bioanalytical Chemistry* 390 (2008) 89–111.
- [2] K. Geyer, J.D.C. Codée, P.H. Seeberger, Microreactors as tools for synthetic chemists—the chemists' round-bottomed flask of the 21st century? *Chemistry—A European Journal* 12 (2006) 8434–8442.
- [3] W. Ehrfeld, V. Hessel, L. Löwe, *Microreactors: New Technology for Modern Chemistry*, Wiley-VCH, 2000.
- [4] P. Watts, C. Wiles, Recent advances in synthetic micro reaction technology, *Chemical Communications* (2007) 443–467.
- [5] B.P. Mason, K.E. Price, J.L. Steinbacher, A.R. Bogdan, D.T. McQuade, Greener approaches to organic synthesis using microreactor technology, *Chemical Reviews* 107 (2007) 2300–2318.
- [6] M. Brivio, W. Verboom, D.N. Reinholdt, Miniaturized continuous flow reaction vessels: influence on chemical reactions, *Lab on a Chip* 6 (2006) 329–344.
- [7] J. Kobayashi, Y. Mori, S. Kobayashi, Multiphase organic synthesis in microchannel reactors, *Chemistry—An Asian Journal* 1 (2006) 22–35.
- [8] R.L. Hartman, K.F. Jensen, Microchemical systems for continuous-flow synthesis, *Lab on a Chip* 9 (2009) 2495–2507.
- [9] M.W. Losey, M.A. Schmidt, K.F. Jensen, Microfabricated multiphase packed-bed reactors: characterization of mass transfer and reactions, *Industrial & Engineering Chemistry Research* 40 (2001) 2555–2562.
- [10] S.J. Haswell, B. O'Sullivan, P. Styring, Kumada–Corriu reactions in a pressure-driven microflow reactor, *Lab on a Chip* 1 (2001) 164–166.
- [11] M. Baumann, I.R. Baxendale, S.V. Ley, C.D. Smith, G.K. Tranmer, Fully automated continuous flow synthesis of 4,5-disubstituted oxazoles, *Organic Letters* 8 (2006) 5231–5234.

- [12] M.W. Losey, R.J. Jackman, S.L. Firebaugh, M.A. Schmidt, K.F. Jensen, Design and fabrication of microfluidic devices for multiphase mixing and reaction, *Journal of Microelectromechanical Systems* 11 (2002) 709–717.
- [13] K.F. Bolton, A.J. Canty, J.A. Deverell, R.M. Guijt, E.F. Hilder, T. Rodemann, J.A. Smith, Macroporous monolith supports for continuous flow capillary microreactors, *Tetrahedron Letters* 47 (2006) 9321–9324.
- [14] A. Gömann, J.A. Deverell, K.F. Munting, R.C. Jones, T. Rodemann, A.J. Canty, J.A. Smith, R.M. Guijt, Palladium-mediated organic synthesis using a porous polymer monolith formed in situ as a continuous catalyst support structure for application in microfluidic devices, *Tetrahedron* 65 (2009) 1450–1454.
- [15] R.C. Jones, A.J. Canty, J.A. Deverell, M.G. Gardiner, R.M. Guijt, T. Rodemann, J.A. Smith, V.-A. Tolhurst, Supported palladium catalysis using a heteroleptic 2-methylthiomethylpyridine –N,S– donor motif for Mizoroki–Heck and Suzuki–Miyaura coupling, including continuous organic monolith in capillary microscale flow-through mode, *Tetrahedron* 65 (2009) 7474–7481.
- [16] A.J. Canty, J.A. Deverell, A. Gömann, R.M. Guijt, T. Rodemann, J.A. Smith, Microfluidic devices for flow-through supported palladium catalysis on porous organic monolith, *Australian Journal of Chemistry* 61 (2008) 630–633.
- [17] F. Svec, My favorite materials: porous polymer monoliths, *Journal of Separation Science* 32 (2009) 3–9.
- [18] C. Viklund, F. Svec, J.M.J. Fréchet, K. Irgum, Monolithic, “molded”, porous materials with high flow characteristics for separations, catalysis, or solid-phase chemistry: Control of porous properties during polymerization, *Chemical Materials* 8 (1996) 744–750.
- [19] Q.C. Wang, F. Svec, J.M.J. Fréchet, Hydrophilization of porous polystyrene-based continuous rod column, *Analytical Chemistry* 67 (1995) 670–674.
- [20] S.F. Xie, F. Svec, J.M.J. Fréchet, Preparation of porous hydrophilic monoliths: effect of the polymerization conditions on the porous properties of poly(acrylamide-co-N,N'-methylenebisacrylamide) monolithic rods, *Journal of Polymer Science, Part A, Polymer Chemistry* 35 (1997) 1013–1021.
- [21] M.R. Buchmeiser, Polymeric monolithic materials: syntheses, properties, functionalization and applications, *Polymer* 48 (2007) 2187–2198.
- [22] E.G. Vlahk, T.B. Tennikova, Preparation of methacrylate monoliths, *Journal of Separation Science* 30 (2007) 2801–2813.
- [23] C. Yu, F. Svec, J.M.J. Fréchet, Towards stationary phases for chromatography on a microchip: molded porous polymer monoliths prepared in capillaries by photoinitiated in situ polymerization as separation media for electrochromatography, *Electrophoresis* 21 (2000) 120–127.
- [24] D.A. Mair, T.R. Schwei, T.S. Dinio, F. Svec, J.M.J. Fréchet, Use of photopatterned porous polymer monoliths as passive micromixers to enhance mixing efficiency for on-chip labeling reactions, *Lab on a Chip* 9 (2009) 877–883.
- [25] W. Rutsch, K. Dietliker, D. Leppard, M. Kohler, L. Misev, U. Kolczak, G. Rist, Recent developments in photoinitiators, *Progress in Organic Coatings* 27 (1996) 227–239.
- [26] T. Rohr, C. Yu, M.H. Davey, F. Svec, J.M.J. Fréchet, Porous polymer monoliths: simple and efficient mixers prepared by direct polymerization in the channels of microfluidic chips, *Electrophoresis* 22 (2001) 3959–3967.
- [27] C. Yu, F. Svec, J.M.J. Fréchet, Towards stationary phases for chromatography on a microchip: molded porous polymer monoliths prepared in capillaries by photoinitiated in situ polymerization as separation media for electrochromatography, *Electrophoresis* 21 (2000) 120–127.
- [28] S. Abele, F.Q. Nie, F. Foret, B. Paull, M. Macka, UV-LED photopolymerised monoliths, *Analyst* 133 (2008) 864–866.
- [29] W. Zarah, A.L. Pavel, J. Vijay, P. Brett, S. Frantisek, M. Mirek, Visible light initiated polymerization of styrenic monolithic stationary phases using 470 nm light emitting diode arrays, *Journal of Separation Science* 33 (2010) 61–66.
- [30] N.E. Leadbeater, M. Marco, Preparation of polymer-supported ligands and metal complexes for use in catalysis, *Chemical Reviews* 102 (2002) 3217–3273.
- [31] C. Yu, M.C. Xu, F. Svec, J.M.J. Fréchet, Preparation of monolithic polymers with controlled porous properties for microfluidic chip applications using photoinitiated free-radical polymerization, *Journal of Polymer Science, Part A, Polymer Chemistry* 40 (2002) 755–769.
- [32] Z. Walsh, S. Abele, B. Lawless, D. Heger, P. Klan, M.C. Breadmore, B. Paull, M. Macka, Photoinitiated polymerisation of monolithic stationary phases in polyimide coated capillaries using visible region LEDs, *Chemical Communications* (2008) 6504–6506.
- [33] M.C. Breadmore, R.M. Guijt, High intensity light emitting diode array as an alternative exposure source for the fabrication of electrophoretic microfluidic devices, *Journal of Chromatography A* 1213 (2008) 3–7.
- [34] N.S. Kenning, B.A. Ficek, C.C. Hoppe, A.B. Scranton, Spatial and temporal evolution of the photoinitiation rate for thick polymer systems illuminated by polychromatic light: selection of efficient photoinitiators for LED or mercury lamps, *Polymer International* 57 (2008) 1134–1140.
- [35] D.A. Mair, E. Geiger, A.P. Pisano, J.M.J. Fréchet, F. Svec, Injection molded microfluidic chips featuring integrated interconnects, *Lab on a Chip* 6 (2006) 1346–1354.
- [36] B. Rånby, W.T. Yang, O. Tretinnikov, Surface photografting of polymer fibers, films and sheets, *Nuclear Instruments & Methods in Physics Research Section B-Beam Interactions with Materials and Atoms* 151 (1999) 301–305.
- [37] T.B. Stachowiak, T. Rohr, E.F. Hilder, D.S. Peterson, M.Q. Yi, F. Svec, J.M.J. Fréchet, Fabrication of porous polymer monoliths covalently attached to the walls of channels in plastic microdevices, *Electrophoresis* 24 (2003) 3689–3693.
- [38] T.B. Stachowiak, D.A. Mair, T.G. Holden, L.J. Lee, F. Svec, J.M.J. Fréchet, Hydrophilic surface modification of cyclic olefin copolymer microfluidic chips using sequential photografting, *Journal of Separation Science* 30 (2007) 1088–1093.

- [39] J. Urban, S. Eeltink, P. Jandera, P.J. Schoenmakers, Characterization of polymer-based monolithic capillary columns by inverse size-exclusion chromatography and mercury-intrusion porosimetry, *Journal of Chromatography A* 1182 (2008) 161–168.
- [40] N. Karbass, V. Sans, E. Garcia-Verdugo, M.I. Burguete, S.V. Luis, Pd(0) supported onto monolithic polymers containing IL-like moieties. Continuous flow catalysis for the Heck reaction in near-critical EtOH, *Chemical Communications* (2006) 3095–3097.

Biographies

Jeremy Deverell recieved his BSc from the University of Tasmania in 2004. In 2006, Jeremy entered the graduate program in Chemistry at the same university. He is currently in the final stages of completing his doctoral research in the development of microreactors using polymer monolith for immobilization of palladium catalysts and has recently commenced a position at the Ian Wark Research Institute, University of South Australia as a Microfluidic Technologist.

Thomas Rodemann obtained his BSc(Hons) in 1998 and PhD in 2001 at La Trobe University with Dr Leslie Deady. After five years as a postdoctoral research fellow with Prof. Allan Canty at the University of Tasmania he joined the Central Science Laboratory at the University of Tasmania where he is currently the Deputy Director. His research activities include vibrational spectroscopy, the development of microreactors and organic and organometallic synthesis.

Jason Smith is a graduate of the Flinders University of South Australia where he obtained both his BSc (Hons) and PhD degrees (with Professor Rolf Prager). He has carried out post-doctoral research at The Texas A&M University (with Professor Sir Derek H. R. Barton) and at The Australian National University (with Professor Martin G. Banwell). In 2001 he joined the faculty in the School of Chemistry at The University of Tasmania where his research activities focus on the development of new synthetic methodologies and their application to the synthesis of biologically active and/or structurally complex molecules.

Allan Canty received his PhD degree from Monash University in 1971, and after a year as an 1851 Scholar at Cambridge University, U.K. He joined the University of Tasmania in 1974 where he is now a Distinguished Professor and a Fellow of the Australian Academy of Science. His research interests have encompassed the bioinorganic and fundamental chemistry of mercury; applications of polydentate nitrogen donor ligands; cyclometallation chemistry; the fundamental chemistry of palladium and platinum including relevance to applications in organic synthesis and catalysis; and recently, the development of flow-through microreactor technology for supported catalysis on organic monolith.

Rosanne Guijt After completing her undergraduate studies in Biopharmaceutical Sciences at Leiden University, the Netherlands, she did her PhD research at the Kluyver Institute of Biotechnology, Delft University of Technology under supervision of Prof. Gijs van Dedem and Prof. Sabeth Verpoorte (IMT, University of Neuchâtel, Switzerland; currently at Groningen University, the Netherlands). After graduating, she moved to the University of Tasmania in 2003 to start up a Lab on a Chip research group. Her research activities have focused on the fabrication and application of Lab on a Chip devices in Life Sciences.